CERN-EP-2024-062
2025/04/10

CMS-B2G-23-002

Searches for Higgs boson production through decays of heavy resonances

The CMS Collaboration*

Abstract

The discovery of the Higgs boson has led to new possible signatures for heavy resonance searches at the LHC. Since then, search channels including at least one Higgs boson plus another particle have formed an important part of the program of new physics searches. In this report, the status of these searches by the CMS Collaboration is reviewed. Searches are discussed for resonances decaying to two Higgs bosons, a Higgs and a vector boson, or a Higgs boson and another new resonance. All analyses use proton-proton collision data collected at $\sqrt{s} = 13$ TeV in the years 2016–2018. A combination of the results of these searches is presented together with constraints on different beyond-the-standard model scenarios, including scenarios with extended Higgs sectors, heavy vector bosons and extra dimensions. Studies are shown for the first time by CMS on the validity of the narrow-width approximation in searches for the resonant production of a pair of Higgs bosons. The potential for a discovery at the High Luminosity LHC is also discussed.

Published in Physics Reports as doi:10.1016/j.physrep.2024.09.004.

Contents

1	Introduction	1
1.1	The Higgs boson at the LHC	2
1.2	Resonant Higgs boson production in models beyond the SM	6
2	Detector and analysis techniques	15
2.1	The CMS Detector	17
2.2	Physics objects	17
2.3	Search for resonances in VH channels	21
2.4	Search for resonances in the HH channel	29
2.5	Search for resonances in the YH channel	34
2.6	Statistical combination	39
3	Upper limits on the cross sections	39
3.1	The $X \rightarrow VH$ decays	40
3.2	The $X \rightarrow HH$ decays	41
3.3	The $X \rightarrow YH$ decays	43
4	Model-specific interpretation	46
4.1	Extended Higgs sector models	46
4.2	Warped extra dimensions	52
4.3	Heavy vector triplet models	54
4.4	Effects of finite width and interference in resonant HH production	54
5	Discovery potential at the HL-LHC	61
5.1	Methodology for estimation of the discovery potential	64
5.2	Discovery potential for $X \rightarrow HH$	64
5.3	Discovery potential for $X \rightarrow YH$	69
6	Summary	75
A	The CMS Collaboration	97

1 Introduction

The discovery of the Higgs (H) boson in 2012 [1–3], at a mass of about 125 GeV, represented a breakthrough for elementary particle physics. Its observation brought a direct confirmation of the principle of spontaneous symmetry breaking, which lies at the origin of elementary particle masses, and is a cornerstone of today’s standard model (SM) of particle physics.

Since the H boson discovery, subsequent research has shown that the measured production and decay modes of the H boson are in agreement with the SM expectations [4]. Thanks to the high luminosity of the CERN Large Hadron Collider (LHC), the very sizable data set of proton-proton (pp) collisions at a center-of-mass energy of 13 TeV accumulated during Run 2 (2015–2018), and the considerable advances in analysis methodology, the very elusive SM Higgs boson pair (HH) production process gradually comes into reach. HH production allows the probing of the trilinear Higgs coupling and thus the investigation of the shape of the Higgs potential.

The H boson also provides an excellent instrument to probe hitherto unknown physics beyond the SM (BSM). A very striking feature of such extensions would be the existence of heavy resonances coupling directly to the H boson, which might, even dominantly, decay into final

states involving H bosons. This would lead to an additional source of H boson production in resonant topologies, which is absent in the SM. Given the small cross section of SM HH production due to the destructive interference between several contributing processes, an excess of HH production with respect to the SM prediction could reveal the existence of heavy BSM resonances. Similarly, the associated production of H and vector bosons could be significantly modified by resonant contributions.

Extended Higgs sectors, which comprise more than the single complex Higgs doublet of the SM, would provide natural candidates for heavy scalar bosons that decay into final states with one or more H bosons. Examples of such models are two-Higgs-doublet models (2HDM) [5–8], 2HDMs extended with a scalar singlet (2HDM+S) [9–11], and the two-real-singlet model (TRSM) [12]. Supersymmetry naturally incorporates extended Higgs sectors. The minimal supersymmetric model (MSSM) [13–16] features a 2HDM-type Higgs sector, while the next-to-minimal supersymmetric model (NMSSM) [17–19] includes a 2HDM+S-type Higgs sector.

Models of warped extra dimensions (WED) [20–29] predict the existence of an additional spatial dimension in which the field quanta of gravity, the gravitons, propagate. The Randall–Sundrum bulk model gives rise to heavy resonances such as the spin-0 radion, and a tower of Kaluza–Klein excitations of the spin-2 graviton, which might have sizable branching fractions into HH. In certain models, which might potentially solve the hierarchy problem, heavy vector resonances, like W' and Z' bosons, form a heavy vector triplet (HVT) [30]. They could manifest themselves through decays into ZH and WH, where W and Z denote the electroweak (EW) gauge bosons.

This report is organized as follows: Section 1 provides a brief introduction to the H boson and the theoretical concepts underlying the resonant production of H bosons. Section 2 summarizes the techniques of the respective CMS analyses on 13 TeV data. Section 3 presents a coherent picture of the results of these analyses, as well as combinations of these results. Section 4 is dedicated to interpretations of the results in the various models. Section 5 discusses projections towards higher integrated luminosities, including the potential for a discovery at the High-Luminosity LHC (HL-LHC). A summary is given in Section 6.

Tabulated results unique to this report are provided in a HEPData record [31].

1.1 The Higgs boson at the LHC

The Higgs boson was first proposed in the 1960s [32–34], and was finally discovered at the LHC in 2012, by the ATLAS [1] and CMS [2, 3] collaborations.

In the SM, the Higgs field has a nonzero vacuum expectation value, which breaks the EW symmetry and generates the masses of the W and Z bosons, while leaving the photon massless. This process is called the EW symmetry breaking of the Brout–Englert–Higgs mechanism.

There are several ways that H bosons can be produced at the LHC in pp collisions, each with their own unique experimental signature. The production cross sections are shown in Fig. 1 (left).

The dominant H boson production mechanism is through the “gluon fusion” process (ggF), which involves the fusion of two gluons from the colliding protons. This process accounts for around 88% of all H bosons produced at the LHC. “Vector boson fusion” (VBF) describes the scattering of two vector bosons V (W or Z bosons) exchanged between the colliding protons, and accounts for around 8% of all Higgs bosons produced at the LHC. Other processes include associated H boson production with vector bosons (VH), with top quarks ($t\bar{t}H$), or with bottom

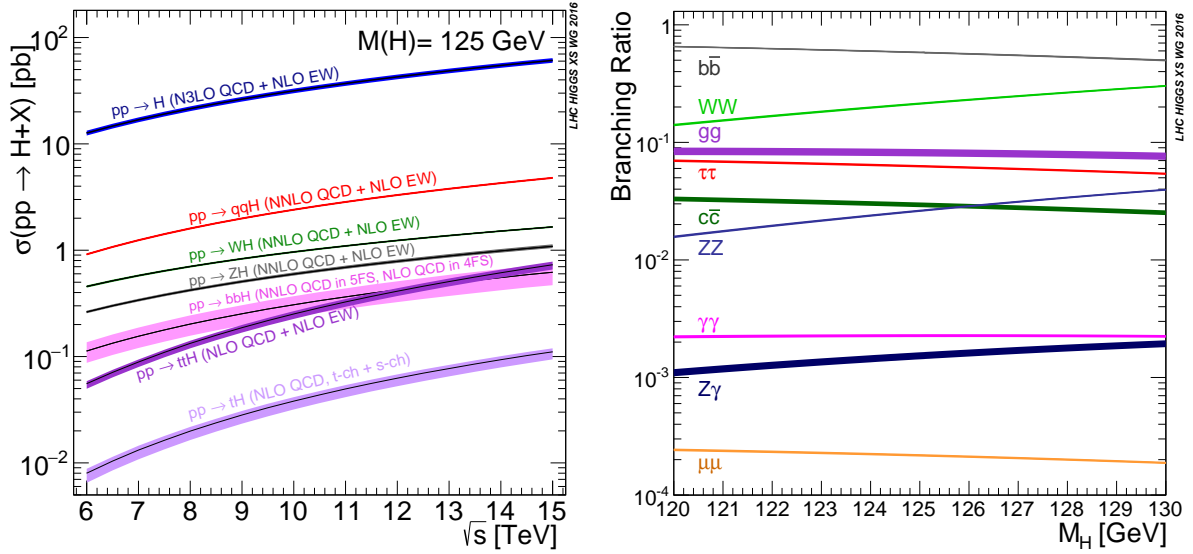


Figure 1: Higgs boson production cross sections in the SM as a function of the collider center-of-mass energy (left), and Higgs boson branching fractions in the SM as a function of the Higgs boson mass (right). Both figures are taken from Ref. [35].

quarks ($b\bar{b}H$).

Once produced, Higgs bosons can decay in various ways, each producing a different final state of particles. The most common and experimentally accessible H boson decay modes are to a pair of bottom quarks, W bosons, τ leptons, and Z bosons as shown in Fig. 1 (right). The H boson does not directly couple to gluons or photons, but can decay into them via fermion or W boson loops.

The properties and couplings of the H boson have been extensively studied at the LHC. The SM does not predict the mass of the H boson, but once the mass is given, all its other properties are defined. The most recent and precise measurement of the H boson mass is $m_H = 125.22 \pm 0.14$ GeV [36]. The CMS Collaboration has measured the H boson width to be $\Gamma_H = 3.2^{+2.4}_{-1.7}$ MeV via off-shell production in the 4ℓ and $2\ell + 2\nu$ final states [37]. This value is in agreement with the SM prediction of 4.1 MeV [38].

To quantify the agreement between the data and the SM predictions, the concept of a signal strength can be used, which is defined as $\mu = \sigma/\sigma_{SM}$, where σ is the measured production cross section and σ_{SM} is the SM prediction. After performing a combined fit of all the data collected at $\sqrt{s} = 13$ TeV, in all production modes and decay channels, the observed H signal strength is $\mu = 1.002 \pm 0.057$ [4], in agreement with the SM prediction. Figure 2 shows the CMS measurements of the signal strength parameter for each production mode, $\mu_i = \sigma_i/\sigma_{i,SM}$, and several decay channels, $\mu^f = \mathcal{B}^f/\mathcal{B}_{SM}^f$, where \mathcal{B} is the branching fraction. The production modes ggF, VBF, WH, ZH, and $t\bar{t}H$ are all observed with a significance of five standard deviations (s.d.) or above [4].

To quantify the impact of new physics on the interaction between the H boson and other particles, we scale the coupling strengths as predicted in the SM by a factor κ_i (the coupling modifiers) [38], where i is the coupling which the modifier corresponds to. Two coupling modifiers are introduced, κ_V and κ_f , to scale the couplings to the EW gauge bosons and fermions, respectively. When differentiating between the two heavy gauge bosons W and Z, we can define κ_W and κ_Z . Equivalently, for the fermions we define κ_t , κ_b , κ_τ , and κ_μ . In extensions of the

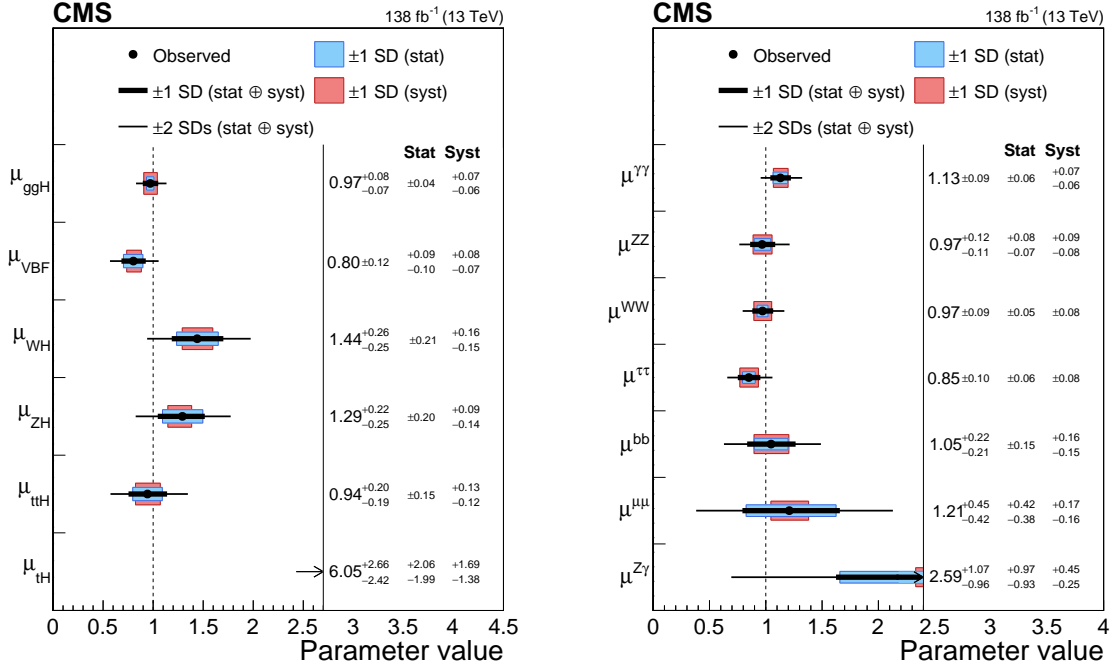


Figure 2: Signal strength parameters extracted for various production modes μ_i , assuming the branching fractions $\mathcal{B}^f = \mathcal{B}_{SM}^f$ (left), and decay channels μ^f , assuming the production cross sections as predicted by the SM (right). The thick and thin black lines indicate the one and two s.d. confidence intervals (labelled by SD in the figures), with the systematic and statistical components of the former indicated by the red and blue bands, respectively. The vertical dashed line at unity represents the values of μ_i (resp. μ^f) in the SM. Taken from Ref [4].

SM with new particles, loop-induced processes may receive additional contributions, therefore introducing additional modifiers for the effective couplings of the H boson to gluons (κ_g), photons (κ_γ), and $Z\gamma$ ($\kappa_{Z\gamma}$). According to the latest combined results on these effective couplings shown in Fig. 3, the measured coupling modifiers are compatible with the SM expectations within 1.5 s.d., with uncertainties around 10% for most couplings [4]. The invisible and undetected decays of the Higgs boson are also considered, where the latter expression refers to Higgs boson decays into final states that can not be distinguished from background processes, at the LHC.

The H boson trilinear coupling is a measure of the Higgs field's self-interaction strength and determines the shape of its potential. The Higgs boson self-coupling can be accessed directly at the LHC via Higgs boson pair production. This rare process has a very low SM cross section because of the destructive interference of the two contributing processes at leading order (LO), the box and triangle diagrams shown in Fig. 4 (left and middle). Only the triangle diagram is sensitive to the H trilinear coupling. As a result, detecting the production of Higgs boson pairs and determining the trilinear self-coupling is a major experimental challenge.

The CMS Collaboration has constrained the coupling modifier for the trilinear H boson self-coupling to be within -1.24 and 6.49 at 95% confidence level (CL) using pp data corresponding to an integrated luminosity of 138 fb^{-1} , and assuming SM values for the Higgs boson couplings to top quarks and vector bosons. The production cross section for inclusive HH production has been constrained to be smaller than 3.4 times the value predicted in the SM at 95% CL [4].

To understand the Higgs sector is essential for particle physics and cosmology. Determining the exact behavior of the Higgs field will help us understand the formation of structures in the

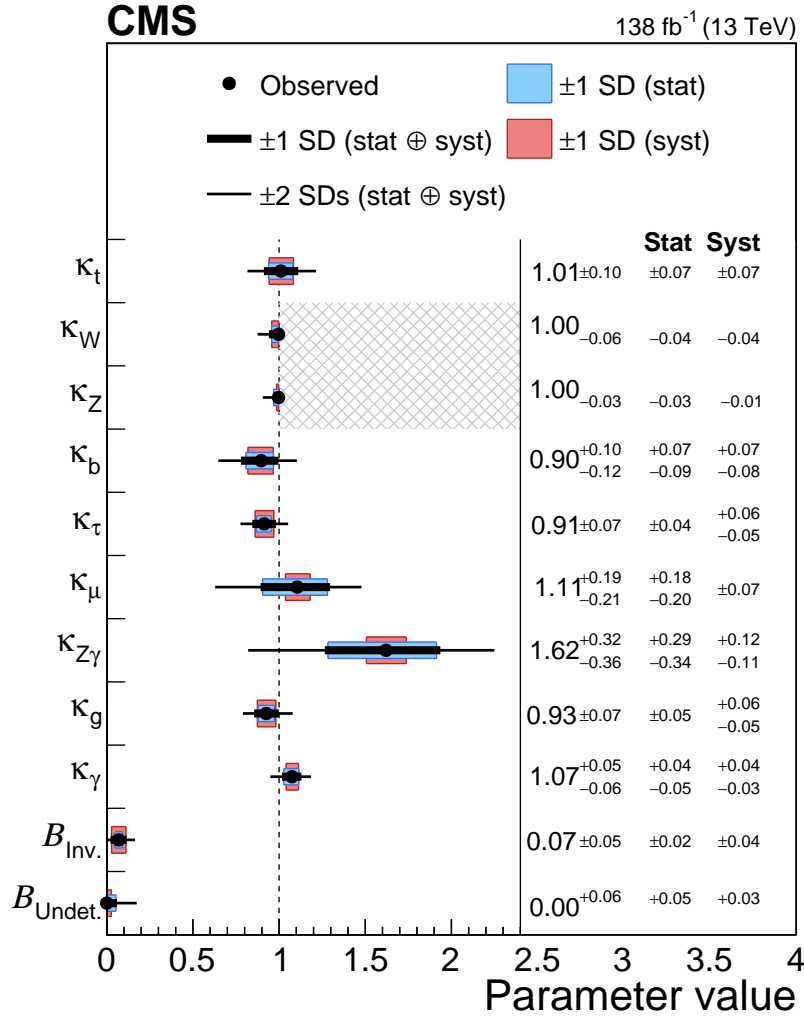


Figure 3: Measurements of the coupling modifiers κ_i , allowing both invisible and undetected decay modes, with the SM value used as an upper bound on both κ_W and κ_Z . The thick and thin black lines indicate the ± 1 and ± 2 s.d. confidence intervals, respectively, with the systematic and statistical components of the ± 1 s.d. interval indicated by the red and blue bands. The resulting branching fractions for invisible and undetected decay modes are also displayed. Taken from Ref. [4].

early universe immediately after the Big Bang, and the stability of the vacuum. Some theories of inflation involve a scalar field as the inflaton, the field responsible for driving the expansion of the universe [39, 40]. The fact that the Higgs field is the only scalar field currently known motivates a theory based on the idea that the Higgs field caused inflation. In addition, the behavior of the Higgs field during the phase transition in the early universe can explain leptogenesis [41] and baryogenesis [42, 43] and could potentially shed light on the matter-antimatter asymmetry we observe today [44]. However, the Higgs sector does not have to be minimal. The presence of additional fields would have an impact on the mechanisms of inflation, leptogenesis, and baryogenesis. Studying the Higgs interactions in detail and exploring the Higgs sector more broadly provide a promising avenue for discovering BSM physics and understanding the evolution of the early universe.

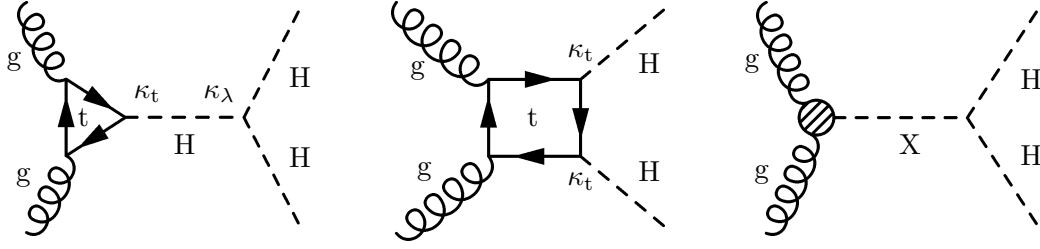


Figure 4: Leading order Feynman diagrams of Higgs boson pair production via gluon fusion. The left and middle parts of the figure show the “triangle” and “box” diagrams, respectively for nonresonant H production, as expected from the SM. The right part of the figure shows a diagram for H boson production through a new resonance labeled as X.

1.2 Resonant Higgs boson production in models beyond the SM

The production of H bosons through the decay of heavy resonances is not possible within the SM. A generic example of a Feynman diagram for such a process is shown in Fig. 4 (right), where X denotes a sufficiently heavy resonance. In the following, we briefly review BSM models in which such production mechanisms occur.

1.2.1 Extended Higgs sectors

The SM Higgs sector consists of one complex Higgs doublet and leads to the prediction of one physical H boson. However, there is no guarantee that the Higgs sector is minimal. The SM Higgs sector can be extended with additional singlets, doublets, or triplets, or combinations thereof [6, 45–48]. Extended Higgs sectors imply the presence of additional Higgs bosons: Neutral Higgs bosons appear in singlet, doublet, and triplet extensions; charged Higgs bosons H^\pm appear in doublet and triplet extensions; and doubly charged Higgs bosons, like e.g., H^{++} , appear in triplet extensions. In this report, we focus on extensions with singlets and doublets since these lead to final states with SM-like H bosons. Furthermore, it is assumed that the singlets and doublets acquire a vacuum expectation value and couple to the SM particles.

The phenomenology of the additional neutral bosons also depends on their CP structure. Here, we only consider CP eigenstates: pure scalars are denoted by either X or Y, with $m_X > m_Y$, and pseudoscalars are denoted by A or a, with $m_A > m_a$. Depending on the structure of the extended Higgs sector and on the masses of the additional scalars and pseudoscalars, the following decays involve SM-like H bosons in the decay chain:

1. decays of a heavy neutral scalar to two SM-like Higgs bosons, $X \rightarrow HH$,
2. decays of a heavy neutral scalar to an SM-like Higgs boson and another scalar, $X \rightarrow YH$,
3. decays of a heavy pseudoscalar to an SM-like Higgs boson and another pseudoscalar, $A \rightarrow Ha$, and
4. decays of a heavy pseudoscalar to an SM-like Higgs boson and a Z boson, $A \rightarrow ZH$.
5. For large m_X and if $m_Y \gtrsim 250$ GeV, there can also be chained decays leading to the production of multiple H bosons, $X \rightarrow YY \rightarrow HHHH$ and $X \rightarrow YH \rightarrow HHH$.

In general, the additional singlets and doublets mix with the SM doublet and therefore modify the couplings of the SM-like scalar H [49]. The couplings of the observed H boson agree well with the SM predictions, leading to significant constraints on the parameter space of extended Higgs models [4, 50–52].

Additional singlets The most straightforward extension of the SM Higgs sector is to introduce an additional real-singlet field S [53–56]. The ratio of the vacuum expectation values v of the SM complex doublet and of the singlet, $\langle S \rangle$, defines the parameter $\tan \beta = v / \langle S \rangle$. The real-singlet model leads to one additional scalar X , which can be heavier or lighter than H . When applying a \mathbb{Z}_2 symmetry that requires invariance under transformation of the field $S \rightarrow -S$, the scalar X obtains its couplings to SM particles from mixing with the SM-like H boson, with a mixing angle α . The couplings to SM particles hence correspond to those of the H boson, albeit suppressed by a factor $\sin \alpha$ if $m_X > m_H$.

For this reason, also the branching fractions of the scalar X equal those of an SM-like Higgs boson, unless $m_X > 2m_H$, in which case the decay $X \rightarrow HH$ becomes kinematically possible. In this case, the decays to other SM particles are suppressed depending on the partial width of the X decay to HH , which depends on $\tan \beta$. In summary, the extension with a real additional scalar with \mathbb{Z}_2 symmetry involves three new free parameters — the mass of the additional scalar m_X , the mixing angle α , and the ratio of the two vacuum expectation values $\tan \beta$ — and leads to $X \rightarrow HH$ decays if kinematically possible, with a relative rate compared to the other decay modes depending on $\tan \beta$.

Adding a second real singlet field, again imposing \mathbb{Z}_2 symmetry, defines the two real singlet model (TRSM) [12]. Compared to the real-singlet extension, the TRSM introduces four new parameters: the mass of a second new scalar Y , the mixing angles between the second real singlet field and the complex SM doublet as well as the other real singlet field, and the vacuum expectation value of the second real singlet field. The main difference in terms of phenomenology is that, depending on the masses of the additional Higgs bosons, decays of type $X \rightarrow YH$, $X \rightarrow HH$ (or $Y \rightarrow HH$), and $X \rightarrow YY$ become possible, including the chained decays $X \rightarrow YY \rightarrow HHHH$ and $X \rightarrow YH \rightarrow HHH$. All of the decays involving H bosons can have large branching fractions and are hence of experimental interest. The final states that provide the largest sensitivity after the decays of the H bosons depend on the branching fractions of H (discussed in Section 1.1) and Y . The Y branching fractions correspond to those of an SM-like Higgs boson of mass m_Y . Therefore, decays into W and Z bosons dominate above the WW and ZZ production thresholds, and decays to $t\bar{t}$ become relevant above the $t\bar{t}$ production threshold. This is different from 2HDMs where decays into fermions are dominant for a large fraction of the parameter space.

Additional doublets In 2HDMs, the SM is extended with a second Higgs doublet leading to the emergence of three neutral and two charged Higgs bosons [5–8]. Most commonly it is required that each Higgs doublet only couples to charged fermions of one type (up-type quarks, down-type quarks, or charged leptons) and CP -violating terms at the tree level are forbidden to evade constraints from flavor-changing neutral currents and the negative results of searches for CP violation in the Higgs sector. These constraints give rise to four types of 2HDMs that are distinguished by which of the Higgs doublet fields couples to which type of fermions:

1. Type I, with all charged fermions coupled to the second Higgs doublet,
2. Type II, with only up-type quarks coupled to the second Higgs doublet,
3. Lepton-specific (Type X), with only up-type and down-type quarks coupled to the second Higgs doublet, and
4. Flipped (Type Y), with only up-type quarks and charged leptons coupled to the second Higgs doublet.

The free parameters of the model can be expressed in terms of the masses of the Higgs bosons (m_H , with H being the SM-like Higgs boson, as well as m_X , m_A , and m_{H^\pm}), the vacuum expectation value of the SM-like doublet v , the ratio of the two vacuum expectation values $\tan\beta$, the mixing angle α , and a parameter m_{12} that softly breaks the \mathbb{Z}_2 symmetry. Since m_H and v are known, there are six free parameters in these 2HDM scenarios. However, there are important constraints on the parameter space. Constraints from EW precision data require the masses of at least two of the additional Higgs bosons to be close to each other [57], which is why mass-degenerate scenarios are studied most frequently. In addition, flavor observables lead to strong constraints in the overall parameter space, and in particular to lower bounds on m_{H^\pm} of around 600 GeV in Type II and Type Y models [58–61]. Furthermore, in the so-called alignment limit with $\cos(\beta - \alpha) \rightarrow 0$ the H boson becomes SM-like. In turn, the measurements of the H boson couplings, which are consistent with the SM predictions within uncertainties [4, 52], lead to constraints on $|\cos(\beta - \alpha)|$ between 0.02 and 0.3, depending on the type of 2HDM and on $\tan\beta$ [50–52, 57].

The couplings of additional heavy Higgs bosons X and A that involve an H boson crucially depend on $\cos(\beta - \alpha)$. For $\cos(\beta - \alpha) \rightarrow 0$, the branching fractions for the decays $X \rightarrow HH$ and $A \rightarrow ZH$ vanish. While the couplings remain the same for different types of 2HDMs, the branching fractions can be different because these depend on the partial widths of all decay modes. Example branching fractions for 2HDMs of Type I and Type II are shown in Fig. 5. For non-mass-degenerate 2HDMs, decays of type $A \rightarrow ZX$ and $X \rightarrow ZA$ are possible. If allowed, these decays usually have large branching fractions that are not suppressed in the alignment limit.

An important special case of a 2HDM of Type II is the Higgs sector of the minimal supersymmetric standard model (MSSM) [13–16]. At the tree level, the MSSM Higgs sector can be described by two parameters, m_A and $\tan\beta$. The MSSM naturally predicts an H boson that has nearly SM-like couplings, in particular when m_A is large. Furthermore, the mass of the SM-like H boson follows from the MSSM parameter values. For small values of $\tan\beta$, i.e., $\tan\beta \gtrsim 1$, a large supersymmetry (SUSY) breaking scale is needed to achieve $m_H = 125$ GeV. This is, however, consistent with the nonobservation of SUSY partners at the LHC.

Various MSSM benchmark scenarios have been proposed [35, 64–67, 70]. Searches for $A/X \rightarrow \tau\tau$ exclude a large fraction of parameter space at medium to high $\tan\beta$ [71], such that the phenomenologically interesting parameter space is at low to medium $\tan\beta$. Figure 6 shows the $X \rightarrow HH$ branching fractions in two scenarios that are particularly designed to give non-excluded predictions at low $\tan\beta$. The branching fractions for masses below the $t\bar{t}$ threshold can reach values of more than 80%, making this channel very important, though measurements of the H boson couplings indicate that $m_A > 400$ –500 GeV [50, 51]. For intermediate values of $\tan\beta$, the branching fraction $\mathcal{B}(X \rightarrow HH)$ can still be of order 10% and the search remains important, whereas $\mathcal{B}(A \rightarrow ZH)$ is found to become negligible.

Models with additional singlets and doublets Models that combine singlets and doublets include the next-to-minimal 2HDM (N2HDM), which extends the 2HDM with a real singlet, and the 2HDM+S, which extends the 2HDM with a complex singlet [9–11]. Considering only CP -conserving versions of the model, the N2HDM predicts three CP -even neutral Higgs bosons (again denoted as H , X , and Y), one CP -odd neutral Higgs boson A , and two charged Higgs bosons H^\pm . Compared to 2HDMs, the N2HDM adds four additional parameters [11]: two mixing angles α_2 and α_3 , responsible for the mixing of the additional singlet with the two doublets, the mass of the additional CP -even Higgs boson m_Y , and the vacuum expectation value of the real singlet v_S . The N2HDMs can be categorized in the same four scenarios as

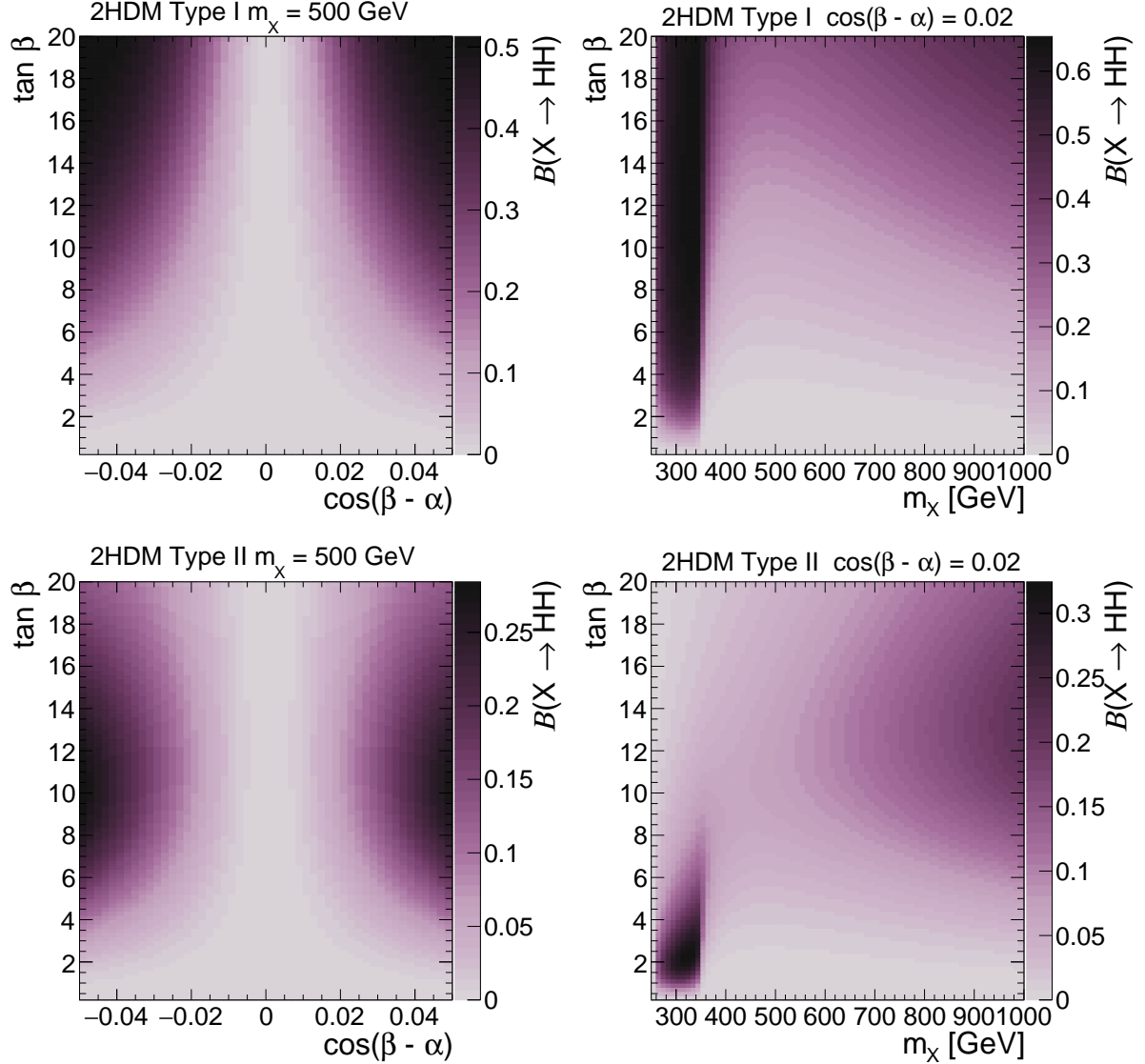


Figure 5: Branching fractions of $X \rightarrow HH$ decays in 2HDMs of Type I (upper) and Type II (lower) in the $\cos(\beta - \alpha)$ - $\tan \beta$ plane for $m_X = 500$ GeV (left) and in the m_X - $\tan \beta$ plane for $\cos(\beta - \alpha) = 0.02$ (right). The masses of all non-SM-like Higgs bosons are set to be the same, $m_X = m_A$, and $m_{12}^2 = m_A^2 \tan \beta / (1 + \tan^2 \beta)$. The branching fractions have been calculated with 2HDMC v1.8.0 [62, 63].

2HDMs, depending on the Yukawa couplings.

Phenomenologically, N2HDMs share many similarities and constraints with 2HDMs, in particular, those related to EW constraints and flavor observables. However, the singlet admixture can affect the couplings of the SM-like H boson. Most importantly, the additional scalar Y can either be produced directly or in decays of heavier Higgs bosons, $X \rightarrow YH$ and $X \rightarrow YY$. Unlike decays to two SM-like Higgs bosons like $X \rightarrow HH$, these decays are not suppressed in the alignment limit, which is at least approximately realized given the SM-like nature of the H boson. The decays $X \rightarrow YH$ and $X \rightarrow YY$ can hence be dominant if kinematically allowed. The branching fractions of the Y boson to SM particles depend on the Yukawa type and the other model parameters. This leads to a variety of experimentally relevant final states [72, 73].

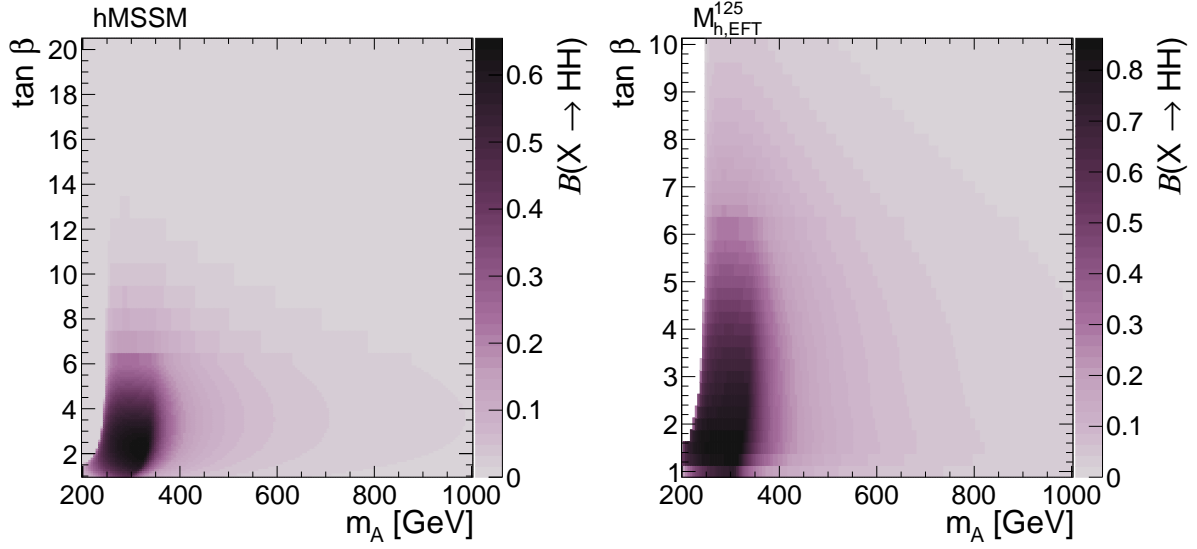


Figure 6: Branching fraction of $X \rightarrow HH$ decays in the MSSM, for the hMSSM [64–66] (left) and the $M_{h,EFT}^{125}$ [67] benchmarks, in the m_A – $\tan \beta$ plane. The branching fractions are taken from benchmark files produced by the MSSM subgroup of the LHC Higgs Working Group [68, 69].

The 2HDM+S model adds a second CP -odd Higgs boson, leading to the additional $A \rightarrow Ha$ decay, which is experimentally consistent with the $X \rightarrow HY$ signature [74]. The Higgs sector of the next-to-minimal MSSM (NMSSM) is a 2HDM+S of Type II [17–19]. The NMSSM generally leads to the same signatures as the N2HDM and 2HDM+S models, but, like the MSSM, is more constrained due to the characteristics of SUSY, and these constraints differ from the MSSM because of the additional particle content [55, 75, 76].

1.2.2 Warped extra dimensions (radion and Randall–Sundrum graviton)

Models with a warped extra dimension (WED), as proposed by Randall and Sundrum (RS) [20], postulate the existence of one extra spatial dimension compactified between two fixed “branes”. The region between the branes is referred to as bulk and possesses an exponential metric. The gap between the two fundamental scales of nature, such as the Planck scale (M_{Pl}) and the EW scale, is controlled by a warp factor (k) in the metric, which corresponds to one of the fundamental parameters of the model. The brane where the extra-dimensional metric’s density is localized is called the “Planck brane”, while the other, where the Higgs field is localized, is called the “TeV brane”. This class of models predicts the existence of new particles that can decay to HH , such as the spin-0 radion R [21–23], and the first spin-2 Kaluza-Klein (KK) excitation of the graviton, G [24–26]. The radion is an additional element of WED models, needed to stabilize the size of the extra dimension l , where the distance between the branes is connected to its vacuum expectation value [21].

There are two possible ways of describing a KK graviton in WED models, that depend on the localization choice for the SM matter fields, as shown in Fig. 7. In the RS1 model, only gravity is allowed to propagate in the extra-dimensional bulk. In this model, the KK graviton couplings to matter fields are controlled by the dimensionless quantity $\tilde{k} = k/\bar{M}_{Pl}$ [20], with the reduced Planck mass \bar{M}_{Pl} defined by $M_{Pl}/\sqrt{8\pi}$. The second possibility is to have SM particles propagate in the bulk, the bulk-RS model. In this scenario, the KK graviton couplings to the matter fields depend on the localization of the SM fields in the bulk. This report uses the phenomenology of Ref. [27]. The SM particles are allowed to propagate in the bulk and follow the SM gauge group’s characteristics, with the right-handed top quark localized very near the TeV brane (the

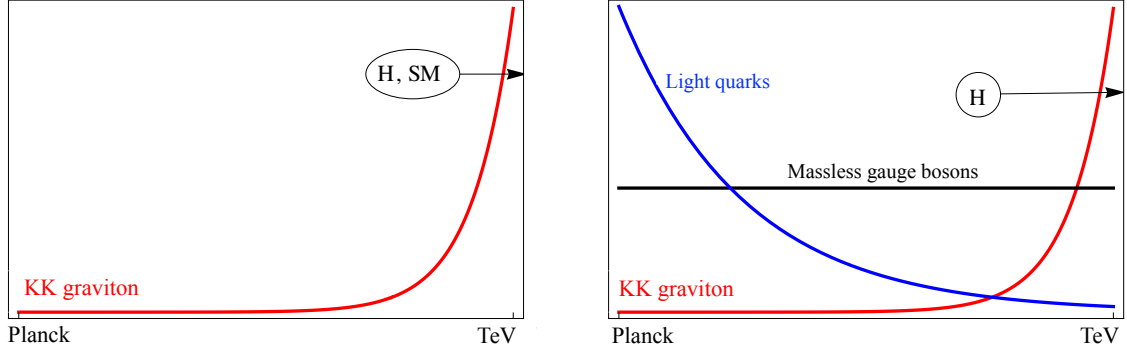


Figure 7: Localization of fields on the branes, in different types of the Randall-Sundrum (RS) model: RS1 (left) and bulk-RS (right). The x -axis represents the 5th dimension with the Planck brane on the left and the TeV brane on the right. The y -axis is the probability density. Adapted from Ref. [28].

so-called elementary top quark hypothesis).

It is common practice to express the benchmark points of the model in terms of \tilde{k} , and the mass scale $\Lambda_R = \sqrt{6} e^{-kl} \overline{M}_{\text{Pl}}$, where the latter is interpreted as the ultraviolet cutoff of the model [29]. The addition of a scalar-curvature term can induce mixing between the scalar R and the H boson [29, 77, 78]. Precision EW studies suggest that this mixing is small [79], so we neglect the possibility of R - H mixing in this report.

The choice of localization of the SM matter fields for the KK-graviton resonance impacts the kinematics of the signal and drastically modifies its production and decay properties [80], so that a distinction of the RS1 and bulk-RS models is necessary for the G phenomenology. In contrast, the physics of the radion depends only very weakly on the choice of the model [29], which obviates the need to distinguish the RS1 and bulk-RS possibilities in this case. More details on WED models can be found in Ref. [28].

In RS1, with all the SM fields localized on the TeV brane, a heavy graviton would decay to a wide range of final states with significant branching fractions as shown in Fig. 8 (upper left), and constraints on the RS1 model are mainly obtained from fermionic channels [81]. In the bulk-RS model, the maximum branching fraction to a pair of Higgs bosons is below 10% under the hypothesis of an elementary H boson, as shown in Fig. 8 (upper right). Accordingly, the HH final state is usually not the most important one for placing constraints on the bulk-RS model, where the largest sensitivity arises from searches in WW , ZZ , or $t\bar{t}$ signatures. However, the branching fraction to HH can reach 25% if the top quark coupling becomes small, such that investigations of HH signatures are necessary in the context of bulk-RS models, because the branching fractions are very model dependent.

The dominant R decay modes are into pairs of massive gauge bosons, H bosons, and top quarks, as shown in Fig. 8 (lower). Since the couplings are determined by the masses of the final-state particles, and these masses arise from the H boson localized on the TeV brane, the RS1 and bulk-RS couplings are identical at LO. For large resonance mass m_χ , the corresponding widths are

$$\Gamma(R \rightarrow HH) = \Gamma(R \rightarrow ZZ) = \Gamma(R \rightarrow WW)/2 = \frac{1}{32\pi} \frac{m_\chi^3}{\Lambda_R^2} \quad (1)$$

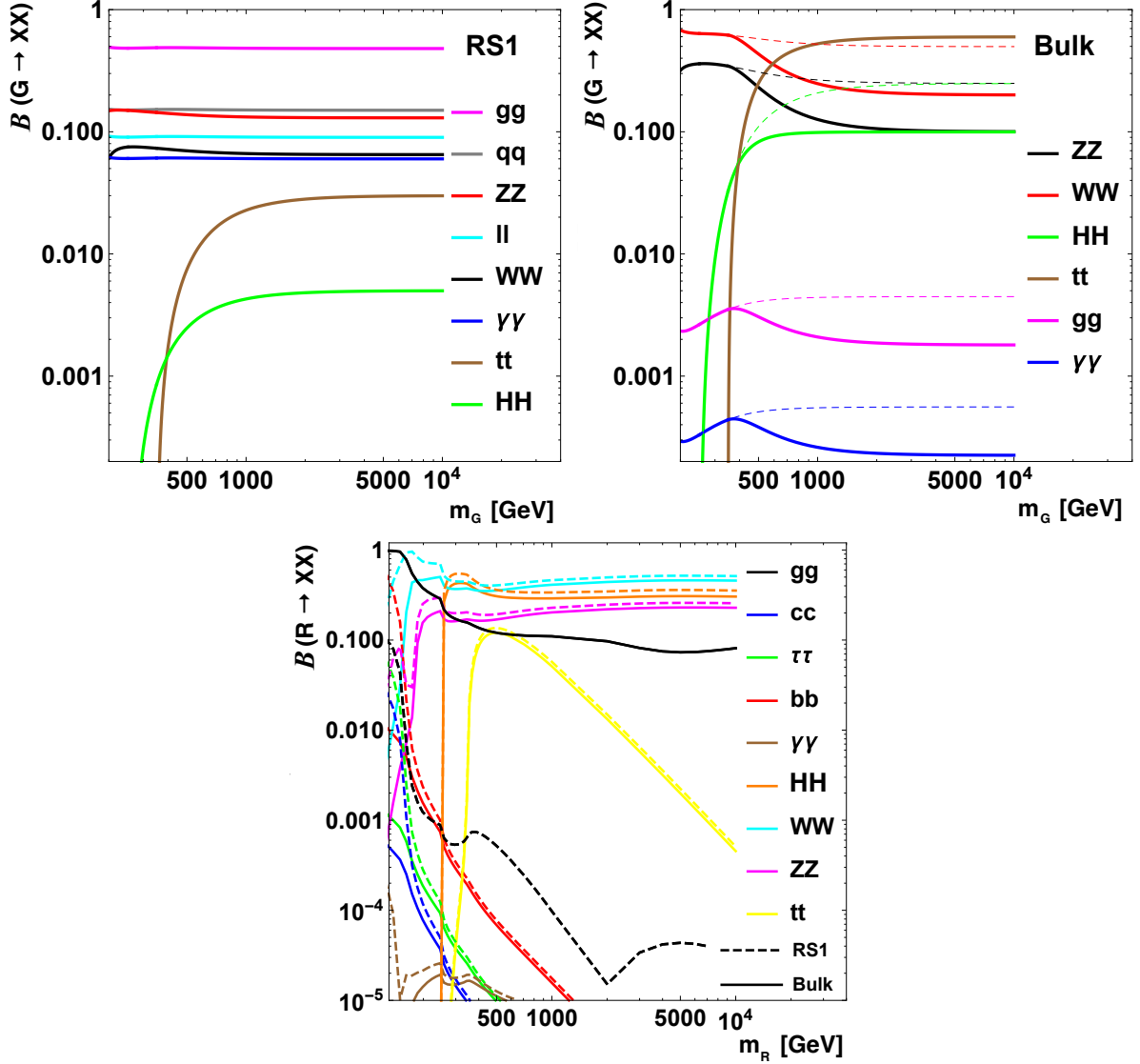


Figure 8: The decay branching fractions of an RS1 graviton (upper left), bulk graviton (upper right), and radion (lower). Solid lines assume a fully elementary top quark, while the dashed lines ignore the coupling of the graviton to top quarks. Adapted from Ref. [28].

and

$$\Gamma(R \rightarrow t\bar{t}) = \frac{3}{8\pi} \left(\frac{m_t}{m_\chi} \right)^2 \frac{m_\chi^3}{\Lambda_R^2}. \quad (2)$$

For large radion masses, the branching fraction to HH is approximately 25%, independent of Λ_R , because the contribution from decays to $t\bar{t}$ is suppressed by $(m_t/m_\chi)^2$. This makes $R \rightarrow HH$ an important channel in the search for a radion resonance.

1.2.3 Heavy vector triplet (W' and Z')

A class of models extending the gauge groups of the SM predicts new force-carrying vector bosons. They may form a heavy vector triplet (HVT) [30] consisting of W' and Z' , in analogy with the carriers of the weak force. Examples of such theories include weakly coupled W' and Z' models [82–84], little Higgs models [85, 86], and composite Higgs scenarios [87–91]. The latter are of particular interest as they offer a potential solution to the hierarchy problem. In

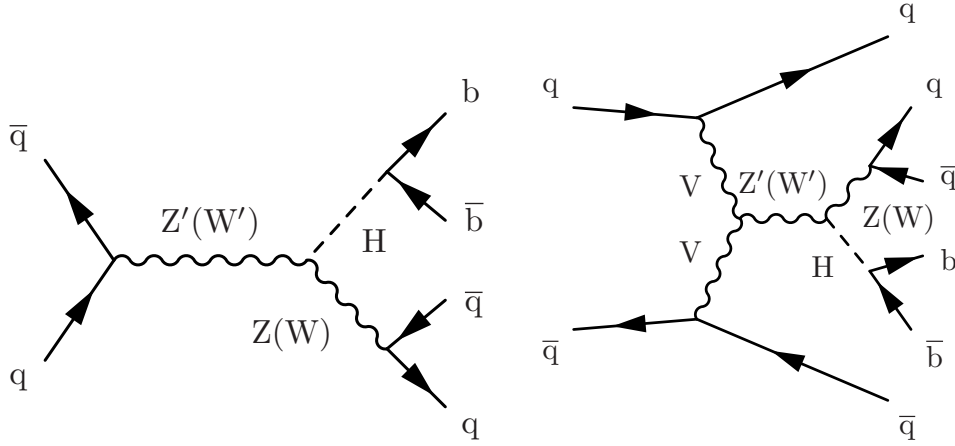


Figure 9: Feynman diagrams for the production of Z' and W' bosons produced through the (left) Drell–Yan and (right) vector boson fusion process. The Z' (resp. W') boson subsequently decays into ZH and WH , respectively.

these scenarios, the H boson is a strongly coupled bound state, a pseudo-Nambu–Goldstone boson, sharing constituents with new heavy vector bosons. One possible signature of such models at the LHC is H boson production through new heavy vector resonances.

The phenomenology of models including an HVT can be deduced from a simplified Lagrangian [30]. The HVT model is characterized in terms of four parameters: the masses of the W' and Z' resonances, which are degenerate, a coefficient c_F , which scales the W' and Z' couplings to fermions, another coefficient c_H , which scales the W' and Z' couplings to the H boson and longitudinally polarized SM vector bosons, and g_V , which represents the typical strength of the new vector boson interaction.

The two main W' and Z' production modes at the LHC and their decays to VH are shown in Fig. 9. The triplet field, which mixes with the SM gauge bosons, couples to the fermionic current through the combination of parameters $g_F = g^2 c_F / g_V$ and to the H and V bosons through $g_H = g_V c_H$, where g is the $SU(2)_L$ gauge coupling, taken to be $2m_W/v = 0.6534$ with the W boson mass m_W and the vacuum expectation value v from Ref. [48]. We will derive the constraints on the couplings g_H and g_F for several values of g_V below.

Three benchmark scenarios are typically considered in searches.

- Model A, with $g_V = 1$, $c_H = -0.556$, and $c_F = -1.316$, corresponding to $g_F = -0.562$ and $g_H = -0.556$. This scenario reproduces a model with a weakly coupled extended gauge theory [92].
- Model B, with $g_V = 3$, $c_H = -0.976$, and $c_F = 1.024$, corresponding to $g_F = 0.146$ and $g_H = -2.928$. It mimics a minimal strongly coupled composite Higgs model [88].
- Model C, with $g_V = 1$, $c_H = 1 - 3$, and $c_F = 0$, is a model where couplings to fermions are suppressed, such that no production via a Drell–Yan (DY) process is possible at the LHC and the production of W' and Z' bosons happens exclusively via VBF.

In all three scenarios, fermion universality is assumed. In model A, the vector resonances have larger couplings to fermions than to bosons, with the branching fractions to quarks enhanced by the color factor in QCD. Thus, searches for resonances in fermion pair production are most sensitive. Models B and C have large branching fractions to boson pairs, while the fermionic

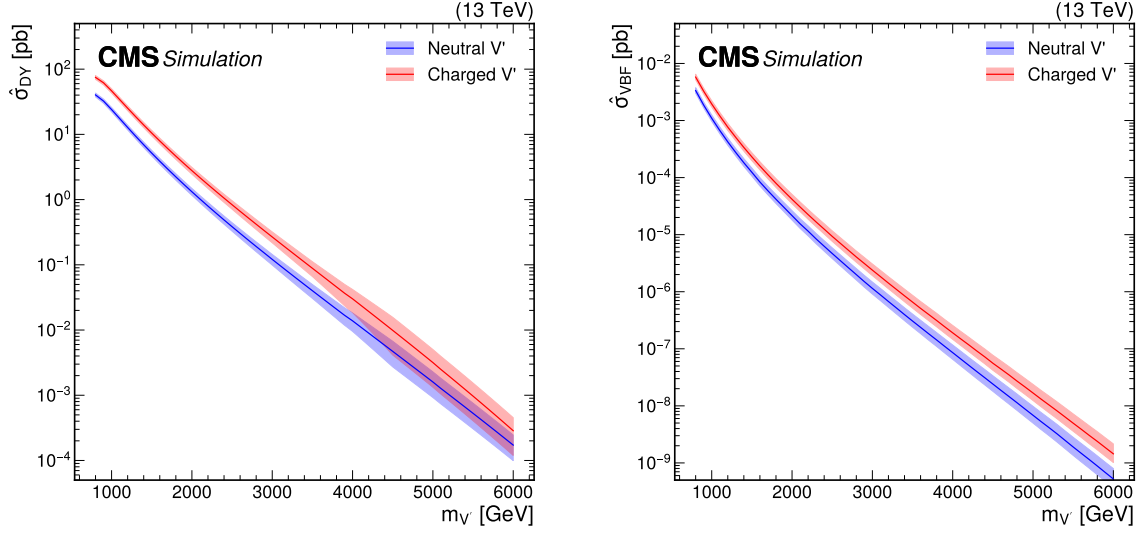


Figure 10: Cross sections for (left) Drell–Yan production ($\hat{\sigma}_{\text{DY}}$) and (right) production through vector boson fusion ($\hat{\sigma}_{\text{VBF}}$), as defined in Eqs. (3) and (4), for Z' and W' bosons in the heavy vector triplet (HVT) model B at $\sqrt{s} = 13$ TeV. Calculations are based on the work of Ref. [30].

couplings are suppressed.

The analyses discussed in this paper derive results using the narrow-width approximation. In this approximation, the production of a certain final state through the W' and Z' resonances can be factorized into the production of the W' and Z' resonances, followed by the decay with the respective branching fractions to the final state under consideration. We parametrize the W' and Z' production cross sections as

$$\sigma_{\text{DY}}(g_F, g_H, g_V) = g_F^2 \hat{\sigma}_{\text{DY}} \quad (3)$$

$$\sigma_{\text{VBF}}(g_F, g_H, g_V) = g_H^2 \hat{\sigma}_{\text{VBF}} \quad (4)$$

where $\hat{\sigma}_{\text{DY}}$ and $\hat{\sigma}_{\text{VBF}}$ for model B are shown in Fig. 10. Compared to the production cross sections of heavy scalar resonances discussed in Section 1.2.1, where the smallness of the cross sections restricts the sensitivity at the LHC to masses of order 1 TeV, the W' and Z' cross sections are large enough to probe masses of multiple TeV.

The branching fractions of W' and Z' bosons as functions of the coupling parameter g_H times the sign of g_F are shown in Fig. 11. These are computed for g_F values corresponding to the benchmark models A and B, and for two distinct resonance masses of 1 and 2 TeV. For a resonance mass of 1 TeV, a subtle distinction between positive and negative values of g_F is observed, whereas branching fractions are symmetric with respect to the sign of g_F for higher masses. When g_H is small, the branching fractions for decays into quark final states are large. The leptonic decay modes are suppressed due to the QCD color factors. Conversely, for large values of g_H , the bosonic decay modes dominate the branching fractions, indicating that the searches for VH resonances have the best sensitivity together with searches for VV resonances.

The dependence of the branching fraction of the decay $Z' \rightarrow \text{VH}$ on the parameter g_F is shown in Fig. 12 (left) for a resonance with a mass of 2 TeV. This branching fraction increases for decreasing g_F , asymptotically approaching the maximum value of about 50% as g_H increases. The total width of the Z' boson is shown in Fig. 12 (right) for a resonance mass of 2 TeV. The

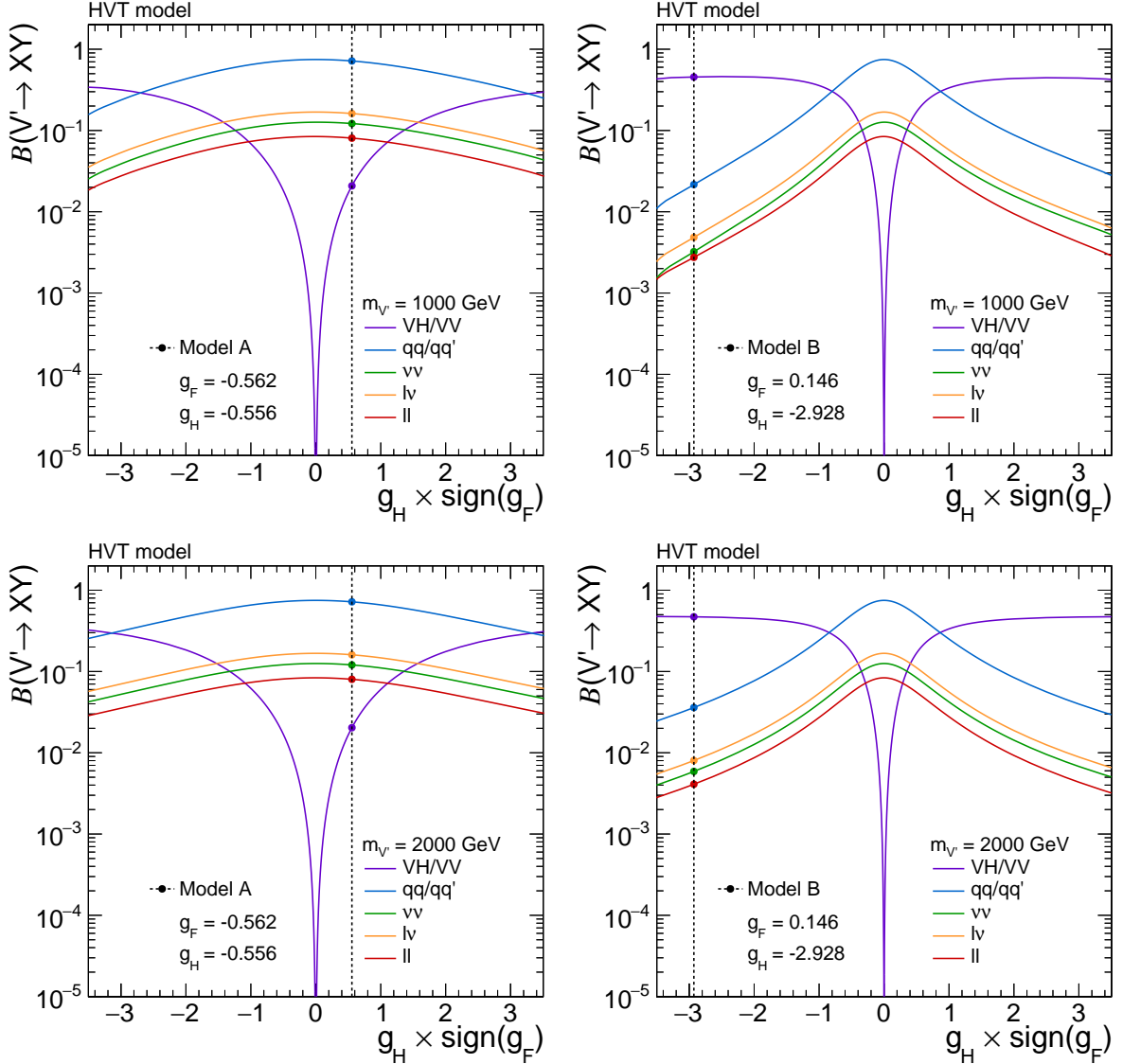


Figure 11: Branching fractions for heavy vector triplet (HVT) bosons with masses of (upper) 1 and (lower) 2 TeV for values of the parameter g_F corresponding to models (left) A and (right) B. The exact branching fractions of each model are indicated by the crossing points of the individual curves with the dashed vertical lines. Calculations are based on the work of Ref. [30].

width increases for increasing values of g_F and g_H . For small values of g_F , the width changes more rapidly as a function of g_H . The W' boson branching fractions and decay widths exhibit very similar behavior as a function of g_F and g_H to those of Z' bosons, and are not shown here. Previous searches by the CMS and ATLAS Collaborations in the VH channel have not observed significant deviations from the SM [93–107].

2 Detector and analysis techniques

The analyses described in the following sections are searches for a new heavy resonance X in the $X \rightarrow HH$, $X \rightarrow VH$, and $X \rightarrow YH$ decays, where V denotes a W or Z boson, H the observed Higgs boson, and Y another new particle like an additional Higgs boson, as predicted in several extensions of the SM Higgs sector. This report focuses on analyses by the CMS Collaboration;

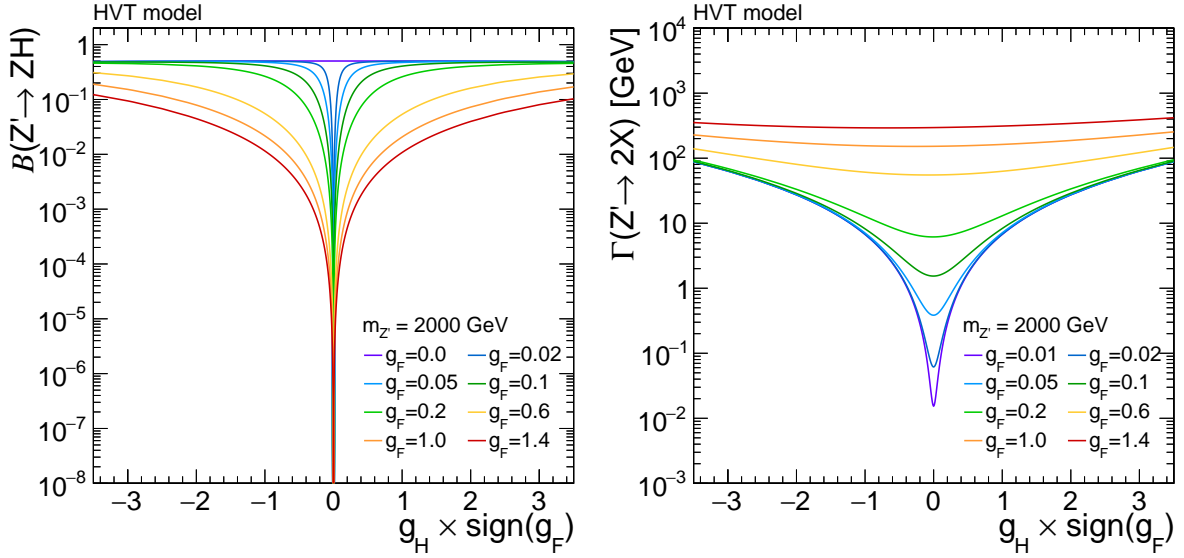


Figure 12: (left) Branching fraction for the decay $Z' \rightarrow ZH$, and (right) total width of the Z' boson, for a resonance with 2 TeV mass, for different values of the parameter g_F . Calculations are based on the work of Ref. [30].

related results from the ATLAS Collaboration can be found in Refs. [101, 108–113].

In most analyses, the intermediate particles V or Y are targeted in decay modes involving b quarks, leptons or photons. This choice is made to profit from the accuracy with which these particles can be reconstructed and identified to distinguish the resulting final states from the overwhelming amount of purely hadronic processes at the LHC. In all searches the natural decay widths of the X and Y particles are assumed to be small compared to the experimental resolution. Implications of this assumption are discussed in Section 4.4.

The search signatures are rich in characteristic features, most notably there are three resonance masses in the full decay chain, of which the masses of the V bosons and m_H are known to a precision of better than 1%. To include this information in the process description, we introduce a notation where the final-state particles are associated with the V , H , or Y particles. For example, with this notation the decay $X \rightarrow Y(bb)H(\tau\tau)$ indicates the subsequent decays of $Y \rightarrow bb$ and $H \rightarrow \tau\tau$. An overview is given in Table 1 of all the analyses discussed in the following sections and the kinematic ranges of their sensitivity.

The analyses span resonance mass ranges of $90 < m_X < 6000 \text{ GeV}$ and $60 < m_Y < 2800 \text{ GeV}$. Such large ranges in mass require different reconstruction techniques even for the same final state [125]. In the case of small m_X , the decay products of Y and H are produced with large angular separation and can be reconstructed as separate objects. This characterizes a regime with fully resolved final states. In contrast, for large m_X and sufficiently small m_Y , the decay products of Y and H are strongly collimated because of the large Lorentz boost; such kinematic regimes are referred to as boosted throughout this report. Final state objects being part of such collimated decays are referred to as merged. In the boosted regime, the hadronic decay products of the intermediate resonances, e.g., $H(bb)$, are reconstructed as a single large- R jet with substructure identification and grooming of soft and large-angle radiation [126–128], where the parameter R denotes the distance parameter of the jet finding algorithm, as described in Section 2.2.1. Typically for the values of R used in this paper, the resolved regime corresponds to $m_X \lesssim 1 \text{ TeV}$, and the boosted regime to $m_X \gtrsim 1 \text{ TeV}$ with $m_Y \ll m_X$. For $m_X \approx 1 \text{ TeV}$ both merged and resolved final states might be encountered depending on the helicity angles of the

Table 1: Summary of all analyses discussed in Section 2. Note that the list of sub-channels is not exhaustive in all cases. All analyses listed under YH also contribute to the HH measurements.

Target final state		Ref.	Mass coverage (GeV)		Comment
V	H		m_χ		
$Z(\ell\ell)$	$\tau\tau$	[114]	220–400		
$Z(\ell\ell + \nu\nu)$	bb	[115]	225–1000		resolved jets
$W(\ell\nu)$	bb	[116]	1000–4500		$W \rightarrow \ell\nu$ and merged bb jet
$Z(\ell\ell)$	bb	[117]	800–4600		$Z \rightarrow \ell\ell/\nu\nu$ and merged bb jet
$Z(qq)$	bb	[118]	1300–6000		two merged jets
H	H		m_χ		
bb	$W(\ell\nu)W(\ell\nu + qq)$	[119]	250–900		resolved
bb	$W(\ell\nu)W(\ell\nu + qq)$	[120]	800–4500		merged
$WW + \tau\tau$	$WW + \tau\tau$	[121]	250–1000		multilepton final state
Y	H		m_χ	m_Y	
bb	$\tau\tau$	[122]	240–3000	60–2800	resolved jets and τ leptons
bb	$\gamma\gamma$	[123]	300–1000	90–800	resolved jets and photons
bb	bb	[124]	900–4000	60–600	two merged bb jets

boson decays.

Unless stated otherwise, all analyses are based on pp collision data collected between 2016 and 2018, at a center-of-mass energy of 13 TeV, corresponding to an integrated luminosity of 137–138 fb⁻¹.

2.1 The CMS Detector

The central feature of the CMS apparatus is a superconducting solenoid of 6 m internal diameter, providing a magnetic field of 3.8 T. Within the solenoid volume are a silicon pixel and strip tracker, a lead tungstate crystal electromagnetic calorimeter (ECAL), and a brass and scintillator hadron calorimeter (HCAL), each composed of a barrel and two endcap sections. Forward calorimeters extend the pseudorapidity coverage provided by the barrel and endcap detectors. Muons are measured in gas-ionization detectors embedded in the steel flux-return yoke outside the solenoid. A more detailed description of the CMS detector, together with a definition of the coordinate system used and the relevant kinematic variables, can be found in Ref. [129].

Events of interest are selected using a two-tiered trigger system. The first level, composed of custom hardware processors, uses information from the calorimeters and muon detectors to select events at a rate of around 100 kHz within a fixed latency of 4 μ s [130]. The second level, known as the high-level trigger, consists of a farm of processors running a version of the full event reconstruction software optimized for fast processing, and reduces the event rate to around 1 kHz before data storage [131].

2.2 Physics objects

The reconstruction of the pp collision products is based on the particle-flow (PF) algorithm [132], combining the available information from all CMS subdetectors to reconstruct individual particle candidates, categorized into charged and neutral hadrons, electrons, photons, and muons. The average number of interactions per bunch crossing was 23 in the year 2016 and 32 in the years 2017–2018. The fully recorded detector data of a bunch crossing define an event for further processing. The primary interaction vertex (PV) is taken to be the vertex corresponding

to the hardest scattering in an event, evaluated using tracking information alone, as described in Ref. [133]. Secondary vertices, which are detached from the PV, might be associated with decays of long-lived particles emerging from the PV. Any other collision vertices in an event are associated with additional mostly soft inelastic pp collisions referred to as pileup (PU).

2.2.1 Jets and missing transverse momentum

AK4 and AK8 jets All PF candidates are clustered into jets using the anti- k_T clustering algorithm [134] as implemented in the FASTJET software package [135]. By default, a distance parameter of $R = 0.4$ is used. The resulting jet collection will be referred to as AK4 jets. Ideally, the kinematic properties of AK4 jets resemble those of the single quarks or gluons initiating them. In the boosted regime the fragmentation products of the individual quarks, resulting from hadronic V, H, or Y decays, start to overlap and cannot be properly reconstructed as AK4 jets. For this purpose, a second collection of large- R jets is obtained with a distance parameter of 0.8, referred to as AK8 jets. The larger jet radius allows the inclusion of all hadronic decay products in a single jet, and subsequently jet substructure techniques can be applied to identify the boosted decay within this jet, as explained further down.

In each case, the jet momenta are determined from the vectorial sum of the momenta of all PF candidates contained in a jet. The value of this sum is measured to be within 5 to 10% of the same quantity calculated from the momenta of stable particles inside equally clustered generated jets in simulation, which holds over the entire transverse momentum (p_T) spectrum and geometrical detector acceptance. Jet energy corrections to the stable-particle level are obtained from simulation, and are confirmed with *in situ* measurements of the energy balance in dijet, multijet, γ +jets, and Z+jets events, where the Z boson decays into light leptons [136]. Residual corrections to the simulated energies to match the observed spectra usually amount to no more than 2–3%. When combining information from the entire detector, the jet energy resolution typically amounts to 15–20% at 30 GeV, 10% at 100 GeV, and 5% at 1 TeV [136].

The AK4 jets are restricted to $p_T > 30$ GeV. Depending on the analysis, these are either used in a range of $|\eta| < 2.4$, well contained in the coverage of the tracker, or in a range of $|\eta| < 4.7$, where the extension is based on the calorimeters but not covered by the tracker. The AK8 jets are restricted to $p_T > 200$ GeV and $|\eta| < 2.4$ or 2.5, depending on the analysis, where the higher value in $|\eta|$ has been used from 2017 on after the upgrade of the silicon pixel detector. Ideally, their properties match those of the decaying resonance. In a first step, AK8 jets are used for the selection of events of interest. In a second step, their specific properties are used to distinguish signal from background processes, based on dedicated algorithms, as discussed below. To reduce the dependence of the related observables on PU, the pileup-per-particle identification (PUPPI) algorithm [137, 138] is applied to the AK8 jets, weighting all PF candidates by their probability to originate from the PV [139]. For AK4 jets the charged-hadron subtraction (CHS) technique, as described in Refs. [132, 138] is used. In addition, both AK4 and AK8 jets are required to pass tight identification requirements [140] to remove jets originating from calorimetric noise and track misreconstruction. Several properties of the selected jets are of importance for the analyses described in this report and will be discussed in more detail in the following.

Identification of b jets To identify jets resulting from the hadronization of b quarks (b jets) several strategies and tagging algorithms are used, depending on the analysis. These comprise the DEEPCSV [141] and DEEPJET [141, 142] algorithms, which are applied either to AK4 jets or to the subjets of the selected AK8 jet. The subjets are obtained with the soft drop algorithm, where the Cambridge–Aachen algorithm [143, 144] is reversed until the soft drop condi-

tion [145] is fulfilled. The two resulting clusters are identified as subjects of the AK8 jet. Alternatively, the “double-b tagger” [141], the DEEPAK8 jet tagging [146], or the PARTICLENET [147] algorithms are used to identify AK8 jets that are consistent with being initiated by two b quarks, a process referred to as “double-b tagging”. These algorithms usually result in a multiclass output from which a suitable discriminant is built. This discriminant is used to distinguish AK8 jets produced from light-flavor quarks or gluons versus AK8 jets from two near-collinear b quarks. All algorithms use secondary vertex and impact parameter information, as well as the multiplicities and kinematic properties of the clustered PF candidates. The resonance tagging algorithms are usually trained to be insensitive to the mass of the corresponding resonance. For all algorithms, predefined working points corresponding to an expected b jet identification efficiency for a given misidentification rate for jets initiated by light-flavor quarks or gluons, as defined in Ref. [148], are used, exhibiting efficiencies of 70–90% for misidentification rates of 1–10%.

Mass of AK8 jets The mass of the hadronically decaying boson resonance associated with an AK8 jet is estimated using the “soft-drop” mass m_{SD} [145], obtained with the soft-drop algorithm with an angular exponent $\beta = 0$, soft-cutoff threshold $z_{\text{cut}} = 0.1$, and characteristic radius $R_0 = 0.8$. The soft-drop algorithm is a generalization of the modified mass-drop algorithm [149, 150], which is identical to soft drop for $\beta = 0$. The reconstruction of m_{SD} is tested and calibrated in $t\bar{t}$ -enriched event selections, where the mass of hadronically decaying W bosons can be reconstructed with a resolution of 10%.

Jet substructure To exploit the substructure of a selected AK8 jet, the ratio $\tau_{21} = \tau_2/\tau_1$ is used, where τ_1 and τ_2 are the 1- and 2-subjettiness observables [151], respectively. The quantity τ_{21} takes lower values for jets originating from two-prong V, H, or Y decays and larger values for one-prong jets initiated, e.g., by single quarks or gluons. However, a selection on τ_{21} alters the distribution in m_{SD} , such that the monotonically falling distribution might feature a resonant structure after selecting jets with a minimum value of τ_{21} . This feature prevents typical background estimation methods from working for important background processes, like W+jets production [116]. To overcome this drawback, we use the “designing decorrelated tagger” (DDT) procedure [152] leading to

$$\tau_{21}^{\text{DDT}} = \tau_{21} + 0.08 \log \left(\frac{m_{\text{SD}}^2}{p_{\text{T}} \mu} \right), \quad (5)$$

where p_{T} refers to the transverse momentum of the AK8 jet and $\mu = 1 \text{ GeV}$. A selection based on τ_{21}^{DDT} does not alter the distribution in m_{SD} , such that the shape of this distribution can be derived from control regions (CRs) to estimate the background from SM processes in signal regions (SRs).

Event observables The two-dimensional vector in the x and y coordinates, $\vec{p}_{\text{T}}^{\text{miss}}$, describes the missing transverse momentum and is computed as the negative \vec{p}_{T} sum of all PF candidates in the event [139]. The magnitude of $\vec{p}_{\text{T}}^{\text{miss}}$ is referred to as $p_{\text{T}}^{\text{miss}}$. It is used for the event selection and in the calculation of the transverse mass

$$m_{\text{T}} = \sqrt{2p_{\text{T}}p_{\text{T}}^{\text{miss}}(1 - \cos \Delta\phi)}, \quad (6)$$

where $\Delta\phi$ refers to the azimuthal angular difference between the transverse momentum vector \vec{p}_{T} of the visible decay product of the particle whose transverse mass is to be estimated, and $\vec{p}_{\text{T}}^{\text{miss}}$. Depending on the analysis, sometimes the PUPPI algorithm is used to mitigate PU effects

on \vec{p}_T^{miss} . Alternatively, the quantity H_T^{miss} is used, defined as the magnitude of the \vec{p}_T sum of all AK4 jets with $p_T > 30 \text{ GeV}$ and $|\eta| < 3.0$. In the same context also the observable H_T is used, which corresponds to the scalar p_T -sum of all selected AK4 jets. It indicates the overall magnitude of hadronic activity in an event.

2.2.2 Leptons and photons

Electrons, muons, and photons Electron candidates are reconstructed from matching clusters of energy deposits in the ECAL with tracks, which are fitted to form hits in the tracker [153, 154]. To increase their purity, reconstructed electrons are required to pass a multivariate electron identification discriminant, which combines information on the track quality, shower shape, and kinematic quantities [154]. Predefined working points corresponding to electron identification efficiencies of 70–90% and misidentification rates of 2–15% are used. Energy deposits in the ECAL that are not linked to any charged-particle trajectory associated with a pp collision are identified as photons.

Muons in an event are reconstructed by performing a simultaneous track fit to hits in the tracker and in the muon chambers [155, 156]. The presence of hits in the muon chambers already leads to a strong suppression of particles misidentified as muons. Additional identification requirements on the track-fit quality and the compatibility of individual track segments with the fitted track reduce the misidentification rate further.

The contributions from backgrounds to the electron and muon selections are usually further reduced by requiring the corresponding lepton to be isolated from any hadronic activity in the detector. This property is quantified by an isolation variable

$$I_{\text{rel}} = \frac{1}{p_T^\ell} \left(\sum p_T^{\text{charged}} + \max \left(0, \sum E_T^{\text{neutral}} + \sum E_T^\gamma - p_T^{\text{PU}} \right) \right), \quad (7)$$

where p_T^ℓ corresponds to the measured electron or muon p_T . The variables $\sum p_T^{\text{charged}}$, $\sum E_T^{\text{neutral}}$, and $\sum E_T^\gamma$ are calculated from the sum over p_T or transverse energy E_T of all charged particles, neutral hadrons, and photons, respectively. These sums include all particles in a predefined cone of radius $\Delta R = \sqrt{(\Delta\eta)^2 + (\Delta\phi)^2}$ around the lepton direction at the PV, where $\Delta\eta$ and $\Delta\phi$ are the angular distances between the corresponding particle and the lepton in the η and azimuthal ϕ directions. The lepton itself is excluded from the calculation of I_{rel} . Typical values for cone sizes are $\Delta R = 0.3$ and 0.4 for electrons and muons, respectively. To mitigate effects from PU on I_{rel} , only charged particles with tracks associated with the PV are taken into account. Since for neutral hadrons and photons an unambiguous association with the PV or PU is not possible, an estimate of the contribution from PU (p_T^{PU}) is subtracted from the sum of $\sum E_T^{\text{neutral}}$ and $\sum E_T^\gamma$. This estimate is obtained from tracks not associated with the PV in the case of muons, and from the mean energy flow per unit area in the case of electrons. If the sum is negative, the result is set to zero. The I_{rel} selection threshold is optimized for each analysis separately. If a lepton isolation requirement is imposed in an analysis, leptons failing this requirement are not considered further.

Hadronic τ lepton decays The reconstruction of hadronic τ lepton decays (τ_h) starts from AK4 jets, further exploiting their substructure with the hadrons-plus-strips algorithm [157]. This algorithm acts like a tagger, with different working points as defined in [157]. The decays into one or three charged hadrons with up to two neutral pions with $p_T > 2.5 \text{ GeV}$ are used. The neutral pions are reconstructed as strips in the ECAL with a dynamic size in η - ϕ from reconstructed electrons and photons contained in a jet, where the strip size varies as a function of

the p_T of the electron or photon candidate. Electrons, which may emerge from photon conversions, are considered in the reconstruction of the strips. The τ_h decay mode is then obtained by combining the charged hadrons with the strips.

To distinguish τ_h candidates from jets originating from the hadronization of quarks or gluons, and from electrons or muons, the DEEPTAU (DT) algorithm [158] is used. This algorithm exploits basic tracking and clustering information in the tracker, ECAL, and HCAL, the kinematic and object-identification properties of both the PF candidates forming the τ_h candidate and all remaining PF candidates in the vicinity of the τ_h candidate, and several characterizing quantities of the whole event. It results in a multiclassification output y_α^{DT} , where $\alpha = \tau, \text{jet}, e, \mu$. The output can be identified with a Bayesian probability of the τ_h candidate to originate from a genuine τ lepton decay, the hadronization of a quark or gluon, an isolated electron, or an isolated muon. From this output three discriminants are built according to

$$D_i = \frac{y_\tau^{\text{DT}}}{y_\tau^{\text{DT}} + y_i^{\text{DT}}} \quad \text{with } i = \text{jet}, e, \text{ or } \mu. \quad (8)$$

For the identification of τ_h candidates based on D_i predefined working points with varying efficiencies for given misidentification rates are used as described in Ref. [158]. For D_{jet} the efficiencies vary within 50–70% for misidentification rates of $<0.5\%$. For D_e and D_μ , the efficiencies vary within 80–99% for misidentification rates between 0.05 and 2.50%.

2.3 Search for resonances in VH channels

Searches for VH resonances are optimized either for the mass range up to about 1 TeV, motivated by neutral members of an extended Higgs sector, or masses greater than 1 TeV, where heavy vector bosons might be found. The latter case corresponds to the boosted regime, where the V and H bosons are strongly Lorentz-boosted and dedicated reconstruction and identification techniques are applied.

All searches presented in the following target the $H \rightarrow b\bar{b}$ or $H \rightarrow \tau\tau$ decays. The V bosons are reconstructed either through the leptonic decays $W(\ell\nu)$ [116], $Z(\ell\ell)$ or $Z(\nu\nu)$ [114, 115, 117], or by the hadronic decays $V(qq)$ [118]. Where allowed by the signal signature, the trigger selection is based on the presence of a single high- p_T electron or muon within the geometrical acceptance of $|\eta| < 2.4$ (2.5) for electrons (muons), large p_T^{miss} , or large H_T^{miss} . Also, dilepton triggers are used. Otherwise, triggers based on the presence of high- p_T AK4 jets or large values of H_T are required. Offline, search regions are defined by the presence of exactly one (1ℓ category), two (2ℓ category), or no (0ℓ category) charged leptons. This categorization ensures that the analyses are mutually exclusive, allowing for a combined statistical interpretation subsequently to the completion of all analyses.

2.3.1 The sub-TeV mass region

The analyses searching for CP -odd Higgs bosons through their $A \rightarrow ZH$ decay, in the mass region below 1 TeV, are based on the 2016 data set. The H boson is reconstructed in the $H \rightarrow b\bar{b}$ [115] and $H \rightarrow \tau\tau$ [114] decay channels.

In the $H \rightarrow b\bar{b}$ case, the two b jet candidates with the highest b tagging scores are selected to form the H boson candidate. Both gluon-gluon fusion and b quark-associated production are considered. In the 0ℓ category, which targets decays of the Z boson into neutrinos, the mass of the A resonance cannot be reconstructed directly. In this case, its mass is estimated by computing the transverse mass m_{ZH}^T using Eq. (6). It is calculated using \vec{p}_T^{miss} and the four-momentum of the H boson candidate, and must be larger than 500 GeV, where triggers are

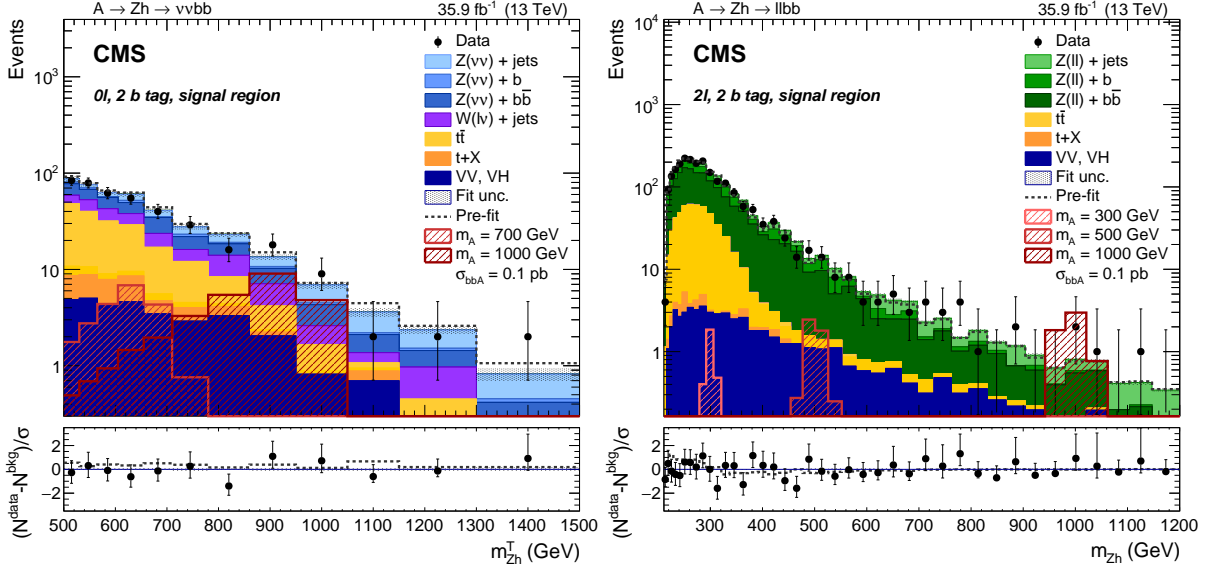


Figure 13: Search for $A \rightarrow ZH(bb)$: Distributions of the m_{ZH}^T and m_{ZH} variables, as introduced in the text, in the (left) 0ℓ and (right) 2ℓ categories, in the 2 b tag signal region of the $A \rightarrow ZH(bb)$ analysis [115]. In the 2ℓ categories, the contributions of the $2e$ and 2μ channels have been summed. The gray dotted line represents the sum of all background processes before the fit to data; the shaded area represents the post-fit uncertainty. The hatched red histograms represent signal hypotheses for b quark associated A production corresponding to $\sigma_A \mathcal{B}(A \rightarrow ZH) \mathcal{B}(H \rightarrow bb) = 0.1$ pb. The lower panels depict $(N^{data} - N^{bkg})/\sigma$ in each bin, where σ refers to the statistical uncertainty in the given bin. Figure from Ref. [115].

fully efficient. The resulting efficiency for signal events with $m_A \lesssim 500$ GeV is small because the p_T of the Z boson is not sufficient to produce a p_T^{miss} large enough to pass this selection. Therefore, the sensitivity of the 0ℓ category is significant only for large values of m_A .

In the $2e$ and 2μ categories, events are required to have at least two isolated electrons or muons within the detector's geometrical acceptance. The Z boson candidate is formed from the two highest p_T , opposite-sign, same-flavor leptons, and must have an invariant mass $m_{\ell\ell}$ between 70 and 110 GeV. The $m_{\ell\ell}$ selection lowers the contamination from $t\bar{t}$ dileptonic decays and significantly reduces the contribution from $Z \rightarrow \tau\tau$ decays. The A boson candidate is reconstructed from the invariant mass m_{ZH} of the Z and H boson candidates.

If the two jets originate from an H boson, their invariant mass is expected to peak close to 125 GeV. Events with a dijet invariant mass m_{jj} between 100 and 140 GeV enter the SRs; otherwise, if $m_{jj} < 400$ GeV, they fall in the dijet mass sidebands, which are used as CRs to estimate the contributions of the main backgrounds. The SRs are further divided by the number of jets passing the b tagging requirement (1, 2, or at least 3 b tags). The 3 b tag category has been defined to select the additional b quarks from b quark associated production. In this region, at least one additional jet, other than the two used to reconstruct the H boson, has to pass the kinematic selections and b tagging requirements. Comparisons between data and background predictions, together with examples for signal distributions are shown in Fig. 13 in the 2 b tag SR for the 0ℓ and 2ℓ categories. The data are well described by the backgrounds expected from SM processes. The 0ℓ and 2ℓ categories can be combined using the known branching fractions of the Z boson.

In the $H \rightarrow \tau\tau$ case, only the dielectron and dimuon decays of the Z boson are used. For the

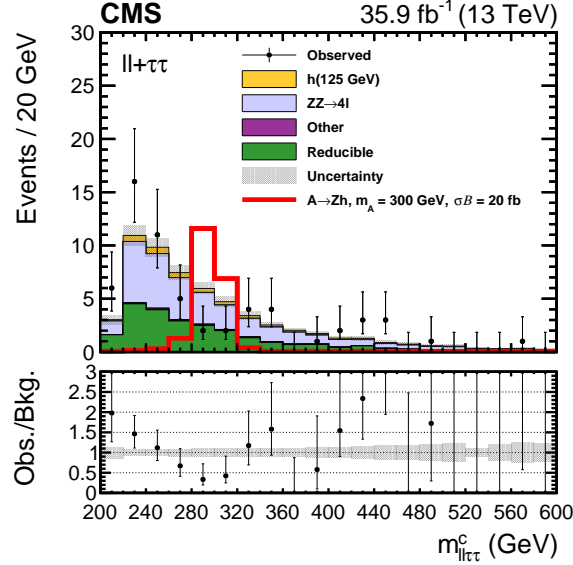


Figure 14: Search for $A \rightarrow ZH(\tau\tau)$: Distribution of the $m_{\ell\ell\tau\tau}^c$ variable, as introduced in the text, of the $A \rightarrow ZH(\tau\tau)$ analysis [114], after a fit of the background-only hypothesis in all eight final states. While the fit is based on corresponding distributions, for each final state individually, these have been combined into a single distribution, for visualization purposes for this figure. Uncertainties include both statistical and systematic components. The expected contribution from the $A \rightarrow ZH$ signal process is shown for a pseudoscalar Higgs boson with $m_A = 300$ GeV with the product of the cross section and branching fraction of 20 fb. Figure from Ref. [114].

H boson reconstruction, the $e\tau_h$, $\mu\tau_h$, $e\mu$, and $\tau_h\tau_h$ topologies are considered. The leptons associated with the H boson decay are required to have opposite signs. In case of the $e\tau_h$, $\mu\tau_h$, and $e\mu$ decay channels, tighter selection criteria are applied to the light leptons to decrease the background contributions from Z+jets and other reducible backgrounds. These four H $\rightarrow \tau\tau$ decay patterns are combined with the Z boson decays into two light leptons, i.e., $Z \rightarrow \ell\ell$ with $\ell = e, \mu$, resulting in eight distinct final states of the A boson decay.

The mass resolution of the reconstructed A boson candidate can be significantly improved by accounting for the neutrinos associated with the leptonic and hadronic τ decays. We use the SVFIT algorithm [159] to estimate the mass of the H boson, denoted as $m_{\tau\tau}^{\text{fit}}$. The SVFIT algorithm combines the \vec{p}_T^{miss} with the four-vectors of both τ candidates (e, μ , or τ_h), resulting in an improved estimate of the four-vector of the H boson, which is further improved by giving the measured mass of the Higgs boson (125 GeV) as an input to the SVFIT algorithm. This yields a constrained estimate of the four-vector of the H boson, which results in an even more precise estimate of the A boson candidate mass, denoted as $m_{\ell\ell\tau\tau}^c$. The resolution of $m_{\ell\ell\tau\tau}^c$ is as good as 3% at 300 GeV, which improves the expected 95% CL model-independent limits by approximately 40% compared to using the visible mass of the A boson $m_{\ell\ell\tau\tau}^{\text{vis}}$ as the discriminating variable.

The resulting distribution in $m_{\ell\ell\tau\tau}^c$, summed over all eight categories, is shown in Fig. 14, together with the expected signal shape for $m_A = 300$ GeV. No excess above the SM background expectation is observed in the data.

2.3.2 The high-mass region: leptonic V boson decays

In the high-mass analyses targeting leptonic V boson decays, the presence of an isolated electron with $p_T > 115$ GeV and $|\eta| < 2.4$ or muon with $p_T > 55$ GeV and $|\eta| < 2.5$ is required. The high p_T thresholds are imposed to guarantee a sufficiently high selection efficiency at the trigger level.

For $W(\ell\nu)$ decays, this selection is complemented by the requirement of $p_T^{\text{miss}} > 80$ GeV in the electron channel and $p_T^{\text{miss}} > 40$ GeV in the muon channel. Events with additional leptons fulfilling looser selection criteria are discarded from the selection. To reconstruct a $W(\ell\nu)$ boson candidate, the \vec{p}_T^{miss} is used as an estimate of the \vec{p}_T of the neutrino. The longitudinal component p_z of the neutrino momentum is estimated by imposing the constraint that the mass of the system formed from the selected lepton and the neutrino should equal m_W . This leads to a quadratic equation in p_z , of which the solution with the smallest magnitude is chosen. When no real solution is found, only the real part of the two complex solutions is considered.

For $Z(\ell\ell)$ decays, a second lepton with the same flavor and η range as the first lepton, and $p_T > 20$ GeV is required. The system formed by the two leptons is used to reconstruct the Z boson candidate. It must have $p_T^{\ell\ell} > 200$ GeV and $70 < m_{\ell\ell} < 110$ GeV. The window in $m_{\ell\ell}$ has not been chosen tighter, since a narrowing would reduce the signal efficiency while not improving the relation of the signal to the main background from Z+jets events. In all cases, all leptons are required to have a large enough distance in ΔR to any AK4 jet. For the $Z(\nu\nu)$ channel, the absence of leptons and a value of $p_T^{\text{miss}} > 250$ GeV are required.

In addition to the identification of the reconstructed objects forming the V boson candidate, all events are required to have an AK8 jet with $p_T > 200$ GeV and $|\eta| < 2.4$ [116] or 2.5 [117]. In the case that more than one AK8 jet is found in an event, the leading one in p_T is interpreted to originate from the $H \rightarrow b\bar{b}$ decay, hence referred to as the H candidate.

In the $W(\ell\nu)$ channel [116], the H candidate is required to have a distance of $\Delta R > \pi/2$ from the selected lepton and a distance larger than 2 in $\Delta\phi$ from both \vec{p}_T^{miss} and the $W(\ell\nu)$ candidate. Furthermore, it is required to have a value of $\tau_{21}^{\text{DDT}} < 0.8$. All accepted events are assigned to 24 high-purity (HP) and low-purity (LP) event categories according to the flavor of the selected lepton (e or μ), the value of the double-b-tagger output of the H candidate, the distance between the $W(\ell\nu)$ and the H candidate in rapidity $|\Delta y| < 1$ (LDy) or $|\Delta y| > 1$ (HDy), a tightened requirement of $\tau_{21}^{\text{DDT}} < 0.5$ (defining the HP and LP categories), and a VBF tag requiring the pseudorapidity difference of the two VBF jets $|\Delta\eta| > 4$ and the dijet mass larger than 500 GeV. The VBF tag is imposed to increase the sensitivity of the search to the production of the VH system through VBF. The categorization in Δy is imposed to tag different spin hypotheses for X. A two-dimensional (2D) discriminant composed of m_{SD} of the H candidate and an estimate of m_X obtained from the four-vectors of the H and the $W(\ell\nu)$ candidates is used for the final signal extraction in these categories. We note that this analysis is not restricted to the VH process, which is the subject of this report, but extends towards VV final states as well. The data are interpreted under both signal hypotheses each time considering all event categories, including those enriched and depleted in VH and VV by the value of the double-b tagger of the H candidate.

Distributions of m_{SD} and the reconstructed m_X in the event category with a selected muon, $\tau_{21}^{\text{DDT}} < 0.5$, double-b tag, and $|\Delta y| > 1$ are shown in Fig. 15. The background processes are split into two categories: (i) processes exhibiting resonant structures close to the t quark and/or V boson mass in m_{SD} ($W + V/t$), comprising $t\bar{t}$, single-t quark, and diboson production, and (ii) processes without resonant structure in the m_{SD} distribution, dominated by W+jets events. All

backgrounds are characterized by a falling spectrum in m_X . These are estimated with the help of simulation, where the smoothness of the background shape is ensured by using conditional probability density functions in m_{SD} and the reconstructed m_X , as detailed in Ref. [116].

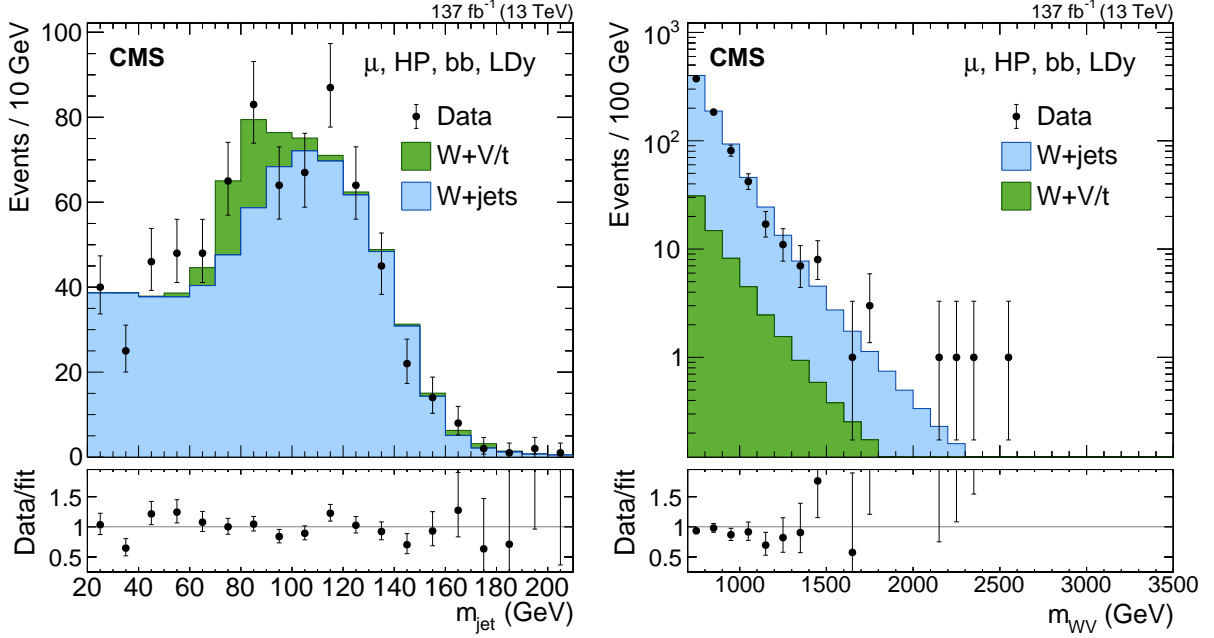


Figure 15: Search for $X \rightarrow VH(bb)$: Distributions of (left) the jet soft drop mass of a boosted Higgs boson candidate, labeled m_{jet} , and (right) the mass of the X resonance candidate, labeled m_{WV} in the $W(\ell\nu)H(bb)$ channel. The notation m_{WV} is used as a shorthand since the analysis also searches for resonances in the WW and WZ final states. Figures from Ref. [116].

In the $Z(\ell\ell)$ channel, the H candidate is required to have a distance of $\Delta R > 0.8$ from each selected lepton. For the $Z(\nu\nu)$ channel $\Delta R(\vec{p}_T^{\text{miss}}, H) > 2$ and a ratio of $p_T^{\text{miss}}/p_T^H > 0.6$ are required. Finally, the value of m_{SD} of the H candidate is required to lie within $105 < m_{SD} < 135 \text{ GeV}$, compatible with m_H . The DEEPCSV algorithm is applied to the two subjets of the AK8 jet with the highest p_T . All remaining events are assigned to 12 event categories based on the flavor of the selected leptons ($\mu\mu$, ee , or $\nu\nu$), the number of b -tagged subjets of the H candidate (≤ 1 , or 2), and a VBF tag identical to the one defined above. The signal is extracted in the $Z(\ell\ell)$ channel from the distribution in m_X , obtained from the four-vectors of the H and the Z candidates. In the $Z(\nu\nu)$ channel the variable m_T , as obtained from \vec{p}_T^H and \vec{p}_T^{miss} , is chosen. Distributions of m_{SD} , m_X , and m_T in the $\mu\mu$ and $\nu\nu$ event categories with two b -tagged subjets, and no VBF tag are shown in Fig. 16. The dominant background in this search is from Z +jets events, which is estimated from data using low-mass (LSB) and high-mass (HSB) CRs in m_{SD} . A veto region with $65 < m_{SD} < 105 \text{ GeV}$ is excluded from the CRs to minimize the event overlap with dedicated searches in the VV decay channel [160–162]. Minor backgrounds originate from $t\bar{t}$, single t quark, and SM VH production. In all cases, analytical functions are fitted to the observed distributions in m_X in the LSB and HSB CRs, where the functions are predefined with the help of simulation. For the minor backgrounds from diboson (including VH) production these functions are purely determined from simulation. For $t\bar{t}$ production and for the dominating background from Z +jets events, these are fitted to the data in dedicated sideband regions, after subtracting the estimates of the minor backgrounds in these regions. The functions are then extrapolated to the SR through transfer functions, which have been obtained from simulation. This method has been validated with slightly modified sideband

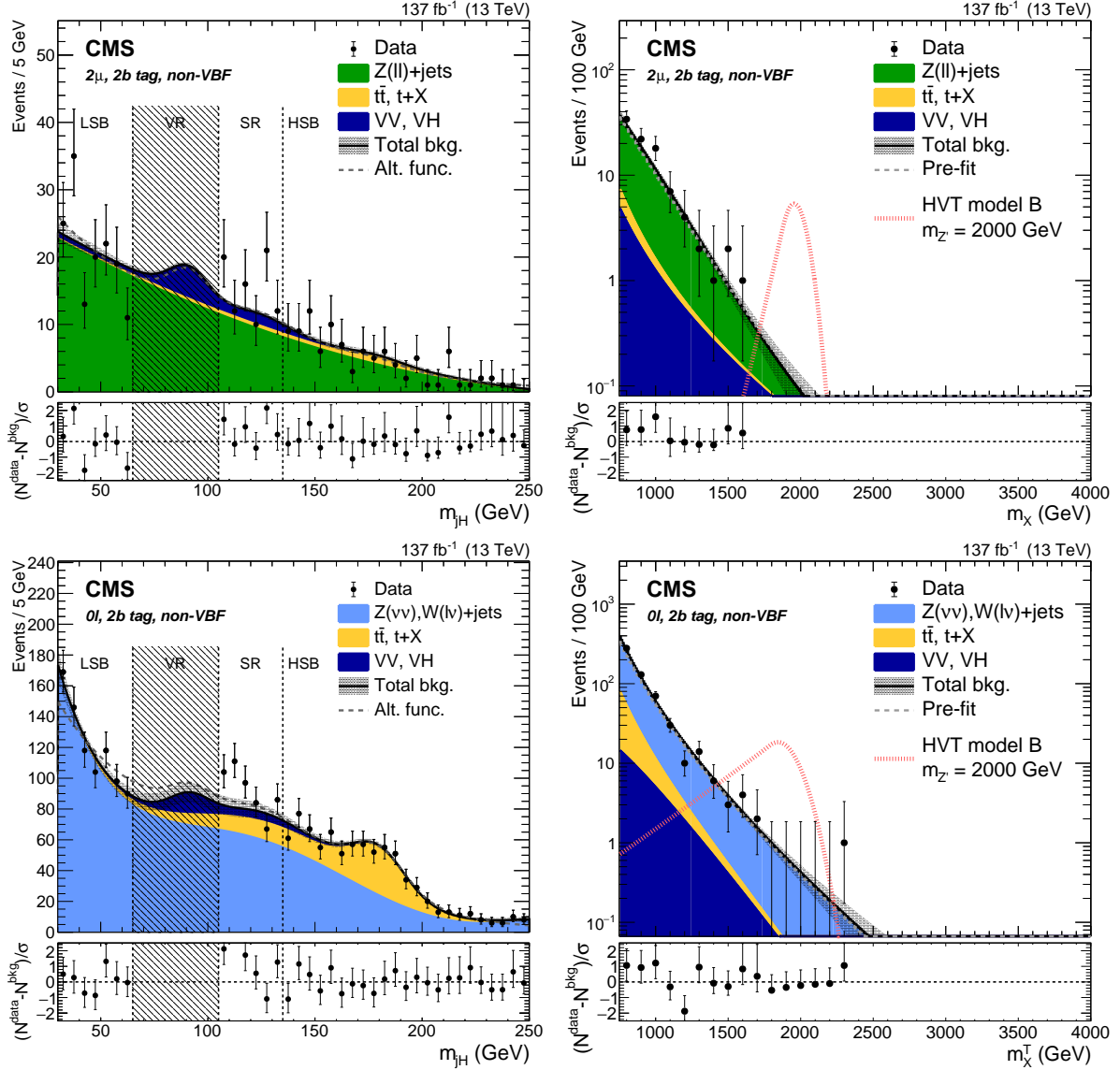


Figure 16: Search for $X \rightarrow VH(bb)$: Distributions of (left) the jet soft drop mass of a boosted Higgs boson candidate, labeled m_{jH} , and (right) the mass or transverse mass of the X resonance candidate, labeled m_X and m_X^T , respectively, in the $Z(\ell\ell)H(bb)$ (upper) and $Z(\nu\nu)H(bb)$ channels (lower). The shaded area depicts a veto region excluded from the analysis to minimize the event overlap with dedicated searches in the VV decay channel. Figures from Ref. [117].

definitions providing independent control regions close to the SRs. Several functional forms have been tested and a bias test has been conducted to ensure that the method is capable of describing the data in the validation regions and that no spurious signal may emerge this way.

2.3.3 The high-mass region: hadronic V boson decays

In the high-mass analysis targeting hadronic V boson decays [118], the presence of two AK8 jets with $p_T > 200$ GeV and $|\eta| < 2.5$ is required. In cases where more than two AK8 jets are found in an event, the leading ones in p_T are interpreted to originate from the $V \rightarrow qq$ and $H \rightarrow bb$ decays. To guarantee an efficiency of $>99\%$ of the trigger selection, the invariant mass of the selected AK8 jets is required to be larger than $m_{jj}^{\text{AK8}} > 1250$ GeV. Furthermore, the jets are required to have a distance $\Delta R > 0.8$ from any reconstructed electron or muon with $p_T > 20$ or 30 GeV satisfying identification criteria optimized for high-momentum leptons, respectively.

To reduce the background from events with purely QCD-induced light-quark and gluon jets, referred to as QCD multijet production in the following, the selected AK8 jets are required to be separated by no more than $|\Delta\eta_{jj}^{\text{AK8}}| < 1.3$. In addition, $55 < m_{\text{SD}} < 215$ GeV and a loose requirement of

$$\rho = \log(m_{\text{SD}}^2/p_T^2) < 1.8 \quad (9)$$

are imposed. The requirement on ρ is imposed to prevent high values for m_{SD} while the p_T of the AK8 jet is low. In those cases, the cone size of $\Delta R = 0.8$ is too small to contain the full jet, affecting both the m_{SD} resolution and the efficiency to assign each AK8 jet to a W, Z, or H boson.

The DEEPAK8 jet tagging algorithm [146] is used to identify AK8 jets originating from a W, Z, or H boson. The algorithm consists of a staggered two-step deep neural network (NN) architecture, based on the properties of the clustered PF candidates, such as the p_T , charge, and angular distance to the jet axis, as well as track and secondary vertex information. The latter is used to infer whether a jet contains heavy-quark decays or not. The input features of both, the PF candidates and the secondary vertices and tracks are processed in two independent convolutional NNs. The outputs of these NNs are passed to a third, fully connected deep NN (DNN) to assign a jet to one of the following classes: single quark or gluon, W boson decaying to cq or qq , and H or Z boson, each decaying into bb , cc , or light flavor quarks. For the reported analysis two discriminants are of relevance, both discriminating between signal jets and jets from single quarks or gluons. A qq discriminant is built to identify the decay of a W or Z boson into light quarks, and a bb discriminant is built to identify the H and Z boson decays into bb .

The strategy of the search is to distinguish the signal, which is peaking in three distributions, namely m_{SD} of each selected AK8 jet and the dijet mass of the two AK8 jets m_{jj}^{AK8} , from the considered backgrounds that exhibit a smoothly falling spectrum in at least one of these observables. To guarantee that the m_{SD} distributions of the considered background processes are not kinematically biased by the selection based on the DEEPAK8 tagger, an adversarial training of the NNs is performed that leads to a reduced correlation between m_{SD} and the output of the tagger [146]. The remaining correlations are further suppressed by a DDT method [152] applied on the tagger output. Eventually, the selection of the output of the DEEPAK8 tagger is chosen such that it yields a constant tagging rate as a function of p_T and m_{SD} for the quark or gluon jets with the highest p_T in QCD multijet production, based on simulation.

The qq tagging efficiency, and the probability of hadronic t quark decays to be misidentified by the qq tagger are calibrated in a $t\bar{t}$ event selection enriched in hadronic W boson decays.

The bb discriminant is calibrated in an event sample enriched with jets from $g \rightarrow bb$ splitting using a double-muon tag, as described in Ref. [141].

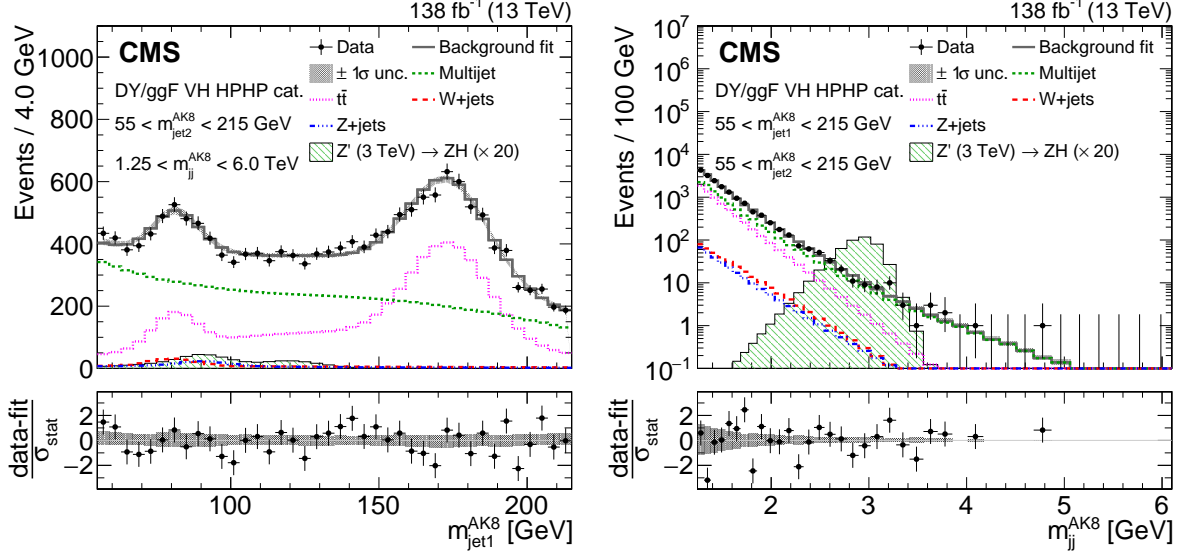


Figure 17: Search for $X \rightarrow V(qq)H(bb)$: Distributions of (left) the soft drop mass m_{SD} variable, labelled as m_{jet1}^{AK8} , and (right) the dijet mass m_{jj}^{AK8} in the $V(qq)H(bb)$ channel [118]. The individual contributions of the background model are shown by open histograms with different colors and line styles. The signal of a Z' boson with a mass of 3 TeV decaying via $Z \rightarrow qq$ and $H \rightarrow bb$ is also shown, by a green filled histogram. Figure from Ref. [118].

To increase the sensitivity of the search after selection, all remaining events are assigned to one of 10 mutually exclusive event categories based on a VBF tag and the outputs of the qq and bb discriminants from each of the selected AK8 jets. The VBF tag is defined by requiring at least two AK4 jets with $p_T > 30$ GeV and $|\eta| < 5.0$ that do not overlap with the selected AK8 jets within $\Delta R < 1.2$. For the two AK4 jets, which are leading in p_T , $m_{jj} > 800$ GeV and a separation of $|\Delta\eta| > 4.5$ are required. The event categories target VV and VH decays.

Distributions of m_{SD} and m_{jj}^{AK8} in the non-VBF VH event category, where one of the selected AK8 jets (the V candidate) exhibits a high-purity classification score in the qq discriminant, while the other one (the H candidate) exhibits a high purity classification score in the bb discriminant, are shown in Fig. 17. To simplify the modelling of the three-dimensional (3D) $(m_{jj}^{AK8}, m_{SD}^{jet1}, m_{SD}^{jet2})$ shapes, the assignment of AK8 jets to “Jet 1” and “Jet 2” is performed randomly, so that both m_{SD} distributions exhibit the same shape. The largest background originates from QCD multijet production, which is estimated from a parametric functional form obtained through a forward-folding technique applied to a set of simulated samples at the level of stable particles [163]. This functional form can be constrained through nuisance parameters attached to physics-motivated alternative shapes. All other processes are obtained from simulation. The production of $t\bar{t}$ events is expected to contribute 40%, the expected background from W +jets and Z +jets production amounts to up to 4% of the selected events. Backgrounds from single t quark and diboson production are expected to contribute less than 1.5%. While all backgrounds are nonresonant in m_{jj}^{AK8} , some exhibit one or two resonant structures at different values in the m_{SD} distribution of only one or both AK8 jets. The signal is obtained from analytic functional forms as in the case of the analyses described in Section 2.3.2.

2.4 Search for resonances in the HH channel

This section describes searches for resonances decaying into two H bosons with a mass of 125 GeV. Various further decay mode combinations are covered by the more general searches in the $X \rightarrow YH$ analyses, and are discussed in Section 2.5.

2.4.1 The $X \rightarrow H(bb)H(WW)$ decay in resolved jet topology

For a pair of Higgs bosons, the $bbWW$ decay channel has the second-largest branching fraction of all HH decay modes, of about 24%. The analysis described in this section focuses on the single lepton (SL) $bb\ell\nu qq$ and dilepton (DL) $bb\ell\nu\ell\nu$ final states [119].

The data have been collected with a combination of single- and double-lepton triggers. The event selection requires one or two isolated leptons, in the second case with opposite signs. The analysis considers $H \rightarrow bb$ in both resolved and merged jet topologies, and requires suitable numbers of AK4 and AK8 jets. Jets associated with the $H \rightarrow bb$ candidate are b tagged by passing the medium working point of the DEEPCSV algorithm [142] in the AK4 case, or the medium working point of the DEEPCSV algorithm [141] in case of AK8 subjects.

The selection vetoes pairs of leptons, which according to their invariant mass are likely to originate from quarkonia or Z boson decays. Overlap with events selected by the analysis in the $bb\tau\tau$ channel (discussed in Section 2.5.1) is removed by vetoing events containing at least one τ_h candidate passing the selection described in Ref. [122].

The events are classified into processes based on the output of multiclass deep neural networks (DNNs), separately trained for the SL and DL cases. The DNNs feature output nodes for a number of backgrounds and one signal node. The DNNs are trained on all signal samples; they are parameterized in the nominal signal mass and contain five background nodes for the SL and seven for the DL category. Depending on the highest scoring node, events are subdivided into signal and background categories. The network inputs include a number of high-level features, such as invariant masses and the hadronic activity of the event, but in addition also the output of a Lorentz-boost network [164] performing automated feature engineering based on the four-momenta of selected leptons and jets. Due to similarity of the DNN score distributions for various background classes, they are merged into process groups prior to the signal extraction.

The signal categories are further divided into subcategories according to the b jet topology and multiplicity, referred to as resolved 1b, resolved 2b, and merged. The merged jet subcategories are excluded in the HH combination (Section 2.6) as they would overlap with the analysis described in Section 2.4.2. Background contributions dominantly originating from $t\bar{t}$ production are estimated from simulation, with two exceptions: contributions arising from jets misidentified as leptons are estimated with the misidentification-factor method [165], while the DY background is addressed with a different method using the 0b CR in data and transfer factors determined in the Z boson peak region.

In the SL case, the signal extraction is performed by a simultaneous maximum likelihood fit to the distributions of the DNN outputs of the signal and the background process groups. In the DL case, the DNN output of the signal category is combined into an unrolled 2D variable with the output of a heavy-mass estimator (HME) [166], a variable that estimates the most likely invariant mass of the HH system considering the presence of two neutrinos and the \vec{p}_T^{miss} measurement.

Examples of the signal extraction are shown in Fig. 18. The distribution in the DNN score (SL case) and the unrolled combination of the DNN score and the HME bin (DL case) are shown

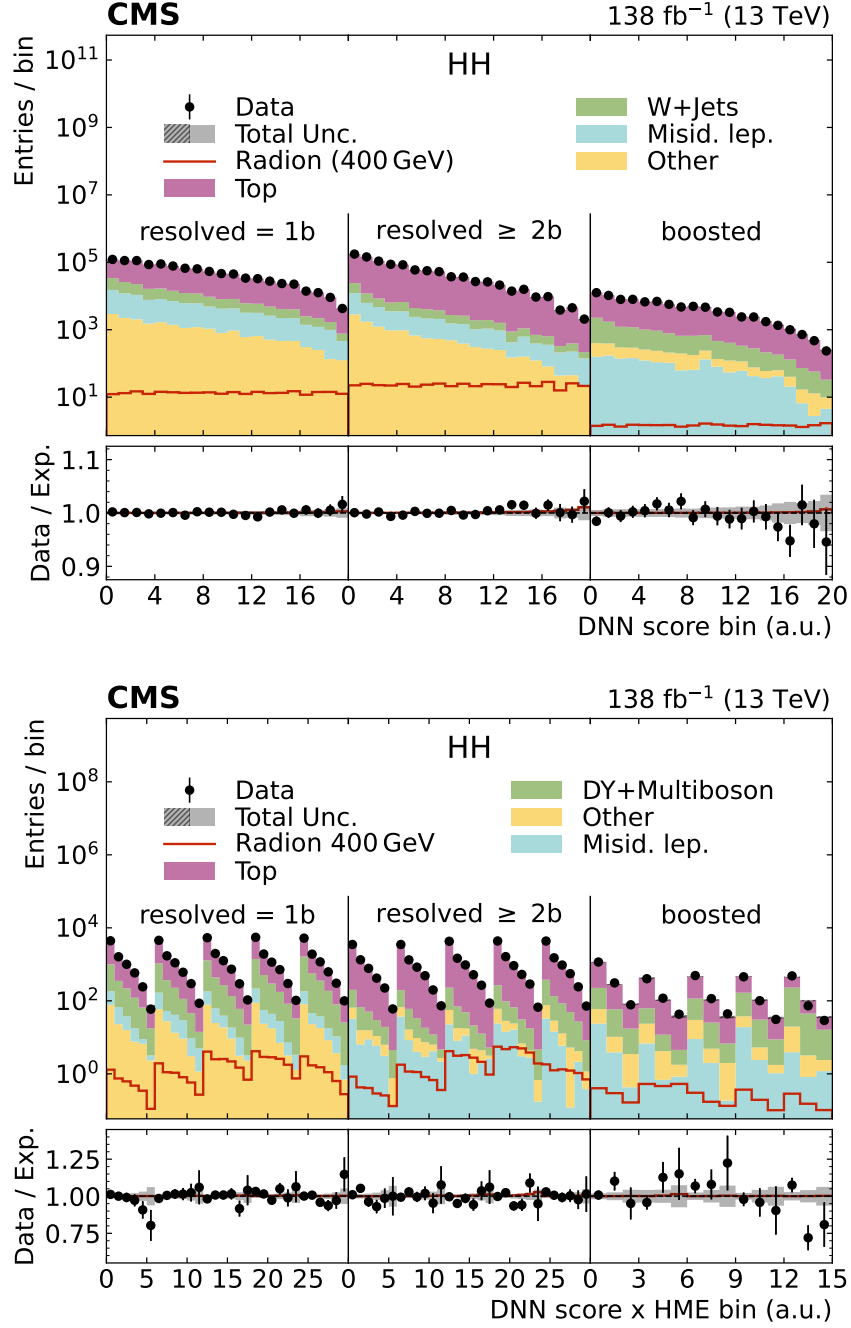


Figure 18: Search for $X \rightarrow H(bb)H(WW)$: Distributions of the DNN output for events in the signal nodes of the (upper) SL and (lower) DL categories of the $H(bb)H(WW)$ analysis based on merged and resolved jets [119]. The distributions for a signal of a resonant radion with a mass of 400 GeV are also shown, by open red histograms. Figure from Ref. [119].

for the SR for the three event categories, for an assumed resonance mass of $m_X = 400$ GeV. The signal expected for a radion of this mass with a cross section of 1 pb is also displayed. The observed distributions agree well with the expectation from SM backgrounds and no significant signal is observed.

2.4.2 The $X \rightarrow H(bb)H(WW)$ decay in merged-jet topology

This study extends the search in the bbWW channel towards higher X masses [120]. As in Section 2.4.1, the SL selection targets the $HH \rightarrow bbWW \rightarrow bb\ell\nu qq$ decay mode. The DL selection covers both the $HH \rightarrow bbWW \rightarrow bb\ell\nu\ell\nu$ and the $HH \rightarrow bb\tau\tau \rightarrow bb\ell\nu\ell\nu\ell\nu$ decay modes, and the latter comprises 30–35% of the total expected DL signal yield. As this analysis targets resonance masses of $m_X > 0.8$ TeV, the H bosons emerge with a large Lorentz boost with respect to the laboratory rest frame, and their decay products are contained in collimated cones. For this reason, the hadronically decaying H and W bosons are each reconstructed with a single AK8 jet.

The signal is searched for in the two-dimensional distribution in the (m_{bb}, m_{HH}) mass plane, hence the kinematics of both Higgs boson candidates need to be reconstructed.

In the SL final state, the highest p_T lepton in the event is selected as the lepton candidate from the leptonic W decay. The $W(qq)$ decay is reconstructed with a high- p_T AK8 jet. The AK8 jet nearest to the lepton satisfying $\Delta R < 1.2$ is taken to be the W candidate. The $H \rightarrow WW$ decay chain is reconstructed using a likelihood-based technique, which provides an estimate of the neutrino momentum vector and also a correction to the p_T of the $W(qq)$ candidate jet.

In the DL final state, two opposite-sign light leptons with the highest p_T are taken to be the leptons arising from the $H \rightarrow WW$ decay. Due to the collimation of the Higgs boson decay products, the polar angles of the dineutrino and dilepton systems can be assumed to be the same. Using this assumption, and by approximating the invariant mass of the two neutrinos with its expected mean value of 55 GeV, the sum of the four-momenta of the two neutrinos is estimated using p_T^{miss} . These assumptions are guided by simulation studies. The leptons are required to be close by satisfying $\Delta R < 1$, and their invariant mass is required to be in the range of 6–75 GeV to reduce contamination from DY production. Events are required to have large p_T^{miss} , pointing in approximately the same direction in the transverse plane as the dilepton system, satisfying $\Delta\phi < \pi/2$.

In all considered final states, the $H \rightarrow bb$ decay is reconstructed as a single AK8 jet with two-prong substructure and high p_T . The double-b tagging is performed with the DEEPAK8 algorithm. The SR is defined by requiring m_{SD} of the $H \rightarrow bb$ candidate to be within 30–210 GeV. This allows us to also capture the neighboring background, which is important for the signal extraction described below. Events containing any b-tagged AK4 jets outside the $H \rightarrow bb$ candidate AK8 jet are vetoed, as they are likely to arise from $t\bar{t}$ production.

Events with the production of one or more top quarks constitute the majority of the background, where particles from a hadronic top quark decay are captured in the $H \rightarrow bb$ candidate jet, particularly in the SL final state. The invariant mass distributions of such backgrounds may resonate in m_t , m_W , or neither, depending on which daughter partons are captured, and the backgrounds are classified accordingly. Events originating from other processes, primarily from W+jets and QCD multijet production in the SL channel and DY production in the DL channel, are taken as a separate component.

Events are divided into twelve categories according to the lepton flavor, the purity of the $H \rightarrow bb$ flavor tagging, and, for the SL final states, the purity of the $H \rightarrow WW$ decay re-

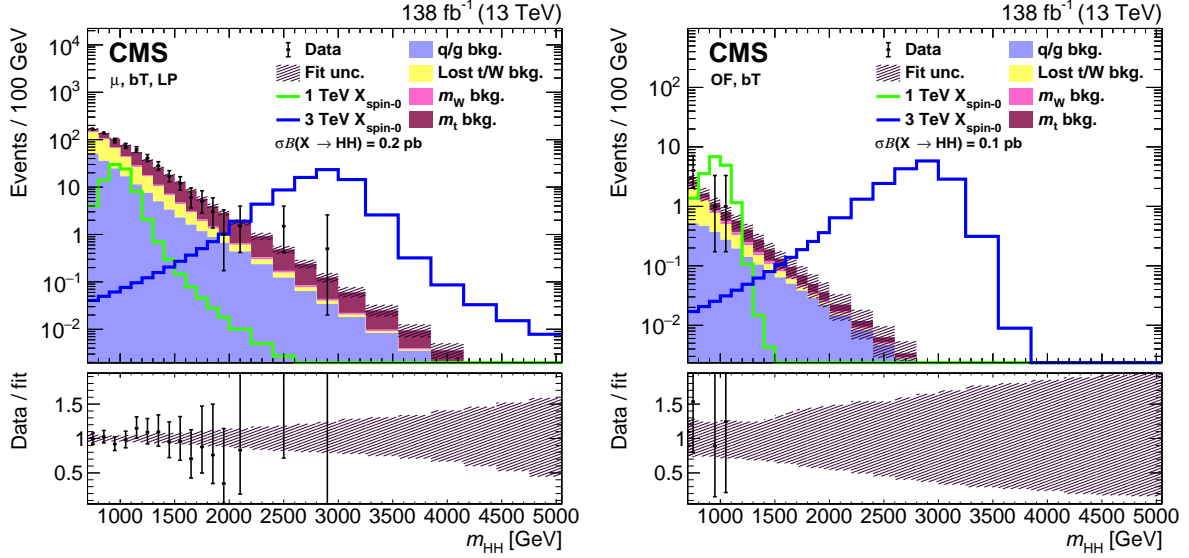


Figure 19: Search for $X \rightarrow H(bb)H(WW)$: Distributions of the m_{HH} variable, in the (left) SL and (right) DL categories of the $H(bb)H(WW)$ analysis with merged jets [120]. Expected signal distributions from a spin-0 resonance with a mass of 1 or 3 TeV are also shown, by the open green and blue histograms. Figure from Ref. [120].

construction. Results are extracted by performing a maximum likelihood fit in the 2D (m_{bb} , m_{HH}) mass plane. The background-only model is found to describe the observed distributions well. The distributions of events projected into m_{HH} for two selected categories in SL and DL final states are shown in Fig. 19. In both cases high purity of the $H \rightarrow bb$ flavor tagging (bT) is required. The chosen SL category is further characterized by a muon and a low purity (LP) requirement of the $H \rightarrow WW$ decay reconstruction. The DL category is characterized by different flavors.

2.4.3 The $X \rightarrow HH$ decays into multilepton final states

The analysis of multilepton final states [121] does not assume at least one $H \rightarrow bb$ decay, unlike all other HH analyses discussed in this report, and thus gains access to various hitherto uncovered HH signatures. This search is focused on resonant HH production in the WWWW, WW $\tau\tau$, and $\tau\tau\tau\tau$ decay modes. The chosen final states provide a good compromise between a relatively large HH branching fraction and a clean leptonic event signature. The latter provides a series of almost background-free categories with low event counts, which are especially sensitive at low resonance masses. The data are collected using triggers combining single and multiple lepton and τ_h signatures.

The selected events are split into seven event categories with different multiplicities of reconstructed leptons and hadronically decaying taus, denoted as $2\ell ss$ (same sign), 3ℓ , 4ℓ , $3\ell + 1\tau_h$, $2\ell + 2\tau_h$, $1\ell + 3\tau_h$, and $4\tau_h$. The lower multiplicity $2\ell ss$ and 3ℓ categories also require additional jets, as expected from hadronic W boson decays. To reduce the impact of backgrounds involving the decay of top quarks, such as $t\bar{t}$ production, and to avoid overlap with other HH analyses, events with b jets identified with the DEEPIET algorithm [142] are explicitly vetoed. Similarly, events with two opposite-sign same-flavor lepton pairs and a combined invariant mass below 140 GeV are vetoed to avoid overlap with the $HH \rightarrow bbZZ$ signature, the analysis of which is not included in this Report. To exclude phase space regions enriched in low mass resonances, which are not well modelled in simulation, and to reduce the impact of backgrounds involving Z boson decays, events containing DL pairs with a mass of $m_{\ell\ell} < 12$ GeV

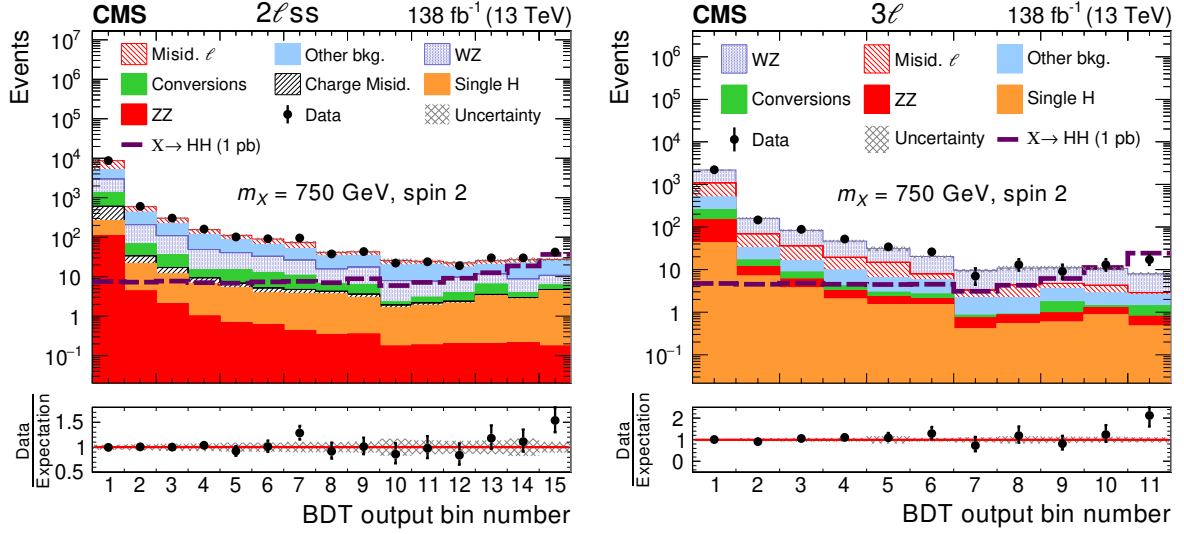


Figure 20: Search for $X \rightarrow HH$ in multi-lepton final states: Distributions of the BDT classifier output for events in the (left) $2\ell ss$ and (right) 3ℓ categories of the $H(WW + \tau\tau)H(WW + \tau\tau)$ analysis in multilepton final states [121]. The expected signal for a spin-2 resonance with a mass of 750 GeV is shown by the open dashed histogram. The signal is normalized to a cross section of 1 pb. The distributions of the estimated background processes and corresponding uncertainties are shown after a fit of the signal plus background hypothesis to the data. Figure from Ref. [121].

or in the vicinity of the Z boson mass are vetoed as well.

The main backgrounds arise from genuine multiboson processes, such as ZZ production in all categories, as well as WZ production in the $2\ell ss$ and 3ℓ categories. These backgrounds, as well as smaller backgrounds, such as contributions from DY, $t\bar{t}$, and single H production together with backgrounds from photon conversions in the detector material are estimated from the simulation. Background events from charge misidentification in the $2\ell ss$ category, however, are also estimated from data extrapolating events with opposite-sign electrons from $Z \rightarrow ee$ decays into the SR. In most categories, backgrounds arising from jets misidentified as either leptons or τ_h also play an important role; these are estimated with the misidentification-rate factor method [165].

The signal extraction is based on maximum likelihood fits to the distributions of boosted decision tree (BDT) discriminants. The BDTs are trained to discriminate signal from background in each of the seven categories and for each resonance spin assumption (spin 0 or 2). The BDTs are parameterized in the nominal resonance mass.

The selection of BDT input variables is optimized for each signal category, and includes kinematic variables of ℓ and τ_h candidates as well as angular separations and invariant masses of their combinations. Also, the reconstructed HH mass is used. The fits also include two kinematic distributions in control regions enriched in the dominant prompt backgrounds from ZZ and WZ production.

As an example of the SR composition, Fig. 20 shows the BDT output in the two highest signal yield categories $2\ell ss$ and 3ℓ for a spin-2 particle with $m_X = 750$ GeV. A small excess is observed in the rightmost bin of both distributions, amounting to a local significance of about 2.1 standard deviations in both categories. This leads to a mild local excess of the observed limits

corresponding to about 1.5–2 standard deviations for masses above 600 GeV, which is visible in Fig. 27.

2.5 Search for resonances in the YH channel

Recently, direct searches for new physics in the Higgs sector have been extended towards YH decays, where Y denotes another unknown bosonic resonance. Such decays are expected, e.g., in 2HDM+S models like the NMSSM, where X and Y can be identified with additional heavy or light Higgs bosons. In cases where Y carries a large singlet component its couplings to SM particles are suppressed and its dominant production at the LHC proceeds via the decay $X \rightarrow YH$. The first analysis presenting such a search was performed in $Y(bb)H(\tau\tau)$ final states [122], covering mass ranges of $260 < m_X < 3000$ GeV and $60 < m_Y < 2800$ GeV. Later on, this analysis was complemented by similar searches in the $Y(bb)H(bb)$ [124] and $Y(bb)H(\gamma\gamma)$ [123] final states. The search in the $Y(bb)H(bb)$ final state covers mass ranges of $900 < m_X < 4000$ GeV and $60 < m_Y < 600$ GeV, targeting kinematic regimes where both bb decays are reconstructed as large- R AK8 jets. The $Y(bb)H(\gamma\gamma)$ analysis covers mass ranges of $300 < m_X < 1000$ GeV and $90 < m_Y < 800$ GeV, where the upper bound on m_X is implied by the requirement that it should be possible to resolve the b quarks originating from the Y decay as two distinct AK4 jets. All final states have the $Y(bb)$ decay in common. The $H(bb)$ decay utilizes the large branching fraction of the H boson to b quarks; the $H(\tau\tau)$ decay comprises the second largest branching fraction with advantageous reconstruction and identification properties; the $H(\gamma\gamma)$ decay contributes through the excellent mass resolution of the ECAL.

2.5.1 The $X \rightarrow Y(bb)H(\tau\tau)$ decays

The analysis in $Y(bb)H(\tau\tau)$ final states [122] evolved from an analysis of $H \rightarrow \tau\tau$ [167], adding loose requirements on the $Y \rightarrow bb$ decay where the b quarks are reconstructed as AK4 jets. For the $H(\tau\tau)$ decay the $e\tau_h$, $\mu\tau_h$, and $\tau_h\tau_h$ final states are considered. These final states have been shown to have the largest sensitivity to this signature, while the contribution from $\tau\tau$ decays into an e and μ , mostly due to the large background from $t\bar{t}$ production in the kinematic phase space with additionally selected b jets is marginal.

The trigger selection of the events proceeds via the presence of high- p_T electrons, muons, or τ_h decays, or combinations of those at the trigger level. Due to the trigger requirements evolving with time, the offline p_T thresholds range from 25–33 GeV for electrons, from 20–25 GeV for muons, and from 30–40 GeV for τ_h candidates, the latter depending also on the $\tau\tau$ final state. The τ_h candidates are identified using the DEEPTAU algorithm [158], as discussed in Section 2.2. Jets are b tagged using the DEEPTAU algorithm, with a working point of 80% efficiency with a misidentification rate for light-flavor or gluon jets of $\approx 1\%$ [141, 142]. For the event selection, a $\tau\tau$ pair in one of the targeted $\tau\tau$ final states and at least one b jet are required. Events that contain only one b jet and no other jet are discarded from the analysis. If more than two b jets are found, the $Y(bb)$ decay is built from those jets that are leading in p_T . If only one b jet exists, the Y candidate is built from this b jet and the jet with the highest b jet score of the DEEPTAU algorithm, even if this lies below the threshold of the chosen working point. The energies of the jets used to form the Y candidate are corrected using the multivariate energy-momentum regression [168].

Depending on the $\tau\tau$ final state, all selected events are then passed through one of three NNs exploiting multiclass classification to distinguish signal, for given values of m_X and m_Y , from four background classes: (i) events with genuine τ pairs in the final state; (ii) events with quark- or gluon-induced jets misidentified as τ_h candidates; (iii) $t\bar{t}$ events where the intermediate W bosons in the decay chain decays into any combination of electrons and muons or into a

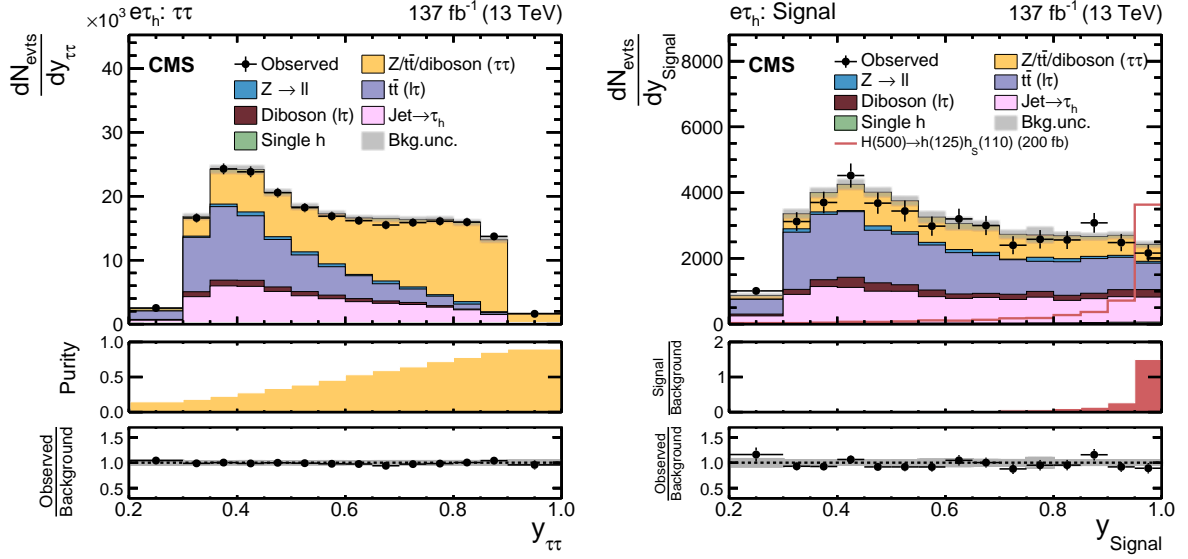


Figure 21: Search for $X \rightarrow Y(bb)H(\tau\tau)$: Distributions of the NN output scores y_i , in different event categories after NN classification, based on a training for a resonance X with $m_X = 500$ GeV and a resonance Y with $100 \leq m_Y < 150$ GeV in the $e\tau_h$ final state of the $H(\tau\tau)Y(bb)$ analysis [122]. Shown are the (left) $\tau\tau$ and (right) signal categories. For these figures, the data of all years have been combined. The uncertainty bands correspond to the combination of statistical and systematic uncertainties after the fit of the signal plus background hypothesis for $m_X = 500$ GeV and $m_Y = 110$ GeV to the data. In the lower panels of the figures the (left) purity and (right) fraction of the expected signal over background yields for a signal with a cross section of 200 fb, as well as the ratio of the obtained yields in data over the expectation based on only the background model, are shown. Figure from Ref. [122].

single τ lepton and an electron or muon (not included in (i) or (ii)); (iv) events from remaining background processes that are of minor importance for the analysis and not yet included in any of the previous classes. This last class comprises single H , single t quark, and diboson production, as well as Z boson decays into electrons or muons. For single H production, rates and branching fractions as predicted by the SM are assumed.

Inputs to the NNs are 20–25 features, of which the following have been identified to be most discriminating, according to an unambiguous metric as given in Ref. [169]: the invariant masses of the bb , $\tau\tau$, and $bb\tau\tau$ systems, and the χ^2 -value of a kinematic fit to the data of the signal hypothesis for given values of m_X and m_Y . Since the discrimination depends on the signal hypothesis, individual NNs have been trained for 68 groups of kinematically adjacent and similar signal hypotheses. Each event has been assigned to the class with the highest NN output score. Eventually, the NN output scores have been chosen as discriminating variables for a maximum likelihood fit in 45 individual event categories, split by $\tau\tau$ final state and data-taking year. Typical output distributions are shown in Fig. 21.

2.5.2 The $X \rightarrow Y(bb)H(\gamma\gamma)$ decays

As in the previous case, the analysis in the $Y(bb)H(\gamma\gamma)$ final state [123] starts from the well-identified $H \rightarrow \gamma\gamma$ decay complemented by the selection of two additional AK4 jets to form the $Y(bb)$ candidate.

The trigger selection proceeds through the requirement of two photons with thresholds of $p_T > 30$ GeV for the leading (γ_1) and $p_T > 18$ GeV for the subleading (γ_2) photon in p_T , for data taken

in 2016. For data taken in the years 2017–2018, the requirement on γ_2 is raised to $p_T > 22$ GeV because of the larger amount of PU in data. The photons are required to pass identification and isolation criteria, already through the trigger selection, and the mass of the two photons is required to be $m_{\gamma\gamma} > 90$ GeV.

In the offline selection, the photons from which the H candidate is formed are required to be well contained in the ECAL and tracker fiducial volumes of $|\eta| < 2.5$, excluding the transition region of $1.44 < |\eta| < 1.57$ between the ECAL barrel and endcaps, and to fulfill kinematic requirements of $100 < m_{\gamma\gamma} < 180$ GeV, $p_T^{\gamma_1}/m_{\gamma\gamma} > 1/3$, and $p_T^{\gamma_2}/m_{\gamma\gamma} > 1/4$. In addition to the photons at least two AK4 jets originating from the same PV as the photons are required, where the assignment of the photons to the PV is achieved with the help of an MVA technique, as described in Ref. [170]. The jets must fulfill identification requirements as described in Section 2.2, have $p_T > 25$ GeV and $|\eta| < 2.4$ or 2.5, for the data taken in 2016 and 2017–2018, respectively, and be separated from each of the selected photons by $\Delta R > 0.4$. Of all jets in an event that match these criteria, those with the highest sum of their DEEPIET discriminant scores are chosen to form the Y candidate with a requirement on the dijet mass of $70 < m_{jj} < 1200$ GeV. The lower bound on m_{jj} is implied by the kinematic turn-on in the m_{jj} distribution, the upper bound is defined by the transition towards Lorentz-boosted regimes, where the bb system may not be resolved by two spatially separated AK4 jets.

The X candidate is reconstructed from the jets and photons forming the H and Y candidates. To improve the resolution, its mass m_X is estimated from

$$\tilde{m}_X = m_{\gamma\gamma jj} - (m_{\gamma\gamma} - m_H) - (m_{jj} - m_Y), \quad (10)$$

where $m_{\gamma\gamma jj}$ is the mass calculated from the two jets and the two photons. It is corrected by subtracting $m_{\gamma\gamma}$ and m_{jj} , with their values replaced by the nominal values of the masses m_H and m_Y . This estimate has been shown to lead to a 30 to 90% improvement in signal resolution compared to $m_{\gamma\gamma jj}$ alone, in the high- and low- m_X regimes, respectively. For the signal extraction, events are required to be located inside a window in \tilde{m}_X , depending on the m_X hypothesis under test. The width of this window has been defined such that it contains at least 60% of the signal.

Resonant backgrounds to the analysis originate from single H production, which is strongly suppressed already by the selection in \tilde{m}_X . For hypotheses of $m_X < 550$ GeV a sizeable contribution from $t\bar{t}H$ production is further reduced by an NN-based discriminant developed for the search for nonresonant $H(\gamma\gamma)H(bb)$ production [171], exploiting the decays of W bosons arising from the $t\bar{t}$ decay chains.

Nonresonant backgrounds in this search mostly originate from the production of one (γ +jets) and two ($\gamma\gamma$ +jets) photons in association with jets. To separate these backgrounds from the signal a BDT with three output classes, one for each background and one for signal, and 22 input features is used. The input features comprise kinematic and identification observables of the selected jets and photons, estimates of the mass, energy, and p_T resolutions, and an estimate of the p_T density from PU. For training, six exclusive kinematic regions are defined, based on the hypothesized values of m_X and m_Y , where in each region all contained signal samples and the two background processes in question, as obtained from simulation, are used with equal weight. These training regions are defined to resemble similar kinematic properties for signals inside the given m_X – m_Y window. For each kinematic region, three event categories are defined, based on the output of the corresponding BDT. These categories are introduced to indicate regimes of varying signal purity. For each m_X hypothesis the signal is inferred from an unbinned likelihood fit of a parametric model to the data in the 2D discriminating distributions

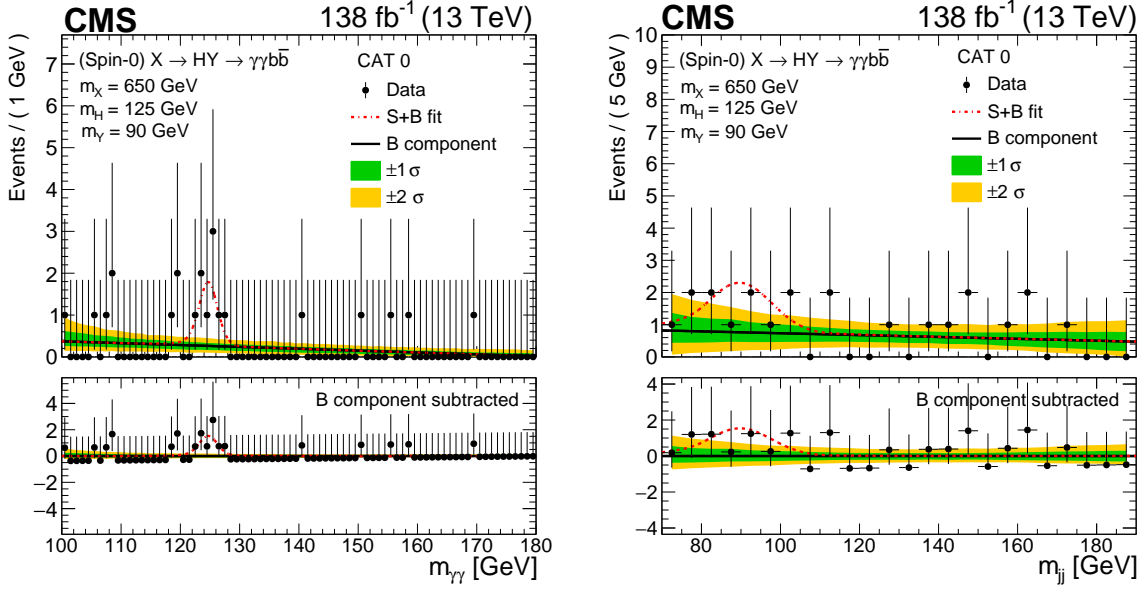


Figure 22: Search for $X \rightarrow Y(bb)H(\gamma\gamma)$: Marginal distributions of the (left) $m_{\gamma\gamma}$ and (right) m_{jj} variables, in the high-purity SR (labeled “CAT 0”) of the $Y(bb)H(\gamma\gamma)$ analysis [123]. The figure is shown, for a hypothesis of $m_X = 650$ GeV and $m_Y = 90$ GeV, for which the largest excess of events over the background model is observed. In the lower panels, the numbers of background-subtracted events are shown after the fit of the background model to the data. Figure from Ref. [123].

given by the values of $m_{\gamma\gamma}$ and m_{jj} , in each of the BDT categories. The data are found to be compatible with the SM predictions. In Fig. 22 the marginal distributions of $m_{\gamma\gamma}$ and m_{jj} in the BDT category with the highest expected signal purity for a selection corresponding to $m_X = 650$ GeV and $m_Y = 90$ GeV, are shown together with the results of the fit to the data. For these mass values, the largest deviation from the background-only hypothesis is observed, with a local (global) significance of 3.8 (below 2.8) standard deviations. A hypothesized signal for $m_X = 650$ GeV and $m_Y = 90$ GeV with an arbitrary normalization is also shown.

2.5.3 The $X \rightarrow Y(bb)H(bb)$ decays in merged jet topology

This analysis in the $Y(bb)H(bb)$ final state [124] explicitly targets ranges in m_X and m_Y where both, the $Y(bb)$ and $H(bb)$ decays can be reconstructed with AK8 jets, as described in Section 2.2.

The trigger selection proceeds through a logical OR of a mixture of trigger paths requiring the presence of high- p_T AK8 jets, large values of H_T , or combinations of those. In addition, b tagging requirements and a requirement on the mass of the two leading jets, in cases where more than one AK8 jet is present in an event, are imposed. This setup aims at a trigger efficiency close to 100% for the offline selected events. Residual corrections to the trigger efficiency have been derived from CRs. These corrections usually range below 5%.

In the offline selection, the events are required to contain at least two AK8 jets with $p_T > 350$ GeV and $|\eta| < 2.4$ for the data taken in 2016 and $p_T > 400$ GeV and $|\eta| < 2.5$ for data taken in 2017–2018. The dominant backgrounds for this analysis arise from $t\bar{t}$ production in the all-hadronic decay of the intermediate W bosons and QCD multijet production. To further suppress the latter an additional pairwise requirement of $|\Delta\eta| < 1.3$ for the selected AK8 jets is imposed. Eventually the two leading jets in p_T are identified as the H and Y candidates, where

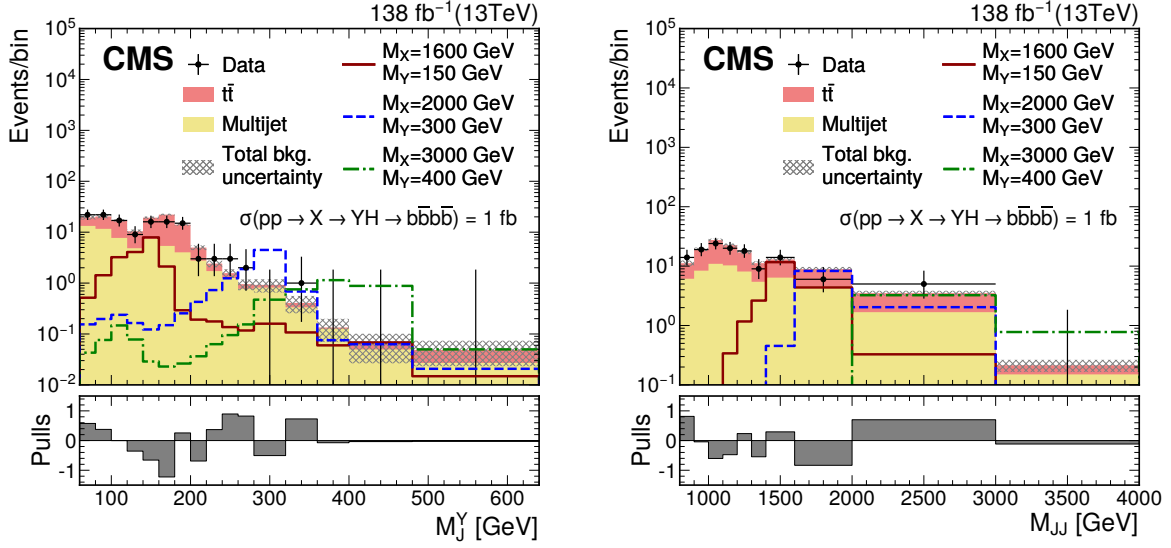


Figure 23: Search for $X \rightarrow Y(bb)H(bb)$: Distributions of the (left) soft-drop mass of the boosted Y candidate, labeled M_J^Y , and (right) the dijet mass of the Y and H candidates, M_{JJ} , in the high-purity SR of the $Y(bb)H(bb)$ analysis with two merged bb jets [124]. The distributions as expected for signals with three different values of m_X and m_Y (labeled M_X and M_Y) are also shown. In the lower panels the statistical pull in each bin is displayed. Figure from Ref. [124].

requirements of $110 < m_{SD} < 140$ GeV for the H candidate and $m_{SD} > 60$ GeV for the Y candidate are imposed. When both AK8 jets satisfy the first mass requirement, the Y jet is chosen at random. The H and Y candidates are then passed to the PARTICLENET algorithm [147] to discriminate the decays of a boosted resonance, $H(bb)$ or $Y(bb)$, from light-flavor quark or gluon jets.

Based on the output of the PARTICLENET algorithm for each of the AK8 jets, a loose and a tight SR, with varying expected signal purity, are defined. In addition, corresponding side-band regions for the estimation of the background from QCD multijet production and a series of regions to validate this background estimate are constructed. The background from $t\bar{t}$ production is estimated from simulation and monitored in a dedicated CR in data, obtained from a selection of either an isolated electron or muon with $p_T > 40$ GeV and $|\eta| < 2.4$, and an AK4 jet tagged as a b jet with the DEEPIET algorithm, with a distance of $\Delta R < 1.5$ from the selected lepton. For this purpose, a working point of the DEEPIET algorithm with an efficiency of 90% with a misidentification rate of $\approx 10\%$ has been chosen. In addition, requirements of $p_T^{\text{miss}} > 60$ GeV and $H_T > 500$ GeV are imposed. The lepton, p_T^{miss} , and the b -tagged jet provide the signature of a leptonically decaying t quark. A hadronically decaying t quark candidate is reconstructed from an AK8 jet fulfilling the same kinematic requirement as in the SR and $m_{SD} > 60$ GeV. In addition the selected AK8 jet must have a distance of $\Delta R > 2$ from the selected lepton. This selection reaches a purity in $t\bar{t}$ events of greater than 90%. The signal is obtained from a fit of the signal and background models to the observed 2D distribution in the (m_J^Y, m_{JJ}) plane, where m_J^Y is the soft-drop mass of the Y boson candidate, and m_{JJ} is the invariant mass of the H and Y boson candidates. The loose and tight SRs are fit jointly with the corresponding CRs that constrain the QCD multijet and $t\bar{t}$ backgrounds. Distributions in m_J^Y and m_{JJ} in the high-purity signal region are shown in Fig. 23.

2.6 Statistical combination

Combinations are performed based on the HH and YH decay channels presented in this report, and the results will be presented in Sec 3. A combination of VH decay channels is foreseen at a later date as various analyses are still ongoing. The combination is performed by integrating the signal extraction procedures of the respective decay channels into a combined likelihood analysis determining a single combined signal strength. In the HH case, this combined signal strength measures the product $\sigma(pp \rightarrow X)\mathcal{B}(X \rightarrow HH)$. It is linked to the signal strength in each individual HH decay mode combination by the product of the corresponding H branching fractions, where the SM values for a Higgs boson with $m_H = 125 \text{ GeV}$ are used. In the YH case, the combined signal strength measures the product $\sigma(pp \rightarrow X)\mathcal{B}(X \rightarrow YH)\mathcal{B}(Y \rightarrow bb)$. It is connected to the signal strength in each YH decay mode by the corresponding SM H branching fraction. The branching fraction $\mathcal{B}(Y \rightarrow bb)$ is unknown, model dependent, and no attempt is made to correct for it. This way of combination is possible because all considered YH channels share the $Y \rightarrow bb$ decay mode.

For this combined analysis, those systematic variations that should act in the same way for each individual search in consideration, are treated as correlated. A typical example of this kind is the uncertainty in the integrated luminosities of the used data sets. According to the values of m_X and m_Y , different channels may contribute at different levels of relative sensitivity. This is due to differences in the selection efficiency, the acceptance of the CMS detector, the trigger efficiency and the branching fractions. Therefore a combination might be either dominated by one channel or benefit from the joint effect of many channels with similar sensitivity depending on the phase-space region.

For the $X \rightarrow HH$ decay, the combination is performed separately for the spin-0 and spin-2 hypotheses on the X boson. For the $X \rightarrow YH$ case, spin-0 is assumed for both the X and Y bosons. For all measurements described in the following, the H boson mass is fixed to $m_H = 125 \text{ GeV}$. In case of the $Y(bb)H(\tau\tau)$ analysis (Section 2.5.1), for which no limits at $m_Y = 125 \text{ GeV}$ are available, we use $m_Y = 130 \text{ GeV}$ instead to estimate the result for the HH case. This is justified by the limited mass resolution. We make this particular choice because a comparison of the limits with $m_Y = 120 \text{ GeV}$ and $m_Y = 130 \text{ GeV}$ shows that the latter choice yields more conservative limits. Theoretical uncertainties in the branching fractions and in the HH cross sections are taken into account [35].

The used grids in points of m_X and (m_X, m_Y) can differ across the various analyses. In general, the combination is performed only for the points common to all analyses considered in the combination.

As theoretical systematic uncertainties, we consider normalization uncertainties related to PDF, QCD scale, and α_s in the total cross section for the main backgrounds and for the single H production process, which follows the recommendations by the LHC cross section working group [35]. These uncertainties are considered to be uncorrelated across processes, and fully correlated across channels that share the same process.

3 Upper limits on the cross sections

We now turn to the results of the searches for heavy resonances X decaying into VH, HH, and YH channels. Each search features at least one instance of the H boson at a mass of 125 GeV originating from the decay of a heavy resonance X. The analyses are performed in a variety of final states with complementary sensitivity in the masses m_X and m_Y .

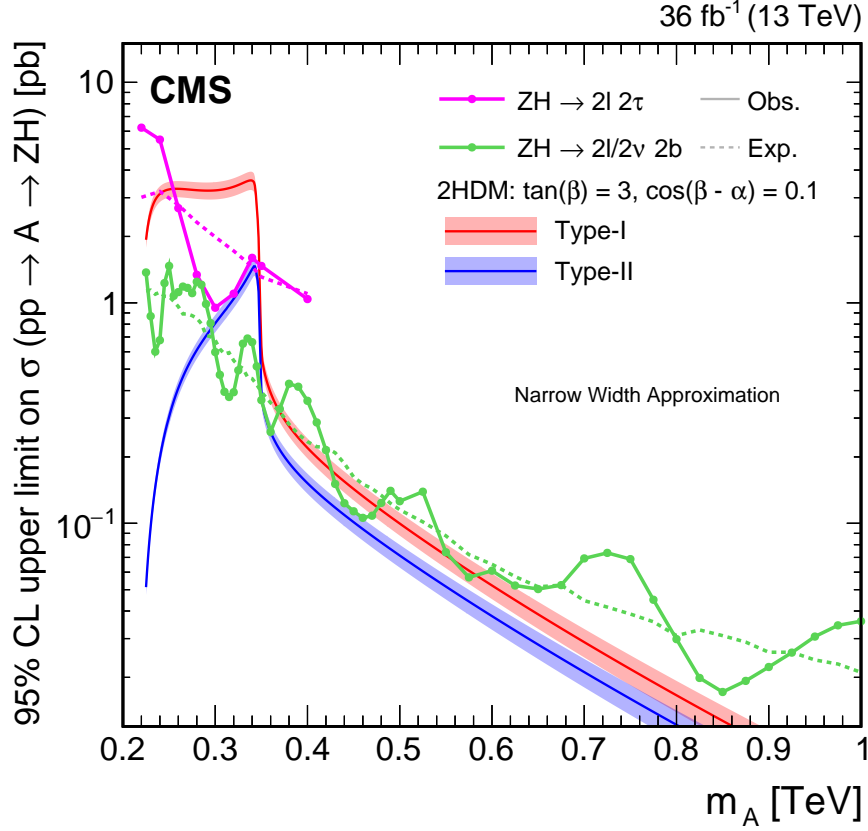


Figure 24: Search for $X \rightarrow ZH$: Observed and expected 95% CL upper limits on the product of the cross section σ for the production of an A boson, via gluon-gluon fusion and the branching fraction \mathcal{B} for the $A \rightarrow ZH$ decay. The limits are given in pb as functions of m_A . The markers connected with solid lines (dashed lines) indicate the observed (expected) limits. The green (magenta) lines refer to the $Z(\ell\ell + \nu\nu)H(bb)$ [115] ($Z(\ell\ell)H(\tau\tau)$ [114]) analysis. The red and blue solid lines indicate the product $\sigma\mathcal{B}$ as expected by the 2HDM Type I and Type II models, respectively, for the parameters $\tan\beta = 3$ and $\cos(\beta - \alpha) = 0.1$. The shaded areas associated with these predictions indicate the corresponding model uncertainties. The results and model predictions have been adapted from Refs. [114, 115].

The observed data for all searches are found to be in agreement with the SM expectations in the corresponding SRs. We set upper limits on the product of the production cross section of the resonance and the branching fraction, $\sigma\mathcal{B}$. The upper limits are set at 95% CL, using the CL_s criterion [172–174]. Statistical combinations of the different HH and YH analyses are performed as described in Section 2.6 to extract the maximum information from the data.

3.1 The $X \rightarrow VH$ decays

Five searches for VH resonances are presented in Section 2.3. These target final states with 0, 1, and 2 leptons, originating from the decay of the vector boson (W or Z) produced together with the H boson. The H boson is assumed to either decay to bb or $\tau\tau$. The results are shown as upper limits on $\sigma\mathcal{B}$ as functions of the resonance mass X . This can either be a scalar particle, which can occur, e.g., in 2HDM models, or a vector boson resonance, like W' and Z' , as predicted in the HVT models.

Figure 24 shows the upper limits on $\sigma(pp \rightarrow A)\mathcal{B}(A \rightarrow ZH)$ as functions of the mass of the CP -odd Higgs boson A , using H decays to bb [115] and $\tau\tau$ [114], obtained with the data set

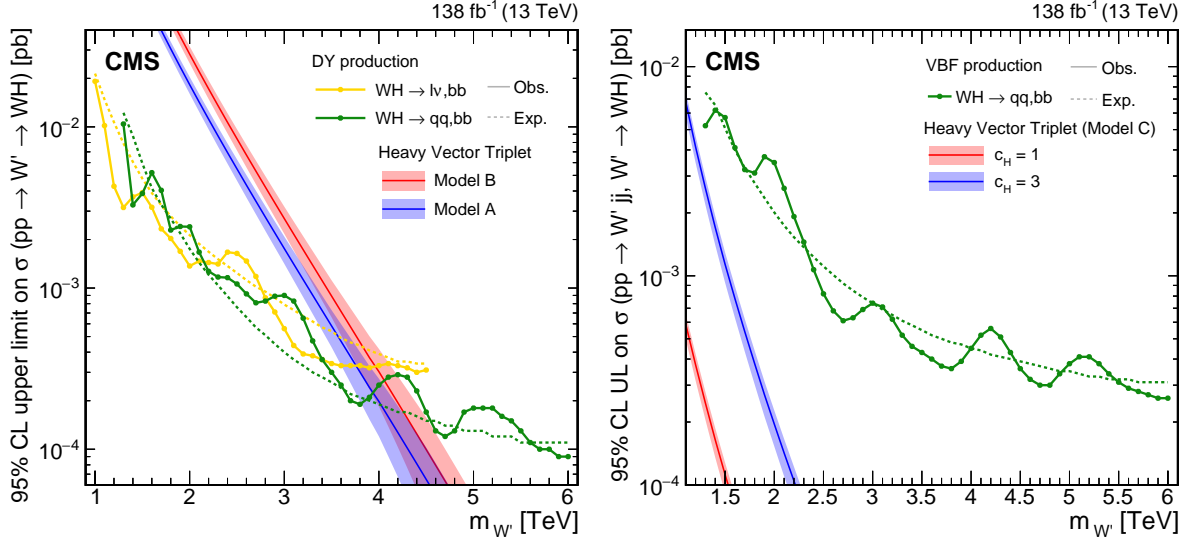


Figure 25: Search for $X \rightarrow WH$: Observed and expected 95% CL upper limits on the product of the cross section σ for the production of a W' spin-1 resonance, via (left) DY production or (right) vector boson fusion and the branching fraction \mathcal{B} for the $W' \rightarrow WH$ decay. The solid lines represent the observed and the dotted lines the expected limits. The theory predictions from the heavy vector triplet models A, B, and C are also shown.

recorded in 2016. This plot also shows the expected cross sections for A bosons in two typical 2HDM scenarios. These feature a drop beyond the $t\bar{t}$ threshold because of the $A \rightarrow t\bar{t}$ channel opening up.

Figures 25 and 26 show the upper limits on $\sigma\mathcal{B}$ for spin-1 W' and Z' resonances, as a function of the masses $m_{W'}$ and $m_{Z'}$, respectively. The limits are derived for DY (left) and VBF (right) production separately. The exclusion limits reach values of $\sigma\mathcal{B}$ below 0.1 and 0.3 fb for the DY and VBF topologies, respectively. In DY production the results from searches with leptons in the final state yield a stronger exclusion for $m_{W'}$ masses below 1.7 TeV and $m_{Z'}$ below 3.2 TeV. For higher masses, the fully hadronic final state shows higher sensitivity. The interpretations of these upper limits on $\sigma\mathcal{B}$ in HVT models will be discussed in detail in Section 4.3.

3.2 The $X \rightarrow HH$ decays

The six searches for $X \rightarrow HH$ discussed in Section 2.4 target a variety of final states with b jets, photons, light leptons, and τ_h leptons. The searches study spin-0 and spin-2 resonances in the mass range 0.28–4.5 TeV. We denote the spin-0 resonance as X since interpretations in warped extra dimension and extended Higgs sector models are both possible. We denote the spin-2 resonance as G having a graviton in mind.

Figure 27 shows the upper limits on $\sigma\mathcal{B}$ as functions of the resonance mass for both spin hypotheses. The exclusion in terms of $\sigma\mathcal{B}$ extends down to 0.2 fb for both spin scenarios probed. The best sensitivity at low masses is obtained by the diphoton search, while at high masses the two searches with b-tagged merged jets show the best sensitivity. The results of the statistical combination as described in Section 2.6 are shown as red lines. These combined results are presented again separately in Fig. 28 along with the ± 1 and ± 2 s.d. intervals on the expected limits. No deviation larger than 2 s.d. from the expected limits is observed. Large improvements in sensitivity relative to the best individual channel are achieved in the range of $m_X \sim 0.5$ –1 TeV, where many channels contribute with about the same weight to the com-

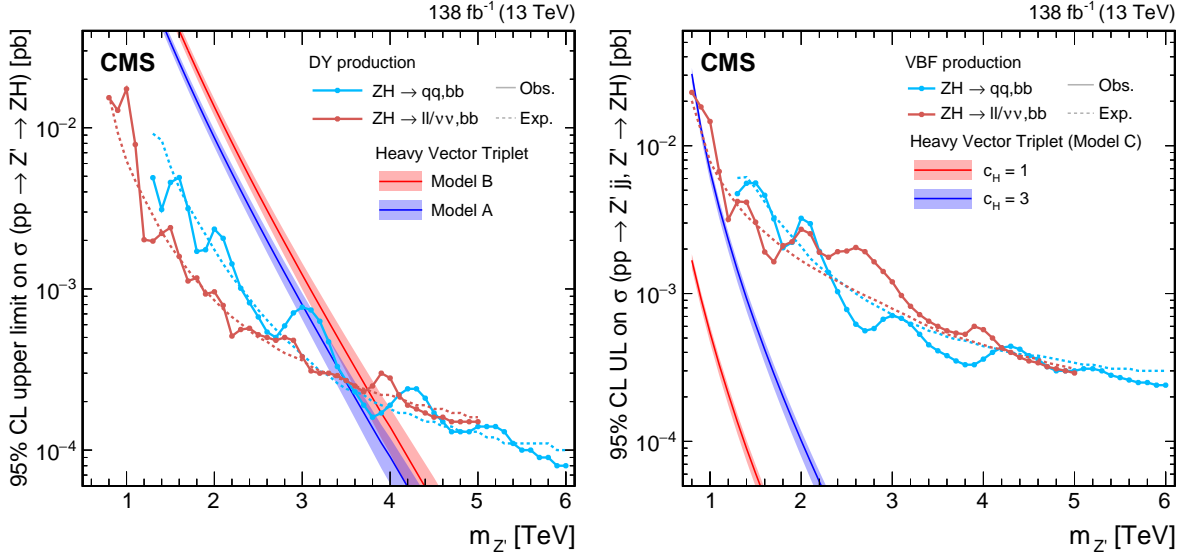


Figure 26: Search for $X \rightarrow ZH$: Observed and expected 95% CL upper limits on the product of the cross section σ for the production of a Z' spin-1 resonance, via (left) DY production or (right) vector boson fusion and the branching fraction \mathcal{B} for the $Z' \rightarrow ZH$ decay. The solid lines represent the observed and the dotted lines the expected limits. The theory predictions from the heavy vector triplet models A, B and C are also shown.

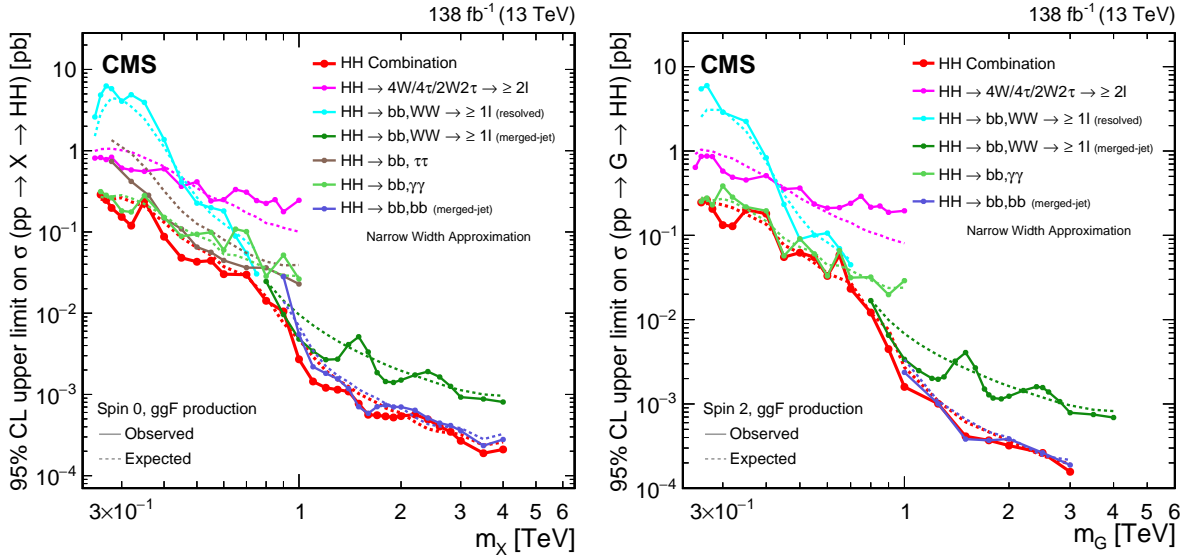


Figure 27: Search for $X \rightarrow HH/G \rightarrow HH$: Observed and expected 95% CL upper limits on the product of the cross section σ for the production of a (left) spin-0 resonance X and (right) a spin-2 resonance G , via gluon-gluon fusion and the branching fraction \mathcal{B} for the corresponding HH decay. The results of the individual analyses presented in this report, corrected for the branching fractions of the respective H decay modes, and the result of their combined likelihood analysis are shown. The observed limits are indicated by markers connected with solid lines and the expected limits by dashed lines.

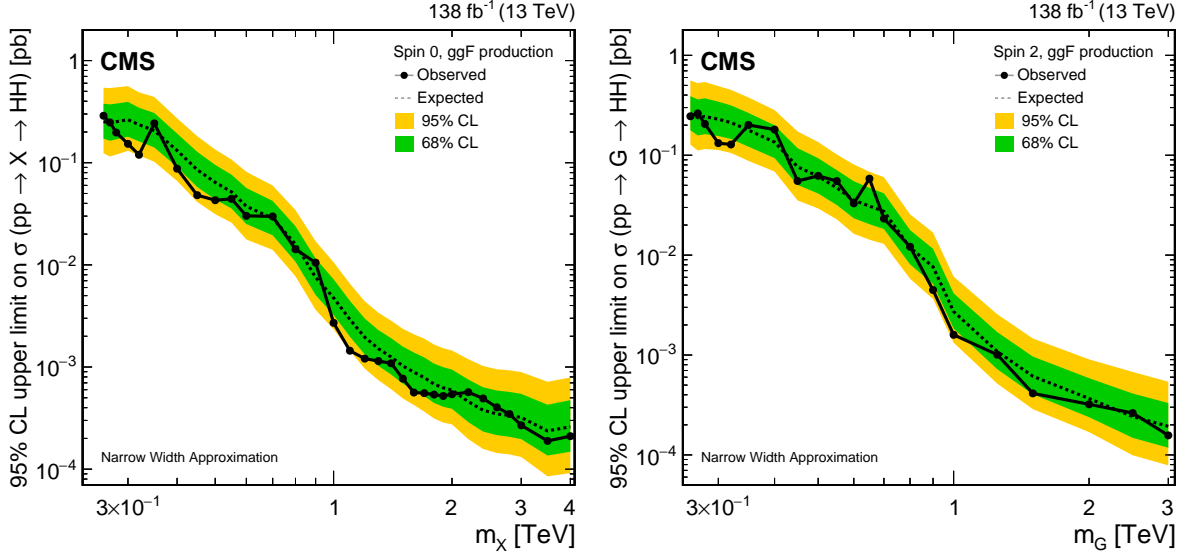


Figure 28: Search for $X \rightarrow HH/G \rightarrow HH$: Observed and expected 95% CL upper limits on the product of the cross section σ for the production of a (left) spin-0 resonance X and (right) a spin-2 resonance G , via gluon-gluon fusion, and the branching fraction \mathcal{B} for the corresponding HH decay, as obtained from the combined likelihood analysis of all contributing individual analyses presented in this report and shown in Fig. 27. In addition to the limit from the combined likelihood analysis the 68 and 95% central intervals for the expected upper limits in the absence of a signal are shown as colored bands.

bination. Below masses of 0.32 TeV and above 0.8 TeV, this combination gives the strongest observed limits to date on resonant HH production. A recent combination of HH searches performed by the ATLAS Collaboration can be found in Ref. [175].

3.3 The $X \rightarrow YH$ decays

Three searches target the $X \rightarrow YH$ decay. Two are dedicated to lower masses with the H boson decaying to $\gamma\gamma$ or $\tau\tau$ with two b -tagged AK4 jets for the reconstruction of the Y boson (as discussed in Section 2.5). The search in the fully hadronic final state with two double- b -tagged AK8 jets targets the high-mass regime. As the Y boson decays to bb in all cases considered, this allows for a direct comparison of the results from these three searches, without the assumption of a specific model. Furthermore, this makes a model-independent combination possible, where only the branching fractions of the H boson need to be taken into account.

Figures 29 and 30 show the upper limits on $\sigma\mathcal{B}$ as functions of the m_Y for $m_X \leq 1$ TeV and for $m_X \geq 1.2$ TeV, respectively. The results have been achieved by adjusting each channel to the corresponding SM branching fraction of the H boson decay under consideration. No correction has been made for the unknown branching fraction of $Y \rightarrow bb$, which is the same in all searches.

At low m_X , the $Y(bb)H(\tau\tau)$ and $Y(bb)H(\gamma\gamma)$ analyses provide the best sensitivity. For $m_X = 1$ TeV and higher, the $Y(bb)H(bb)$ in the merged jet topology dominates for small and medium values of m_Y . At the largest values of m_Y , however, approaching the kinematic limit, the sensitivity of the $Y(bb)H(bb)$ analysis is reduced because the Lorentz boost of the Y boson rest frame is too small for the fragmentation products of the two b quarks to merge into a single jet.

The three analyses are statistically combined as described in Section 2.6, and the resulting expected and observed limits are shown in Figs. 29 and 30. Covering the full mass grid, however,

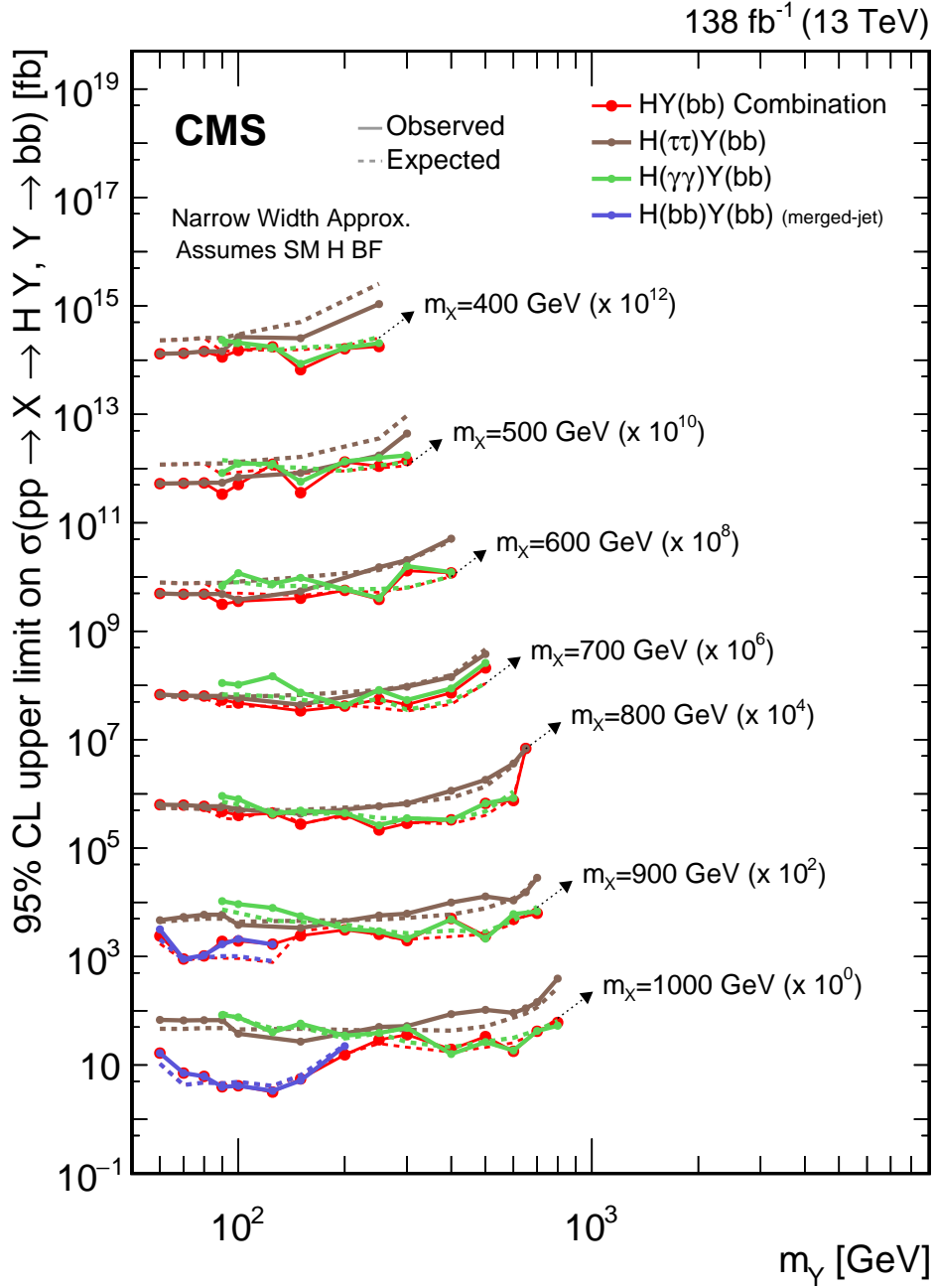


Figure 29: Search for $X \rightarrow YH$: Observed and expected upper limits, at 95% CL, on the product of the cross section σ for the production of a resonance X via gluon-gluon fusion and the branching fraction \mathcal{B} for the $X \rightarrow Y(bb)H$ decay. For the branching fractions of the $H \rightarrow \tau\tau$, $H \rightarrow \gamma\gamma$ and $H \rightarrow bb$ decays, the SM values are assumed. The results derived from the individual analyses presented in this report and the result of their combined likelihood analysis are shown as functions of m_Y and m_X for $m_X \leq 1$ TeV. Observed limits are indicated by markers connected with solid lines, expected limits by dashed lines. For presentation purposes, the limits have been scaled in successive steps by two orders of magnitude, each. For each set of graphs, a black arrow points to the m_X related legend.

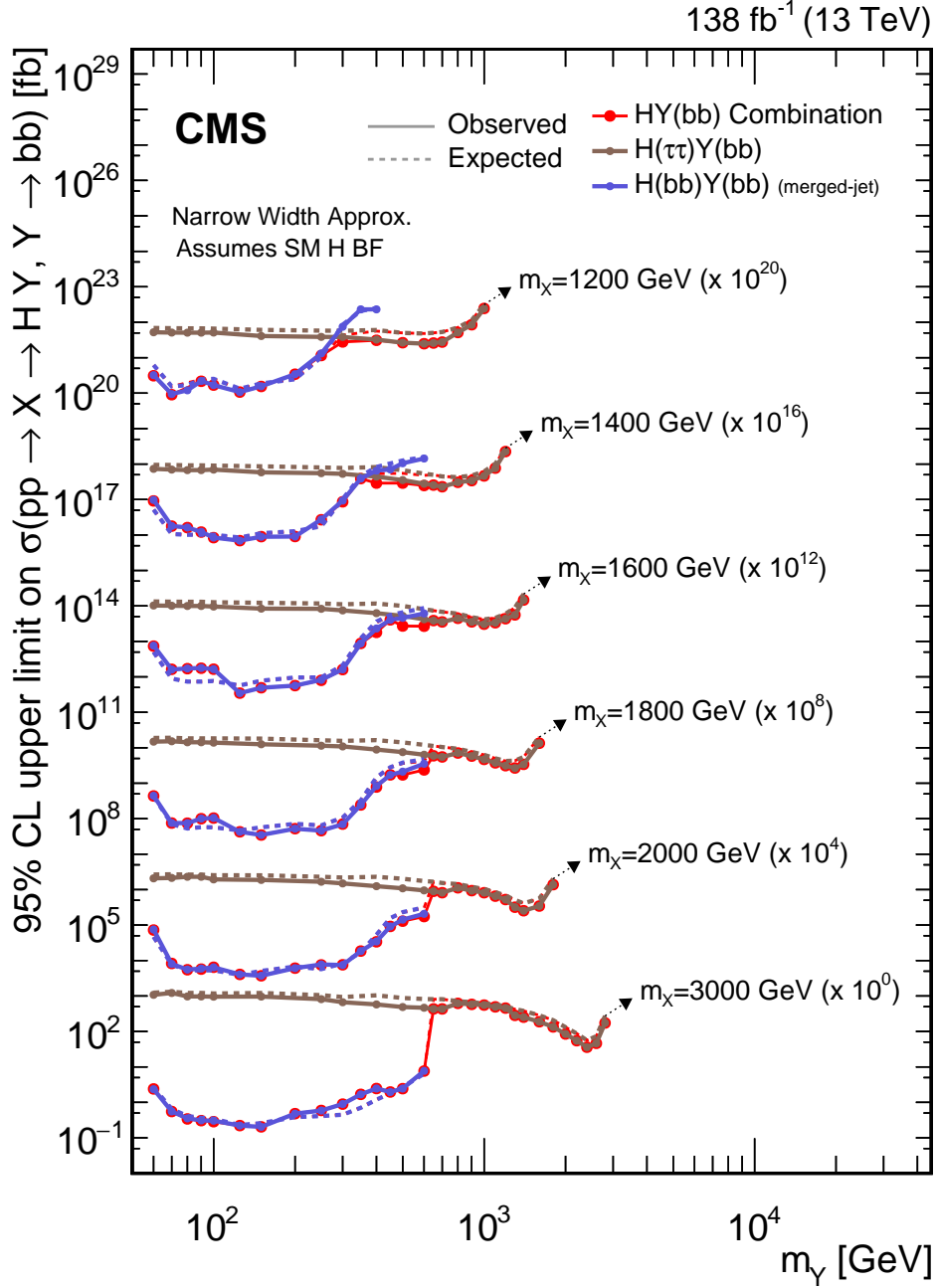


Figure 30: Search for $X \rightarrow YH$: Observed and expected upper limits, at 95% CL, on the product of the cross section σ for the production of a resonance X via gluon-gluon fusion and the branching fraction \mathcal{B} for the $X \rightarrow Y(bb)H$ decay. For the branching fractions of the $H \rightarrow \tau\tau$ and $H \rightarrow bb$ decays, the SM values are assumed. The results derived from the individual analyses presented in this report and the result of their combined likelihood analysis are shown as functions of m_Y and m_X for $m_X \geq 1.2$ TeV. Observed limits are indicated by markers connected with solid lines, expected limits by dashed lines. For presentation purposes, the limits have been scaled in successive steps by four orders of magnitude, each. For each set of graphs, a black arrow points to the m_X related legend.

is beyond the scope of this Report. This combination is shown as an example for the given mass points, and a separate publication in the near future will include a full combination featuring a larger set of decay modes. The typical exclusion upper limits on $\sigma\mathcal{B}$ are about 50, 5, and 0.3 fb for $m_\chi = 0.5, 1$, and 3 TeV, respectively. No excess larger than two s.d. above the expected limit is observed at any of these mass points. A two-dimensional representation of the experimental limits in the (m_χ, m_γ) parameter space is shown as part of the interpretation in Section 4.1.3.

4 Model-specific interpretation

We interpret the results of the individual searches and their combinations in specific models. The interpretations highlight the coverage of the analyses in the corresponding parameter space and show which regions are excluded by the current data. The first three subsections address how the measurements can constrain the parameter space of models with an extended Higgs sector, warped extra dimensions, and in a HVT framework. Section 4.4 is dedicated to studies going beyond the narrow-width approximation (NWA), where we investigate the effects of non-negligible resonance widths and interference.

4.1 Extended Higgs sector models

4.1.1 The MSSM

The decays $X \rightarrow HH$ and $A \rightarrow ZH$ can have sizable branching fractions in models with two complex Higgs doublets. However, as discussed previously, the branching fractions get suppressed when approaching the alignment limit, where the H boson becomes SM-like. Searches for HH and ZH can nonetheless set important constraints in these models, in particular at low to intermediate values of $\tan\beta$, and for masses below or near the $t\bar{t}$ threshold, $m_{X/A} \lesssim 350$ GeV.

Figure 31 shows exclusion regions in the $(m_A, \tan\beta)$ plane of the hMSSM [64–66, 69]. For this and the following model interpretations, the version numbers of the corresponding tools are documented in Ref. [69]. The branching fractions are obtained with HDECAY [178, 179]. The gluon fusion cross section is obtained with SUSHI [180, 181], which includes higher-order QCD corrections [182–188] and EW effects from light quarks [189, 190]. The $X \rightarrow HH$ searches result in an exclusion for $\tan\beta \lesssim 6$ for m_A just above the HH production threshold of 250 GeV, decreasing to $\tan\beta \lesssim 1$ for $m_A \approx 600$ GeV. This is complementary to the exclusion regions from searches for fermionic decays, such as $A \rightarrow \tau\tau$, which exclude regions of large $\tan\beta$. The $A \rightarrow ZH$ search in the $H \rightarrow \tau\tau$ channel provides sensitivity for $220 < m_A < 350$ GeV and excludes regions below $\tan\beta = 3.6$ for $m_A \lesssim 330$ GeV. Compared to other direct searches, there is a unique sensitivity of the $X \rightarrow HH$ searches for $m_A \gtrsim 450$ GeV and $\tan\beta < 5$. At the same time, the constraints derived from the measurements of the H boson couplings are somewhat more stringent, albeit these place only indirect constraints on this model.

The frequently used M_h^{125} benchmark model is not very suitable for interpretations of results from $X \rightarrow HH$ searches as these exclude regions at low $\tan\beta$ where the SM-like scalar has a mass inconsistent with 125 GeV and thus with the observed H boson. Instead, we choose to interpret these results in the $M_{h,\text{EFT}}^{125}$ scenario [67, 69]. Higgs boson masses and mixings are obtained with FEYNHIGGS [15, 191–197]. The branching fraction calculations make use of both FEYNHIGGS, HDECAY, and PROPHECY4F [198, 199]. The cross section for gluon fusion production is obtained from the same tools and predictions as in the hMSSM scenario. The resulting exclusion regions in the $(m_A, \tan\beta)$ plane are shown in Fig. 32. In this scenario, the parameter regions excluded by the HH combination are found not to be in conflict with the measured H boson mass. For $m_A \gtrsim 400$ GeV the results from the combination provide unique

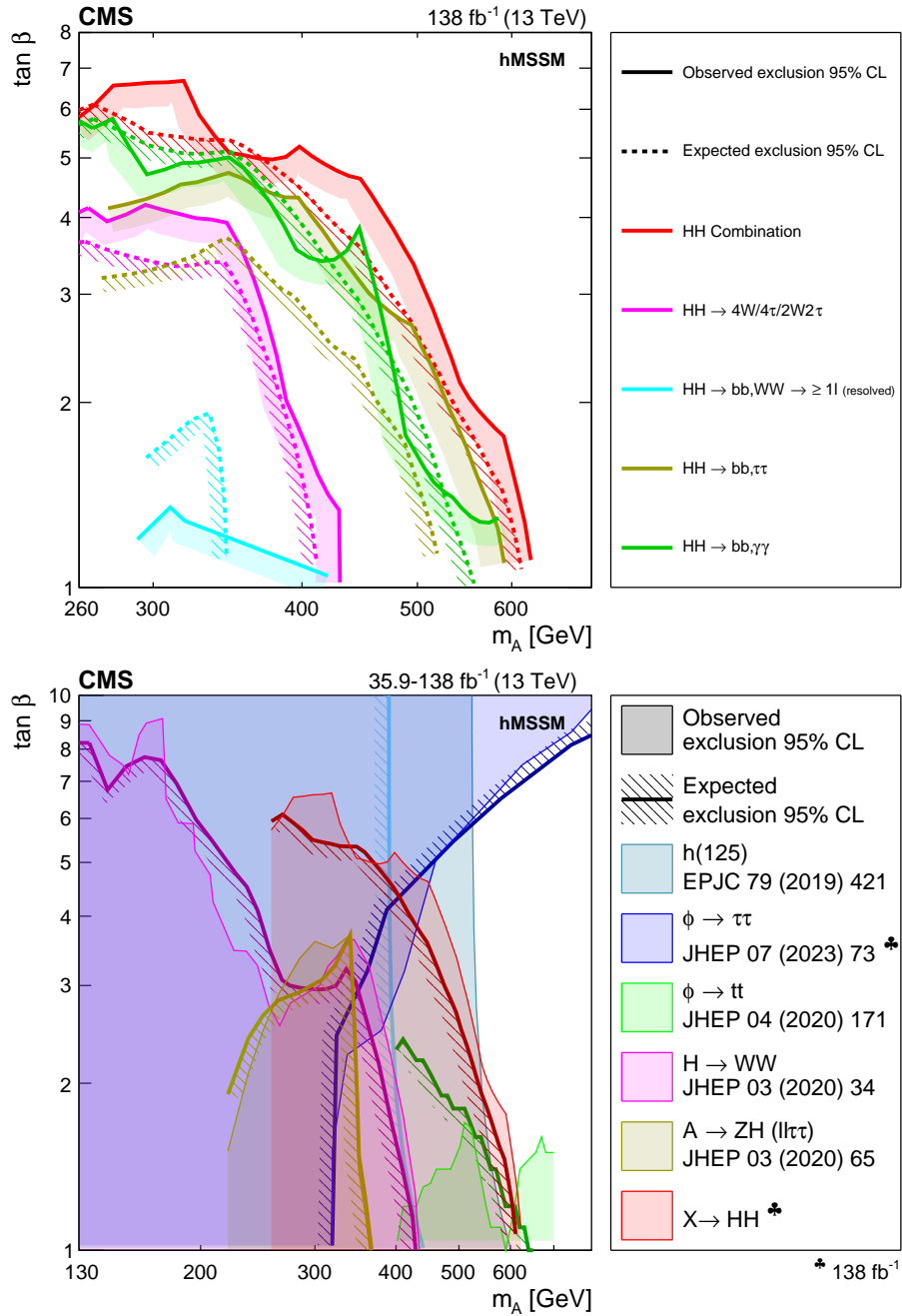


Figure 31: Interpretation of the results from the searches for the $X \rightarrow HH$ decay, in the hMSSM model. In the upper part of the figure, the observed and expected exclusion contours at 95% CL, in the $(m_A, \tan \beta)$ plane, from the individual HH analyses presented in this report and their combined likelihood analysis are shown. In the lower part of the figure, a comparison of the region excluded by the combined likelihood analysis shown in the upper part of the figure with selected results from other searches for the production of heavy scalar bosons in the hMSSM, in $\tau\tau$ [71], $t\bar{t}$ [176] and WW [177] decays is shown. Also shown, are the results from one representative search for $A \rightarrow ZH$ [114] and indirect constraints obtained from measurements of the coupling strength of the observed H boson [50]. Results not marked by a club symbol are based on an integrated luminosity of 35.9 fb $^{-1}$.

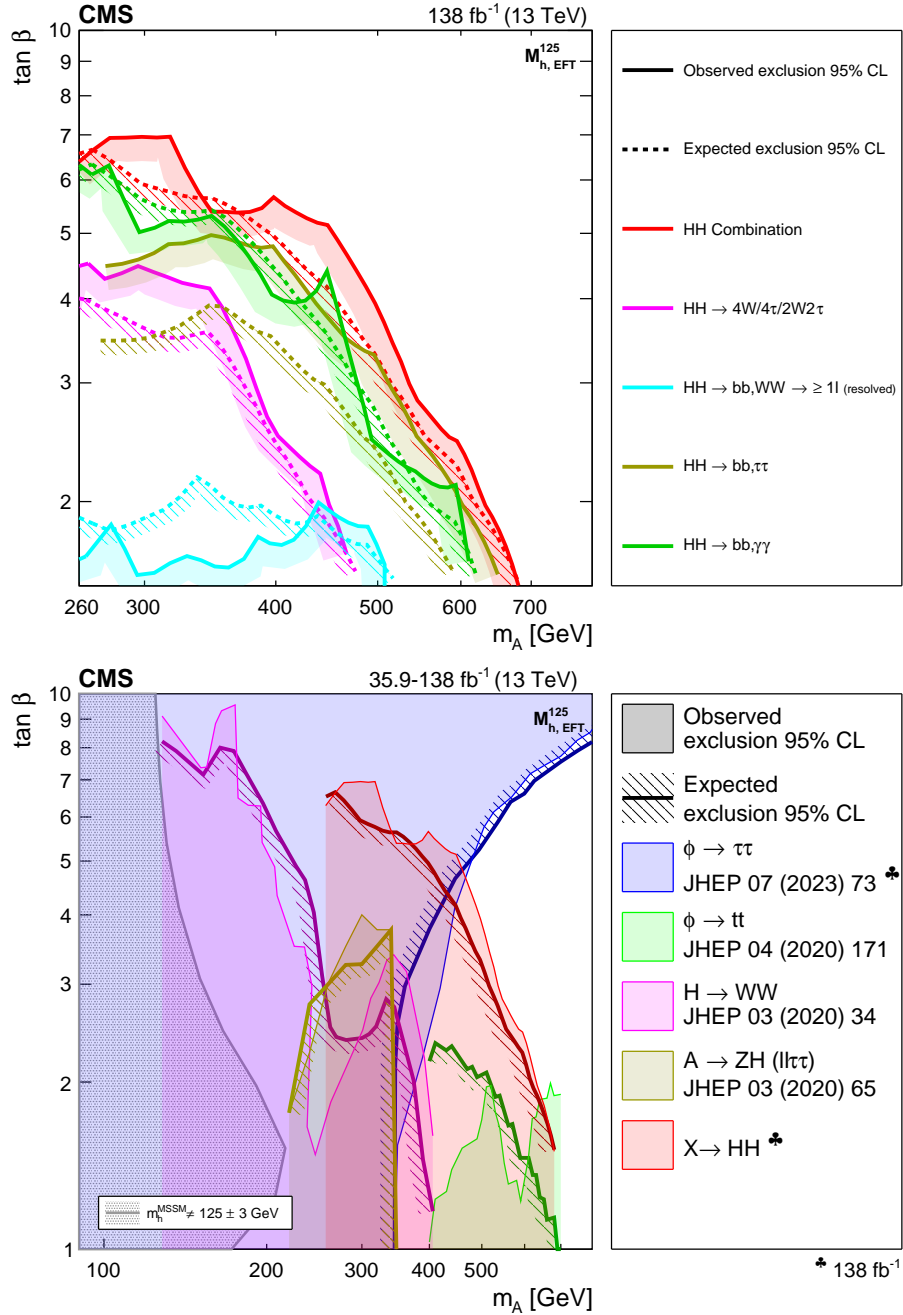


Figure 32: Interpretation of the results from the searches for the $X \rightarrow HH$ decay, in the $M_{h,EFT}^{125}$ benchmark scenario. In the upper part of the figure, the observed and expected exclusion contours at 95% CL are shown, in the $(m_A, \tan \beta)$ plane from the individual HH analyses presented in this report and their combined likelihood analysis. In the lower part of the figure, a comparison of the region excluded by the combined likelihood analysis shown in the upper part of the figure with selected results from other searches for the production of heavy scalar bosons in the $M_{h,EFT}^{125}$ scenario, in $\tau\tau$ [71], $t\bar{t}$ [176] and WW [177] decays is shown. Also shown, are the results from one representative search for $A \rightarrow ZH$ [114]. The parameter region in which the mass of the lightest MSSM Higgs boson does not coincide with 125 GeV within a 3 GeV margin is indicated by the dark hatched area. Results not marked by a club symbol are based on an integrated luminosity of 35.9 fb⁻¹.

exclusions. Otherwise, the overall picture is similar to the hMSSM scenario.

4.1.2 The 2HDM

Exclusion limits in the 2HDM are derived from the results of the search for $A \rightarrow ZH(bb)$ [115]. The 2HDM cross sections and branching fractions are computed with 2HDMC [62] and SUSHi, respectively. The light H boson mass is set to 125 GeV and $m_\chi = m_{H^\pm} = m_A$ is used. The Z boson branching fractions are set to the measured values [48]. Figure 33 shows the constraints in the $(\tan \beta, \cos(\beta - \alpha))$ plane for $m_A = 300$ GeV [115]. The search excludes nearly the whole region of low $\tan \beta$ in all four 2HDM scenarios, except for a narrow region around $\cos(\beta - \alpha) = 0$ for which the branching fraction goes to zero, another narrow region at negative $\cos(\beta - \alpha)$ for the Type I and lepton-specific scenarios, and at positive $\cos(\beta - \alpha)$ for the other two scenarios. At high $\tan \beta$, the excluded region widens in the Type II and flipped scenarios, whereas there is no sensitivity in the Type I and lepton-specific scenarios because the production cross section for the A boson becomes too small.

4.1.3 The NMSSM and TRSM models

The searches for $X \rightarrow YH$ decays are interpreted in the NMSSM and TRSM models. In both models, there are various free parameters besides the masses of the additional X and Y bosons that affect the cross sections and branching fractions. To check whether the searches are sensitive to a point in the (m_X, m_Y) plane, a parameter scan is performed to determine the maximally allowed cross section, taking all previous constraints on the models into account.

In the NMSSM case, we obtain the maximally allowed cross section values for $\sigma(X \rightarrow YH \rightarrow bbbb)$ from the scans in Ref. [200], which are based on version 5.6.2 of the program NMSSM-TOOLS [200, 201]. These numbers are divided by the corresponding branching fraction $\mathcal{B}(H \rightarrow bb)$ to obtain an approximation for the maximally allowed values of $\sigma(X \rightarrow Y(bb)H)$. Uncertainties arising from the precision of the measured branching fractions of the H boson are neglected.

Figure 34 shows the observed and expected upper limits at 95% CL on $\sigma\mathcal{B}$ of the combined $X \rightarrow YH$ searches (upper panel), together with the maximally allowed model values (lower panel). While the experimental limits appear to touch the model predictions in several places, there is not much additional exclusion. This is expected because many relevant measurements, including the CMS searches for $X \rightarrow Y(bb)H(\tau\tau)$ and $X \rightarrow Y(bb)H(bb)$ presented in this article, are already accounted for in this version of NMSSMTOOLS, which lowers the maximally allowed NMSSM cross sections correspondingly. Therefore, no new constraints are expected from these channels compared to those in the original publications [123, 124, 167].

Comparisons of the measured limits for $X \rightarrow Y(bb)H(bb)$ in merged final states with the maximally allowed TRSM values can be found in Ref. [124]. The measurement excludes part of the allowed TRSM parameter space in a wedge-shaped region between $m_X \approx 1000\text{--}1300$ GeV and around $m_Y \approx 125$ GeV. An interpretation of the $X \rightarrow Y(bb)H(\tau\tau)$ measurements within the TRSM benchmark planes can be found in Ref. [202].

4.1.4 The real-singlet extension

The additional scalar boson X predicted in the real-singlet model has the same relative couplings to SM particles as the SM H boson. Most searches for $X \rightarrow HH$ assume that the width of the X boson is much smaller than the reconstructed mass resolution, such that the NWA holds. We use the real-singlet model for a dedicated study of nonnegligible width and interference

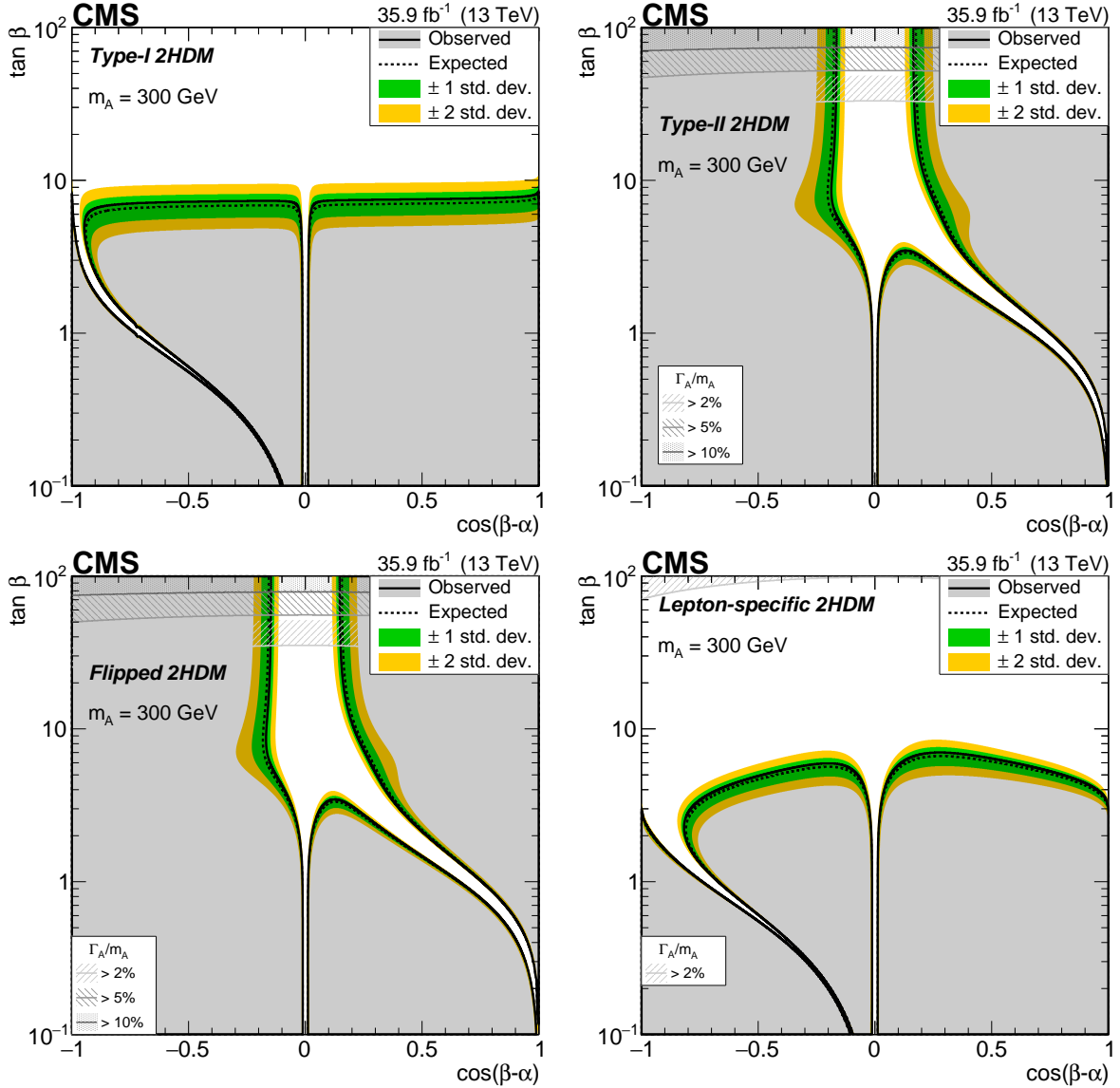


Figure 33: Interpretation of the results of the $A \rightarrow ZH(bb)$ analysis [115], in the (upper left) Type I, (upper right) Type II, (lower left) flipped, and (lower right) lepton-specific 2HDM models. In each case observed and expected exclusion contours at 95% CL, in the plane defined by $\cos(\beta - \alpha)$ and $\tan \beta$, are shown. The excluded regions are represented by the shaded gray areas. The 68 and 95% central intervals of the expected exclusion contours in the absence of a signal are indicated by the green and yellow bands. Contours are derived from the projection on the corresponding 2HDM parameter space for $m_A = 300$ GeV. The regions of parameter space where the natural width of the A boson Γ_A is comparable to or larger than the experimental resolution and thus the narrow-width approximation is not valid are represented by hatched gray areas. Figure from Ref. [115].

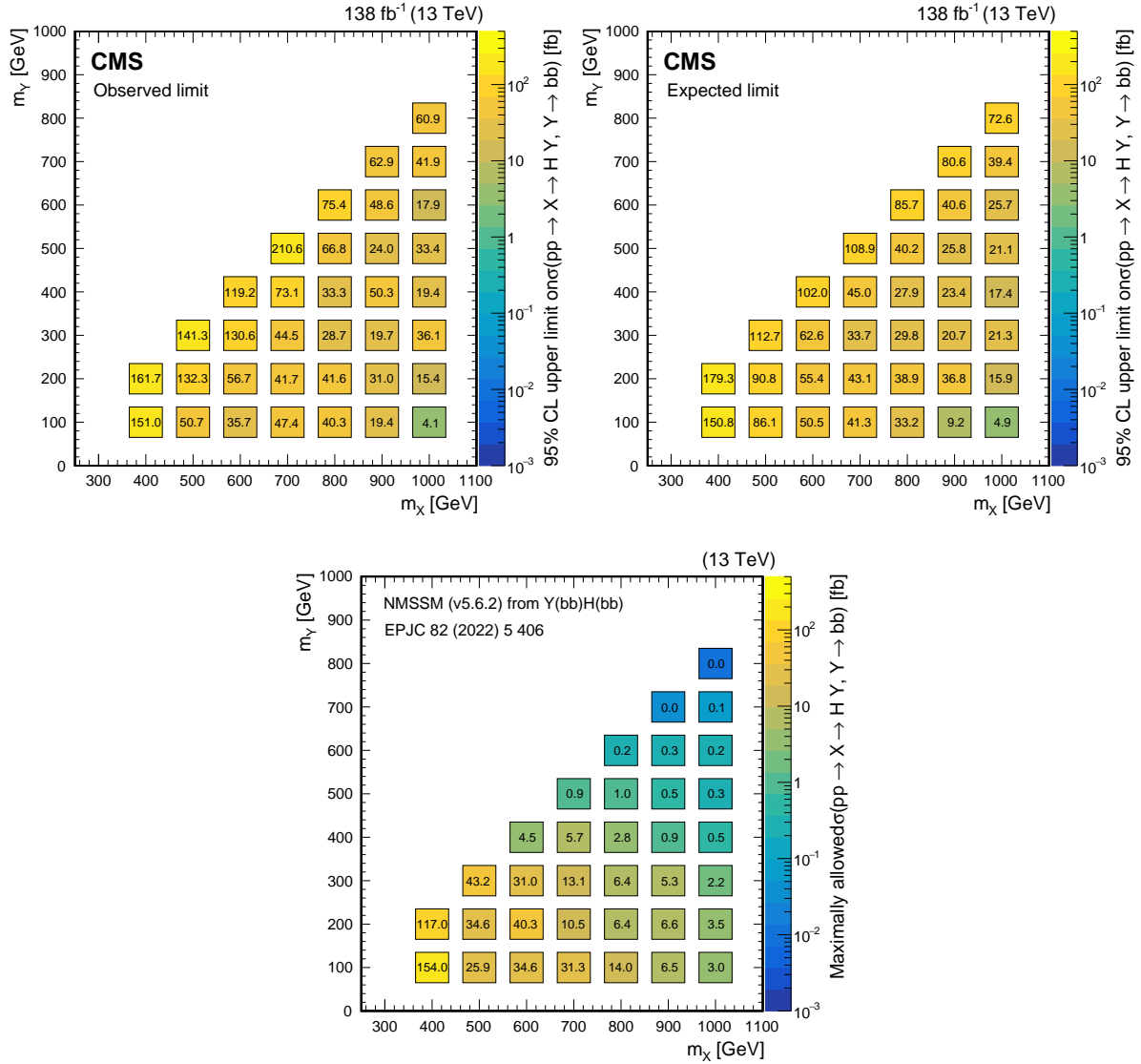


Figure 34: (Upper left) Observed and (upper right) expected upper limits at 95% CL, on the product of the cross section σ for the production of a resonance X via gluon-gluon fusion and the branching fraction \mathcal{B} for the $X \rightarrow Y(bb)H$ decay, as obtained from a combined likelihood analysis of the individual analyses presented in this report and shown in Fig. 29. The results are presented in a plane defined by m_X and m_Y . The limits have been evaluated in discrete steps corresponding to the centers of the boxes. The numbers in the boxes are given in fb. The corresponding maximally allowed values of $\sigma\mathcal{B}$ in the NMSSM are also shown for comparison (lower plot), as adapted from Ref. [200].

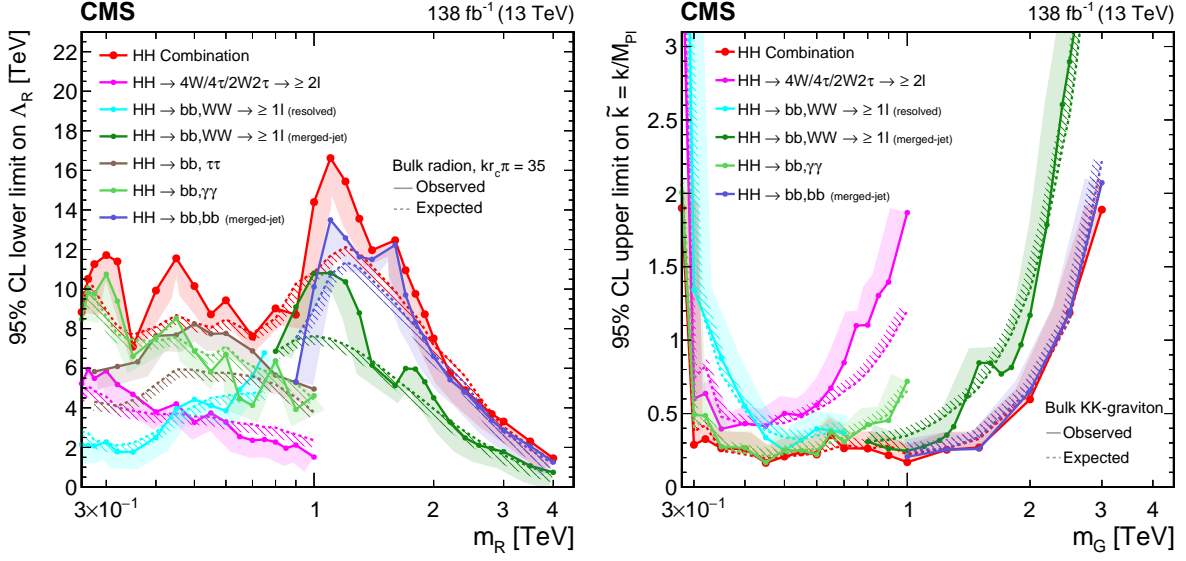


Figure 35: Observed and expected limits, at 95% CL, on the parameters of models with warped extra dimensions, as obtained from the $X \rightarrow HH$ analyses presented in this report and their combined likelihood analysis. Shown are lower limits (left) on the bulk radion ultraviolet cutoff parameter Λ_R , as a function of the radion mass m_R , and upper limits (right) on the parameter \tilde{k} of the spin-2 bulk graviton G , as a function of m_G . Excluded areas are indicated by the direction of the hatching along the exclusion contours.

effects and present the results in Section 4.4. The corresponding model interpretations for the $X \rightarrow HH$ combination in the real-singlet model are presented there.

4.2 Warped extra dimensions

The measured upper limits on resonant HH production can also be interpreted in the context of WED models (as discussed in Section 1.2.2). Figure 35 (left) shows the lower limit on the bulk radion ultraviolet cutoff parameter Λ_R as a function of the radion mass m_R for all presented HH analyses and their combination. The individual analyses with the best sensitivity are from the searches of $X \rightarrow H(bb)H(\gamma\gamma)$ for $m_X \lesssim 1$ TeV, and $X \rightarrow H(bb)H(bb)$ for $m_X \gtrsim 1$ TeV. In the regions $0.5 \lesssim m_X \lesssim 1$ TeV and $1 \lesssim m_X \lesssim 1.5$ TeV, the $X \rightarrow H(bb)H(\tau\tau)$ and $X \rightarrow H(bb)H(WW)$ analyses contribute significantly to the combination. In the mass region below 1 TeV, the expected lower limit from the combination ranges from 8 to 10 TeV, with observed limits reaching up to 12 TeV. The strongest exclusion limits of about 12 TeV expected and 16 TeV observed are reached near $m_R = 1.2$ TeV. The combination improves the sensitivity over the full mass range probed. Figure 35 (right) shows the corresponding upper limits of the parameter \tilde{k} of the spin-2 bulk graviton G . The combination excludes values of \tilde{k} larger than about 0.3 at 95% CL for the large mass range $0.3 < m_G < 1.5$ TeV.

We compare the limits obtained from the HH combination with limits from searches for $X \rightarrow ZZ$ [203–205] and $X \rightarrow WW$ [116, 118, 177] in Fig. 36. The HH combination is found to be very competitive, and it places stronger constraints on the WED models in some mass regions. For radions, shown on the left, the HH combination shows about the same sensitivity as the $Z(\ell\ell)Z(qq/\nu\nu/\ell\ell)$ final state [203] for $m_R \lesssim 1$ TeV. The HH combination has the best sensitivity in the region $1 < m_R < 2$ TeV, and for higher masses it has a comparable sensitivity as searches in final states from hadronic and semileptonic WW decays [116, 118]. For gravitons, the HH combination places the best upper limits on \tilde{k} for $250 < m_G < 450$ GeV and $700 < m_G < 2000$ GeV.

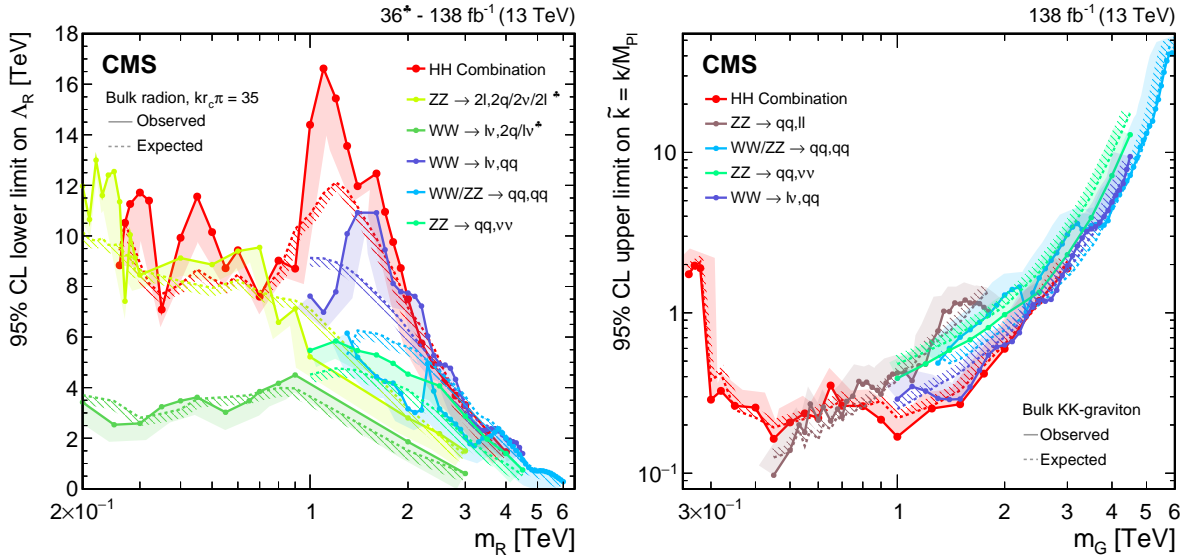


Figure 36: Observed and expected limits, at 95% CL, on the parameters of models with warped extra dimensions, as obtained from the combined likelihood analysis of the individual $X \rightarrow HH$ analyses presented in this report and shown in Fig. 35. The exclusion contours obtained from the combined likelihood analysis are compared to similar exclusions obtained from individual searches in the decays $Z(\ell\ell)Z(qq/\nu\nu/\ell\ell)$ [203], $W(\ell\nu)W(\ell\nu/qq)$ [177], $W(\ell\nu)W(qq)$ [116], $V(qq)V(qq)$ [118], and $Z(\nu\nu)Z(qq)$ [204], in case of the radion interpretation, and from individual searches in the decays $Z(qq)Z(\ell\ell)$ [205], $V(qq)V(qq)$ [118], $Z(\nu\nu)Z(qq)$ [204], and $W(\ell\nu)W(qq)$ [116], in the case of the graviton interpretation. Excluded areas are indicated by the direction of the hatching along the exclusion contours.

4.3 Heavy vector triplet models

The three searches for $X \rightarrow VH$ introduced in Section 2.3 probe for a new vector boson V' (either W' or Z') in final states with 0, 1, and 2 leptons. The resulting upper limits on $\sigma\mathcal{B}$ presented in Section 3.1 are now interpreted in the HVT model. The theoretical cross sections are calculated at NLO in QCD with the models detailed in Ref. [28, 30]. The theory predictions with the corresponding $\mathcal{B}(W' \rightarrow WH)$ and $\mathcal{B}(Z' \rightarrow ZH)$ in the models A, B, and C, where couplings of V' to bosons are enhanced, have been shown in Figs. 25 and 26. The upper limits on $\sigma\mathcal{B}$ are translated into lower limits on the vector boson masses. The W' and Z' masses are excluded up to 4.1 and 3.9 TeV, respectively, in model B interpretations.

Figure 37 shows the upper limits on the DY production cross section of V' in the WH and ZH channels, compared to those obtained from VV [116, 118, 204, 205] and fermion pair production channels [206–209] assuming branching fractions of the HVT models A and B. The corresponding theory predictions are overlaid. The all-jets channels are sensitive to both W' and Z' production and are thus interpreted in combined V' production. While in model A, searches for fermion pair production dominate the sensitivity, in model B, where couplings of V' to bosons are large, the VV and VH searches are most sensitive.

For four resonance mass hypotheses, the cross section exclusion limits from DY production are translated into two-dimensional upper limits on the coupling parameters for fermions and bosons of the HVT model. Figure 38 shows only the constraints from VH production, while Fig. 39 includes also VV and fermion pair production channels for comparison. The constraints from VH searches are most stringent, apart from the region with small boson couplings, where the complementary searches with fermion final states provide stronger constraints.

In model C, where the V' is produced exclusively via VBF, the data set is not sufficient to exclude couplings below $g_H = 3$ in any range of $m_{V'}$. The corresponding results are shown in Fig. 40.

4.4 Effects of finite width and interference in resonant HH production

Most of the HH and YH analyses performed by the CMS Collaboration make use of the NWA, where the width of BSM particles is neglected and no interference with nonresonant Higgs boson pair production occurs. However, in general, interference effects can strongly impact the HH cross section [210, 211]. The interference can be either constructive or destructive, enhancing or decreasing the HH production rate [212, 213], and have a nonnegligible effect in BSM exclusion limits. We study the impact of the interference between nonresonant and resonant production in the inclusive $pp \rightarrow HH$ production, which can receive contributions from resonant $X \rightarrow HH$ production. This work provides the first measure of interference effects, identifying phase space regions where the NWA is valid. We use as a benchmark a simplified scenario based on the real-singlet model introduced in Section 1.2.1, as it includes the smallest number of additional free parameters [214]. We note that interference effects are model dependent and may be different for other BSM scenarios.

For this specific study, we modify the singlet model by not imposing the \mathbb{Z}_2 symmetry. The \mathbb{Z}_2 symmetry precludes terms of odd powers of the additional singlet scalar field, which are known to be responsible for a stronger first-order EW phase transition [215, 216]. Exploiting EW symmetry breaking on the singlet model scalar potential, we are left with two mixing states. After mass diagonalization, the identification of one of the states with the SM H boson reduces the number of uncorrelated parameters further from seven to five. The other state is

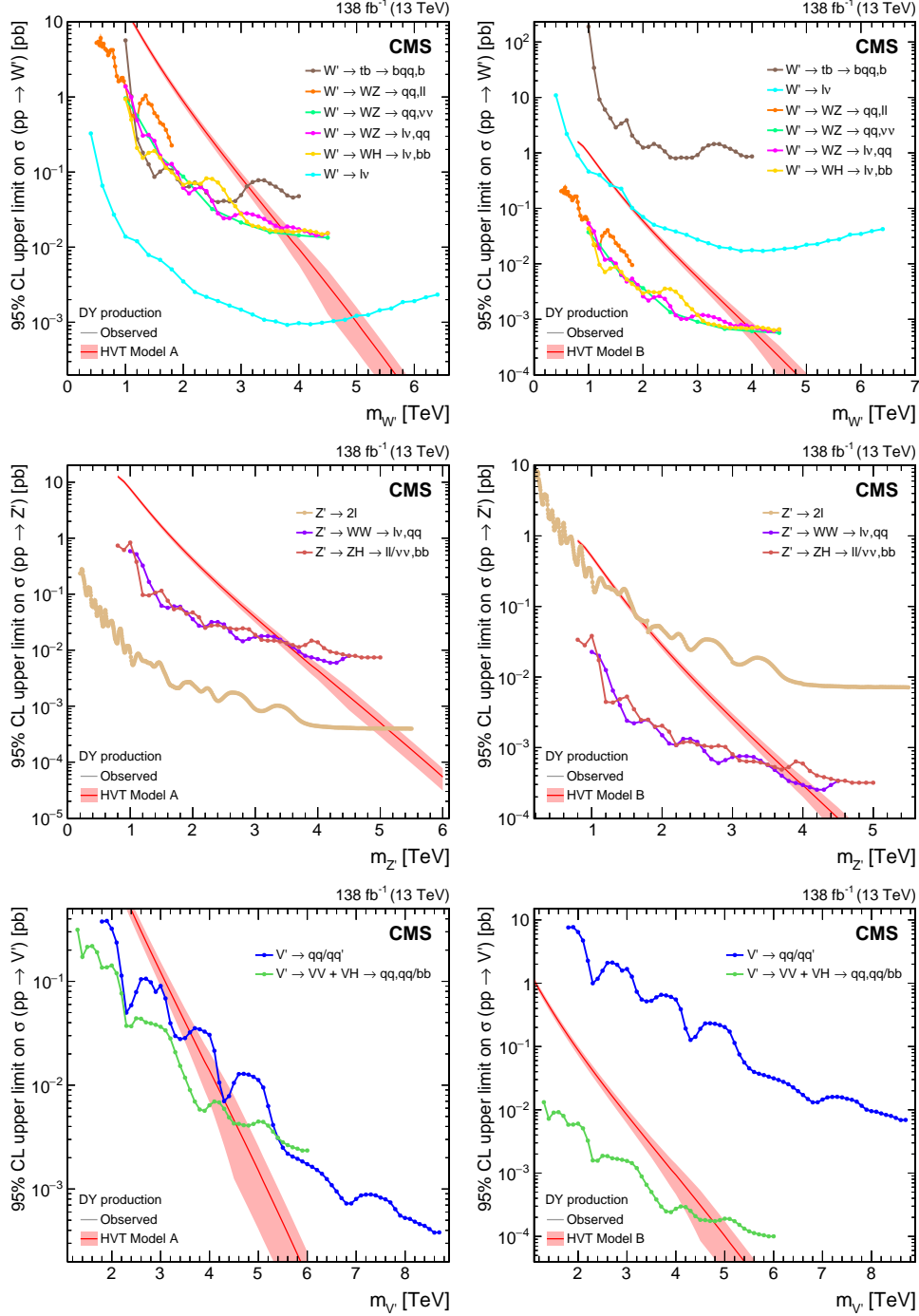


Figure 37: Observed upper limits, at 95% CL, on the Drell–Yan production cross section of (upper) W' , (middle) Z' , and (lower) combined V' spin-1 resonances assuming branching fractions of the heavy vector triplet models (left) A and (right) B. The theory predictions from these models are also shown. Results from the VH [116–118] and VV channels [116, 118, 204, 205], as well as results from dijet [209], $t\bar{b}$ [207], $\ell\bar{\ell}$ [206], and $\ell\nu$ [208] final states are shown for comparison.

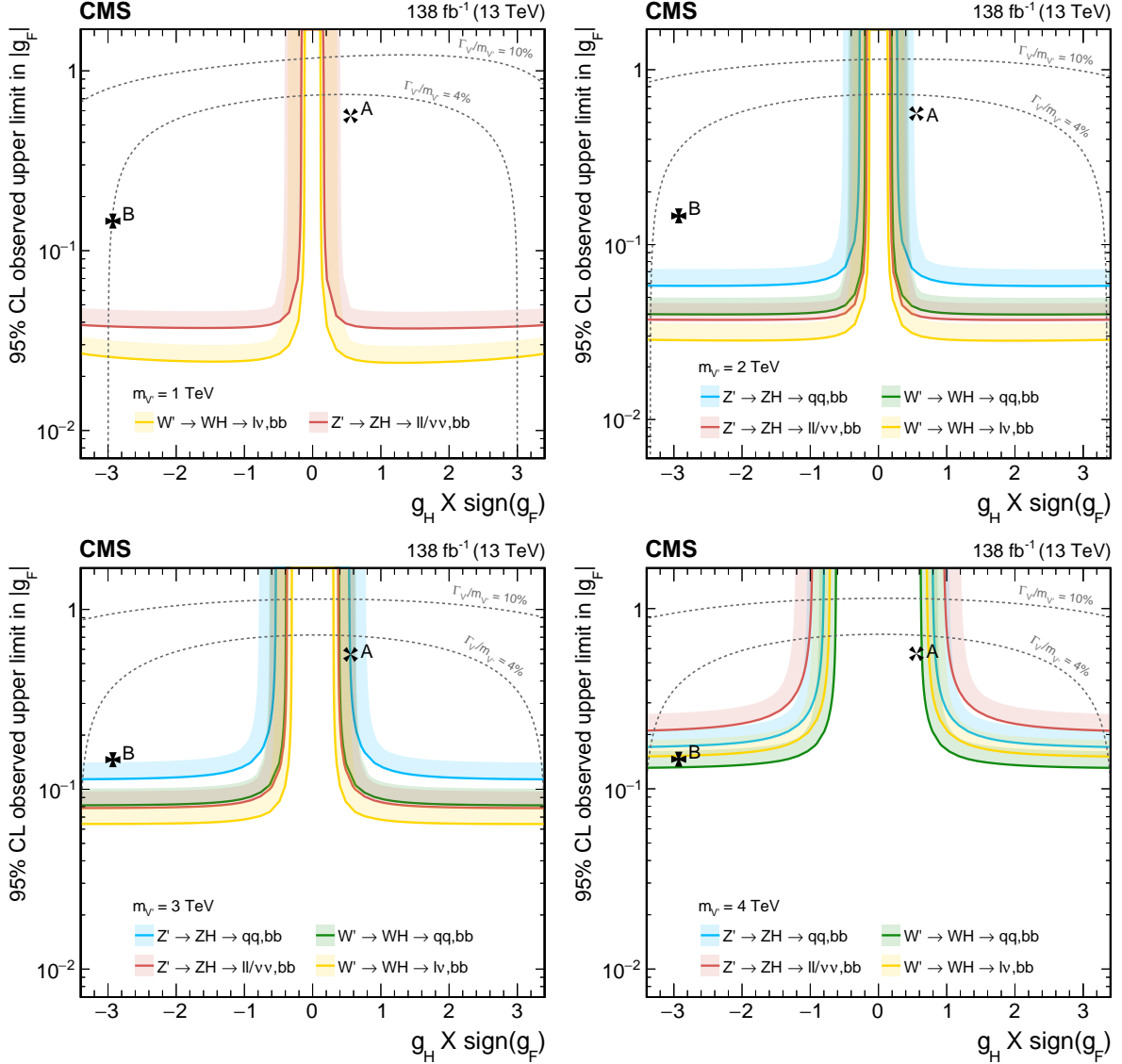


Figure 38: Observed upper limits, at 95% CL, on the V' couplings g_F and g_H within the HVT model for V' masses of (upper left) 1, (upper right) 2, (lower left) 3, and (lower right) 4 TeV, from DY production, derived from VH channels of Refs. [116–118] discussed in this report. Excluded areas are indicated by the direction of the shading along the exclusion contours. The dotted lines denote coupling values above which the relative width of the resonance, $\Gamma_{V'}/m_{V'}$, exceeds 4 and 10%. These dotted lines are to be compared with the experimental resolution to identify where the narrow width approximation no longer applies. The experimental resolution in final states with jets decreases as a function of resonance mass from 7% at 1 TeV to as low as 4% at 4 TeV. The couplings corresponding to the heavy vector triplet models A and B are indicated by cross markers.

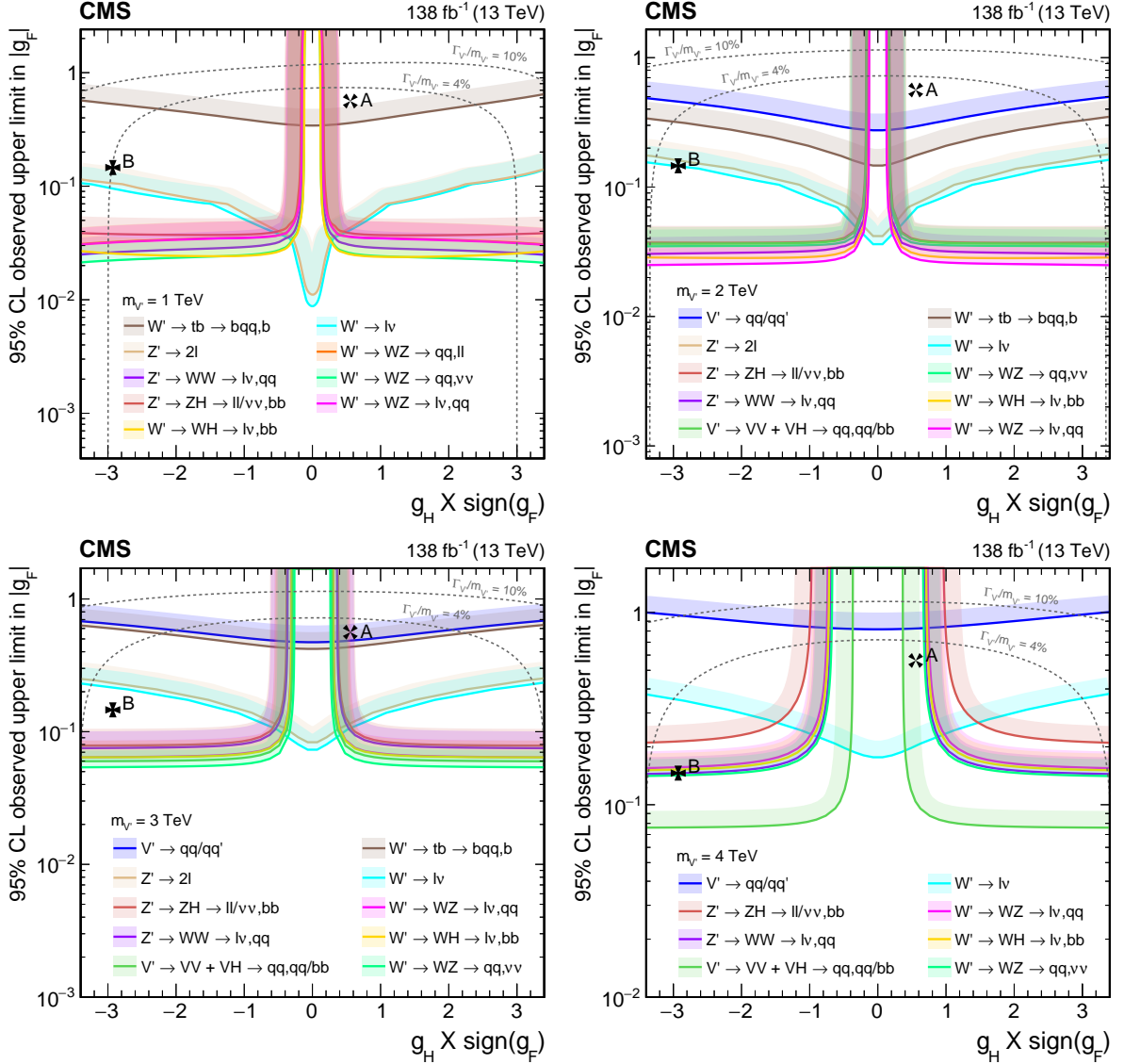


Figure 39: Observed upper limits, at 95% CL, on the V' couplings g_F and g_H within the HVT model for V' masses of (upper left) 1, (upper right) 2, (lower left) 3, and (lower right) 4 TeV, from DY production, derived from VH channels of Refs. [116–118] discussed in this report and the VV channels of Refs. [116, 118, 204, 205], as well as results from dijet [209], tb [207], $\ell\ell$ [206] and $\ell\nu$ [208] final states. Excluded areas are indicated by the direction of the shading along the exclusion contours. The dotted lines denote coupling values above which the relative width of the resonance, $\Gamma_{V'}/m_{V'}$, exceeds 4 and 10%. These dotted lines are to be compared with the experimental resolution to identify where the narrow width approximation no longer applies. The experimental resolution in final states with jets decreases as a function of resonance mass from 7% at 1 TeV to as low as 4% at 4 TeV. The couplings corresponding to the heavy vector triplet models A and B are indicated by cross markers.

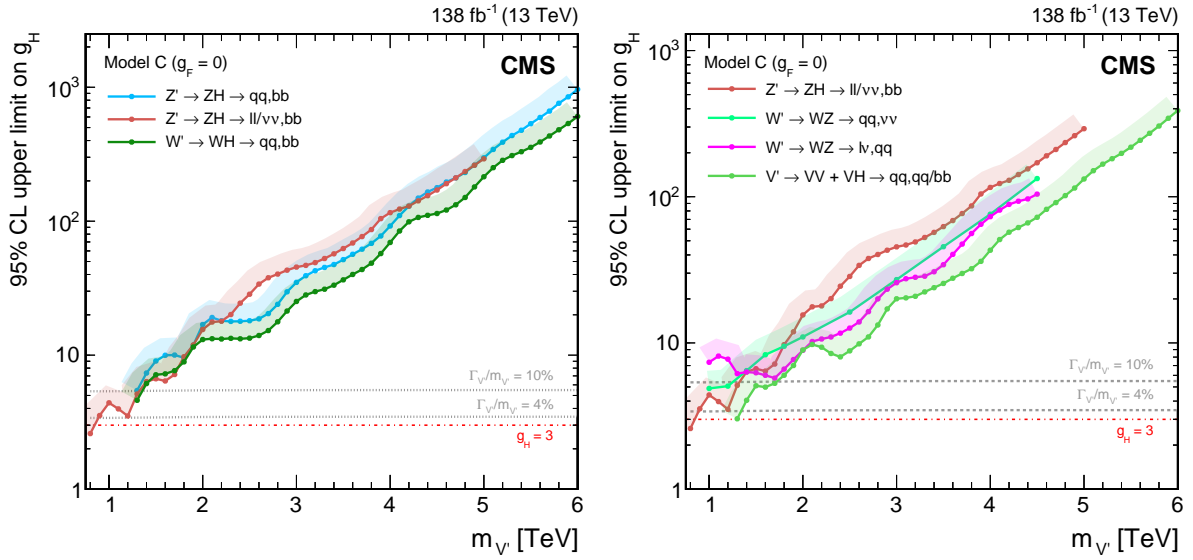


Figure 40: Observed upper limits, at 95% CL, on the coupling g_H within the heavy vector triplet model, as a function of the V' mass. The limits are shown for the vector boson fusion production mode in the context of model C, in which $g_F = 0$. The results are shown (left) for the WH and ZH analyses of Refs. [116–118], individually, and for a combination with the WZ final states of Refs. [116, 118, 204] (right), where the WH and ZH results from all-hadronic final states have been combined with the corresponding VV channels. The dotted lines denote coupling values above which the relative width of the resonance, $\Gamma_{V'}/m_{V'}$, exceeds 4 and 10%. These dotted lines are to be compared with the experimental resolution to identify where the narrow width approximation no longer applies. The experimental resolution in final states with jets decreases as a function of resonance mass from 7% at 1 TeV to as low as 4% at 4 TeV.

associated with a new particle X. The couplings of the H boson and the X particle are given by

$$g_{Hkk} = g_{Hkk}^{\text{SM}} \cos \alpha \quad \text{and} \quad g_{Xkk} = -g_{Hkk}^{\text{SM}} \sin \alpha, \quad (11)$$

where α is the mixing angle, and k represents any SM particle. For $m_X > 2m_H$ the width of the X resonance can be calculated as

$$\Gamma_X = \sin^2 \alpha \Gamma^{\text{SM}}(m_X) + \frac{\lambda_{\text{HHX}}^2 \sqrt{1 - 4m_H^2/m_X^2}}{8\pi m_X}, \quad (12)$$

where λ_{HHX} is the trilinear coupling between two H bosons and the new particle X, and $\Gamma^{\text{SM}}(m_X)$ represents the width of a scalar boson of mass m_X with the same decay modes as the SM H boson. The latter has been calculated by interpolating the values published in Ref. [35]. In addition to α , m_X and λ_{HHX} , this singlet model also depends on the trilinear H coupling modifier $k_\lambda \equiv \lambda_{\text{HHH}}/\lambda_{\text{HHH}}^{\text{SM}}$, and on an additional scalar coupling.

We use the MADGRAPH5_aMC@NLO generator version 2.9.7 [217], to simulate inclusive HH events in the singlet model at LO. A custom universal FEYNRULES [218] output (UFO) model based on Ref. [215] adds a heavy scalar boson to the SM with couplings to SM particles as defined in Eq. (11). The samples are created according to the following parameter grid with $k_\lambda = 1$:

- m_X [GeV]: 280, 300, 400, 500, 600, 700, 800, 900, 1000,
- $\sin \alpha$: 0.00, 0.10, 0.20, 0.30, 0.40, 0.50, 0.60, 0.70, 0.80, 0.90, 0.95, 0.99,
- λ_{HHX} [GeV]: -600, -500, -400, -300, -200, -100, -50, 0, 50, 100, 200, 300, 400, 500, 600,

where m_X is chosen based on the signal samples used in the HH combination presented in Section 3.2. The resonant, nonresonant, and total cross sections for each combination of grid points are generated separately. We perform a parameter scan in the parameters m_X , $\sin \alpha$, and λ_{HHX} of the interference ratio defined as

$$R_{\text{int}} = \frac{\sigma^{\text{full}} - (\sigma^{\text{resonant-only}} + \sigma^{\text{nonresonant}})}{\sigma^{\text{resonant-only}} + \sigma^{\text{nonresonant}}}. \quad (13)$$

We obtain the nonresonant cross section by setting the coupling g_{Xkk} defined in Eq. (11) to zero, and the resonant-only cross section by setting the coupling g_{Hkk} to zero. The variable R_{int} provides information concerning the relative strength of the interference between the SM and BSM processes. The larger the deviation of R_{int} from zero, the stronger the modification of the cross section due to the interference. We consider the gluon fusion production mode due to its dominant contribution to the cross section. The UFO model and procedure are validated using the program HPAIR [213, 219] where the results varying k_λ in the nonresonant scenario are found to agree with the NLO predictions of Ref. [4].

Exact conclusions from this study naturally depend on the allowed size of R_{int} and the relative width Γ_X/m_X . In the following, we choose as benchmark points $R_{\text{int}} = \pm 10$ and $\pm 20\%$, and $\Gamma_X/m_X = 5, 10$ and 20% . The corresponding contours and exclusion limits derived from the HH combination in the singlet model are shown in Fig. 41.

Contours of positive (green) and negative (blue) interference ratios are shown as solid (for $R_{\text{int}} = \pm 10\%$) and dashed (for $R_{\text{int}} = \pm 20\%$) lines. They are found to swap positions at $m_X = 400$ GeV, likely because of the peak of the nonresonant HH distribution. The dotted

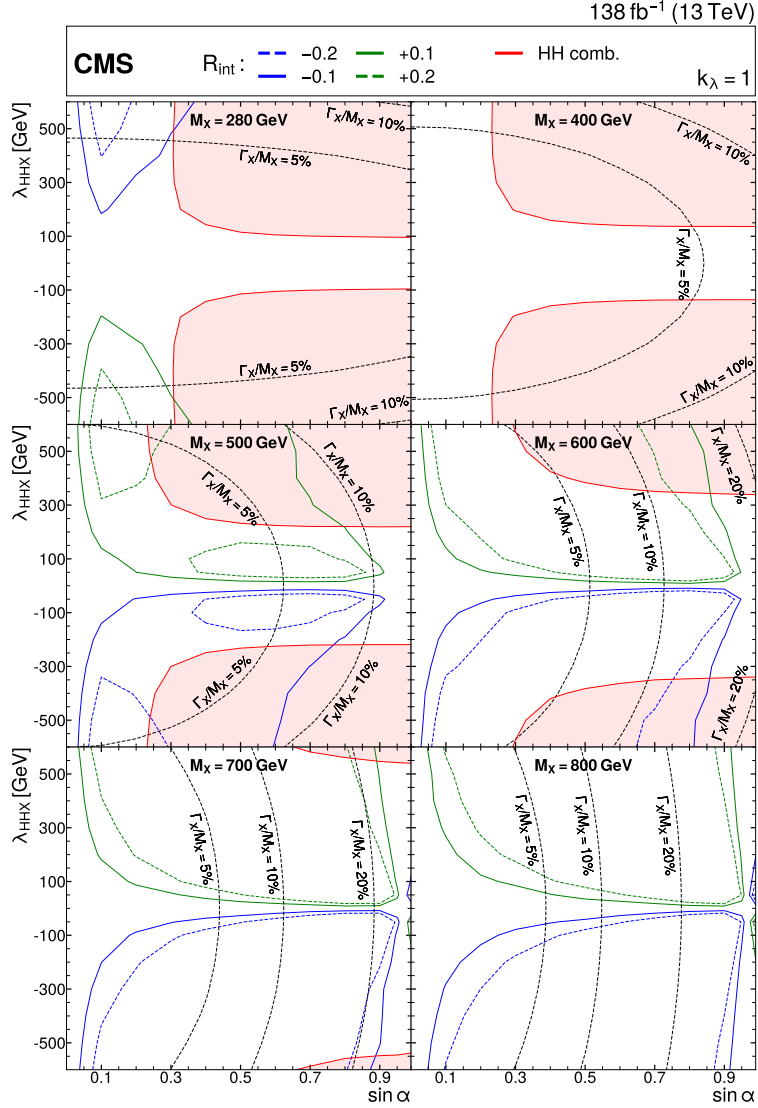


Figure 41: Contours of the variable R_{int} as defined in Eq. (13) and discussed in the text, in the $(\sin \alpha, \lambda_{\text{HHX}})$ plane for the singlet model with $k_\lambda = 1$ and different resonance masses m_χ between (upper left) 280 and (lower right) 800 GeV. Contours are shown for R_{int} values of (dashed blue) -0.2 , (solid blue) -0.1 , (solid green) $+0.1$, and (dashed green) $+0.2$. Regions that are excluded, at 95% CL, from the combined likelihood analysis of the HH analyses presented in this report are indicated by red filled areas. Dashed black lines indicate constant relative widths of 5, 10, and 20%.

lines denote coupling value combinations beyond which the relative width of the resonance, Γ_X/m_X , exceeds 5 and 10%, respectively, implying the narrow width approximation not being accurate anymore. For a given m_X , the quadratic dependence of Γ_X on both $\sin \alpha$ and λ_{HHX} according to Eq. (12) leads to elliptical isolines of constant Γ_X/m_X . The experimental bound from the HH combination discussed in Section 3.2 is obtained from the 95% CL upper limit on $\sigma(\text{pp} \rightarrow \text{X})\mathcal{B}(\text{X} \rightarrow \text{HH})$, with the X production cross section growing with increasing $\sin \alpha$, and $\mathcal{B}(\text{X} \rightarrow \text{HH})$ growing with increasing λ_{HHX} . We note that large values of $\sin \alpha$, corresponding to regions where the H boson is less SM-like, also tend to be excluded by precision measurements of the H boson [215].

For most of the studied mass points, sizable interference ratios occur only in parameter regions to which the current measurements are either not yet sensitive, or at too large values of $\sin \alpha$. In particular, for large resonance masses, where interference effects tend to grow, they are far below the current sensitivity and might only play a role when the full data set from HL-LHC becomes available [220], as discussed in Section 5.3. However, there are regions at intermediate m_X where the interpretation of NWA-based limits for HH derived in the singlet model would solicit some care already in the Run 2 combination (e.g., $m_X = 500$ GeV, $\sin \alpha = 0.2$ and $\lambda_{\text{HHX}} = 400$ GeV). It is important to note that such interpretations are generally model dependent.

The differential cross sections as a function of m_{HH} are shown for representative points from the $(\sin \alpha, \lambda_{\text{HHX}})$ parameter space in Fig. 42 for $m_X = 280$ GeV, and in Fig. 43 for $m_X = 500$ GeV. The parameters are chosen such that $\Gamma_X/m_X = 5\%$, which is well below the detector resolution for resonance masses below 1 TeV, and $R_{\text{int}} = \pm 10\%$ or $\pm 20\%$, so that sizable interference effects are expected. The lineshapes show points in parameter space where the R_{int} contours intersect with lines of constant $\Gamma_X/m_X = 5\%$ in Fig. 41.

The mass points of $m_X = 280$ and 500 GeV have been chosen because these values are on the left- and right-hand side of the peak in the m_{HH} distribution for nonresonant SM HH production. The total signal contribution of the resonance, including the interference effect, can be assessed as the difference between σ^{full} (red graph) and $\sigma^{\text{nonresonant}}$ (green graph). In the $m_X = 280$ GeV case, the resonance peak is at a mass where the non-resonant background is low in comparison; hence the central part of the peak is not much affected in its shape, and a classical bump hunt should still work. However, the total cross section is modified as specified by R_{int} . For a precision measurement, which is not yet in our reach, a distortion of the signal shape, either a peak-dip or peak-tail pattern depending on the relative sign of the amplitudes, would have to be taken into account. At $m_X = 500$ GeV, in the top panels of Fig. 43, the signal shape is found to be strongly modified by the interference effect. However, this occurs in a parameter region still relatively far away from the regions currently probed, as can be seen in Fig. 41. Although the expected interference effects clearly depend on the underlying model, they can be expected to be of mounting importance in the future as the LHC data set increases.

5 Discovery potential at the HL-LHC

The HL-LHC [221] is planned to start in 2029 and aims to deliver a pp collision data set corresponding to about 3000 fb^{-1} of integrated luminosity in the baseline scenario, and up to 4000 fb^{-1} in the ultimate scenario, at an unprecedented center-of-mass energy of 14 TeV. The CMS detector will be upgraded to cope with the large size of 140 (200) PU events on average for the baseline (ultimate) scenario. The upgraded detector will also meet the challenges from the adverse effects due to the radiation dose to which the detector components are exposed, which is one order of magnitude higher than at the current LHC. Furthermore, major improvements

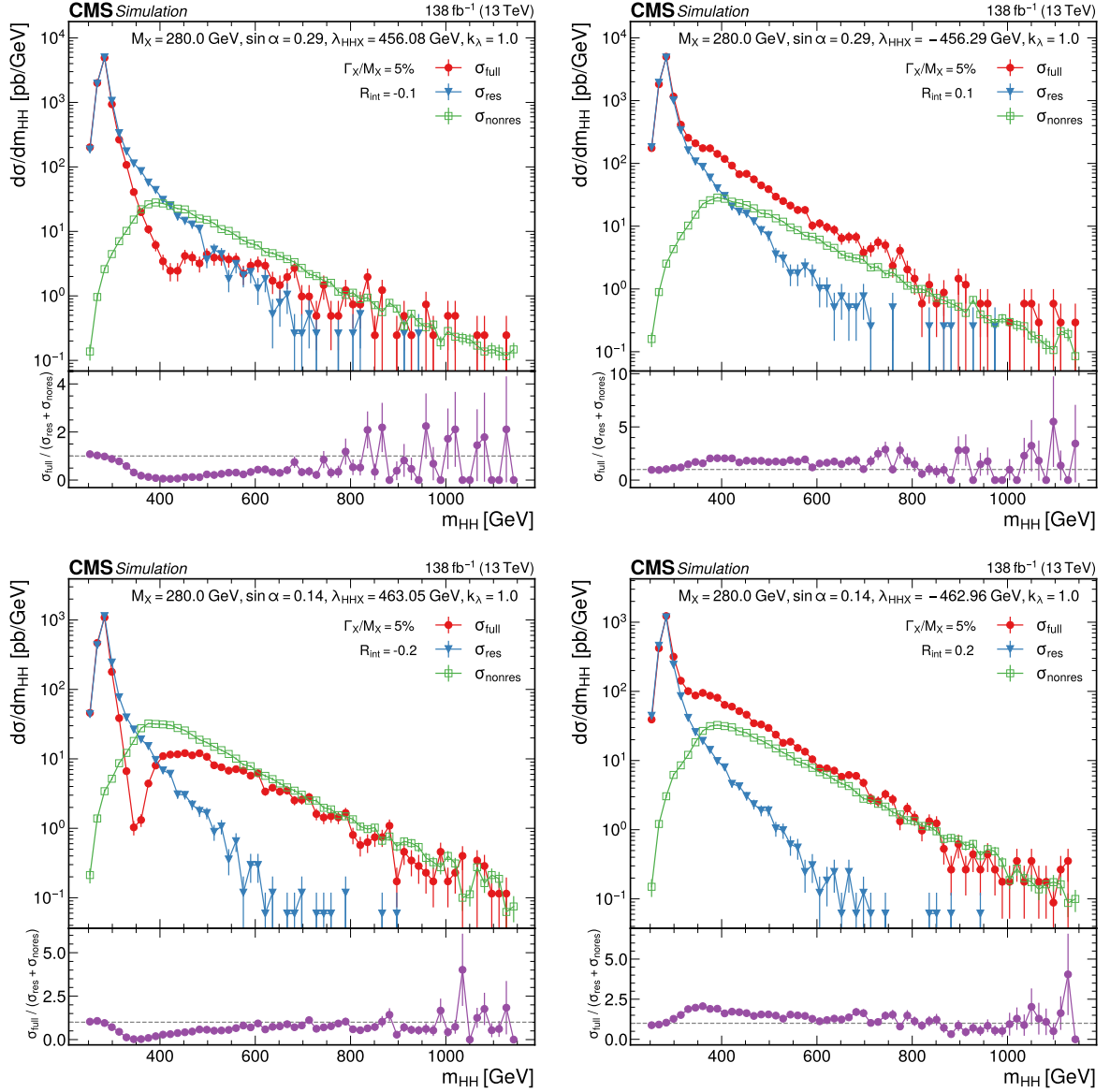


Figure 42: Expected differential cross sections for HH production, as a function of m_{HH} , for the real-singlet model with $m_X = 280$ GeV and $\Gamma_X/m_X = 5\%$. The parameters $\sin \alpha$ and λ_{HHX} have been chosen such that (upper row) $R_{\text{int}} = \pm 10\%$ and (lower row) $R_{\text{int}} = \pm 20\%$, for (left) negative and (right) positive values of R_{int} . The total cross section for HH production σ^{full} (red line, labelled as σ_{full}) is compared to the cross sections $\sigma^{\text{resonant-only}}$ (blue line, labelled as σ_{res}) and $\sigma^{\text{nonresonant}}$ (green line, labelled as σ_{nonres}) considering only resonant and nonresonant production. In the lower panels the ratio of σ^{full} over $(\sigma^{\text{resonant-only}} + \sigma^{\text{nonresonant}})$ is shown.

of the software for the online and offline event reconstruction are under development to fully exploit the potential of the upgraded detector. Searches for scalars X decaying to HH or YH are among the most relevant targets of research at the HL-LHC, and thus projection studies are very important to motivate the ongoing hardware and software upgrades. Meanwhile, such studies can provide an estimate of the sensitivity to the relevant BSM theories which can be achieved with the HL-LHC data.

This section describes the perspectives for the searches for X boson resonances decaying to HH or YH at the HL-LHC, in the most sensitive decay channels $bb\gamma\gamma$, $bb\tau\tau$, and $bbbb$, in the

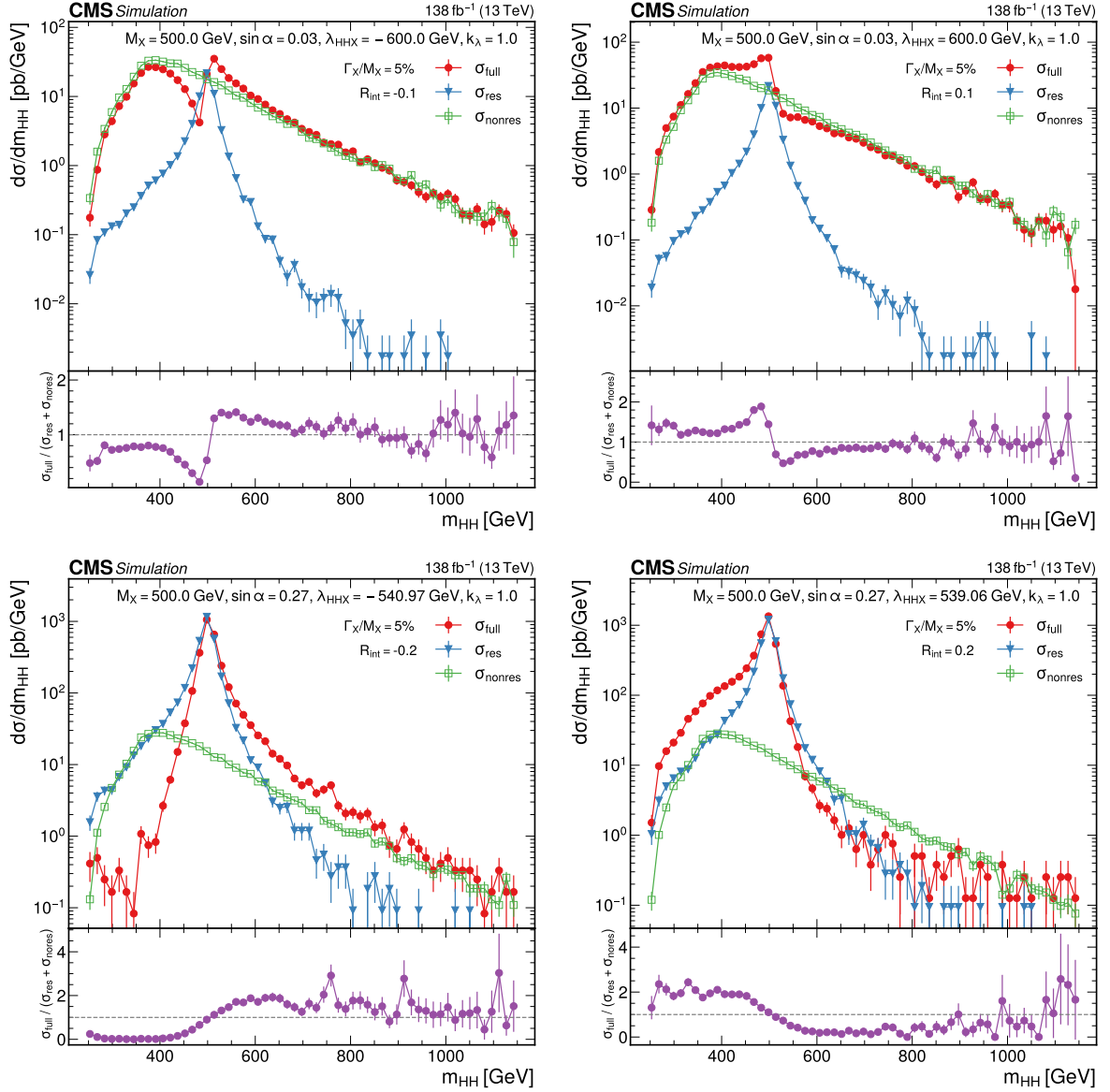


Figure 43: Expected differential cross sections for HH production, as a function of m_{HH} for the real-singlet model with $m_\chi = 500$ GeV and $\Gamma_\chi/m_\chi = 5\%$. The parameters $\sin \alpha$ and λ_{HHX} have been chosen such that (upper row) $R_{\text{int}} = \pm 10\%$ and (lower row) $R_{\text{int}} = \pm 20\%$, for (left) negative and (right) positive values of R_{int} . The total cross section for HH production σ^{full} (red line, labelled as σ_{full}) is compared to the cross sections $\sigma^{\text{resonant-only}}$ (blue line, labelled as σ_{res}) and $\sigma^{\text{nonresonant}}$ (green line, labelled as σ_{nonres}) considering only resonant and nonresonant production. In the lower panels the ratio of σ^{full} over $(\sigma^{\text{resonant-only}} + \sigma^{\text{nonresonant}})$ is shown.

baseline scenario of the HL-LHC. Using the combined likelihood method, individual channels are statistically combined to exploit their complementarity in sensitivity to different regions in parameter space of the tested BSM theories. The expected upper limits at 95% CL on the cross sections of the BSM processes of interest are provided as functions of the masses of the BSM scalars. The expected exclusion in the parameters of the relevant BSM theories is estimated, as well as the expected discovery significance for benchmark BSM signals.

Table 2: Searches for resonant HH and YH production considered for the projection study.

Final state	Reference	Section
$bb\tau\tau$	[122]	2.5.1
$bb\gamma\gamma$	[123]	2.5.2
$bbbb$ (merged-jet)	[124]	2.5.3

5.1 Methodology for estimation of the discovery potential

The projection studies are based on the resonant HH and YH searches in the most sensitive channels from the CMS Run 2 data set corresponding to an integrated luminosity of 138 fb^{-1} , as summarized in Table 2. Descriptions of the Run 2 HH and YH searches are given in the sections indicated in the table.

Using the same approach as studies in Ref. [220], searches using the Run 2 data set are projected to an integrated luminosity of 3000 fb^{-1} . Where appropriate, the signal cross sections have been scaled to the center-of-mass energy of 14 TeV [35]. As the upgraded CMS detector will ensure a performance comparable to Run 2, the efficiency in the reconstruction and identification of photons, leptons, jets and b jets, as well as the resolution in their energy and momentum measurements are assumed to be unchanged. The experimental sensitivity expected at the HL-LHC is derived using the following three systematic uncertainty scenarios.

S1: All the systematic uncertainties are assumed to remain the same as in Run 2. This is an over-conservative scenario because the CMS detector upgrade, the progress in the reconstruction techniques, and the very large data set available for the experimental calibrations are expected to bring a substantial reduction of several systematic uncertainties. Furthermore, progress in the theory calculations is expected to reduce the uncertainties in the predictions.

S2: The theory uncertainties are halved, while the experimental uncertainties are set according to the recommendations of Ref. [222].

Statistical only: The results are derived considering only the statistical uncertainty in data.

The projected results from the channels considered are statistically combined following the same procedure as adopted for the Run 2 combination which is described in Section 2.6. In particular, the systematic uncertainties affecting multiple channels, such as the uncertainties in the luminosity and on the b jet identification efficiency, are treated as correlated among all the input channels.

5.2 Discovery potential for $X \rightarrow \text{HH}$

The expected upper limits at 95% CL on the $X \rightarrow \text{HH}$ cross section from the channels considered projected to 3000 fb^{-1} are shown for the three different systematic uncertainty scenarios in Fig. 44. The projected upper limits from the $bb\gamma\gamma$ decay mode range between 60 and 3 fb for m_X within 300–1000 GeV. The overall impact of the systematic uncertainties on the $bb\gamma\gamma$ upper limits is below 1% because of the small uncertainty on the background modeling thanks to the estimation procedure based on the fit to the data in sideband regions.

The $bb\tau\tau$ channel provides upper limits on the cross section at 95% CL between 300 and 7 fb for m_X within 300–1000 GeV. The systematic uncertainty with the largest impact in the S1 scenario has its origin in the limited size of the MC simulation used for the background estimation. In the S2 scenario, the statistical uncertainties on the simulated events are assumed to be

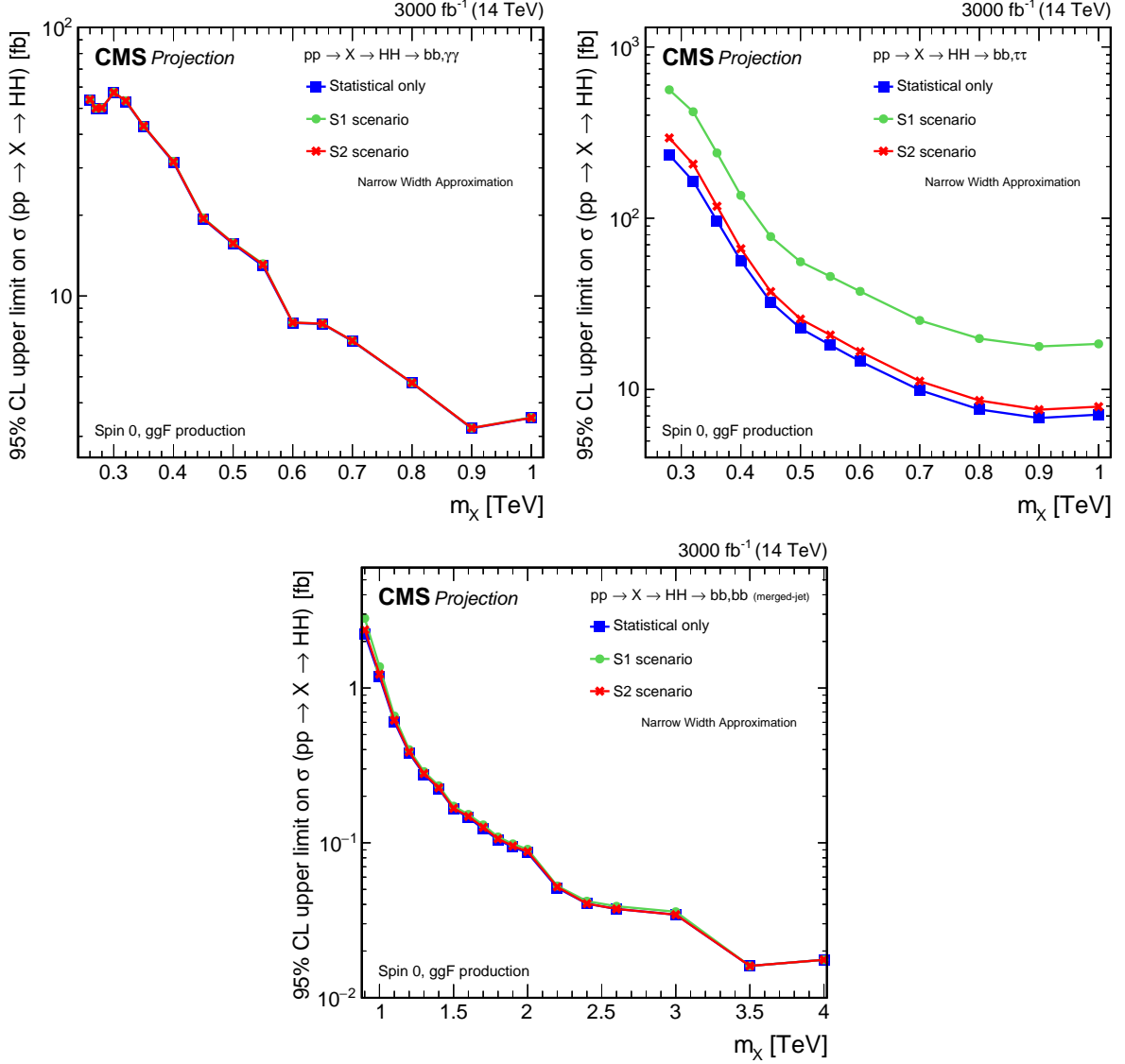


Figure 44: Expected upper limits at 95% CL, on the product of the cross section for the production of a spin-0 resonance X and the branching fraction $\mathcal{B}(X \rightarrow HH)$, as functions of m_X from the (upper left) $bb\tau\tau$ [122], (upper right) $bb\gamma\gamma$ [123], and (lower) $bbbb$ with two merged bb jets [124] analyses discussed in this report, projected to an integrated luminosity of 3000 fb^{-1} under the assumption of different systematic uncertainty scenarios, as discussed in the text. All estimates include the anticipated statistical uncertainties.

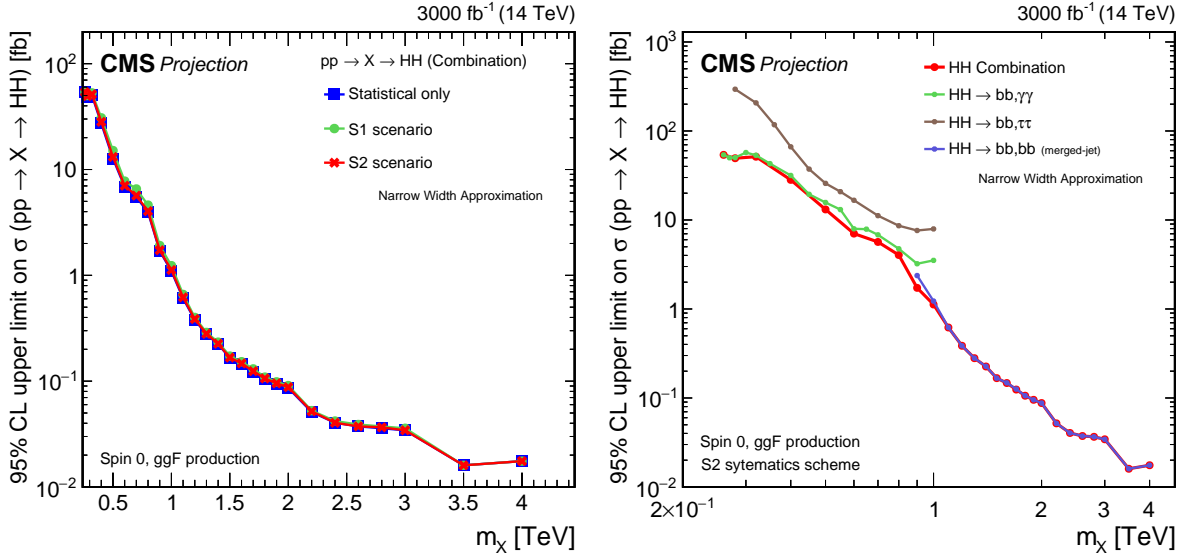


Figure 45: Expected upper limits at 95% CL, on the product of the cross section for the production of a spin-0 resonance X and the branching fraction $\mathcal{B}(X \rightarrow HH)$, as a function of m_X , for an integrated luminosity of 3000 fb^{-1} and the combination of the three analyses shown in Fig. 44. Shown are the effects of the different systematic uncertainty scenarios (left), and the reach of the individual analyses for the S2 systematic scenario (right). All estimates include the anticipated statistical uncertainties.

negligible and the main systematic uncertainties arise from the efficiencies of the b jet and τ identification and misidentification.

The bbbb channel in the boosted regime, in the following simply referred to as bbbb, covers m_X values between 900 and 4000 GeV, and is expected to provide upper limits between 0.04 and 0.02 fb at an integrated luminosity of 3000 fb^{-1} . The impact of the systematic uncertainties is very small, as the sensitivity of the analysis is mainly limited by the statistical uncertainty in the data.

The results of the combination of the resonant HH searches considered are shown in Fig. 45 in the different systematic uncertainty scenarios, and in comparison to the results from the individual channels. The $bb\gamma\gamma$ channel is found to dominate the sensitivity in the region $m_X < 500 \text{ GeV}$; around 900 GeV the channel with the best sensitivity is bbbb, followed by $bb\gamma\gamma$ and $bb\tau\tau$. For $m_X > 1000 \text{ GeV}$ the only channel considered is bbbb which is expected to be the most sensitive in this kinematic region. Thanks to the small impact of the systematic uncertainties on the $bb\gamma\gamma$ and bbbb channels, the differences between the three systematic uncertainty scenarios are rather small.

5.2.1 Perspectives for the discovery of BSM benchmark signals

The expected significance for the discovery of a benchmark BSM signal from a spin-0 resonance with a mass of 1 TeV is calculated for several signal cross sections and represented as a function of the integrated luminosity in Fig. 46. Based on the three channels considered in this projection, the significance of a signal of $X \rightarrow HH$ with a cross section of 10 fb corresponds to about three standard deviations at Run 2, while an integrated luminosity of 300 fb^{-1} would yield 4.8 standard deviations, indicating an attractive discovery potential already for Run 3 and its combination with Run 2. The significance of the same signal would reach about 15 standard deviations at 3000 fb^{-1} . A signal with a cross section of 3 fb would be sufficient to reach an

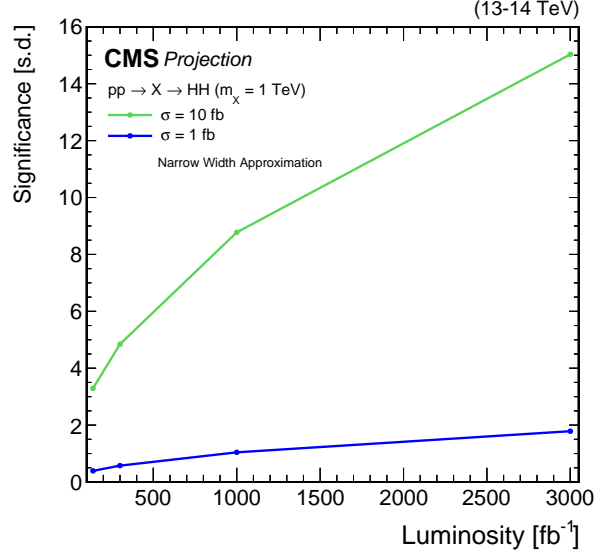


Figure 46: Expected discovery significance for a spin-0 resonance X with $m_X = 1$ TeV and cross sections of 1 and 10 fb, obtained for the combined likelihood analysis of the resonant HH searches as discussed in Section 5 and shown in Figs. 44 and 45, shown as function of the integrated luminosity.

observation at the level of five standard deviations with 3000 fb^{-1} .

5.2.2 Perspectives for MSSM scenarios

The projected exclusion limits at 95% CL of the hMSSM and $M_{h,\text{EFT}}^{125}$ benchmark scenarios from resonant HH searches are shown in Fig. 47. The S1 systematic uncertainty scenario is used for the Run 2 result and conservatively also for the result with 300 fb^{-1} , while the S2 systematic uncertainty scenario is used for the projected 1000 and 3000 fb^{-1} results. Over the full accessible range in $\tan \beta$, the exclusion in m_A increases by about 250–300 GeV when moving from the Run 2 integrated luminosity to 3000 fb^{-1} , for both the hMSSM and $M_{h,\text{EFT}}^{125}$ scenarios. This exclusion from the resonant HH searches will complement the searches for X decaying to a pair of fermions or vector bosons.

5.2.3 Perspectives for the WED bulk scenario

The expected lower limits at 95% CL on the bulk radion parameter Λ_R as a function of the radion mass m_R are shown in Fig. 48. The limits are obtained from the combination of resonant HH searches in the WED bulk scenario. The S1 systematic uncertainty scenario is used for the Run 2 result and conservatively also for the result with 300 fb^{-1} , while the S2 systematic uncertainty scenario is used for the projected 1000 and 3000 fb^{-1} results. Over the full range in m_R , the limit on Λ_R is expected to increase by a factor of at least two with the full HL-LHC data set.

5.2.4 Perspectives for the singlet scenarios

In the singlet model of Section 4.4 with $k_\lambda = 1$, limits are derived in the $(\sin \alpha, \lambda_{\text{HHX}})$ plane from the combination of resonant HH searches. Resonance masses between 280 and 800 GeV are probed using Run 2 data and projected to integrated luminosities corresponding to 300, 1000, and 3000 fb^{-1} . Projected exclusion regions at 95% CL are shown in Fig. 49. The HL-LHC dataset of 3000 fb^{-1} has the potential to considerably expand the present exclusion regions

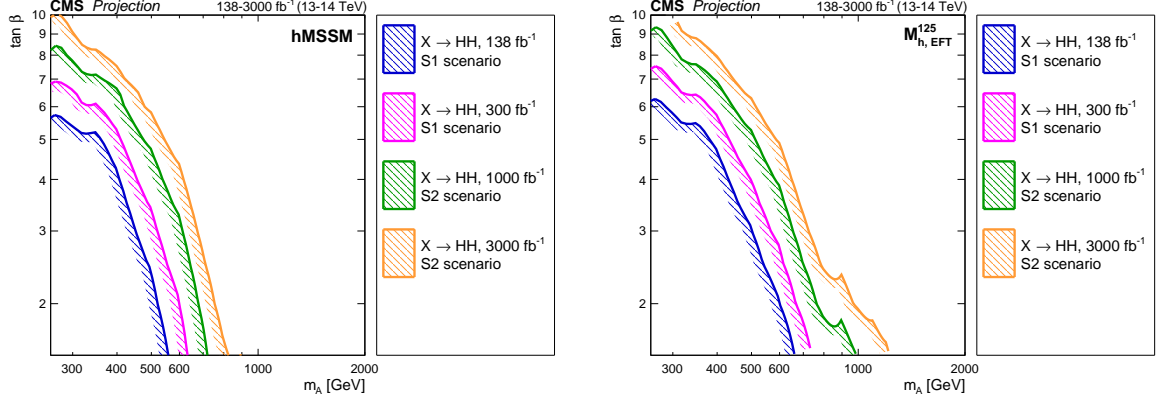


Figure 47: Expected exclusion contours at 95% CL, in the $(\tan\beta, m_A)$ plane of the (left) hMSSM and (right) $M_{h,EFT}^{125}$ scenarios obtained from the combined likelihood analysis of the HH searches discussed in Section 4.1 and shown in Figs. 31 and 32, for different integrated luminosities and compared to the Run 2 result obtained at $\sqrt{s} = 13$ TeV. The projections assume $\sqrt{s} = 14$ TeV.

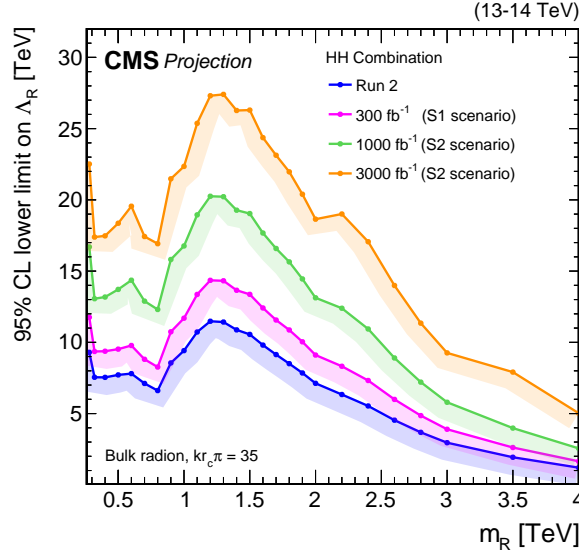


Figure 48: Expected lower limit at 95% CL, on Λ_R in the warped extra dimensions bulk scenario for the production of a radion R , as a function of m_R . The limits are derived from the combined likelihood analysis of the HH searches discussed in Section 4.2 and shown in Fig. 35, for different values of the integrated luminosity. Excluded areas are indicated by the direction of the hatching along the exclusion contours.

in the $(\sin \alpha, \lambda_{HHX})$ plane for all values of m_X . Compared to the present limits, the largest improvement is observed for large masses, $m_X = 600$ GeV and higher, where large regions of the $(\sin \alpha, \lambda_{HHX})$ plane can be probed.

5.3 Discovery potential for $X \rightarrow YH$

The upper limits on the cross section for $X \rightarrow YH$ are also projected to an integrated luminosity of 3000 fb^{-1} for the three systematic uncertainty scenarios. The projections are derived for the individual channels in the $bb\gamma\gamma$, $bb\tau\tau$, and $bbbb$ final states, and for a combination with the assumption of SM H boson branching fractions, where we use the same procedure as for the HH projections. The differences between the upper limits in the S1, S2, and statistical-only scenarios are analogous to the findings for the corresponding channels in the $X \rightarrow HH$ projections.

The results of the $X \rightarrow YH$ projections are presented in Figs. 50 and 51 for m_X up to and above 1 TeV, respectively. The regions of the (m_X, m_Y) parameter space with the largest ratios of m_Y/m_X correspond to a Y particle with low transverse momentum, and can be probed with the $bb\gamma\gamma$ channel. In the regions with small ratios of m_Y/m_X , the Y particle receives a large Lorentz boost, such that the $bbbb$ boosted channel has the highest sensitivity and only this final state is considered. In the intermediate region, the $bb\gamma\gamma$ and $bb\tau\tau$ channels provide comparable sensitivity and about equal weight in the combination.

Selected bins of the projections from the YH combination are used for presenting expected upper limits as functions of m_X and m_Y , and are shown in Fig. 52. In comparison with Fig. 34, the improvement is clearly visible.

5.3.1 Perspectives for the NMSSM and TRSM

We compare the maximally allowed cross sections predicted by the NMSSM model scans with the expected upper limits at 95% CL on the $X \rightarrow YH$ cross sections, projected to an integrated luminosity of 3000 fb^{-1} . The NMSSM model scans are obtained with NMSSMTOOLS version 5.6.2 [200], as described in Section 4.1.3, and take many relevant experimental constraints from Run 2 into account. Figure 53 shows the projected exclusion contours for the final states $Y(bb)H(\gamma\gamma)$ (upper left), $Y(bb)H(\tau\tau)$ (upper right), and $Y(bb)H(bb)$ in the merged-jet topology (lower left). The maximized model $\sigma\mathcal{B}$ values may depend non-monotonically on m_Y which can be reflected in the contours. Substantial regions of the parameter space can be excluded in the probed mass region with $m_X = 500\text{--}1000$ GeV and $m_Y = 100\text{--}350$ GeV, as well as up to $m_Y = 200$ GeV for $m_X = 1100\text{--}1500$ GeV. This indicates a huge increase in sensitivity for the HL-LHC compared to the results from Run 2. Similarly, we compare the predictions of the TRSM model [12] with the projected results from the $Y(bb)H(bb)$ channel in the merged-jet topology in Fig. 53 (lower right), which results in a sizable exclusion region for $m_X = 900\text{--}1500$ GeV and $m_Y = 110\text{--}135$ GeV.

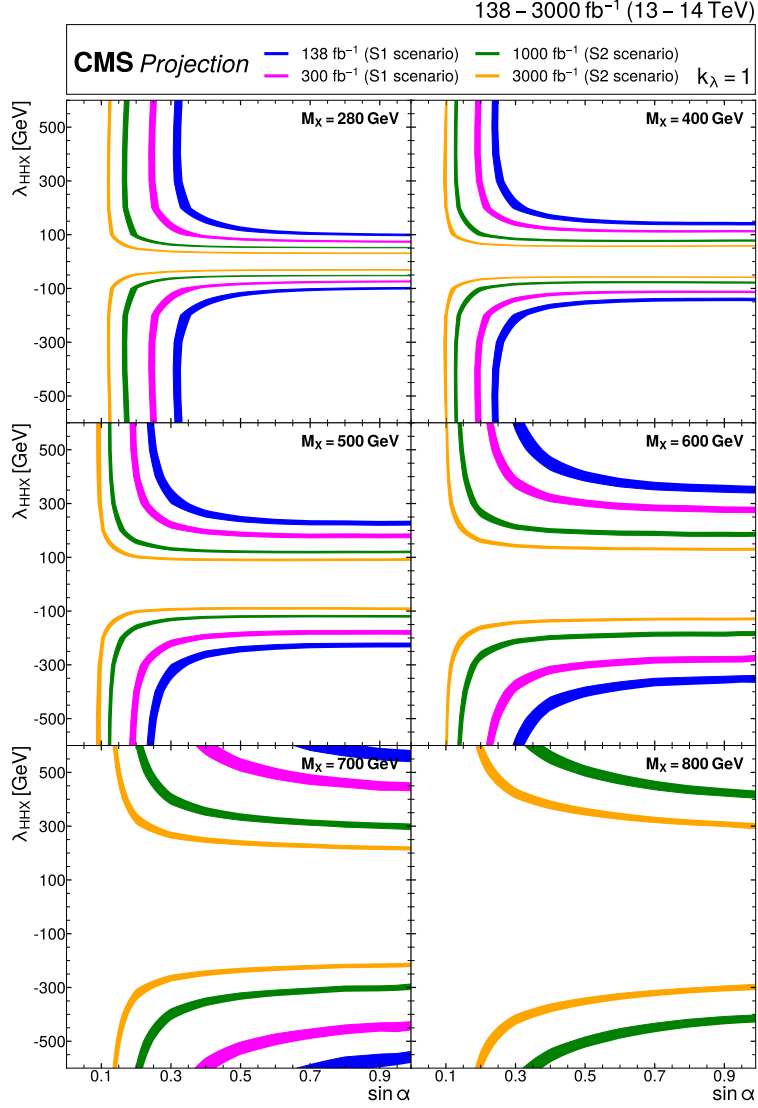


Figure 49: Exclusion contours at 95% CL, in the $(\sin \alpha, \lambda_{HHX})$ plane for $k_\lambda = 1$ in the real-singlet model. These contours are obtained from the combined likelihood analysis of the HH searches discussed in Section 4.1 for (upper left to lower right) $m_\chi = 280, 400, 500, 600, 700$, and 800 GeV. The expected limits from the Run 2 dataset have been projected to integrated luminosities of $300, 1000$, and 3000 fb^{-1} . Excluded areas are indicated by the direction of the hatching along the exclusion contours.

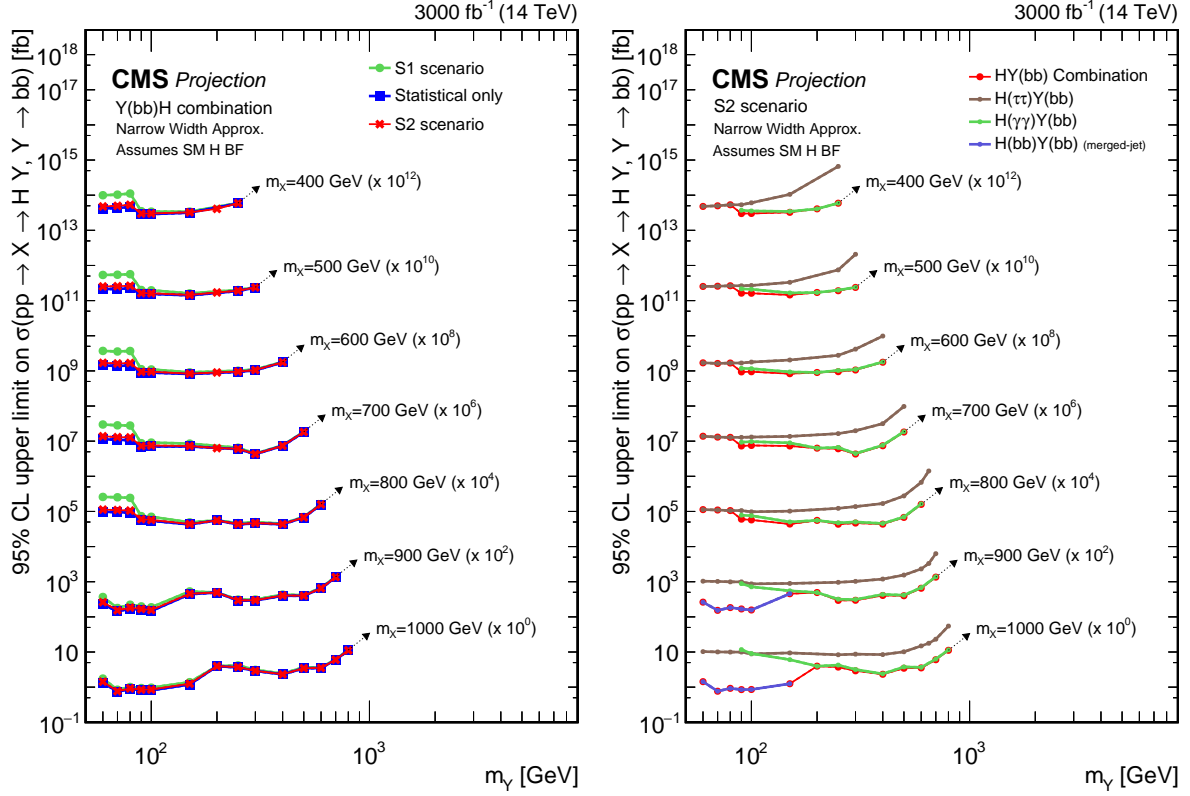


Figure 50: Expected upper limits at 95% CL, on the product of the cross section σ for the production of a resonance X via gluon-gluon fusion and the branching fraction \mathcal{B} for the $X \rightarrow Y(bb)H$ decay, as functions of m_Y , for $m_X \leq 1$ TeV. For the branching fractions of the $H \rightarrow \tau\tau$, $H \rightarrow \gamma\gamma$ and $H \rightarrow bb$ decays, the SM values are assumed. The limits are obtained from the combined likelihood analysis of all analyses discussed in Section 3.3 and shown in Fig. 29, projected to an integrated luminosity of 3000 fb^{-1} . Shown are the projections for the combined likelihood analysis for different systematic uncertainty scenarios (left), and the projections for the combined likelihood analysis and the individual contributing analyses assuming the S2 scenario (right). For presentation purposes, the limits have been scaled in successive steps by two orders of magnitude. For each set of graphs, a black arrow points to the m_X related legend.

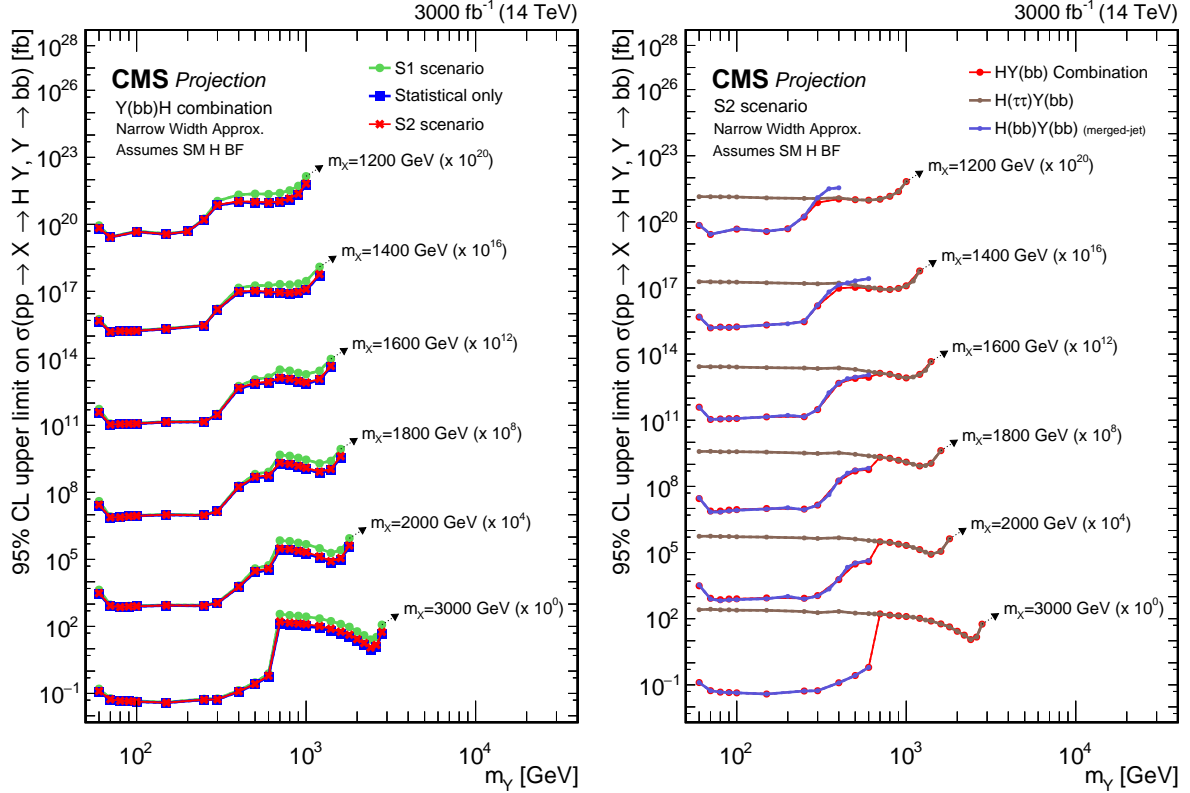


Figure 51: Expected upper limits at 95% CL, on the product of the cross section σ for the production of a resonance X via gluon-gluon fusion and the branching fraction \mathcal{B} for the $X \rightarrow Y(bb)H$ decay, as functions of m_Y , for $m_X \geq 1.2$ TeV. For the branching fractions of the $H \rightarrow \tau\tau$ and $H \rightarrow bb$ decays, the SM values are assumed. The limits are obtained from the combined likelihood analysis of all analyses discussed in Section 3.3 and shown in Fig. 30, projected to an integrated luminosity of 3000 fb^{-1} . Shown are the projections for the combined likelihood analysis for different systematic uncertainty scenarios (left), and the projections for the combined likelihood analysis and the individual contributing analyses assuming the S2 scenario (right). For presentation purposes, the limits have been scaled in successive steps by four orders of magnitude. For each set of graphs, a black arrow points to the m_X related legend.

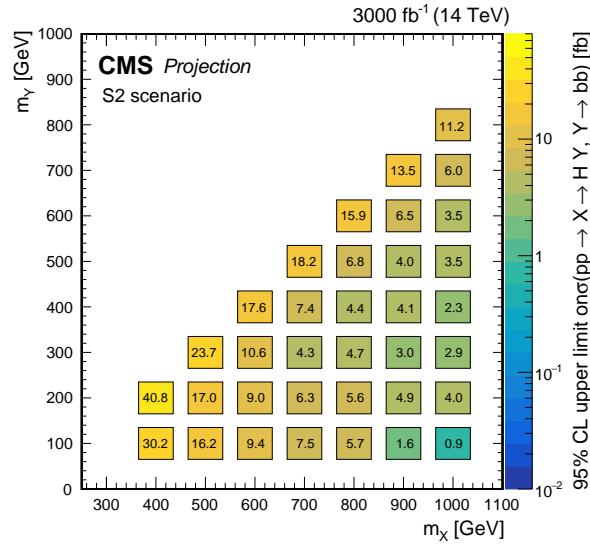


Figure 52: Expected upper limits at 95 % CL on the product of the cross section σ for the production of a resonance X via gluon-gluon fusion and the branching fraction \mathcal{B} for the $X \rightarrow Y(bb)H$ decay, as obtained from the combined likelihood analysis of the individual analyses presented in Section 3.3 and Figure 29. The results are shown in the plane spanned by m_Y and m_X for $m_X \leq 1$ TeV, and projected to an integrated luminosity of 3000 fb^{-1} , assuming the S2 systematic uncertainty scenario. The numbers in the boxes are given in fb.

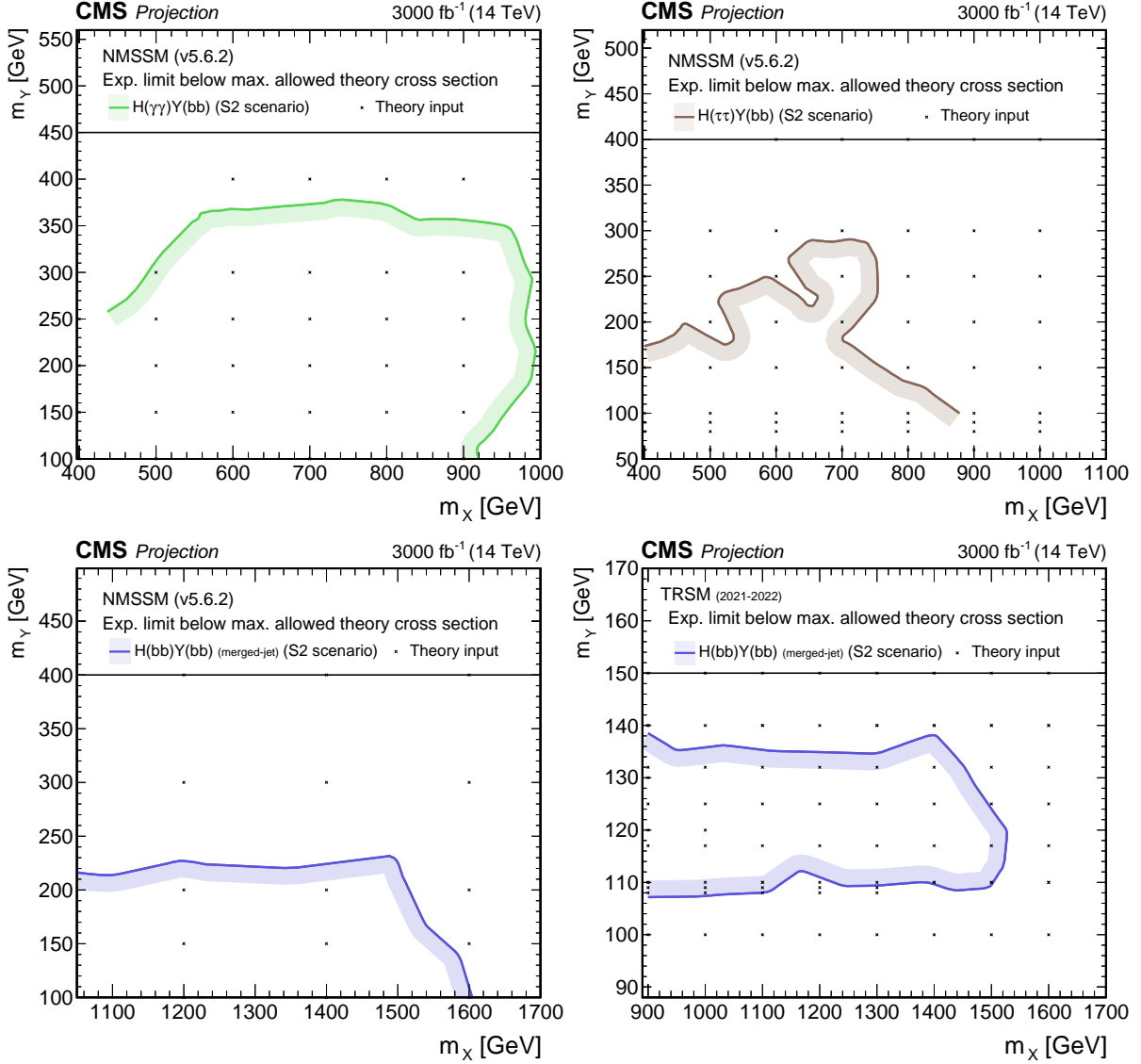


Figure 53: Interpretation of the upper limits at 95% CL, on the product of the cross section σ for the production of a resonance X via gluon-gluon fusion and the branching fraction \mathcal{B} for the $X \rightarrow Y(bb)H$ decay, obtained from the projections to an integrated luminosity of 3000 fb^{-1} of the (upper left) $Y(bb)H(\gamma\gamma)$ [123], (upper right) $Y(bb)H(\tau\tau)$ [122], and (lower row) $Y(bb)H(bb)$ [124] analyses, assuming the S2 systematic uncertainty scenario. The projected limits are mapped onto the (m_X, m_Y) plane, and compared with the maximally allowed cross sections of the NMSSM (left and upper right), and TRSM models (lower right) discussed in Section 4.1.3. The points indicate the available theory predictions. The mass dependences of both the projected experimental limits and the maximally allowed theory cross sections have been interpolated to obtain approximate exclusion contours. The NMSSM predictions based on NMSSMTOOLS version 5.6.2 are adapted from Ref. [200], whereas the TRSM is described in Ref. [12]. In both cases, the model predictions have been scaled to $\sqrt{s} = 14 \text{ TeV}$.

6 Summary

The analyses searching for the production of the Higgs (H) boson through decays of heavy resonances, performed by the CMS Collaboration using the Run 2 data set, are reviewed. This Report covers final states with two bosons with at least one an H boson, namely an H boson and a vector boson (VH), a pair of H bosons (HH), and an H boson joined by a new boson Y (YH), where V represents a W or a Z boson.

The analyses cover a wide range of H boson decay modes, in particular, decays into photons, b quarks, τ leptons, and W bosons. The Y boson is exclusively searched for in b quark final states. Topologies involving both resolved and merged jet objects are used to cover a wide range of the phase space. Multivariate methods are employed in various ways to improve the performance.

The results are presented as summary plots which show the sensitivity of all channels in direct comparison. For the HH and YH final states, the results obtained by combining all decay channels are presented for the first time.

The results are interpreted in the context of various beyond-the-standard model scenarios for resonances decaying into VH, HH and YH final states. These include various extended Higgs sector models, warped extra-dimension models, and heavy vector triplet models. The results from resonant H boson production searches are compared with results from searches in other channels.

While all presented analyses assume the validity of the narrow-width approximation, a dedicated study of the impact of finite width and interference is performed for the first time in CMS for the real singlet extension of the standard model. This study shows the modification of the HH cross section and line shape in regions of the parameter space where the narrow-width approximation is not valid anymore.

The expected sensitivity of the analyses in the HH and YH final states is estimated for future data sets with integrated luminosities of 300, 1000, and 3000 fb^{-1} , the last number corresponding to the baseline scenario of the High-Luminosity LHC (HL-LHC) over its full lifetime. The expected upper limits for resonant HH production for the HL-LHC scenario range from about 50 fb at a resonance mass of 300 GeV to nearly 0.01 fb for masses of 3 TeV and above. The exclusions in terms of $\tan \beta$ in the hMSSM and $M_{h,\text{EFT}}^{125}$ scenarios are expanded by almost a factor of two compared to the Run 2 data set.

This review shows how the specific strengths of many different experimental signatures can be combined to chart very thoroughly the territory where resonant Higgs boson production might reveal beyond the standard model physics, and gives a promising outlook towards the achievement potential of future measurements in this sector.

Acknowledgments

We congratulate our colleagues in the CERN accelerator departments for the excellent performance of the LHC and thank the technical and administrative staffs at CERN and at other CMS institutes for their contributions to the success of the CMS effort. In addition, we gratefully acknowledge the computing centers and personnel of the Worldwide LHC Computing Grid and other centers for delivering so effectively the computing infrastructure essential to our analyses. Finally, we acknowledge the enduring support for the construction and operation of the LHC, the CMS detector, and the supporting computing infrastructure provided

by the following funding agencies: the Armenian Science Committee, project no. 22rl-037; the Austrian Federal Ministry of Education, Science and Research and the Austrian Science Fund; the Belgian Fonds de la Recherche Scientifique, and Fonds voor Wetenschappelijk Onderzoek; the Brazilian Funding Agencies (CNPq, CAPES, FAPERJ, FAPERGS, and FAPESP); the Bulgarian Ministry of Education and Science, and the Bulgarian National Science Fund; CERN; the Chinese Academy of Sciences, Ministry of Science and Technology, the National Natural Science Foundation of China, and Fundamental Research Funds for the Central Universities; the Ministerio de Ciencia Tecnología e Innovación (MINCIENCIAS), Colombia; the Croatian Ministry of Science, Education and Sport, and the Croatian Science Foundation; the Research and Innovation Foundation, Cyprus; the Secretariat for Higher Education, Science, Technology and Innovation, Ecuador; the Estonian Research Council via PRG780, PRG803, RVTT3 and the Ministry of Education and Research TK202; the Academy of Finland, Finnish Ministry of Education and Culture, and Helsinki Institute of Physics; the Institut National de Physique Nucléaire et de Physique des Particules / CNRS, and Commissariat à l'Énergie Atomique et aux Énergies Alternatives / CEA, France; the Shota Rustaveli National Science Foundation, Georgia; the Bundesministerium für Bildung und Forschung, the Deutsche Forschungsgemeinschaft (DFG), under Germany's Excellence Strategy – EXC 2121 “Quantum Universe” – 390833306, and under project number 400140256 - GRK2497, and Helmholtz-Gemeinschaft Deutscher Forschungszentren, Germany; the General Secretariat for Research and Innovation and the Hellenic Foundation for Research and Innovation (HFRI), Project Number 2288, Greece; the National Research, Development and Innovation Office (NKFIH), Hungary; the Department of Atomic Energy and the Department of Science and Technology, India; the Institute for Studies in Theoretical Physics and Mathematics, Iran; the Science Foundation, Ireland; the Istituto Nazionale di Fisica Nucleare, Italy; the Ministry of Science, ICT and Future Planning, and National Research Foundation (NRF), Republic of Korea; the Ministry of Education and Science of the Republic of Latvia; the Research Council of Lithuania, agreement No. VS-19 (LMTLT); the Ministry of Education, and University of Malaya (Malaysia); the Ministry of Science of Montenegro; the Mexican Funding Agencies (BUAP, CINVESTAV, CONACYT, LNS, SEP, and UASLP-FAI); the Ministry of Business, Innovation and Employment, New Zealand; the Pakistan Atomic Energy Commission; the Ministry of Education and Science and the National Science Centre, Poland; the Fundação para a Ciência e a Tecnologia, grants CERN/FIS-PAR/0025/2019 and CERN/FIS-INS/0032/2019, Portugal; the Ministry of Education, Science and Technological Development of Serbia; MCIN/AEI/10.13039/501100011033, ERDF “a way of making Europe”, Programa Estatal de Fomento de la Investigación Científica y Técnica de Excelencia María de Maeztu, grant MDM-2017-0765, projects PID2020-113705RB, PID2020-113304RB, PID2020-116262RB and PID2020-113341RB-I00, and Plan de Ciencia, Tecnología e Innovación de Asturias, Spain; the Ministry of Science, Technology and Research, Sri Lanka; the Swiss Funding Agencies (ETH Board, ETH Zurich, PSI, SNF, UniZH, Canton Zurich, and SER); the Ministry of Science and Technology, Taipei; the Ministry of Higher Education, Science, Research and Innovation, and the National Science and Technology Development Agency of Thailand; the Scientific and Technical Research Council of Turkey, and Turkish Energy, Nuclear and Mineral Research Agency; the National Academy of Sciences of Ukraine; the Science and Technology Facilities Council, UK; the US Department of Energy, and the US National Science Foundation.

Individuals have received support from the Marie-Curie programme and the European Research Council and Horizon 2020 Grant, contract Nos. 675440, 724704, 752730, 758316, 765710, 824093, 101115353, 101002207, and COST Action CA16108 (European Union) the Leventis Foundation; the Alfred P. Sloan Foundation; the Alexander von Humboldt Foundation; the Belgian Federal Science Policy Office; the Fonds pour la Formation à la Recherche dans l'Industrie

et dans l'Agriculture (FRIA-Belgium); the Agentschap voor Innovatie door Wetenschap en Technologie (IWT-Belgium); the F.R.S.-FNRS and FWO (Belgium) under the "Excellence of Science – EOS" – be.h project n. 30820817; the Beijing Municipal Science & Technology Commission, No. Z191100007219010 and USTC Research Funds of the Double First-Class Initiative No. YD2030002017 (China); the Ministry of Education, Youth and Sports (MEYS) of the Czech Republic; the Shota Rustaveli National Science Foundation, grant FR-22-985 (Georgia); the Hungarian Academy of Sciences, the New National Excellence Program - ÚNKP, the NKFIH research grants K 131991, K 133046, K 138136, K 143460, K 143477, K 146913, K 146914, K 147048, 2020-2.2.1-ED-2021-00181, and TKP2021-NKTA-64 (Hungary); the Council of Scientific and Industrial Research, India; ICSC – National Research Centre for High Performance Computing, Big Data and Quantum Computing, funded by the EU NexGeneration program, Italy; the Latvian Council of Science; the Ministry of Education and Science, project no. 2022/WK/14, and the National Science Center, contracts Opus 2021/41/B/ST2/01369 and 2021/43/B/ST2/01552 (Poland); the Fundação para a Ciência e a Tecnologia, grant FCT CEECIND/01334/2018; the National Priorities Research Program by Qatar National Research Fund; the Programa Estatal de Fomento de la Investigación Científica y Técnica de Excelencia María de Maeztu, grant MDM-2017-0765 and projects PID2020-113705RB, PID2020-113304RB, PID2020-116262RB and PID2020-113341RB-I00, and Programa Severo Ochoa del Principado de Asturias (Spain); the Chulalongkorn Academic into Its 2nd Century Project Advancement Project, and the National Science, Research and Innovation Fund via the Program Management Unit for Human Resources & Institutional Development, Research and Innovation, grant B37G660013 (Thailand); the Kavli Foundation; the Nvidia Corporation; the SuperMicro Corporation; the Welch Foundation, contract C-1845; and the Weston Havens Foundation (USA).

References

- [1] ATLAS Collaboration, "Observation of a new particle in the search for the standard model Higgs boson with the ATLAS detector at the LHC", *Phys. Lett. B* **716** (2012) 1, doi:10.1016/j.physletb.2012.08.020, arXiv:1207.7214.
- [2] CMS Collaboration, "Observation of a new boson at a mass of 125 GeV with the CMS experiment at the LHC", *Phys. Lett. B* **716** (2012) 30, doi:10.1016/j.physletb.2012.08.021, arXiv:1207.7235.
- [3] CMS Collaboration, "Observation of a new boson with mass near 125 GeV in pp collisions at $\sqrt{s} = 7$ and 8 TeV", *JHEP* **06** (2013) 081, doi:10.1007/JHEP06(2013)081, arXiv:1303.4571.
- [4] CMS Collaboration, "A portrait of the Higgs boson by the CMS experiment ten years after the discovery", *Nature* **607** (2022) 60, doi:10.1038/s41586-022-04892-x, arXiv:2207.00043.
- [5] T. D. Lee, "A theory of spontaneous T violation", *Phys. Rev. D* **8** (1973) 1226, doi:10.1103/PhysRevD.8.1226.
- [6] G. C. Branco et al., "Theory and phenomenology of two-Higgs-doublet models", *Phys. Rept.* **516** (2012) 1, doi:10.1016/j.physrep.2012.02.002, arXiv:1106.0034.
- [7] H. E. Haber and O. Stål, "New LHC benchmarks for the CP -conserving two-Higgs-doublet model", *Eur. Phys. J. C* **75** (2015) 491, doi:10.1140/epjc/s10052-015-3697-x, arXiv:1507.04281. [Erratum: doi:10.1140/epjc/s10052-016-4151-4].

-
- [8] F. Kling, J. M. No, and S. Su, “Anatomy of exotic Higgs decays in 2HDM”, *JHEP* **09** (2016) 093, doi:10.1007/JHEP09(2016)093, arXiv:1604.01406.
 - [9] G. Chalons and F. Domingo, “Analysis of the Higgs potentials for two doublets and a singlet”, *Phys. Rev. D* **86** (2012) 115024, doi:10.1103/PhysRevD.86.115024, arXiv:1209.6235.
 - [10] C.-Y. Chen, M. Freid, and M. Sher, “Next-to-minimal two Higgs doublet model”, *Phys. Rev. D* **89** (2014) 075009, doi:10.1103/PhysRevD.89.075009, arXiv:1312.3949.
 - [11] M. Mühlleitner, M. O. P. Sampaio, R. Santos, and J. Wittbrodt, “The N2HDM under theoretical and experimental scrutiny”, *JHEP* **03** (2017) 094, doi:10.1007/JHEP03(2017)094, arXiv:1612.01309.
 - [12] T. Robens, T. Stefaniak, and J. Wittbrodt, “Two-real-scalar-singlet extension of the SM: LHC phenomenology and benchmark scenarios”, *Eur. Phys. J. C* **80** (2020) 151, doi:10.1140/epjc/s10052-020-7655-x, arXiv:1908.08554.
 - [13] J. F. Gunion and H. E. Haber, “Higgs bosons in supersymmetric models (1)”, *Nucl. Phys. B* **272** (1986) 1, doi:10.1016/0550-3213(86)90340-8.
 - [14] J. F. Gunion and H. E. Haber, “Higgs bosons in supersymmetric models (II). Implications for phenomenology”, *Nucl. Phys. B* **278** (1986) 449, doi:10.1016/0550-3213(86)90050-7. [Erratum: doi:10.1016/0550-3213(93)90654-8].
 - [15] G. Degrand et al., “Towards high precision predictions for the MSSM Higgs sector”, *Eur. Phys. J. C* **28** (2003) 133, doi:10.1140/epjc/s2003-01152-2, arXiv:hep-ph/0212020.
 - [16] A. Djouadi, “The anatomy of electroweak symmetry breaking Tome II: The Higgs bosons in the minimal supersymmetric model”, *Phys. Rept.* **459** (2008) 1, doi:10.1016/j.physrep.2007.10.005, arXiv:hep-ph/0503173.
 - [17] M. Maniatis, “The next-to-minimal supersymmetric extension of the standard model reviewed”, *Int. J. Mod. Phys. A* **25** (2010) 3505, doi:10.1142/S0217751X10049827, arXiv:0906.0777.
 - [18] U. Ellwanger, C. Hugonie, and A. M. Teixeira, “The next-to-minimal supersymmetric standard model”, *Phys. Rept.* **496** (2010) 1, doi:10.1016/j.physrep.2010.07.001, arXiv:0910.1785.
 - [19] S. F. King, M. Mühlleitner, and R. Nevzorov, “NMSSM Higgs benchmarks near 125 GeV”, *Nucl. Phys. B* **860** (2012) 207, doi:10.1016/j.nuclphysb.2012.02.010, arXiv:1201.2671.
 - [20] L. Randall and R. Sundrum, “Large mass hierarchy from a small extra dimension”, *Phys. Rev. Lett.* **83** (1999) 3370, doi:10.1103/PhysRevLett.83.3370, arXiv:hep-ph/9905221.
 - [21] W. D. Goldberger and M. B. Wise, “Modulus stabilization with bulk fields”, *Phys. Rev. Lett.* **83** (1999) 4922, doi:10.1103/PhysRevLett.83.4922, arXiv:hep-ph/9907447.

- [22] O. DeWolfe, D. Z. Freedman, S. S. Gubser, and A. Karch, “Modeling the fifth dimension with scalars and gravity”, *Phys. Rev. D* **62** (2000) 046008, doi:10.1103/PhysRevD.62.046008, arXiv:hep-th/9909134.
- [23] C. Csáki, M. Graesser, L. Randall, and J. Terning, “Cosmology of brane models with radion stabilization”, *Phys. Rev. D* **62** (2000) 045015, doi:10.1103/PhysRevD.62.045015, arXiv:hep-ph/9911406.
- [24] H. Davoudiasl, J. L. Hewett, and T. G. Rizzo, “Phenomenology of the Randall–Sundrum gauge hierarchy model”, *Phys. Rev. Lett.* **84** (2000) 2080, doi:10.1103/PhysRevLett.84.2080, arXiv:hep-ph/9909255.
- [25] C. Csaki, M. L. Graesser, and G. D. Kribs, “Radion dynamics and electroweak physics”, *Phys. Rev. D* **63** (2001) 065002, doi:10.1103/PhysRevD.63.065002, arXiv:hep-th/0008151.
- [26] K. Agashe, H. Davoudiasl, G. Perez, and A. Soni, “Warped gravitons at the CERN LHC and beyond”, *Phys. Rev. D* **76** (2007) 036006, doi:10.1103/PhysRevD.76.036006, arXiv:hep-ph/0701186.
- [27] A. L. Fitzpatrick, J. Kaplan, L. Randall, and L.-T. Wang, “Searching for the Kaluza-Klein graviton in bulk RS models”, *JHEP* **09** (2007) 013, doi:10.1088/1126-6708/2007/09/013, arXiv:hep-ph/0701150.
- [28] A. Oliveira, “Gravity particles from warped extra dimensions, predictions for LHC”, 2014. arXiv:1404.0102.
- [29] G. F. Giudice, R. Rattazzi, and J. D. Wells, “Graviscalars from higher-dimensional metrics and curvature-Higgs mixing”, *Nucl. Phys. B* **595** (2001) 250, doi:10.1016/S0550-3213(00)00686-6, arXiv:hep-ph/0002178.
- [30] D. Pappadopulo, A. Thamm, R. Torre, and A. Wulzer, “Heavy vector triplets: Bridging theory and data”, *JHEP* **09** (2014) 060, doi:10.1007/JHEP09(2014)060, arXiv:1402.4431.
- [31] “HEPData record for this analysis”, 2024. doi:10.17182/hepdata.146897.
- [32] P. W. Higgs, “Broken symmetries, massless particles and gauge fields”, *Phys. Lett.* **12** (1964) 132, doi:10.1016/0031-9163(64)91136-9.
- [33] P. W. Higgs, “Spontaneous symmetry breakdown without massless bosons”, *Phys. Rev.* **145** (1966) 1156, doi:10.1103/PhysRev.145.1156.
- [34] F. Englert and R. Brout, “Broken symmetry and the mass of gauge vector mesons”, *Phys. Rev. Lett.* **13** (1964) 321, doi:10.1103/PhysRevLett.13.321.
- [35] M. Cepeda et al., “Handbook of LHC Higgs cross sections: 4. Deciphering the nature of the Higgs sector”, CERN Report CERN-2017-002-M, 2016. doi:10.23731/CYRM-2017-002, arXiv:1610.07922.
- [36] ATLAS Collaboration, “Measurement of the Higgs boson mass with $H \rightarrow \gamma\gamma$ decays in 140 fb^{-1} of $\sqrt{s}=13\text{ TeV}$ pp collisions with the ATLAS detector”, *Phys. Lett. B* **847** (2023) 138315, doi:10.1016/j.physletb.2023.138315, arXiv:2308.07216.

-
- [37] CMS Collaboration, “Measurement of the Higgs boson width and evidence of its off-shell contributions to ZZ production”, *Nature Phys.* **18** (2022) 1329, doi:10.1038/s41567-022-01682-0, arXiv:2202.06923.
 - [38] LHC Higgs Cross Section Working Group, “Handbook of LHC Higgs Cross Sections: 3. Higgs Properties: Report of the LHC Higgs Cross Section Working Group”. Number CERN-2013-004 in CERN Yellow Reports: Monographs. CERN, 2013. doi:10.5170/CERN-2013-004.
 - [39] F. Bezrukov and M. Shaposhnikov, “Inflation, LHC and the Higgs boson”, *C. R. Phys.* **16** (2015) 994, doi:10.1016/j.crhy.2015.08.005.
 - [40] F. L. Bezrukov and M. Shaposhnikov, “The standard model Higgs boson as the inflaton”, *Phys. Lett. B* **659** (2008) 703, doi:10.1016/j.physletb.2007.11.072, arXiv:0710.3755.
 - [41] M. Fukugita and T. Yanagida, “Baryogenesis without grand unification”, *Phys. Lett. B* **174** (1986) 45, doi:10.1016/0370-2693(86)91126-3.
 - [42] A. G. Cohen, D. B. Kaplan, and A. E. Nelson, “Progress in electroweak baryogenesis”, *Ann. Rev. Nucl. Part. Sci.* **43** (1993) 27, doi:10.1146/annurev.ns.43.120193.000331, arXiv:hep-ph/9302210.
 - [43] D. E. Morrissey and M. J. Ramsey-Musolf, “Electroweak baryogenesis”, *New J. Phys.* **14** (2012) 125003, doi:10.1088/1367-2630/14/12/125003, arXiv:1206.2942.
 - [44] Y. Hamada and M. Yamada, “Baryogenesis in false vacuum”, *Eur. Phys. J. C* **77** (2017) 643, doi:10.1140/epjc/s10052-017-5215-9, arXiv:1605.06897.
 - [45] I. P. Ivanov, “Building and testing models with extended Higgs sectors”, *Prog. Part. Nucl. Phys.* **95** (2017) 160, doi:10.1016/j.ppnp.2017.03.001, arXiv:1702.03776.
 - [46] S. Dawson, C. Englert, and T. Plehn, “Higgs Physics: It ain’t over till it’s over”, *Phys. Rept.* **816** (2019) 1, doi:10.1016/j.physrep.2019.05.001, arXiv:1808.01324.
 - [47] J. Stegmann, “Extended scalar sectors”, *Ann. Rev. Nucl. Part. Sci.* **70** (2020) 197, doi:10.1146/annurev-nucl-032620-043846.
 - [48] Particle Data Group, “Review of particle physics”, *Prog. Theor. Exp. Phys.* **2022** (2022) 083C01, doi:10.1093/ptep/ptac097.
 - [49] C. Englert et al., “Precision measurements of Higgs couplings: Implications for new physics scales”, *J. Phys. G* **41** (2014) 113001, doi:10.1088/0954-3899/41/11/113001, arXiv:1403.7191.
 - [50] CMS Collaboration, “Combined measurements of Higgs boson couplings in proton–proton collisions at $\sqrt{s} = 13$ TeV”, *Eur. Phys. J. C* **79** (2019) 421, doi:10.1140/epjc/s10052-019-6909-y, arXiv:1809.10733.
 - [51] ATLAS Collaboration, “Combined measurements of Higgs boson production and decay using up to 80 fb⁻¹ of proton-proton collision data at $\sqrt{s} = 13$ TeV collected with the ATLAS experiment”, *Phys. Rev. D* **101** (2020) 012002, doi:10.1103/PhysRevD.101.012002, arXiv:1909.02845.

- [52] ATLAS Collaboration, “A detailed map of Higgs boson interactions by the ATLAS experiment ten years after the discovery”, *Nature* **607** (2022) 52, doi:10.1038/s41586-022-04893-w, arXiv:2207.00092. [Erratum: doi:10.1038/s41586-022-05581-5].
- [53] A. Datta and A. Raychaudhuri, “Next-to-minimal Higgs: Mass bounds and search prospects”, *Phys. Rev. D* **57** (1998) 2940, doi:10.1103/PhysRevD.57.2940, arXiv:hep-ph/9708444.
- [54] V. Barger et al., “Complex singlet extension of the standard model”, *Phys. Rev. D* **79** (2009) 015018, doi:10.1103/PhysRevD.79.015018, arXiv:0811.0393.
- [55] R. Costa, M. Mühlleitner, M. O. P. Sampaio, and R. Santos, “Singlet extensions of the standard model at LHC Run 2: Benchmarks and comparison with the NMSSM”, *JHEP* **06** (2016) 034, doi:10.1007/JHEP06(2016)034, arXiv:1512.05355.
- [56] T. Robens and T. Stefaniak, “Status of the Higgs singlet extension of the standard model after LHC Run 1”, *Eur. Phys. J. C* **75** (2015) 104, doi:10.1140/epjc/s10052-015-3323-y, arXiv:1501.02234.
- [57] J. Haller et al., “Update of the global electroweak fit and constraints on two-Higgs-doublet models”, *Eur. Phys. J. C* **78** (2018) 675, doi:10.1140/epjc/s10052-018-6131-3, arXiv:1803.01853.
- [58] T. Hermann, M. Misiak, and M. Steinhauser, “ $\bar{B} \rightarrow X_s \gamma$ in the two Higgs doublet model up to next-to-next-to-leading order in QCD”, *JHEP* **11** (2012) 036, doi:10.1007/JHEP11(2012)036, arXiv:1208.2788.
- [59] M. Misiak et al., “Updated NNLO QCD predictions for the weak radiative B-meson decays”, *Phys. Rev. Lett.* **114** (2015) 221801, doi:10.1103/PhysRevLett.114.221801, arXiv:1503.01789.
- [60] M. Misiak and M. Steinhauser, “Weak radiative decays of the b meson and bounds on M_{H^\pm} in the two-Higgs-doublet model”, *Eur. Phys. J. C* **77** (2017) 201, doi:10.1140/epjc/s10052-017-4776-y, arXiv:1702.04571.
- [61] M. Misiak, A. Rehman, and M. Steinhauser, “Towards $\bar{B} \rightarrow X_s \gamma$ at the NNLO in QCD without interpolation in m_c ”, *JHEP* **06** (2020) 175, doi:10.1007/JHEP06(2020)175, arXiv:2002.01548.
- [62] D. Eriksson, J. Rathsmann, and O. Stal, “2HDMC: Two-Higgs-doublet model calculator physics and manual”, *Comput. Phys. Commun.* **181** (2010) 189, doi:10.1016/j.cpc.2009.09.011, arXiv:0902.0851.
- [63] R. Harlander et al., “Interim recommendations for the evaluation of Higgs production cross sections and branching ratios at the LHC in the two-Higgs-doublet model”, 2013. arXiv:1312.5571.
- [64] A. Djouadi and J. Quevillon, “The MSSM Higgs sector at a high M_{SUSY} : Reopening the low $\tan \beta$ regime and heavy Higgs searches”, *JHEP* **10** (2013) 028, doi:10.1007/JHEP10(2013)028, arXiv:1304.1787.
- [65] A. Djouadi et al., “The post-Higgs MSSM scenario: Habemus MSSM?”, *Eur. Phys. J. C* **73** (2013) 2650, doi:10.1140/epjc/s10052-013-2650-0, arXiv:1307.5205.

-
- [66] A. Djouadi et al., “Fully covering the MSSM Higgs sector at the LHC”, *JHEP* **06** (2015) 168, doi:10.1007/JHEP06(2015)168, arXiv:1502.05653.
 - [67] H. Bahl, S. Liebler, and T. Stefaniak, “MSSM Higgs benchmark scenarios for Run 2 and beyond: The low $\tan\beta$ region”, *Eur. Phys. J. C* **79** (2019) 279, doi:10.1140/epjc/s10052-019-6770-z, arXiv:1901.05933.
 - [68] E. A. Bagnaschi et al., “Benchmark scenarios for MSSM Higgs boson searches at the LHC”, Technical Report LHCHWG-2021-001, 2021.
 - [69] LHC Higgs Working Group – MSSM subgroup, “LHCHWG MSSM ROOT files”, 2022.
 - [70] E. Bagnaschi et al., “MSSM Higgs boson searches at the LHC: Benchmark scenarios for Run 2 and beyond”, *Eur. Phys. J. C* **79** (2019) 617, doi:10.1140/epjc/s10052-019-7114-8, arXiv:1808.07542.
 - [71] CMS Collaboration, “Searches for additional Higgs bosons and for vector leptoquarks in $\tau\tau$ final states in proton-proton collisions at $\sqrt{s} = 13$ TeV”, *JHEP* **07** (2023) 073, doi:10.1007/JHEP07(2023)073, arXiv:2208.02717.
 - [72] I. Engeln, M. Mühlleitner, and J. Wittbrodt, “N2HDECAY: Higgs boson decays in the different phases of the N2HDM”, *Comput. Phys. Commun.* **234** (2019) 256, doi:10.1016/j.cpc.2018.07.020, arXiv:1805.00966.
 - [73] H. Abouabid et al., “Benchmarking di-Higgs production in various extended Higgs sector models”, *JHEP* **09** (2022) 011, doi:10.1007/JHEP09(2022)011, arXiv:2112.12515.
 - [74] S. Baum and N. R. Shah, “Two Higgs doublets and a complex singlet: Disentangling the decay topologies and associated phenomenology”, *JHEP* **12** (2018) 044, doi:10.1007/JHEP12(2018)044, arXiv:1808.02667.
 - [75] U. Ellwanger and M. Rodriguez-Vazquez, “Simultaneous search for extra light and heavy Higgs bosons via cascade decays”, *JHEP* **11** (2017) 008, doi:10.1007/JHEP11(2017)008, arXiv:1707.08522.
 - [76] S. Baum, N. R. Shah, and K. Freese, “The NMSSM is within reach of the LHC: Mass correlations & decay signatures”, *JHEP* **04** (2019) 011, doi:10.1007/JHEP04(2019)011, arXiv:1901.02332.
 - [77] D. Dominici, B. Grzadkowski, J. F. Gunion, and M. Toharia, “The scalar sector of the Randall–Sundrum model”, *Nucl. Phys. B* **671** (2003) 243, doi:10.1016/j.nuclphysb.2003.08.020, arXiv:hep-ph/0206192.
 - [78] I. Antoniadis and R. Sturani, “Higgs graviscalar mixing in type I string theory”, *Nucl. Phys. B* **631** (2002) 66, doi:10.1016/S0550-3213(02)00214-6, arXiv:hep-th/0201166.
 - [79] N. Desai, U. Maitra, and B. Mukhopadhyaya, “An updated analysis of radion-Higgs mixing in the light of LHC data”, *JHEP* **10** (2013) 093, doi:10.1007/JHEP10(2013)093, arXiv:1307.3765.
 - [80] A. Oliveira and R. Rosenfeld, “Graviscalars from higherdimensional metrics and curvature-Higgs mixing”, *Phys. Lett. B* **702** (2011) 201, doi:10.1016/j.physletb.2011.06.086, arXiv:1009.4497.

- [81] CMS Collaboration, “Search for high-mass resonances in dilepton final states in proton-proton collisions at $\sqrt{s} = 13$ TeV”, *JHEP* **06** (2018) 120, doi:10.1007/JHEP06(2018)120, arXiv:1803.06292.
- [82] C. Grojean, E. Salvioni, and R. Torre, “A weakly constrained W' at the early LHC”, *JHEP* **07** (2011) 002, doi:10.1007/JHEP07(2011)002, arXiv:1103.2761.
- [83] E. Salvioni, G. Villadoro, and F. Zwirner, “Minimal Z' models: Present bounds and early LHC reach”, *JHEP* **11** (2009) 068, doi:10.1088/1126-6708/2009/11/068, arXiv:0909.1320.
- [84] G. Altarelli, B. Mele, and M. Ruiz-Altaba, “Searching for new heavy vector bosons in $p\bar{p}$ colliders”, *Z. Phys. C* **45** (1989) 109, doi:10.1007/BF01556677. [Erratum: doi:10.1007/BF01552335].
- [85] M. Schmaltz and D. Tucker-Smith, “Little Higgs review”, *Ann. Rev. Nucl. Part. Sci.* **55** (2005) 229, doi:10.1146/annurev.nucl.55.090704.151502, arXiv:hep-ph/0502182.
- [86] N. Arkani-Hamed, A. G. Cohen, E. Katz, and A. E. Nelson, “The littlest Higgs”, *JHEP* **07** (2002) 034, doi:10.1088/1126-6708/2002/07/034, arXiv:hep-ph/0206021.
- [87] B. Bellazzini, C. Csáki, and J. Serra, “Composite Higgses”, *Eur. Phys. J. C* **74** (2014) 2766, doi:10.1140/epjc/s10052-014-2766-x, arXiv:1401.2457.
- [88] R. Contino, D. Marzocca, D. Pappadopulo, and R. Rattazzi, “On the effect of resonances in composite Higgs phenomenology”, *JHEP* **10** (2011) 081, doi:10.1007/JHEP10(2011)081, arXiv:1109.1570.
- [89] D. Marzocca, M. Serone, and J. Shu, “General composite Higgs models”, *JHEP* **08** (2012) 013, doi:10.1007/JHEP08(2012)013, arXiv:1205.0770.
- [90] D. Greco and D. Liu, “Hunting composite vector resonances at the LHC: Naturalness facing data”, *JHEP* **12** (2014) 126, doi:10.1007/JHEP12(2014)126, arXiv:1410.2883.
- [91] K. Lane and L. Pritchett, “The light composite Higgs boson in strong extended technicolor”, *JHEP* **06** (2017) 140, doi:10.1007/JHEP06(2017)140, arXiv:1604.07085.
- [92] V. D. Barger, W.-Y. Keung, and E. Ma, “A gauge model with light W and Z bosons”, *Phys. Rev. D* **22** (1980) 727, doi:10.1103/PhysRevD.22.727.
- [93] CMS Collaboration, “Search for heavy resonances decaying into two Higgs bosons or into a Higgs boson and a W or Z boson in proton-proton collisions at 13 TeV”, *JHEP* **01** (2019) 051, doi:10.1007/JHEP01(2019)051, arXiv:1808.01365.
- [94] CMS Collaboration, “Search for heavy resonances decaying into a vector boson and a Higgs boson in final states with charged leptons, neutrinos and b quarks at $\sqrt{s} = 13$ TeV”, *JHEP* **11** (2018) 172, doi:10.1007/JHEP11(2018)172, arXiv:1807.02826.
- [95] CMS Collaboration, “Search for heavy resonances that decay into a vector boson and a Higgs boson in hadronic final states at $\sqrt{s} = 13$ TeV”, *Eur. Phys. J. C* **77** (2017) 636, doi:10.1140/epjc/s10052-017-5192-z, arXiv:1707.01303.

-
- [96] CMS Collaboration, “Search for heavy resonances decaying into a vector boson and a Higgs boson in final states with charged leptons, neutrinos, and b quarks”, *Phys. Lett. B* **768** (2017) 137, doi:10.1016/j.physletb.2017.02.040, arXiv:1610.08066.
 - [97] CMS Collaboration, “Search for massive WH resonances decaying into the $\ell\nu b\bar{b}$ final state at $\sqrt{s} = 8$ TeV”, *Eur. Phys. J. C* **76** (2016) 237, doi:10.1140/epjc/s10052-016-4067-z, arXiv:1601.06431.
 - [98] CMS Collaboration, “Search for a massive resonance decaying into a Higgs boson and a W or Z boson in hadronic final states in proton-proton collisions at $\sqrt{s} = 8$ TeV”, *JHEP* **02** (2016) 145, doi:10.1007/JHEP02(2016)145, arXiv:1506.01443.
 - [99] CMS Collaboration, “Search for narrow high-mass resonances in proton-proton collisions at $\sqrt{s} = 8$ TeV decaying to a Z and a Higgs boson”, *Phys. Lett. B* **748** (2015) 255, doi:10.1016/j.physletb.2015.07.011, arXiv:1502.04994.
 - [100] ATLAS Collaboration, “Search for heavy resonances decaying into a Z or W boson and a Higgs boson in final states with leptons and b jets in 139 fb^{-1} of pp collisions at $\sqrt{s} = 13$ TeV with the ATLAS detector”, *JHEP* **06** (2023) 016, doi:10.1007/JHEP06(2023)016, arXiv:2207.00230.
 - [101] ATLAS Collaboration, “Search for resonances decaying into a weak vector boson and a Higgs boson in the fully hadronic final state produced in proton–proton collisions at $\sqrt{s} = 13$ TeV with the ATLAS detector”, *Phys. Rev. D* **102** (2020) 112008, doi:10.1103/PhysRevD.102.112008, arXiv:2007.05293.
 - [102] ATLAS Collaboration, “Combination of searches for heavy resonances decaying into bosonic and leptonic final states using 36 fb^{-1} of proton-proton collision data at $\sqrt{s} = 13$ TeV with the ATLAS detector”, *Phys. Rev. D* **98** (2018) 052008, doi:10.1103/PhysRevD.98.052008, arXiv:1808.02380.
 - [103] ATLAS Collaboration, “Search for heavy resonances decaying to a photon and a hadronically decaying Z/W/H boson in pp collisions at $\sqrt{s} = 13$ TeV with the ATLAS detector”, *Phys. Rev. D* **98** (2018) 032015, doi:10.1103/PhysRevD.98.032015, arXiv:1805.01908.
 - [104] ATLAS Collaboration, “Search for heavy resonances decaying into a W or Z boson and a Higgs boson in final states with leptons and b-jets in 36 fb^{-1} of $\sqrt{s} = 13$ TeV pp collisions with the ATLAS detector”, *JHEP* **03** (2018) 174, doi:10.1007/JHEP03(2018)174, arXiv:1712.06518. [Erratum: doi:10.1007/JHEP11(2018)051].
 - [105] ATLAS Collaboration, “Search for a new resonance decaying to a W or Z boson and a Higgs boson in the $\ell\ell/\ell\nu/\nu\nu + b\bar{b}$ final states with the ATLAS detector”, *Eur. Phys. J. C* **75** (2015) 263, doi:10.1140/epjc/s10052-015-3474-x, arXiv:1503.08089.
 - [106] ATLAS Collaboration, “Search for new resonances decaying to a W or Z boson and a Higgs boson in the $\ell^+\ell^-b\bar{b}$, $\ell\nu b\bar{b}$, and $\nu\bar{\nu}b\bar{b}$ channels with pp collisions at $\sqrt{s} = 13$ TeV with the ATLAS detector”, *Phys. Lett. B* **765** (2017) 32, doi:10.1016/j.physletb.2016.11.045, arXiv:1607.05621.
 - [107] ATLAS Collaboration, “Search for high-mass diboson resonances with boson-tagged jets in proton-proton collisions at $\sqrt{s} = 8$ TeV with the ATLAS detector”, *JHEP* **12** (2015) 055, doi:10.1007/JHEP12(2015)055, arXiv:1506.00962.

- [108] ATLAS Collaboration, “Search for a heavy Higgs boson decaying into a Z boson and another heavy Higgs boson in the $\ell\ell b\bar{b}$ and $\ell\ell WW$ final states in pp collisions at $\sqrt{s} = 13$ TeV with the ATLAS detector”, *Eur. Phys. J. C* **81** (2021) 396, doi:10.1140/epjc/s10052-021-09117-5, arXiv:2011.05639.
- [109] ATLAS Collaboration, “Search for Higgs boson pair production in the two bottom quarks plus two photons final state in pp collisions at $\sqrt{s} = 13$ TeV with the ATLAS detector”, *Phys. Rev. D* **106** (2022) 052001, doi:10.1103/PhysRevD.106.052001, arXiv:2112.11876.
- [110] ATLAS Collaboration, “Search for resonant and non-resonant Higgs boson pair production in the $b\bar{b}\tau^+\tau^-$ decay channel using 13 TeV pp collision data from the ATLAS detector”, *JHEP* **07** (2023) 040, doi:10.1007/JHEP07(2023)040, arXiv:2209.10910.
- [111] ATLAS Collaboration, “Search for resonant pair production of Higgs bosons in the $b\bar{b}b\bar{b}$ final state using pp collisions at $\sqrt{s} = 13$ TeV with the ATLAS detector”, *Phys. Rev. D* **105** (2022) 092002, doi:10.1103/PhysRevD.105.092002, arXiv:2202.07288.
- [112] ATLAS Collaboration, “Search for a new heavy scalar particle decaying into a Higgs boson and a new scalar singlet in final states with one or two light leptons and a pair of τ -leptons with the ATLAS detector”, *JHEP* **10** (2023) 009, doi:10.1007/JHEP10(2023)009, arXiv:2307.11120.
- [113] ATLAS Collaboration, “Anomaly detection search for new resonances decaying into a Higgs boson and a generic new particle X in hadronic final states using $\sqrt{s} = 13$ TeV pp collisions with the ATLAS detector”, *Phys. Rev. D* **108** (2023) 052009, doi:10.1103/PhysRevD.108.052009, arXiv:2306.03637.
- [114] CMS Collaboration, “Search for a heavy pseudoscalar Higgs boson decaying into a 125 GeV Higgs boson and a Z boson in final states with two tau and two light leptons at $\sqrt{s} = 13$ TeV”, *JHEP* **03** (2020) 065, doi:10.1007/JHEP03(2020)065, arXiv:1910.11634.
- [115] CMS Collaboration, “Search for a heavy pseudoscalar boson decaying to a Z and a Higgs boson at $\sqrt{s} = 13$ TeV”, *Eur. Phys. J. C* **79** (2019) 564, doi:10.1140/epjc/s10052-019-7058-z, arXiv:1903.00941.
- [116] CMS Collaboration, “Search for heavy resonances decaying to WW, WZ, or WH boson pairs in the lepton plus merged jet final state in proton-proton collisions at $\sqrt{s} = 13$ TeV”, *Phys. Rev. D* **105** (2022) 032008, doi:10.1103/PhysRevD.105.032008, arXiv:2109.06055.
- [117] CMS Collaboration, “Search for a heavy vector resonance decaying to a Z boson and a Higgs boson in proton-proton collisions at $\sqrt{s} = 13$ TeV”, *Eur. Phys. J. C* **81** (2021) 688, doi:10.1140/epjc/s10052-021-09348-6, arXiv:2102.08198.
- [118] CMS Collaboration, “Search for new heavy resonances decaying to WW, WZ, ZZ, WH, or ZH boson pairs in the all-jets final state in proton-proton collisions at $\sqrt{s} = 13$ TeV”, *Phys. Lett. B* **844** (2023) 137813, doi:10.1016/j.physletb.2023.137813, arXiv:2210.00043.

-
- [119] CMS Collaboration, “Search for Higgs boson pair production in the $bbWW$ decay mode in proton-proton collisions at $\sqrt{s} = 13$ TeV”, *JHEP* **07** (2024) 293, doi:10.1007/JHEP07(2024)293, arXiv:2403.09430.
 - [120] CMS Collaboration, “Search for heavy resonances decaying to a pair of Lorentz-boosted higgs bosons in final states with leptons and a bottom quark pair at $\sqrt{s} = 13$ TeV”, *JHEP* **05** (2022) 005, doi:10.1007/JHEP05(2022)005, arXiv:2112.03161.
 - [121] CMS Collaboration, “Search for Higgs boson pairs decaying to $WWWW$, $WW\tau\tau$, and $\tau\tau\tau\tau$ in proton-proton collisions at $\sqrt{s} = 13$ TeV”, *JHEP* **07** (2023) 095, doi:10.1007/JHEP07(2023)095, arXiv:2206.10268.
 - [122] CMS Collaboration, “Search for a heavy Higgs boson decaying into two lighter Higgs bosons in the $\tau\tau bb$ final state at 13 TeV”, *JHEP* **11** (2021) 057, doi:10.1007/JHEP11(2021)057, arXiv:2106.10361.
 - [123] CMS Collaboration, “Search for a new resonance decaying into two spin-0 bosons in a final state with two photons and two bottom quarks in proton-proton collisions at $\sqrt{s} = 13$ TeV”, *JHEP* **05** (2024) 316, doi:10.1007/JHEP05(2024)316, arXiv:2310.01643.
 - [124] CMS Collaboration, “Search for a massive scalar resonance decaying to a light scalar and a Higgs boson in the four b quarks final state with boosted topology”, *Phys. Lett. B* **842** (2023) 137392, doi:10.1016/j.physletb.2022.137392, arXiv:2204.12413.
 - [125] M. Gouzevitch et al., “Scale-invariant resonance tagging in multijet events and new physics in Higgs pair production”, *JHEP* **07** (2013) 148, doi:10.1007/JHEP07(2013)148, arXiv:1303.6636.
 - [126] A. J. Larkoski, I. Moult, and B. Nachman, “Jet substructure at the Large Hadron Collider: A review of recent advances in theory and machine learning”, *Phys. Rept.* **841** (2020) 1, doi:10.1016/j.physrep.2019.11.001, arXiv:1709.04464.
 - [127] R. Kogler, B. Nachman, A. Schmidt (editors) et al., “Jet substructure at the Large Hadron Collider”, *Rev. Mod. Phys.* **91** (2019) 045003, doi:10.1103/RevModPhys.91.045003, arXiv:1803.06991.
 - [128] R. Kogler, “Advances in jet substructure at the LHC: Algorithms, measurements and searches for new physical phenomena”, volume 284 of *Springer Tracts Mod. Phys.* Springer, 2021. doi:10.1007/978-3-030-72858-8, ISBN 978-3-030-72857-1, 978-3-030-72858-8.
 - [129] CMS Collaboration, “The CMS experiment at the CERN LHC”, *JINST* **3** (2008) S08004, doi:10.1088/1748-0221/3/08/S08004.
 - [130] CMS Collaboration, “Performance of the CMS Level-1 trigger in proton-proton collisions at $\sqrt{s} = 13$ TeV”, *JINST* **15** (2020) P10017, doi:10.1088/1748-0221/15/10/P10017, arXiv:2006.10165.
 - [131] CMS Collaboration, “The CMS trigger system”, *JINST* **12** (2017) P01020, doi:10.1088/1748-0221/12/01/P01020, arXiv:1609.02366.
 - [132] CMS Collaboration, “Particle-flow reconstruction and global event description with the CMS detector”, *JINST* **12** (2017) P10003, doi:10.1088/1748-0221/12/10/P10003, arXiv:1706.04965.

- [133] CMS Collaboration, “Technical proposal for the Phase-II upgrade of the Compact Muon Solenoid”, CMS Technical Proposal CMS-TDR-15-02, 2015.
- [134] M. Cacciari, G. P. Salam, and G. Soyez, “The anti- k_T jet clustering algorithm”, *JHEP* **04** (2008) 063, doi:10.1088/1126-6708/2008/04/063, arXiv:0802.1189.
- [135] M. Cacciari, G. P. Salam, and G. Soyez, “FastJet user manual”, *Eur. Phys. J. C* **72** (2012) 1896, doi:10.1140/epjc/s10052-012-1896-2, arXiv:1111.6097.
- [136] CMS Collaboration, “Jet energy scale and resolution in the CMS experiment in pp collisions at 8 TeV”, *JINST* **12** (2017) P02014, doi:10.1088/1748-0221/12/02/P02014, arXiv:1607.03663.
- [137] D. Bertolini, P. Harris, M. Low, and N. Tran, “Pileup per particle identification”, *JHEP* **10** (2014) 59, doi:10.1007/JHEP10(2014)059, arXiv:1407.6013.
- [138] CMS Collaboration, “Pileup mitigation at CMS in 13 TeV data”, *JINST* **15** (2020) P09018, doi:10.1088/1748-0221/15/09/P09018, arXiv:2003.00503.
- [139] CMS Collaboration, “Performance of missing transverse momentum reconstruction in proton-proton collisions at $\sqrt{s} = 13$ TeV using the CMS detector”, *JINST* **14** (2019) P07004, doi:10.1088/1748-0221/14/07/P07004, arXiv:1903.06078.
- [140] CMS Collaboration, “Jet algorithms performance in 13 TeV data”, CMS Physics Analysis Summary CMS-PAS-JME-16-003, 2017.
- [141] CMS Collaboration, “Identification of heavy-flavour jets with the CMS detector in pp collisions at 13 TeV”, *JINST* **13** (2018) P05011, doi:10.1088/1748-0221/13/05/P05011, arXiv:1712.07158.
- [142] E. Bols et al., “Jet flavour classification using DeepJet”, *JINST* **15** (2020) P12012, doi:10.1088/1748-0221/15/12/P12012, arXiv:2008.10519.
- [143] Y. L. Dokshitzer, G. D. Leder, S. Moretti, and B. R. Webber, “Better jet clustering algorithms”, *JHEP* **08** (1997) 001, doi:10.1088/1126-6708/1997/08/001, arXiv:hep-ph/9707323.
- [144] M. Wobisch and T. Wengler, “Hadronization corrections to jet cross-sections in deep inelastic scattering”, in *Workshop on Monte Carlo Generators for HERA Physics*, p. 270. 1998. arXiv:hep-ph/9907280.
- [145] A. J. Larkoski, S. Marzani, G. Soyez, and J. Thaler, “Soft drop”, *JHEP* **05** (2014) 146, doi:10.1007/JHEP05(2014)146, arXiv:1402.2657.
- [146] CMS Collaboration, “Identification of heavy, energetic, hadronically decaying particles using machine-learning techniques”, *JINST* **15** (2020) P06005, doi:10.1088/1748-0221/15/06/P06005, arXiv:2004.08262.
- [147] H. Qu and L. Gouskos, “ParticleNet: Jet tagging via particle clouds”, *Phys. Rev. D* **101** (2020) 056019, doi:10.1103/PhysRevD.101.056019, arXiv:1902.08570.
- [148] CMS Collaboration, “Performance of the DeepJet b tagging algorithm using 41.9 fb⁻¹ of data from proton-proton collisions at 13 TeV with Phase 1 CMS detector”, Detector performance note CMS-DP-2018-058, 2018.

-
- [149] M. Dasgupta, A. Fregoso, S. Marzani, and G. P. Salam, “Towards an understanding of jet substructure”, *JHEP* **09** (2013) 029, doi:10.1007/JHEP09(2013)029, arXiv:1307.0007.
- [150] J. M. Butterworth, A. R. Davison, M. Rubin, and G. P. Salam, “Jet substructure as a new Higgs search channel at the LHC”, *Phys. Rev. Lett.* **100** (2008) 242001, doi:10.1103/PhysRevLett.100.242001, arXiv:0802.2470.
- [151] J. Thaler and K. Van Tilburg, “Identifying boosted objects with N-subjettiness”, *JHEP* **03** (2011) 015, doi:10.1007/JHEP03(2011)015, arXiv:1011.2268.
- [152] J. Dolen et al., “Thinking outside the ROCs: Designing decorrelated taggers (DDT) for jet substructure”, *JHEP* **05** (2016) 156, doi:10.1007/JHEP05(2016)156, arXiv:1603.00027.
- [153] CMS Collaboration, “Performance of electron reconstruction and selection with the CMS detector in proton-proton collisions at $\sqrt{s} = 8$ TeV”, *JINST* **10** (2015) P06005, doi:10.1088/1748-0221/10/06/P06005, arXiv:1502.02701.
- [154] CMS Collaboration, “Electron and photon reconstruction and identification with the CMS experiment at the CERN LHC”, *JINST* **16** (2021) P05014, doi:10.1088/1748-0221/16/05/P05014, arXiv:2012.06888.
- [155] CMS Collaboration, “Performance of CMS muon reconstruction in pp collision events at $\sqrt{s} = 7$ TeV”, *JINST* **7** (2012) P10002, doi:10.1088/1748-0221/7/10/P10002, arXiv:1206.4071.
- [156] CMS Collaboration, “Performance of the CMS muon detector and muon reconstruction with proton-proton collisions at $\sqrt{s} = 13$ TeV”, *JINST* **13** (2018) P06015, doi:10.1088/1748-0221/13/06/P06015, arXiv:1804.04528.
- [157] CMS Collaboration, “Performance of reconstruction and identification of τ leptons decaying to hadrons and ν_τ in pp collisions at $\sqrt{s} = 13$ TeV”, *JINST* **13** (2018) P10005, doi:10.1088/1748-0221/13/10/P10005, arXiv:1809.02816.
- [158] CMS Collaboration, “Identification of hadronic tau lepton decays using a deep neural network”, *JINST* **17** (2022) P07023, doi:10.1088/1748-0221/17/07/P07023, arXiv:2201.08458.
- [159] L. Bianchini et al., “Reconstruction of the Higgs mass in events with Higgs bosons decaying into a pair of τ leptons using matrix element techniques”, *Nucl. Instrum. Meth. A* **862** (2017) 54, doi:10.1016/j.nima.2017.05.001, arXiv:1603.05910.
- [160] CMS Collaboration, “Combination of CMS searches for heavy resonances decaying to pairs of bosons or leptons”, *Phys. Lett. B* **798** (2019) 134952, doi:10.1016/j.physletb.2019.134952, arXiv:1906.00057.
- [161] CMS Collaboration, “Search for a heavy resonance decaying into a Z boson and a vector boson in the $\nu\bar{\nu}q\bar{q}$ final state”, *JHEP* **07** (2018) 075, doi:10.1007/JHEP07(2018)075, arXiv:1803.03838.
- [162] CMS Collaboration, “Search for a heavy resonance decaying into a Z boson and a Z or W boson in $2\ell 2q$ final states at $\sqrt{s} = 13$ TeV”, *JHEP* **09** (2018) 101, doi:10.1007/JHEP09(2018)101, arXiv:1803.10093.

- [163] CMS Collaboration, “A multi-dimensional search for new heavy resonances decaying to boosted WW, WZ, or ZZ boson pairs in the dijet final state at 13 TeV”, *Eur. Phys. J. C* **80** (2020) 237, doi:10.1140/epjc/s10052-020-7773-5, arXiv:1906.05977.
- [164] M. Erdmann, E. Geiser, Y. Rath, and M. Rieger, “Lorentz boost networks: Autonomous physics-inspired feature engineering”, *JINST* **14** (2019) P06006, doi:10.1088/1748-0221/14/06/P06006, arXiv:1812.09722.
- [165] CMS Collaboration, “Evidence for associated production of a Higgs boson with a top quark pair in final states with electrons, muons, and hadronically decaying τ leptons at $\sqrt{s} = 13$ TeV”, *JHEP* **08** (2018) 066, doi:10.1007/JHEP08(2018)066, arXiv:1803.05485.
- [166] T. Huang et al., “Resonant di-Higgs boson production in the $b\bar{b}WW$ channel: Probing the electroweak phase transition at the LHC”, *Phys. Rev. D* **96** (2017) 035007, doi:10.1103/PhysRevD.96.035007, arXiv:1701.04442.
- [167] CMS Collaboration, “Measurements of Higgs boson production in the decay channel with a pair of τ leptons in proton-proton collisions at $\sqrt{s} = 13$ TeV”, *Eur. Phys. J. C* **83** (2023) 562, doi:10.1140/epjc/s10052-023-11452-8, arXiv:2204.12957.
- [168] CMS Collaboration, “A deep neural network for simultaneous estimation of b jet energy and resolution”, *Comput. Softw. Big Sci.* **4** (2020) 10, doi:10.1007/s41781-020-00041-z, arXiv:1912.06046.
- [169] S. Wunsch, R. Friese, R. Wolf, and G. Quast, “Identifying the relevant dependencies of the neural network response on characteristics of the input space”, *Comput. Softw. Big Sci.* **2** (2018) 5, doi:10.1007/s41781-018-0012-1, arXiv:1803.08782.
- [170] CMS Collaboration, “Observation of the diphoton decay of the Higgs boson and measurement of its properties”, *Eur. Phys. J. C* **74** (2014) 3076, doi:10.1140/epjc/s10052-014-3076-z, arXiv:1407.0558.
- [171] CMS Collaboration, “Search for nonresonant Higgs boson pair production in final states with two bottom quarks and two photons in proton-proton collisions at $\sqrt{s} = 13$ TeV”, *JHEP* **03** (2021) 257, doi:10.1007/JHEP03(2021)257, arXiv:2011.12373.
- [172] T. Junk, “Confidence level computation for combining searches with small statistics”, *Nucl. Instrum. Meth. A* **434** (1999) 435, doi:10.1016/S0168-9002(99)00498-2, arXiv:hep-ex/9902006.
- [173] A. L. Read, “Presentation of search results: The CL_s technique”, *J. Phys. G* **28** (2002) 2693, doi:10.1088/0954-3899/28/10/313.
- [174] G. Cowan, K. Cranmer, E. Gross, and O. Vitells, “Asymptotic formulae for likelihood-based tests of new physics”, *Eur. Phys. J. C* **71** (2011) 1554, doi:10.1140/epjc/s10052-011-1554-0, arXiv:1007.1727. [Erratum: doi:10.1140/epjc/s10052-013-2501-z].
- [175] ATLAS Collaboration, “Combination of searches for resonant Higgs boson pair production using pp collisions at $\sqrt{s} = 13$ TeV with the ATLAS detector”, *Phys. Rev. Lett.* **132** (2024) 231801, doi:10.1103/PhysRevLett.132.231801, arXiv:2311.15956.

-
- [176] CMS Collaboration, “Search for heavy Higgs bosons decaying to a top quark pair in proton-proton collisions at $\sqrt{s} = 13$ TeV”, *JHEP* **04** (2020) 171, doi:10.1007/JHEP04(2020)171, arXiv:1908.01115. [Erratum: doi:10.1007/JHEP03(2022)187)].
- [177] CMS Collaboration, “Search for a heavy Higgs boson decaying to a pair of W bosons in proton-proton collisions at $\sqrt{s} = 13$ TeV”, *JHEP* **03** (2020) 034, doi:10.1007/JHEP03(2020)034, arXiv:1912.01594.
- [178] A. Djouadi, J. Kalinowski, and M. Spira, “HDECAY: A Program for Higgs boson decays in the standard model and its supersymmetric extension”, *Comput. Phys. Commun.* **108** (1998) 56, doi:10.1016/S0010-4655(97)00123-9, arXiv:hep-ph/9704448.
- [179] A. Djouadi, J. Kalinowski, M. Mühlleitner, and M. Spira, “HDECAY: Twenty++ years after”, *Comput. Phys. Commun.* **238** (2019) 214, doi:10.1016/j.cpc.2018.12.010, arXiv:1801.09506.
- [180] R. V. Harlander, S. Liebler, and H. Mantler, “SusHi: A program for the calculation of Higgs production in gluon fusion and bottom-quark annihilation in the standard model and the MSSM”, *Comput. Phys. Commun.* **184** (2013) 1605, doi:10.1016/j.cpc.2013.02.006, arXiv:1212.3249.
- [181] R. V. Harlander, S. Liebler, and H. Mantler, “SusHi bento: Beyond NNLO and the heavy-top limit”, *Comput. Phys. Commun.* **212** (2017) 239, doi:10.1016/j.cpc.2016.10.015, arXiv:1605.03190.
- [182] M. Spira, A. Djouadi, D. Graudenz, and P. M. Zerwas, “Higgs boson production at the LHC”, *Nucl. Phys. B* **453** (1995) 17, doi:10.1016/0550-3213(95)00379-7, arXiv:hep-ph/9504378.
- [183] R. Harlander and P. Kant, “Higgs production and decay: Analytic results at next-to-leading order QCD”, *JHEP* **12** (2005) 015, doi:10.1088/1126-6708/2005/12/015, arXiv:hep-ph/0509189.
- [184] R. V. Harlander and W. B. Kilgore, “Next-to-next-to-leading order Higgs production at hadron colliders”, *Phys. Rev. Lett.* **88** (2002) 201801, doi:10.1103/PhysRevLett.88.201801, arXiv:hep-ph/0201206.
- [185] C. Anastasiou and K. Melnikov, “Higgs boson production at hadron colliders in NNLO QCD”, *Nucl. Phys. B* **646** (2002) 220, doi:10.1016/S0550-3213(02)00837-4, arXiv:hep-ph/0207004.
- [186] V. Ravindran, J. Smith, and W. L. van Neerven, “NNLO corrections to the total cross-section for Higgs boson production in hadron hadron collisions”, *Nucl. Phys. B* **665** (2003) 325, doi:10.1016/S0550-3213(03)00457-7, arXiv:hep-ph/0302135.
- [187] R. V. Harlander and W. B. Kilgore, “Production of a pseudoscalar Higgs boson at hadron colliders at next-to-next-to leading order”, *JHEP* **10** (2002) 017, doi:10.1088/1126-6708/2002/10/017, arXiv:hep-ph/0208096.
- [188] C. Anastasiou and K. Melnikov, “Pseudoscalar Higgs boson production at hadron colliders in NNLO QCD”, *Phys. Rev. D* **67** (2003) 037501, doi:10.1103/PhysRevD.67.037501, arXiv:hep-ph/0208115.

- [189] U. Aglietti, R. Bonciani, G. Degrassi, and A. Vicini, “Two loop light fermion contribution to Higgs production and decays”, *Phys. Lett. B* **595** (2004) 432, doi:10.1016/j.physletb.2004.06.063, arXiv:hep-ph/0404071.
- [190] R. Bonciani, G. Degrassi, and A. Vicini, “On the generalized harmonic polylogarithms of one complex variable”, *Comput. Phys. Commun.* **182** (2011) 1253, doi:10.1016/j.cpc.2011.02.011, arXiv:1007.1891.
- [191] S. Heinemeyer, W. Hollik, and G. Weiglein, “FeynHiggs: A program for the calculation of the masses of the neutral CP even Higgs bosons in the MSSM”, *Comput. Phys. Commun.* **124** (2000) 76, doi:10.1016/S0010-4655(99)00364-1, arXiv:hep-ph/9812320.
- [192] S. Heinemeyer, W. Hollik, and G. Weiglein, “The masses of the neutral CP-even Higgs bosons in the MSSM: Accurate analysis at the two loop level”, *Eur. Phys. J. C* **9** (1999) 343, doi:10.1007/s100529900006, arXiv:hep-ph/9812472.
- [193] M. Frank et al., “The Higgs boson masses and mixings of the complex MSSM in the Feynman-diagrammatic approach”, *JHEP* **02** (2007) 047, doi:10.1088/1126-6708/2007/02/047, arXiv:hep-ph/0611326.
- [194] T. Hahn et al., “High-precision predictions for the light CP-even Higgs boson mass of the minimal supersymmetric standard model”, *Phys. Rev. Lett.* **112** (2014) 141801, doi:10.1103/PhysRevLett.112.141801, arXiv:1312.4937.
- [195] H. Bahl and W. Hollik, “Precise prediction for the light MSSM Higgs boson mass combining effective field theory and fixed-order calculations”, *Eur. Phys. J. C* **76** (2016) 499, doi:10.1140/epjc/s10052-016-4354-8, arXiv:1608.01880.
- [196] H. Bahl, S. Heinemeyer, W. Hollik, and G. Weiglein, “Reconciling EFT and hybrid calculations of the light MSSM Higgs-boson mass”, *Eur. Phys. J. C* **78** (2018) 57, doi:10.1140/epjc/s10052-018-5544-3, arXiv:1706.00346.
- [197] H. Bahl et al., “Precision calculations in the MSSM Higgs-boson sector with FeynHiggs 2.14”, *Comput. Phys. Commun.* **249** (2020) 107099, doi:10.1016/j.cpc.2019.107099, arXiv:1811.09073.
- [198] A. Bredenstein, A. Denner, S. Dittmaier, and M. M. Weber, “Precise predictions for the Higgs-boson decay $H \rightarrow WW/ZZ \rightarrow 4$ leptons”, *Phys. Rev. D* **74** (2006) 013004, doi:10.1103/PhysRevD.74.013004, arXiv:hep-ph/0604011.
- [199] A. Bredenstein, A. Denner, S. Dittmaier, and M. M. Weber, “Radiative corrections to the semileptonic and hadronic Higgs-boson decays $H \rightarrow WW/ZZ \rightarrow 4$ fermions”, *JHEP* **02** (2007) 080, doi:10.1088/1126-6708/2007/02/080, arXiv:hep-ph/0611234.
- [200] U. Ellwanger and C. Hugonie, “Benchmark planes for Higgs-to-Higgs decays in the NMSSM”, *Eur. Phys. J. C* **82** (2022) 406, doi:10.1140/epjc/s10052-022-10364-3, arXiv:2203.05049.
- [201] U. Ellwanger et al., “Benchmark lines and planes for Higgs-to-Higgs decays in the NMSSM”, **3**, 2024. arXiv:2403.15046.
- [202] T. Robens, “TRSM benchmark planes - EPS-HEP2023 update”, *PoS EPS-HEP2023* (2024) 055, doi:10.22323/1.449.0055, arXiv:2310.18045.

-
- [203] CMS Collaboration, “Search for a new scalar resonance decaying to a pair of Z bosons in proton-proton collisions at $\sqrt{s} = 13$ TeV”, *JHEP* **06** (2018) 127, doi:10.1007/JHEP06(2018)127, arXiv:1804.01939. [Erratum: doi:10.1007/JHEP03(2019)128].
 - [204] CMS Collaboration, “Search for heavy resonances decaying to $Z(\nu\bar{\nu})V(q\bar{q}')$ in proton-proton collisions at $\sqrt{s} = 13$ TeV”, *Phys. Rev. D* **106** (2022) 012004, doi:10.1103/PhysRevD.106.012004, arXiv:2109.08268.
 - [205] CMS Collaboration, “Search for heavy resonances decaying to ZZ or ZW and axion-like particles mediating nonresonant ZZ or ZH production at $\sqrt{s} = 13$ TeV”, *JHEP* **04** (2022) 087, doi:10.1007/JHEP04(2022)087, arXiv:2111.13669.
 - [206] CMS Collaboration, “Search for resonant and nonresonant new phenomena in high-mass dilepton final states at $\sqrt{s} = 13$ TeV”, *JHEP* **07** (2021) 208, doi:10.1007/JHEP07(2021)208, arXiv:2103.02708.
 - [207] CMS Collaboration, “Search for W' bosons decaying to a top and a bottom quark at $\sqrt{s} = 13$ TeV in the hadronic final state”, *Phys. Lett. B* **820** (2021) 136535, doi:10.1016/j.physletb.2021.136535, arXiv:2104.04831.
 - [208] CMS Collaboration, “Search for new physics in the lepton plus missing transverse momentum final state in proton-proton collisions at $\sqrt{s} = 13$ TeV”, *JHEP* **07** (2022) 067, doi:10.1007/JHEP07(2022)067, arXiv:2202.06075.
 - [209] CMS Collaboration, “Search for high mass dijet resonances with a new background prediction method in proton-proton collisions at $\sqrt{s} = 13$ TeV”, *JHEP* **05** (2020) 033, doi:10.1007/JHEP05(2020)033, arXiv:1911.03947.
 - [210] S. Heinemeyer, M. Mühlleitner, K. Radchenko, and G. Weiglein, “Higgs pair production in the 2HDM: Impact of loop corrections to the trilinear Higgs couplings and interference effects on experimental limits”, 3, 2024. arXiv:2403.14776.
 - [211] P. Basler, S. Dawson, C. Englert, and M. Mühlleitner, “Di-Higgs boson peaks and top valleys: Interference effects in Higgs sector extensions”, *Phys. Rev. D* **101** (2020) 015019, doi:10.1103/PhysRevD.101.015019, arXiv:1909.09987.
 - [212] M. Carena, Z. Liu, and M. Riembau, “Probing the electroweak phase transition via enhanced di-Higgs boson production”, *Phys. Rev. D* **97** (2018) 095032, doi:10.1103/PhysRevD.97.095032, arXiv:1801.00794.
 - [213] R. Grober, M. Mühlleitner, and M. Spira, “Higgs pair production at NLO QCD for CP-violating Higgs sectors”, *Nucl. Phys. B* **925** (2017) 1, doi:10.1016/j.nuclphysb.2017.10.002, arXiv:1705.05314.
 - [214] D. O'Connell, M. J. Ramsey-Musolf, and M. B. Wise, “Minimal Extension of the Standard Model Scalar Sector”, *Phys. Rev. D* **75** (2007) 037701, doi:10.1103/PhysRevD.75.037701, arXiv:hep-ph/0611014.
 - [215] A. Papaefstathiou and G. White, “The electro-weak phase transition at colliders: confronting theoretical uncertainties and complementary channels”, *JHEP* **05** (2021) 099, doi:10.1007/JHEP05(2021)099, arXiv:2010.00597.

- [216] A. Papaefstathiou and G. White, “The Electro-Weak Phase Transition at Colliders: Discovery Post-Mortem”, *JHEP* **02** (2022) 185, doi:10.1007/JHEP02(2022)185, arXiv:2108.11394.
- [217] J. Alwall et al., “The automated computation of tree-level and next-to-leading order differential cross sections, and their matching to parton shower simulations”, *JHEP* **07** (2014) doi:10.1007/JHEP07(2014)079, arXiv:1405.0301.
- [218] A. Alloul et al., “FeynRules 2.0 – A complete toolbox for tree-level phenomenology”, *Comput. Phys. Commun.* **185** (2014) 2250, doi:10.1016/j.cpc.2014.04.012, arXiv:1310.1921.
- [219] R. Grober, M. Mühlleitner, M. Spira, and J. Streicher, “NLO QCD corrections to Higgs pair production including dimension-6 operators”, *JHEP* **09** (2015) 092, doi:10.1007/JHEP09(2015)092, arXiv:1504.06577.
- [220] M. Cepeda et al., “Report from Working Group 2: Higgs physics at the HL-LHC and HE-LHC”, *CERN Yellow Rep. Monogr.* **7** (2019) 221, doi:10.23731/CYRM-2019-007.221, arXiv:1902.00134.
- [221] I. Zurbano Fernandez et al., “High-Luminosity Large Hadron Collider (HL-LHC): Technical design report”, technical report, 2020. doi:10.23731/CYRM-2020-0010.
- [222] A. Dainese et al., eds., “Report on the Physics at the HL-LHC, and Perspectives for the HE-LHC”, volume 7/2019 of *CERN Yellow Reports: Monographs*. CERN, 2019. doi:10.23731/CYRM-2019-007, ISBN 978-92-9083-549-3.


Glossary

A, a	<i>CP</i> -odd Higgs bosons in extended Higgs sector models
ATLAS	A Toroidal LHC Apparatus
BDT	Boosted decision tree
BSM	Beyond the standard model
CL	Confidence level
CMS	Compact Muon Solenoid
<i>CP</i>	Charge-parity (symmetry)
CR	Control region
DDT	Designing decorrelated taggers (procedure)
DNN	Deep neural network
DT	Deep tau (identification algorithm)
DY	Drell–Yan (process)
ECAL	Electromagnetic calorimeter
EFT	Effective field theory
EW	Electroweak
G	Graviton
ggF	Gluon-gluon fusion (production process)
HCAL	Hadron calorimeter
HH	Higgs boson pair
HL-LHC	High-Luminosity Large Hadron Collider
hMSSM	Habeat MSSM (scenario)
HVT	Heavy vector triplet (model)
KK	Kaluza-Klein (graviton)
LHC	Large Hadron Collider
LO	Leading order
MC	Monte Carlo (simulation)
MSSM	Minimal supersymmetric standard model
MVA	Multi-variate analysis
NMSSM	Next-to-minimal supersymmetric standard model
NLO	Next-to-leading order
NN	Neural network
NWA	Narrow-width approximation
N2HDM	Next-to-minimal 2HDM
PF	Particle flow (method of reconstructing particle candidates)
pp	Proton-proton
PU	Pileup
PUPPI	Pileup-per-particle identification (algorithm)
QCD	Quantum chromo-dynamics
R	Radion (graviscalar in the RS model), also distance in $(\Delta\eta, \Delta\phi)$ space
RS	Randall–Sundrum (model)
Run 2	The second run of the LHC, during the years 2015–2018
SD	Soft-drop (algorithm)
SM	Standard model
SR	Signal region
SUSY	Supersymmetry
\sqrt{s}	The center-of-mass energy
TRSM	Two-real-singlet Model



















UFO	Universal FeynRules output
V	Vector boson (W or Z)
VBF	Vector boson fusion (production process)
VH	Vector plus Higgs boson (production process or decay channel)
WED	Warped extra dimensions (model)
2HDM	Two-Higgs-doublet Model
2HDM+S	Two-Higgs-doublet-plus-additional-singlet model

A The CMS Collaboration




Yerevan Physics Institute, Yerevan, Armenia

A. Hayrapetyan, A. Tumasyan¹ 




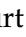








Institut für Hochenergiephysik, Vienna, Austria

W. Adam , J.W. Andrejkovic, T. Bergauer , S. Chatterjee , K. Damanakis , M. Dragicevic , P.S. Hussain , M. Jeitler² , N. Krammer , A. Li , D. Liko , I. Mikulec , J. Schieck² , R. Schöfbeck , D. Schwarz , M. Sonawane , S. Templ , W. Waltenberger , C.-E. Wulz² 










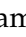




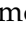

Universiteit Antwerpen, Antwerpen, Belgium

M.R. Darwish³ , T. Janssen , P. Van Mechelen 














Vrije Universiteit Brussel, Brussel, Belgium

N. Breugelmans, J. D'Hondt , S. Dansana , A. De Moor , M. Delcourt , F. Heyen, S. Lowette , I. Makarenko , D. Müller , S. Tavernier , M. Tytgat⁴ , G.P. Van Onsem , S. Van Putte , D. Vannerom 












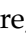


Université Libre de Bruxelles, Bruxelles, Belgium

B. Clerbaux , A.K. Das, G. De Lentdecker , H. Evard , L. Favart , P. Gianneios , D. Hohov , J. Jaramillo , A. Khalilzadeh, F.A. Khan , K. Lee , M. Mahdavihorrami , A. Malara , S. Paredes , L. Thomas , M. Vanden Bemden , C. Vander Velde , P. Vanlaer 








Ghent University, Ghent, Belgium

M. De Coen , D. Dobur , G. Gokbulut , Y. Hong , J. Knolle , L. Lambrecht , D. Marckx , G. Mestdach, K. Mota Amarilo , C. Rendón , A. Samalan, K. Skovpen , N. Van Den Bossche , J. van der Linden , L. Wezenbeek 












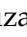



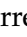
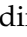
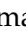
Université Catholique de Louvain, Louvain-la-Neuve, Belgium

A. Benecke , A. Bethani , G. Bruno , C. Caputo , J. De Favereau De Jeneret , C. Delaere , I.S. Donertas , A. Giammanco , A.O. Guzel , Sa. Jain , V. Lemaitre, J. Lidrych , P. Mastrapasqua , T.T. Tran , S. Wertz 


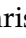
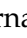

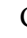




Centro Brasileiro de Pesquisas Físicas, Rio de Janeiro, Brazil

G.A. Alves , E. Coelho , C. Hensel , T. Menezes De Oliveira , A. Moraes , P. Rebello Teles , M. Soeiro, A. Vilela Pereira⁵ 

Universidade do Estado do Rio de Janeiro, Rio de Janeiro, Brazil































W.L. Aldá Júnior , M. Alves Gallo Pereira , M. Barroso Ferreira Filho , H. Brandao Malbouisson , W. Carvalho , J. Chinellato⁶, E.M. Da Costa , G.G. Da Silveira⁷ , D. De Jesus Damiao , S. Fonseca De Souza , R. Gomes De Souza, M. Macedo , J. Martins⁸ , C. Mora Herrera , L. Mundim , H. Nogima , J.P. Pinheiro , A. Santoro , A. Sznajder , M. Thiel 



Universidade Estadual Paulista, Universidade Federal do ABC, São Paulo, Brazil

C.A. Bernardes⁷ , L. Calligaris , T.R. Fernandez Perez Tomei , E.M. Gregores , I. Maietto Silverio , P.G. Mercadante , S.F. Novaes , B. Orzari , Sandra S. Padula 









Institute for Nuclear Research and Nuclear Energy, Bulgarian Academy of Sciences, Sofia, Bulgaria

A. Aleksandrov , G. Antchev , R. Hadjiiska , P. Iaydjiev , M. Misheva , M. Shopova , G. Sultanov 




University of Sofia, Sofia, BulgariaA. Dimitrov , L. Litov , B. Pavlov , P. Petkov , A. Petrov , E. Shumka **Instituto De Alta Investigación, Universidad de Tarapacá, Casilla 7 D, Arica, Chile**S. Keshri , S. Thakur **Beihang University, Beijing, China**T. Cheng , T. Javaid , L. Yuan **Department of Physics, Tsinghua University, Beijing, China**Z. Hu , Z. Liang, J. Liu, K. Yi^{9,10} **Institute of High Energy Physics, Beijing, China**G.M. Chen¹¹ , H.S. Chen¹¹ , M. Chen¹¹ , F. Iemmi , C.H. Jiang, A. Kapoor¹² , H. Liao , Z.-A. Liu¹³ , M.A. Shahzad¹¹, R. Sharma¹⁴ , J.N. Song¹³, J. Tao , C. Wang¹¹, J. Wang , Z. Wang¹¹, H. Zhang , J. Zhao **State Key Laboratory of Nuclear Physics and Technology, Peking University, Beijing, China**A. Agapitos , Y. Ban , A. Carvalho Antunes De Oliveira , S. Deng , B. Guo, C. Jiang , A. Levin , C. Li , Q. Li , Y. Mao, S. Qian, S.J. Qian , X. Qin, X. Sun , D. Wang , H. Yang, L. Zhang , Y. Zhao, C. Zhou **Guangdong Provincial Key Laboratory of Nuclear Science and Guangdong-Hong Kong Joint Laboratory of Quantum Matter, South China Normal University, Guangzhou, China**S. Yang **Sun Yat-Sen University, Guangzhou, China**Z. You **University of Science and Technology of China, Hefei, China**Z. Guo, K. Jaffel , N. Lu **Nanjing Normal University, Nanjing, China**G. Bauer¹⁵, B. Li, J. Zhang **Institute of Modern Physics and Key Laboratory of Nuclear Physics and Ion-beam Application (MOE) - Fudan University, Shanghai, China**X. Gao¹⁶ **Zhejiang University, Hangzhou, Zhejiang, China**Z. Lin , C. Lu , M. Xiao **Universidad de Los Andes, Bogota, Colombia**C. Avila , D.A. Barbosa Trujillo, A. Cabrera , C. Florez , J. Fraga , J.A. Reyes Vega**Universidad de Antioquia, Medellin, Colombia**F. Ramirez , M. Rodriguez , A.A. Ruales Barbosa , J.D. Ruiz Alvarez **University of Split, Faculty of Electrical Engineering, Mechanical Engineering and Naval Architecture, Split, Croatia**D. Giljanovic , N. Godinovic , D. Lelas , A. Sculac **University of Split, Faculty of Science, Split, Croatia**M. Kovac , A. Petkovic , T. Sculac **Institute Rudjer Boskovic, Zagreb, Croatia**P. Bargassa , V. Brigljevic , B.K. Chitroda , D. Ferencek , K. Jakovcic, S. Mishra 

A. Starodumov¹⁷ , T. Susa 


University of Cyprus, Nicosia, Cyprus

A. Attikis , K. Christoforou , A. Hadjiagapiou, A. Ioannou, C. Leonidou , J. Mousa ,
C. Nicolaou, L. Paizanos, F. Ptochos , P.A. Razis , H. Rykaczewski, H. Saka ,
A. Stepennov 


Charles University, Prague, Czech Republic

M. Finger , M. Finger Jr. , A. Kveton 



Universidad San Francisco de Quito, Quito, Ecuador

E. Carrera Jarrin 









Academy of Scientific Research and Technology of the Arab Republic of Egypt, Egyptian Network of High Energy Physics, Cairo, Egypt

Y. Assran^{18,19}, B. El-mahdy , S. Elgammal¹⁹

Center for High Energy Physics (CHEP-FU), Fayoum University, El-Fayoum, Egypt

A. Lotfy , M.A. Mahmoud 

National Institute of Chemical Physics and Biophysics, Tallinn, Estonia

K. Ehataht , M. Kadastik, T. Lange , S. Nandan , C. Nielsen , J. Pata , M. Raidal ,
L. Tani , C. Veelken 

Department of Physics, University of Helsinki, Helsinki, Finland

H. Kirschenmann , K. Osterberg , M. Voutilainen 







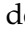
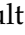



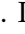





Helsinki Institute of Physics, Helsinki, Finland

S. Bharthuar , N. Bin Norjoharuddeen , E. Brücken , F. Garcia , P. Inkaew ,
K.T.S. Kallonen , R. Kinnunen, T. Lampén , K. Lassila-Perini , S. Lehti , T. Lindén ,
L. Martikainen , M. Myllymäki , M.m. Rantanen , H. Siikonen , J. Tuominiemi 



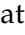
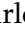
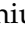
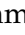





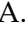
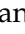


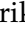





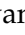



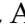
Lappeenranta-Lahti University of Technology, Lappeenranta, Finland

P. Luukka , H. Petrow 











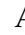






IRFU, CEA, Université Paris-Saclay, Gif-sur-Yvette, France

M. Besancon , F. Couderc , M. Dejardin , D. Denegri, J.L. Faure, F. Ferri , S. Ganjour ,
P. Gras , G. Hamel de Monchenault , V. Lohezic , J. Malcles , F. Orlandi , L. Portales ,
J. Rander, A. Rosowsky , M.Ö. Sahin , A. Savoy-Navarro²⁰ , P. Simkina , M. Titov ,
M. Tornago 

Laboratoire Leprince-Ringuet, CNRS/IN2P3, Ecole Polytechnique, Institut Polytechnique de Paris, Palaiseau, France

F. Beaudette , P. Busson , A. Cappati , C. Charlot , M. Chiusi , F. Damas ,
O. Davignon , A. De Wit , I.T. Ehle , B.A. Fontana Santos Alves , S. Ghosh ,
A. Gilbert , R. Granier de Cassagnac , A. Hakimi , B. Harikrishnan , L. Kalipoliti ,
G. Liu , M. Nguyen , C. Ochando , R. Salerno , J.B. Sauvan , Y. Sirois ,
L. Urda Gómez , E. Vernazza , A. Zabi , A. Zghiche 













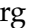



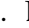

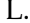
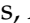




Université de Strasbourg, CNRS, IPHC UMR 7178, Strasbourg, France

J.-L. Agram²¹ , J. Andrea , D. Apparú , D. Bloch , J.-M. Brom , E.C. Chabert ,
C. Collard , S. Falke , U. Goerlach , R. Haeberle , A.-C. Le Bihan , M. Meena ,
O. Poncet , G. Saha , M.A. Sessini , P. Van Hove , P. Vaucelle 

Centre de Calcul de l'Institut National de Physique Nucleaire et de Physique des Particules, CNRS/IN2P3, Villeurbanne, France

A. Di Florio 










Institut de Physique des 2 Infinis de Lyon (IP2I), Villeurbanne, France

D. Amram , S. Beauceron , B. Blancon , G. Boudoul , N. Chanon , D. Contardo , P. Depasse , C. Dozen²² , H. El Mamouni , J. Fay , S. Gascon , M. Gouzevitch , C. Greenberg , G. Grenier , B. Ille , E. Jourd'huy , I.B. Laktineh , M. Lethuillier , L. Mirabito , S. Perries , A. Purohit , M. Vander Donckt , P. Verdier , J. Xiao 












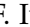



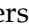




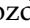


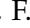



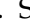




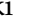
Georgian Technical University, Tbilisi, Georgia

G. Adamov , I. Lomidze , Z. Tsamalaidze¹⁷ 


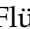






RWTH Aachen University, I. Physikalisches Institut, Aachen, Germany

V. Botta , L. Feld , K. Klein , M. Lipinski , D. Meuser , A. Pauls , D. Pérez Adán , N. Röwert , M. Teroerde 





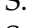
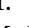
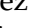

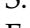
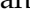




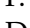

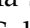


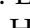
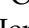



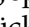






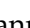




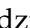

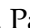










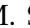



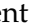


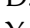
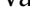

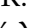
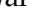

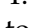
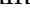

RWTH Aachen University, III. Physikalisches Institut A, Aachen, Germany

S. Diekmann , A. Dodonova , N. Eich , D. Eliseev , F. Engelke , J. Erdmann , M. Erdmann , P. Fackeldey , B. Fischer , T. Hebbeker , K. Hoepfner , F. Ivone , A. Jung , M.y. Lee , F. Mausolf , M. Merschmeyer , A. Meyer , S. Mukherjee , D. Noll , F. Nowotny , A. Pozdnyakov , Y. Rath , W. Redjeb , F. Rehm , H. Reithler , V. Sarkisovi , A. Schmidt , A. Sharma , J.L. Spah , A. Stein , F. Torres Da Silva De Araujo²³ , S. Wiedenbeck , S. Zaleski 




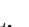



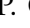

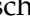


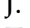
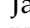

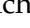


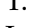
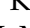

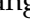


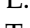
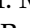
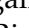
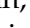


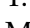
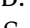
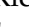
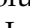


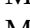

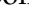
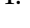
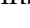
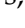


RWTH Aachen University, III. Physikalisches Institut B, Aachen, Germany

C. Dziwok , G. Flügge , T. Kress , A. Nowack , O. Pooth , A. Stahl , T. Ziemons , A. Zotz 

Deutsches Elektronen-Synchrotron, Hamburg, Germany

H. Aarup Petersen , M. Aldaya Martin , J. Alimena , S. Amoroso , Y. An , J. Bach , S. Baxter , M. Bayatmakou , H. Becerril Gonzalez , O. Behnke , A. Belvedere , S. Bhattacharya , F. Blekman²⁴ , K. Borras²⁵ , A. Campbell , A. Cardini , C. Cheng , F. Colombina , S. Consuegra Rodríguez , G. Correia Silva , M. De Silva , G. Eckerlin , D. Eckstein , L.I. Estevez Banos , O. Filatov , E. Gallo²⁴ , A. Geiser , V. Guglielmi , M. Guthoff , A. Hinzmann , L. Jeppe , B. Kaech , M. Kasemann , C. Kleinwort , R. Kogler , M. Komm , D. Krücker , W. Lange , D. Leyva Pernia , K. Lipka²⁶ , W. Lohmann²⁷ , F. Lorkowski , R. Mankel , I.-A. Melzer-Pellmann , M. Mendizabal Morentin , A.B. Meyer , G. Milella , K. Moral Figueroa , A. Mussgiller , L.P. Nair , J. Niedziela , A. Nürnberg , Y. Otariid , J. Park , E. Ranken , A. Raspereza , D. Rastorguev , J. Rübenach , L. Rygaard , A. Saggio , M. Scham^{28,25} , S. Schnake²⁵ , P. Schütze , C. Schwanenberger²⁴ , D. Selivanova , K. Sharko , M. Shchedrolosiev , D. Stafford , F. Vazzoler , A. Ventura Barroso , R. Walsh , D. Wang , Q. Wang , Y. Wen , K. Wichmann , L. Wiens²⁵ , C. Wissing , Y. Yang , A. Zimmermann Castro Santos 






University of Hamburg, Hamburg, Germany

A. Albrecht , S. Albrecht , M. Antonello , S. Bein , L. Benato , S. Bollweg , M. Bonanomi , P. Connor , K. El Morabit , Y. Fischer , E. Garutti , A. Grohsjean , J. Haller , H.R. Jabusch , G. Kasieczka , P. Keicher , R. Klanner , W. Korcari , T. Kramer , C.c. Kuo , V. Kutzner , F. Labe , J. Lange , A. Lobanov , C. Matthies , L. Moureaux , M. Mrowietz , A. Nigamova , Y. Nissan , A. Paasch , K.J. Pena Rodriguez , T. Quadfasel , B. Raciti , M. Rieger , D. Savoivu , J. Schindler , P. Schleper , M. Schröder , J. Schwandt , M. Sommerhalder , H. Stadie , G. Steinbrück , A. Tews , M. Wolf 

Karlsruher Institut fuer Technologie, Karlsruhe, Germany

S. Brommer , M. Burkart , E. Butz , T. Chwalek , A. Dierlamm , A. Droll , N. Faltermann , M. Giffels , A. Gottmann , F. Hartmann²⁹ , R. Hofsaess , M. Horzela , U. Husemann , J. Kieseler , M. Klute , R. Koppenhöfer , J.M. Lawhorn , M. Link , A. Lintuluoto , B. Maier , S. Maier , S. Mitra , M. Mormile , Th. Müller , M. Neukum , M. Oh , E. Pfeffer , M. Presilla , G. Quast , K. Rabbertz , B. Regnery , N. Shadskiy , I. Shvetsov , H.J. Simonis , L. Sowa , L. Stockmeier , K. Tauqeer , M. Toms , N. Trevisani , R.F. Von Cube , M. Wassmer , S. Wieland , F. Wittig , R. Wolf , X. Zuo

Institute of Nuclear and Particle Physics (INPP), NCSR Demokritos, Aghia Paraskevi, Greece

G. Anagnostou , G. Daskalakis , A. Kyriakis , A. Papadopoulos²⁹ , A. Stakia 

National and Kapodistrian University of Athens, Athens, Greece

P. Kontaxakis , G. Melachroinos , Z. Painesis , A. Panagiotou , I. Papavergou , I. Paraskevas , N. Saoulidou , K. Theofilatos , E. Tziaferi , K. Vellidis , I. Zisopoulos



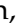



National Technical University of Athens, Athens, Greece

G. Bakas , T. Chatzistavrou , G. Karapostoli , K. Kousouris , I. Papakrivopoulos , E. Siamarkou , G. Tsipolitis , A. Zacharopoulou

University of Ioánnina, Ioánnina, Greece

K. Adamidis , I. Bestintzanos , I. Evangelou , C. Foudas , C. Kamtsikis , P. Katsoulis , P. Kokkas , P.G. Kosmoglou Kioseoglou , N. Manthos , I. Papadopoulos , J. Strogas




HUN-REN Wigner Research Centre for Physics, Budapest, Hungary

C. Hajdu , D. Horvath^{30,31} , K. Márton , A.J. Rádl³² , F. Sikler , V. Veszpremi 





MTA-ELTE Lendület CMS Particle and Nuclear Physics Group, Eötvös Loránd University, Budapest, Hungary

M. Csanád , K. Farkas , A. Fehérkuti³³ , M.M.A. Gadallah³⁴ , Á. Kadlecik , P. Major , G. Pásztor , G.I. Veres

Faculty of Informatics, University of Debrecen, Debrecen, Hungary

P. Raics , B. Ujvari , G. Zilizi 


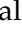

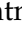
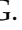

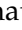



HUN-REN ATOMKI - Institute of Nuclear Research, Debrecen, Hungary

G. Bencze , S. Czellar , J. Molnar , Z. Szillasi 

Karoly Robert Campus, MATE Institute of Technology, Gyongyos, Hungary

T. Csorgo³³ , T. Novak 

Panjab University, Chandigarh, India

J. Babbar , S. Bansal , S.B. Beri , V. Bhatnagar , G. Chaudhary , S. Chauhan , N. Dhingra³⁵ , A. Kaur , A. Kaur , H. Kaur , M. Kaur , S. Kumar , K. Sandeep , T. Sheokand , J.B. Singh , A. Singla

University of Delhi, Delhi, India

A. Ahmed , A. Bhardwaj , A. Chhetri , B.C. Choudhary , A. Kumar , A. Kumar , M. Naimuddin , K. Ranjan , M.K. Saini , S. Saumya 

Saha Institute of Nuclear Physics, HBNI, Kolkata, India

S. Baradia , S. Barman³⁶ , S. Bhattacharya , S. Das Gupta , S. Dutta , S. Dutta , S. Sarkar 

Indian Institute of Technology Madras, Madras, India








M.M. Ameen , P.K. Behera , S.C. Behera , S. Chatterjee , G. Dash , P. Jana 

P. Kalbhor , S. Kamble , J.R. Komaragiri³⁷ , D. Kumar³⁷ , L. Panwar³⁷ , P.R. Pujahari , N.R. Saha , A. Sharma , A.K. Sikdar , R.K. Singh , P. Verma , S. Verma , A. Vijay 













Tata Institute of Fundamental Research-A, Mumbai, India

S. Dugad, M. Kumar , G.B. Mohanty , B. Parida , M. Shelake, P. Suryadevara











Tata Institute of Fundamental Research-B, Mumbai, India

A. Bala , S. Banerjee , R.M. Chatterjee, M. Guchait , Sh. Jain , A. Jaiswal, S. Kumar , G. Majumder , K. Mazumdar , S. Parolia , A. Thachayath 

National Institute of Science Education and Research, An OCC of Homi Bhabha National Institute, Bhubaneswar, Odisha, India

S. Bahinipati³⁸ , C. Kar , D. Maity³⁹ , P. Mal , T. Mishra , V.K. Muraleedharan Nair Bindhu³⁹ , K. Naskar³⁹ , A. Nayak³⁹ , S. Nayak, K. Pal , P. Sadangi, S.K. Swain , S. Varghese³⁹ , D. Vats³⁹ 


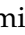





Indian Institute of Science Education and Research (IISER), Pune, India

S. Acharya⁴⁰ , A. Alpana , S. Dube , B. Gomber⁴⁰ , P. Hazarika , B. Kansal , A. Laha , B. Sahu⁴⁰ , S. Sharma , K.Y. Vaish 

Isfahan University of Technology, Isfahan, Iran

H. Bakhshiansohi⁴¹ , A. Jafari⁴² , M. Zeinali⁴³ 


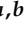

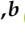




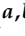








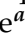
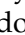










Institute for Research in Fundamental Sciences (IPM), Tehran, Iran

S. Bashiri, S. Chenarani⁴⁴ , S.M. Etesami , Y. Hosseini , M. Khakzad , E. Khazaie⁴⁵ , M. Mohammadi Najafabadi , S. Tizchang 






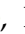

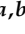


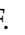


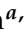



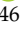


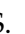









University College Dublin, Dublin, Ireland

M. Felcini , M. Grunewald 

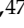
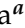
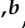


INFN Sezione di Bari^a, Università di Bari^b, Politecnico di Bari^c, Bari, Italy

M. Abbrescia^{a,b} , A. Colaleo^{a,b} , D. Creanza^{a,c} , B. D'Anzi^{a,b} , N. De Filippis^{a,c} , M. De Palma^{a,b} , L. Fiore^a , G. Iaselli^{a,c} , M. Louka^{a,b} , G. Maggi^{a,c} , M. Maggi^a , I. Margjeka^{a,b} , V. Mastrapasqua^{a,b} , S. My^{a,b} , S. Nuzzo^{a,b} , A. Pellecchia^{a,b} , A. Pompili^{a,b} , G. Pugliese^{a,c} , R. Radogna^a , D. Ramos^a , A. Ranieri^a , L. Silvestris^a , F.M. Simone^{a,b} , Ü. Sözbilir^a , A. Stamerra^a , D. Troiano^a , R. Venditti^a , P. Verwilligen^a , A. Zaza^{a,b} 

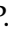


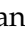
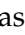





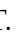








INFN Sezione di Bologna^a, Università di Bologna^b, Bologna, Italy

G. Abbiendi^a , C. Battilana^{a,b} , D. Bonacorsi^{a,b} , L. Borgonovi^a , P. Capiluppi^{a,b} , A. Castro^{a,b} , F.R. Cavallo^a , M. Cuffiani^{a,b} , G.M. Dallavalle^a , T. Diotallevi^{a,b} , F. Fabbri^a , A. Fanfani^{a,b} , D. Fasanella^{a,b} , P. Giacomelli^a , L. Giommi^{a,b} , C. Grandi^a , L. Guiducci^{a,b} , S. Lo Meo^{a,46} , M. Lorusso^{a,b} , L. Lunerti^a , S. Marcellini^a , G. Masetti^a , F.L. Navarria^{a,b} , G. Paggi^a , A. Perrotta^a , F. Primavera^{a,b} , A.M. Rossi^{a,b} , S. Rossi Tisbeni^{a,b} , T. Rovelli^{a,b} , G.P. Siroli^{a,b} 

INFN Sezione di Catania^a, Università di Catania^b, Catania, Italy

S. Costa^{a,b,47} , A. Di Mattia^a , R. Potenza^{a,b} , A. Tricomi^{a,b,47} , C. Tuve^{a,b} 

INFN Sezione di Firenze^a, Università di Firenze^b, Firenze, Italy

P. Assiouras^a , G. Barbagli^a , G. Bardelli^{a,b} , B. Camaiani^{a,b} , A. Cassese^a , R. Ceccarelli^a , V. Ciulli^{a,b} , C. Civinini^a , R. D'Alessandro^{a,b} , E. Focardi^{a,b} , T. Kello^a , G. Latino^{a,b} , P. Lenzi^{a,b} , M. Lizzo^a , M. Meschini^a , S. Paoletti^a , A. Papanastassiou^{a,b} , G. Sguazzoni^a , L. Viliani^a 















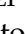


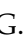







INFN Laboratori Nazionali di Frascati, Frascati, Italy

L. Benussi , S. Bianco , S. Meola⁴⁸ , D. Piccolo 










INFN Sezione di Genova^a, Università di Genova^b, Genova, Italy

P. Chatagnon^a , F. Ferro^a , E. Robutti^a , S. Tosi^{a,b} 









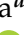



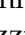
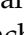



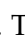










INFN Sezione di Milano-Bicocca^a, Università di Milano-Bicocca^b, Milano, Italy

A. Benaglia^a , G. Boldrini^{a,b} , F. Brivio^a , F. Cetorelli^a , F. De Guio^{a,b} , M.E. Dinardo^{a,b} , P. Dini^a , S. Gennai^a , R. Gerosa^{a,b} , A. Ghezzi^{a,b} , P. Govoni^{a,b} , L. Guzzi^a , M.T. Lucchini^{a,b} , M. Malberti^a , S. Malvezzi^a , A. Massironi^a , D. Menasce^a , L. Moroni^a , M. Paganoni^{a,b} , S. Palluotto^{a,b} , D. Pedrini^a , A. Perego^a , B.S. Pinolini^a, G. Pizzati^{a,b} , S. Ragazzi^{a,b} , T. Tabarelli de Fatis^{a,b} 




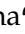


INFN Sezione di Napoli^a, Università di Napoli 'Federico II'^b, Napoli, Italy; Università della Basilicata^c, Potenza, Italy; Scuola Superiore Meridionale (SSM)^d, Napoli, Italy

S. Buontempo^a , A. Cagnotta^{a,b} , F. Carnevali^{a,b}, N. Cavallo^{a,c} , F. Fabozzi^{a,c} , A.O.M. Iorio^{a,b} , L. Lista^{a,b,49} , P. Paolucci^{a,29} , B. Rossi^a , C. Sciacca^{a,b} 





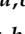
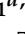
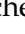
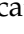




INFN Sezione di Padova^a, Università di Padova^b, Padova, Italy; Università di Trento^c, Trento, Italy

R. Ardino^a , P. Azzi^a , N. Bacchetta^{a,50} , M. Benettoni^a , A. Bergnoli^a , D. Bisello^{a,b} , P. Bortignon^a , G. Bortolato^{a,b}, A. Bragagnolo^{a,b} , A.C.M. Bulla^a , P. Checchia^a , T. Dorigo^a , F. Gasparini^{a,b} , U. Gasparini^{a,b} , E. Lusiani^a , M. Margoni^{a,b} , A.T. Meneguzzo^{a,b} , M. Migliorini^{a,b} , J. Pazzini^{a,b} , P. Ronchese^{a,b} , R. Rossin^{a,b} , F. Simonetto^{a,b} , G. Strong^a , M. Tosi^{a,b} , A. Triossi^{a,b} , S. Ventura^a , M. Zanetti^{a,b} , P. Zotto^{a,b} , A. Zucchetta^{a,b} 




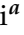



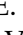



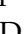

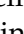











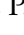






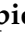
INFN Sezione di Pavia^a, Università di Pavia^b, Pavia, Italy

C. Aimè^a , A. Braghieri^a , S. Calzaferri^a , D. Fiorina^a , P. Montagna^{a,b} , V. Re^a , C. Riccardi^{a,b} , P. Salvini^a , I. Vai^{a,b} , P. Vitulo^{a,b} 







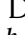






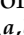






INFN Sezione di Perugia^a, Università di Perugia^b, Perugia, Italy

S. Ajmal^{a,b} , M.E. Ascioti^{a,b}, G.M. Bilei^a , C. Carrivale^{a,b}, D. Ciangottini^{a,b} , L. Fanò^{a,b} , M. Magherini^{a,b} , V. Mariani^{a,b} , M. Menichelli^a , F. Moscatelli^{a,51} , A. Rossi^{a,b} , A. Santocchia^{a,b} , D. Spiga^a , T. Tedeschi^{a,b} 













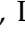







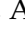

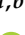








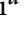

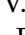
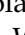
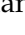
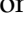
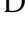




INFN Sezione di Pisa^a, Università di Pisa^b, Scuola Normale Superiore di Pisa^c, Pisa, Italy; Università di Siena^d, Siena, Italy

C.A. Alexe^{a,c} , P. Asenov^{a,b} , P. Azzurri^a , G. Bagliesi^a , R. Bhattacharya^a , L. Bianchini^{a,b} , T. Boccali^a , E. Bossini^a , D. Bruschini^{a,c} , R. Castaldi^a , M.A. Ciocci^{a,b} , M. Cipriani^{a,b} , V. D'Amante^{a,d} , R. Dell'Orso^a , S. Donato^a , A. Giassi^a , F. Ligabue^{a,c} , D. Matos Figueiredo^a , A. Messineo^{a,b} , M. Musich^{a,b} , F. Palla^a , A. Rizzi^{a,b} , G. Rolandi^{a,c} , S. Roy Chowdhury^a , T. Sarkar^a , A. Scribano^a , P. Spagnolo^a , R. Tenchini^a , G. Tonelli^{a,b} , N. Turini^{a,d} , F. Vaselli^{a,c} , A. Venturi^a , P.G. Verdini^a 







INFN Sezione di Roma^a, Sapienza Università di Roma^b, Roma, Italy

C. Baldenegro Barrera^{a,b} , P. Barria^a , C. Basile^{a,b} , M. Campana^{a,b} , F. Cavallari^a , L. Cunqueiro Mendez^{a,b} , D. Del Re^{a,b} , E. Di Marco^a , M. Diemoz^a , F. Errico^{a,b} , E. Longo^{a,b} , J. Mijuskovic^{a,b} , G. Organtini^{a,b} , F. Pandolfi^a , R. Paramatti^{a,b} , C. Quaranta^{a,b} , S. Rahatlou^{a,b} , C. Rovelli^a , F. Santanastasio^{a,b} , L. Soffi^a 

INFN Sezione di Torino^a, Università di Torino^b, Torino, Italy; Università del Piemonte Orientale^c, Novara, Italy

N. Amapane^{a,b} , R. Arcidiacono^{a,c} , S. Argiro^{a,b} , M. Arneodo^{a,c} , N. Bartosik^a , R. Bellan^{a,b} , A. Bellora^{a,b} , C. Biino^a , C. Borca^{a,b} , N. Cartiglia^a , M. Costa^{a,b} , R. Covarelli^{a,b} , N. Demaria^a , L. Finco^a , M. Grippo^{a,b} , B. Kiani^{a,b} , F. Legger^a , F. Luongo^{a,b} , C. Mariotti^a , L. Markovic^{a,b} , S. Maselli^a , A. Mecca^{a,b} , L. Menzio^{a,b} , P. Meridiani^a , E. Migliore^{a,b} , M. Monteno^a , R. Mulargia^a , M.M. Obertino^{a,b} , G. Ortona^a , L. Pacher^{a,b} , N. Pastrone^a , M. Pelliccioni^a , M. Ruspa^{a,c} , F. Siviero^{a,b} , V. Sola^{a,b} , A. Solano^{a,b} , A. Staiano^a , C. Tarricone^{a,b} , D. Trocino^a , G. Umoret^{a,b} , E. Vlasov^{a,b} , R. White^{a,b} 

INFN Sezione di Trieste^a, Università di Trieste^b, Trieste, Italy

S. Belforte^a , V. Candelise^{a,b} , M. Casarsa^a , F. Cossutti^a , K. De Leo^a , G. Della Ricca^{a,b} 




Kyungpook National University, Daegu, Korea

S. Dogra , J. Hong , C. Huh , B. Kim , J. Kim , D. Lee , H. Lee , S.W. Lee , C.S. Moon , Y.D. Oh , M.S. Ryu , S. Sekmen , B. Tae , Y.C. Yang 

Department of Mathematics and Physics - GWNu, Gangneung, Korea

M.S. Kim 


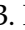






Chonnam National University, Institute for Universe and Elementary Particles, Kwangju, Korea

G. Bak , P. Gwak , H. Kim , D.H. Moon 

Hanyang University, Seoul, Korea

E. Asilar , J. Choi , D. Kim , T.J. Kim , J.A. Merlin , Y. Ryou 

Korea University, Seoul, Korea

S. Choi , S. Han , B. Hong , K. Lee , K.S. Lee , S. Lee , S.K. Park , J. Yoo 

Kyung Hee University, Department of Physics, Seoul, Korea

J. Goh , S. Yang 


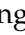


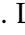


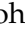


Sejong University, Seoul, Korea

H. S. Kim , Y. Kim , S. Lee 



Seoul National University, Seoul, Korea

J. Almond , J.H. Bhyun , J. Choi , J. Choi , W. Jun , J. Kim , S. Ko , H. Kwon , H. Lee , J. Lee , J. Lee , B.H. Oh , S.B. Oh , H. Seo , U.K. Yang , I. Yoon 

University of Seoul, Seoul, Korea

W. Jang , D.Y. Kang , Y. Kang , S. Kim , B. Ko , J.S.H. Lee , Y. Lee , I.C. Park , Y. Roh , I.J. Watson 


Yonsei University, Department of Physics, Seoul, Korea

S. Ha , H.D. Yoo 

Sungkyunkwan University, Suwon, Korea






















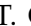






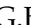







M. Choi , M.R. Kim , H. Lee , Y. Lee , I. Yu 

College of Engineering and Technology, American University of the Middle East (AUM), Dasman, Kuwait













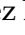








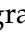



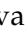
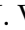

T. Beyrouthy 

Riga Technical University, Riga, Latvia

K. Dreimanis , A. Gaile , G. Pikurs , A. Potrebko , M. Seidel , D. Sidiropoulos Kontos 

University of Latvia (LU), Riga, LatviaN.R. Strautnieks **Vilnius University, Vilnius, Lithuania**M. Ambrozas , A. Juodagalvis , A. Rinkevicius , G. Tamulaitis **National Centre for Particle Physics, Universiti Malaya, Kuala Lumpur, Malaysia**I. Yusuff⁵² , Z. Zolkapli**Universidad de Sonora (UNISON), Hermosillo, Mexico**J.F. Benitez , A. Castaneda Hernandez , H.A. Encinas Acosta, L.G. Gallegos Maríñez, M. León Coello , J.A. Murillo Quijada , A. Sehrawat , L. Valencia Palomo **Centro de Investigacion y de Estudios Avanzados del IPN, Mexico City, Mexico**G. Ayala , H. Castilla-Valdez , H. Crotte Ledesma, E. De La Cruz-Burelo , I. Heredia-De La Cruz⁵³ , R. Lopez-Fernandez , J. Mejia Guisao , C.A. Mondragon Herrera, A. Sánchez Hernández **Universidad Iberoamericana, Mexico City, Mexico**C. Oropeza Barrera , D.L. Ramirez Guadarrama, M. Ramírez García **Benemerita Universidad Autonoma de Puebla, Puebla, Mexico**I. Bautista , I. Pedraza , H.A. Salazar Ibarguen , C. Uribe Estrada **University of Montenegro, Podgorica, Montenegro**I. Bubanja , N. Raicevic **University of Canterbury, Christchurch, New Zealand**P.H. Butler **National Centre for Physics, Quaid-I-Azam University, Islamabad, Pakistan**A. Ahmad , M.I. Asghar, A. Awais , M.I.M. Awan, H.R. Hoorani , W.A. Khan **AGH University of Krakow, Faculty of Computer Science, Electronics and Telecommunications, Krakow, Poland**V. Avati, L. Grzanka , M. Malawski **National Centre for Nuclear Research, Swierk, Poland**H. Bialkowska , M. Bluj , M. Górski , M. Kazana , M. Szleper , P. Zalewski **Institute of Experimental Physics, Faculty of Physics, University of Warsaw, Warsaw, Poland**K. Bunkowski , K. Doroba , A. Kalinowski , M. Konecki , J. Krolikowski , A. Muhammad **Warsaw University of Technology, Warsaw, Poland**K. Pozniak , W. Zabolotny **Laboratório de Instrumentação e Física Experimental de Partículas, Lisboa, Portugal**M. Araujo , D. Bastos , C. Beirão Da Cruz E Silva , A. Boletti , M. Bozzo , T. Camporesi , G. Da Molin , P. Faccioli , M. Gallinaro , J. Hollar , N. Leonardo , G.B. Marozzo , T. Niknejad , A. Petrilli , M. Pisano , J. Seixas , J. Varela , J.W. Wulff **Faculty of Physics, University of Belgrade, Belgrade, Serbia**P. Adzic , P. Milenovic **VINCA Institute of Nuclear Sciences, University of Belgrade, Belgrade, Serbia**M. Dordevic , J. Milosevic , L. Nadderd , V. Rekovic















Centro de Investigaciones Energéticas Medioambientales y Tecnológicas (CIEMAT), Madrid, Spain

J. Alcaraz Maestre , Cristina F. Bedoya , Oliver M. Carretero , M. Cepeda , M. Cerrada , N. Colino , B. De La Cruz , A. Delgado Peris , A. Escalante Del Valle , D. Fernández Del Val , J.P. Fernández Ramos , J. Flix , M.C. Fouz , O. Gonzalez Lopez , S. Goy Lopez , J.M. Hernandez , M.I. Josa , E. Martin Viscasillas , D. Moran , C.M. Morcillo Perez , Á. Navarro Tobar , C. Perez Dengra , A. Pérez-Calero Yzquierdo , J. Puerta Pelayo , I. Redondo , S. Sánchez Navas , J. Sastre , J. Vazquez Escobar 













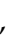






Universidad Autónoma de Madrid, Madrid, Spain

J.F. de Trocóniz 



Universidad de Oviedo, Instituto Universitario de Ciencias y Tecnologías Espaciales de Asturias (ICTEA), Oviedo, Spain

B. Alvarez Gonzalez , J. Cuevas , J. Fernandez Menendez , S. Folgueras , I. Gonzalez Caballero , J.R. González Fernández , P. Leguina , E. Palencia Cortezon , C. Ramón Álvarez , V. Rodríguez Bouza , A. Soto Rodríguez , A. Trapote , C. Vico Villalba , P. Vischia 

Instituto de Física de Cantabria (IFCA), CSIC-Universidad de Cantabria, Santander, Spain

S. Bhowmik , S. Blanco Fernández , J.A. Brochero Cifuentes , I.J. Cabrillo , A. Calderon , J. Duarte Campderros , M. Fernandez , G. Gomez , C. Lasasa García , R. Lopez Ruiz , C. Martinez Rivero , P. Martinez Ruiz del Arbol , F. Matorras , P. Matorras Cuevas , E. Navarrete Ramos , J. Piedra Gomez , L. Scodellaro , I. Vila , J.M. Vizan Garcia 







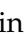


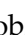

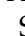








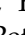
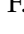

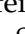
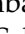


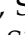





University of Colombo, Colombo, Sri Lanka

B. Kailasapathy⁵⁴ , D.D.C. Wickramarathna 








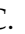




University of Ruhuna, Department of Physics, Matara, Sri Lanka

W.G.D. Dharmaratna⁵⁵ , K. Liyanage , N. Perera 







CERN, European Organization for Nuclear Research, Geneva, Switzerland

D. Abbaneo , C. Amendola , E. Auffray , G. Auzinger , J. Baechler, D. Barney , A. Bermúdez Martínez , M. Bianco , B. Bilin , A.A. Bin Anuar , A. Bocci , C. Botta , E. Brondolin , C. Caillol , G. Cerminara , N. Chernyavskaya , D. d'Enterria , A. Dabrowski , A. David , A. De Roeck , M.M. Defranchis , M. Deile , M. Dobson , G. Franzoni , W. Funk , S. Giani, D. Gigi, K. Gill , F. Glege , L. Gouskos , J. Hegeman , J.K. Heikkilä , B. Huber , V. Innocente , T. James , P. Janot , O. Kaluzinska , S. Laurila , P. Lecoq , E. Leutgeb , C. Lourenço , L. Malgeri , M. Mannelli , A.C. Marini , M. Matthewman, A. Mehta , F. Meijers , S. Mersi , E. Meschi , V. Milosevic , F. Monti , F. Moortgat , M. Mulders , I. Neutelings , S. Orfanelli, F. Pantaleo , G. Petrucciani , A. Pfeiffer , M. Pierini , H. Qu , D. Rabadý , B. Ribeiro Lopes , M. Rovere , H. Sakulin , S. Sanchez Cruz , S. Scarfi , C. Schwick, M. Selvaggi , A. Sharma , K. Shchelina , P. Silva , P. Sphicas⁵⁶ , A.G. Stahl Leiton , A. Steen , S. Summers , D. Treille , P. Tropea , D. Walter , J. Wanczyk⁵⁷ , J. Wang, S. Wuchterl , P. Zehetner , P. Zejdl , W.D. Zeuner








PSI Center for Neutron and Muon Sciences, Villigen, Switzerland

T. Bevilacqua⁵⁸ , L. Caminada⁵⁸ , A. Ebrahimi , W. Erdmann , R. Horisberger , Q. Ingram , H.C. Kaestli , D. Kotlinski , C. Lange , M. Missiroli⁵⁸ , L. Noehte⁵⁸ , T. Rohe 








ETH Zurich - Institute for Particle Physics and Astrophysics (IPA), Zurich, Switzerland

T.K. Aarrestad , K. Androsoy⁵⁷ , M. Backhaus , G. Bonomelli , A. Calandri , C. Cazaniga , K. Datta , P. De Bryas Dexmiers D'archiac⁵⁷ , A. De Cosa , G. Dissertori , M. Dittmar , M. Donegà , F. Eble , M. Galli , K. Gedia , F. Glessgen , C. Grab , N. Härringer , T.G. Harte , D. Hits , W. Lustermann , A.-M. Lyon , R.A. Manzoni , M. Marchegiani , L. Marchese , C. Martin Perez , A. Mascellani⁵⁷ , F. Nessi-Tedaldi , F. Pauss , V. Perovic , S. Pigazzini , C. Reissel , T. Reitenspiess , B. Ristic , F. Riti , R. Seidita , J. Steggemann⁵⁷ , A. Tarabini , D. Valsecchi , R. Wallny







Universität Zürich, Zurich, Switzerland

C. Amsler⁵⁹ , P. Bärtschi , M.F. Canelli , K. Cormier , M. Huwiler , W. Jin , A. Jofrehei , B. Kilminster , S. Leontsinis , S.P. Liehti , A. Macchiolo , P. Meiring , F. Meng , U. Molinatti , J. Motta , A. Reimers , P. Robmann , M. Senger , E. Shokr , F. Stäger , R. Tramontano


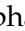
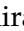
National Central University, Chung-Li, Taiwan

C. Adloff⁶⁰ , D. Bhowmik , C.M. Kuo , W. Lin , P.K. Rout , P.C. Tiwari³⁷ , S.S. Yu 








National Taiwan University (NTU), Taipei, Taiwan

L. Ceard , K.F. Chen , P.s. Chen , Z.g. Chen , A. De Iorio , W.-S. Hou , T.h. Hsu , Y.w. Kao , S. Karmakar , G. Kole , Y.y. Li , R.-S. Lu , E. Paganis , X.f. Su , J. Thomas-Wilsker , L.s. Tsai , H.y. Wu , E. Yazgan



High Energy Physics Research Unit, Department of Physics, Faculty of Science, Chulalongkorn University, Bangkok, Thailand

C. Asawatangkuldee , N. Srimanobhas , V. Wachirapusanand 

Çukurova University, Physics Department, Science and Art Faculty, Adana, Turkey

D. Agyel , F. Boran , F. Dolek , I. Dumanoglu⁶¹ , E. Eskut , Y. Guler⁶² , E. Gurpınar Guler⁶² , C. Isik , O. Kara , A. Kayis Topaksu , U. Kiminsu , G. Onengut , K. Ozdemir⁶³ , A. Polatoz , B. Tali⁶⁴ , U.G. Tok , S. Turkcapar , E. Uslan , I.S. Zorbakir






Middle East Technical University, Physics Department, Ankara, Turkey

G. Sokmen , M. Yalvac⁶⁵ 

Bogazici University, Istanbul, Turkey

B. Akgun , I.O. Atakisi , E. Gülmez , M. Kaya⁶⁶ , O. Kaya⁶⁷ , S. Tekten⁶⁸ 





Istanbul Technical University, Istanbul, Turkey

A. Cakir , K. Cankocak^{61,69} , G.G. Dincer⁶¹ , Y. Komurcu , S. Sen⁷⁰ 

Istanbul University, Istanbul, Turkey

O. Aydılek⁷¹ , V. Epshteyn , B. Hacisahinoglu , I. Hos⁷² , B. Kaynak , S. Ozkorucuklu , O. Potok , H. Sert , C. Simsek , C. Zorbilmez


Yildiz Technical University, Istanbul, Turkey

S. Cerci⁶⁴ , B. Isildak⁷³ , D. Sunar Cerci , T. Yetkin 












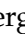


Institute for Scintillation Materials of National Academy of Science of Ukraine, Kharkiv, Ukraine

A. Boyaryntsev , B. Grynyov 













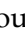

National Science Centre, Kharkiv Institute of Physics and Technology, Kharkiv, Ukraine

L. Levchuk 








University of Bristol, Bristol, United Kingdom

D. Anthony , J.J. Brooke , A. Bundock , F. Bury , E. Clement , D. Cussans , H. Flacher , M. Glowacki , J. Goldstein , H.F. Heath , M.-L. Holmberg , L. Kreczko , S. Paramesvaran , L. Robertshaw , S. Seif El Nasr-Storey , V.J. Smith , N. Stylianou⁷⁴ , K. Walkingshaw Pass



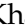


Rutherford Appleton Laboratory, Didcot, United Kingdom

A.H. Ball , K.W. Bell , A. Belyaev⁷⁵ , C. Brew , R.M. Brown , D.J.A. Cockerill , C. Cooke , A. Elliot , K.V. Ellis , K. Harder , S. Harper , J. Linacre , K. Manolopoulos , D.M. Newbold , E. Olaiya , D. Petyt , T. Reis , A.R. Sahasransu , G. Salvi , T. Schuh , C.H. Shepherd-Themistocleous , I.R. Tomalin , K.C. Whalen , T. Williams

Imperial College, London, United Kingdom

I. Andreou , R. Bainbridge , P. Bloch , C.E. Brown , O. Buchmuller , V. Cacchio , C.A. Carrillo Montoya , G.S. Chahal⁷⁶ , D. Colling , J.S. Dancu , I. Das , P. Dauncey , G. Davies , J. Davies , M. Della Negra , S. Fayer , G. Fedi , G. Hall , M.H. Hassanshahi , A. Howard , G. Iles , M. Knight , J. Langford , J. León Holgado , L. Lyons , A.-M. Magnan , S. Mallios , M. Mieskolainen , J. Nash⁷⁷ , M. Pesaresi , P.B. Pradeep , B.C. Radburn-Smith , A. Richards , A. Rose , K. Savva , C. Seez , R. Shukla , A. Tapper , K. Uchida , G.P. Uttley , L.H. Vage , T. Virdee²⁹ , M. Vojinovic , N. Wardle , D. Winterbottom

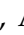

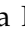



Brunel University, Uxbridge, United Kingdom

K. Coldham , J.E. Cole , A. Khan , P. Kyberd , I.D. Reid 

Baylor University, Waco, Texas, USA

S. Abdullin , A. Brinkerhoff , B. Caraway , E. Collins , J. Dittmann , K. Hatakeyama , J. Hiltbrand , B. McMaster , J. Samudio , S. Sawant , C. Sutantawibul , J. Wilson



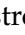




Catholic University of America, Washington, DC, USA

R. Bartek , A. Dominguez , C. Huerta Escamilla , A.E. Simsek , R. Uniyal , A.M. Vargas Hernandez 








The University of Alabama, Tuscaloosa, Alabama, USA

B. Bam , A. Buchot Perraguin , R. Chudasama , S.I. Cooper , C. Crovella , S.V. Gleyzer , E. Pearson , C.U. Perez , P. Rumerio⁷⁸ , E. Usai , R. Yi


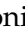





Boston University, Boston, Massachusetts, USA

A. Akpinar , C. Cosby , G. De Castro , Z. Demiragli , C. Erice , C. Fangmeier , C. Fernandez Madrazo , E. Fontanesi , D. Gastler , F. Golf , S. Jeon , J. O'cain , I. Reed , J. Rohlf , K. Salyer , D. Sperka , D. Spitzbart , I. Suarez , A. Tsatsos , A.G. Zecchinelli














Brown University, Providence, Rhode Island, USA

G. Benelli , X. Coubez²⁵ , D. Cutts , M. Hadley , U. Heintz , J.M. Hogan⁷⁹ , T. Kwon , G. Landsberg , K.T. Lau , D. Li , J. Luo , S. Mondal , M. Narain[†] , N. Pervan , S. Sagir⁸⁰ , F. Simpson , M. Stamenkovic , N. Venkatasubramanian , X. Yan , W. Zhang

University of California, Davis, Davis, California, USA

S. Abbott , J. Bonilla , C. Brainerd , R. Breedon , H. Cai , M. Calderon De La Barca Sanchez , M. Chertok , M. Citron , J. Conway , P.T. Cox , R. Erbacher , F. Jensen , O. Kukral , G. Mocellin , M. Mulhearn , S. Ostrom , W. Wei , Y. Yao , S. Yoo , F. Zhang

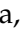





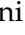

















University of California, Los Angeles, California, USA

M. Bachtis , R. Cousins , A. Datta , G. Flores Avila , J. Hauser , M. Ignatenko ,
M.A. Iqbal , T. Lam , E. Manca , N. Mccoll , A. Nunez Del Prado, D. Saltzberg ,
B. Stone , V. Valuev 

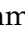

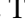
University of California, Riverside, Riverside, California, USA

R. Clare , J.W. Gary , M. Gordon, G. Hanson , W. Si , S. Wimpenny[†] 

University of California, San Diego, La Jolla, California, USA

A. Aportela, A. Arora , J.G. Branson , S. Cittolin , S. Cooperstein , D. Diaz ,
J. Duarte , L. Giannini , Y. Gu, J. Guiang , R. Kansal , V. Krutelyov , R. Lee ,
J. Letts , M. Masciovecchio , F. Mokhtar , S. Mukherjee , M. Pieri , M. Quinnan ,
B.V. Sathia Narayanan , V. Sharma , M. Tadel , E. Vourliotis , F. Würthwein ,
Y. Xiang , A. Yagil 

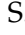













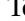

University of California, Santa Barbara - Department of Physics, Santa Barbara, California, USA

A. Barzdukas , L. Brennan , C. Campagnari , K. Downham , C. Grieco , J. Incandela ,
J. Kim , A.J. Li , P. Masterson , H. Mei , J. Richman , S.N. Santpur , U. Sarica ,
R. Schmitz , F. Setti , J. Sheplock , D. Stuart , T.Á. Vámi , S. Wang , D. Zhang










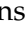




California Institute of Technology, Pasadena, California, USA

A. Bornheim , O. Cerri, A. Latorre, J. Mao , H.B. Newman , G. Reales Gutiérrez,
M. Spiropulu , J.R. Vlimant , C. Wang , S. Xie , R.Y. Zhu 


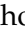








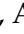




Carnegie Mellon University, Pittsburgh, Pennsylvania, USA

J. Alison , S. An , M.B. Andrews , P. Bryant , M. Cremonesi, V. Dutta , T. Ferguson ,
T.A. Gómez Espinosa , A. Harilal , A. Kallil Tharayil, C. Liu , T. Mudholkar ,
S. Murthy , P. Palit , K. Park, M. Paulini , A. Roberts , A. Sanchez , W. Terrill 



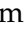



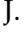



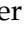


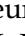
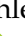
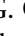





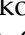
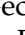


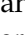
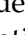




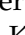
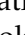
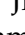

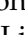


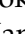
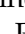





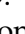








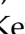





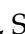










University of Colorado Boulder, Boulder, Colorado, USA

J.P. Cumalat , W.T. Ford , A. Hart , A. Hassani , G. Karathanasis , N. Manganelli ,
A. Perloff , C. Savard , N. Schonbeck , K. Stenson , K.A. Ulmer , S.R. Wagner ,
N. Zipper , D. Zuolo 



















Cornell University, Ithaca, New York, USA

J. Alexander , S. Bright-Thonney , X. Chen , D.J. Cranshaw , J. Fan , X. Fan ,
S. Hogan , P. Kotamnives, J. Monroy , M. Oshiro , J.R. Patterson , M. Reid , A. Ryd ,
J. Thom , P. Wittich , R. Zou 










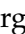



Fermi National Accelerator Laboratory, Batavia, Illinois, USA

M. Albrow , M. Alyari , O. Amram , G. Apollinari , A. Apresyan , L.A.T. Bauerdick ,
D. Berry , J. Berryhill , P.C. Bhat , K. Burkett , J.N. Butler , A. Canepa , G.B. Cerati ,
H.W.K. Cheung , F. Chlebana , G. Cummings , J. Dickinson , I. Dutta , V.D. Elvira ,
Y. Feng , J. Freeman , A. Gandrakota , Z. Gece , L. Gray , D. Green, A. Grummer ,
S. Grünendahl , D. Guerrero , O. Gutsche , R.M. Harris , R. Heller , T.C. Herwig ,
J. Hirschauer , B. Jayatilaka , S. Jindariani , M. Johnson , U. Joshi , T. Klijnsma ,
B. Klima , K.H.M. Kwok , S. Lammel , D. Lincoln , R. Lipton , T. Liu , C. Madrid ,
K. Maeshima , C. Mantilla , D. Mason , P. McBride , P. Merkel , S. Mrenna ,
S. Nahn , J. Ngadiuba , D. Noonan , S. Norberg, V. Papadimitriou , N. Pastika ,
K. Pedro , C. Pena⁸¹ , F. Ravera , A. Reinsvold Hall⁸² , L. Ristori , M. Safdari ,
E. Sexton-Kennedy , N. Smith , A. Soha , L. Spiegel , S. Stoynev , J. Strait ,
L. Taylor , S. Tkaczyk , N.V. Tran , L. Uplegger , E.W. Vaandering , I. Zoi 

University of Florida, Gainesville, Florida, USA

C. Aruta , P. Avery , D. Bourilkov , P. Chang , V. Cherepanov , R.D. Field, E. Koenig , M. Kolosova , J. Konigsberg , A. Korytov , K. Matchev , N. Menendez , G. Mitselmakher , K. Mohrman , A. Muthirakalayil Madhu , N. Rawal , S. Rosenzweig , Y. Takahashi , J. Wang 





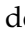


















Florida State University, Tallahassee, Florida, USA

T. Adams , A. Al Kadhimi , A. Askew , S. Bower , R. Habibullah , V. Hagopian , R. Hashmi , R.S. Kim , S. Kim , T. Kolberg , G. Martinez, H. Prosper , P.R. Prova, M. Wulansatiti , R. Yohay , J. Zhang

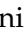









Florida Institute of Technology, Melbourne, Florida, USA

B. Alsufyani , M.M. Baarmand , S. Butalla , S. Das , T. Elkafrawy⁸³ , M. Hohlmann , M. Rahmani, E. Yanes







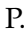




University of Illinois Chicago, Chicago, Illinois, USA

M.R. Adams , A. Baty , C. Bennett, R. Cavanaugh , R. Escobar Franco , O. Evdokimov , C.E. Gerber , M. Hawksworth, A. Hingrajiya, D.J. Hofman , J.h. Lee , D. S. Lemos , A.H. Merritt , C. Mills , S. Nanda , G. Oh , B. Ozek , D. Pilipovic , R. Pradhan , E. Prifti, T. Roy , S. Rudrabhatla , M.B. Tonjes , N. Varelas , M.A. Wadud , Z. Ye , J. Yoo 








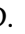

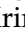







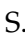






The University of Iowa, Iowa City, Iowa, USA

M. Alhusseini , D. Blend, K. Dilsiz⁸⁴ , L. Emediato , G. Karaman , O.K. Köseyan , J.-P. Merlo, A. Mestvirishvili⁸⁵ , O. Neogi, H. Ogul⁸⁶ , Y. Onel , A. Penzo , C. Snyder, E. Tiras⁸⁷ 









Johns Hopkins University, Baltimore, Maryland, USA

B. Blumenfeld , L. Corcodilos , J. Davis , A.V. Gritsan , L. Kang , S. Kyriacou , P. Maksimovic , M. Roguljic , J. Roskes , S. Sekhar , M. Swartz 






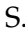









The University of Kansas, Lawrence, Kansas, USA

A. Abreu , L.F. Alcerro Alcerro , J. Anguiano , S. Arteaga Escatel , P. Baringer , A. Bean , Z. Flowers , D. Grove , J. King , G. Krintiras , M. Lazarovits , C. Le Mahieu , J. Marquez , N. Minafra , M. Murray , M. Nickel , M. Pitt , S. Popescu⁸⁸ , C. Rogan , C. Royon , R. Salvatico , S. Sanders , C. Smith , G. Wilson 





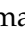






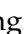




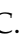






Kansas State University, Manhattan, Kansas, USA

B. Allmond , R. Gujju Gurunadha , A. Ivanov , K. Kaadze , Y. Maravin , J. Natoli , D. Roy , G. Sorrentino 

University of Maryland, College Park, Maryland, USA

A. Baden , A. Belloni , J. Bistany-riebman, Y.M. Chen , S.C. Eno , N.J. Hadley , S. Jabeen , R.G. Kellogg , T. Koeth , B. Kronheim, Y. Lai , S. Lascio , A.C. Mignerey , S. Nabili , C. Palmer , C. Papageorgakis , M.M. Paranjpe, L. Wang 

Massachusetts Institute of Technology, Cambridge, Massachusetts, USA

J. Bendavid , I.A. Cali , P.c. Chou , M. D'Alfonso , J. Eysermans , C. Freer , G. Gomez-Ceballos , M. Goncharov, G. Grosso, P. Harris, D. Hoang, D. Kovalskyi , J. Krupa , L. Lavezzo , Y.-J. Lee , K. Long , C. McGinn , A. Novak , C. Paus , D. Rankin , C. Roland , G. Roland , S. Rothman , G.S.F. Stephans , Z. Wang , B. Wyslouch , T. J. Yang 













University of Minnesota, Minneapolis, Minnesota, USA

B. Crossman , B.M. Joshi , C. Kapsiak , M. Krohn , D. Mahon , J. Mans ,
B. Marzocchi , M. Revering , R. Rusack , R. Saradhy , N. Strobbe 












University of Mississippi, Oxford, Mississippi, USA

L.M. Cremaldi 








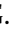


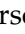

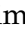



University of Nebraska-Lincoln, Lincoln, Nebraska, USA

K. Bloom , D.R. Claes , G. Haza , J. Hossain , C. Joo , I. Kravchenko , J.E. Siado ,
W. Tabb , A. Vagnerini , A. Wightman , F. Yan , D. Yu 

State University of New York at Buffalo, Buffalo, New York, USA

H. Bandyopadhyay , L. Hay , H.w. Hsia , I. Iashvili , A. Kalogeropoulos ,
A. Kharchilava , M. Morris , D. Nguyen , S. Rappoccio , H. Rejeb Sfar, A. Williams ,
P. Young 








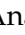


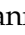

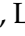
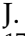












Northeastern University, Boston, Massachusetts, USA

G. Alverson , E. Barberis , J. Dervan , Y. Haddad , Y. Han , A. Krishna , J. Li ,
M. Lu , G. Madigan , R. Mccarthy , D.M. Morse , V. Nguyen , T. Orimoto ,
A. Parker , L. Skinnari , D. Wood 






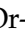


Northwestern University, Evanston, Illinois, USA

J. Bueghly, S. Dittmer , K.A. Hahn , Y. Liu , Y. Miao , D.G. Monk , M.H. Schmitt ,
A. Talierno , M. Velasco

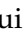



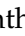










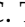

University of Notre Dame, Notre Dame, Indiana, USA

G. Agarwal , R. Band , R. Bucci, S. Castells , A. Das , R. Goldouzian , M. Hildreth ,
K.W. Ho , K. Hurtado Anampa , T. Ivanov , C. Jessop , K. Lannon , J. Lawrence ,
N. Loukas , L. Lutton , J. Mariano, N. Marinelli, I. Mcalister, T. McCauley , C. Mcgrady ,
C. Moore , Y. Musienko¹⁷ , H. Nelson , M. Osherson , A. Piccinelli , R. Ruchti ,
A. Townsend , Y. Wan, M. Wayne , H. Yockey, M. Zarucki , L. Zygalas 

The Ohio State University, Columbus, Ohio, USA

A. Basnet , B. Bylsma, M. Carrigan , L.S. Durkin , C. Hill , M. Joyce , M. Nunez Ornelas ,
K. Wei, B.L. Winer , B. R. Yates 










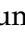



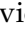
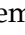

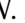

Princeton University, Princeton, New Jersey, USA

H. Bouchamaoui , P. Das , G. Dezoort , P. Elmer , A. Frankenthal , B. Greenberg ,
N. Haubrich , K. Kennedy, G. Kopp , S. Kwan , D. Lange , A. Loeliger , D. Marlow ,
I. Ojalvo , J. Olsen , A. Shevelev , D. Stickland , C. Tully 




University of Puerto Rico, Mayaguez, Puerto Rico, USA

S. Malik 

Purdue University, West Lafayette, Indiana, USA

A.S. Bakshi , V.E. Barnes , S. Chandra , R. Chawla , A. Gu , L. Gutay, M. Jones ,
A.W. Jung , A.M. Koshy, M. Liu , G. Negro , N. Neumeister , G. Paspalaki ,
S. Piperov , V. Scheurer, J.F. Schulte , M. Stojanovic , J. Thieman , A. K. Virdi ,
F. Wang , W. Xie 

Purdue University Northwest, Hammond, Indiana, USA

J. Dolen , N. Parashar , A. Pathak 

Rice University, Houston, Texas, USA

D. Acosta , T. Carnahan , K.M. Ecklund , P.J. Fernández Manteca , S. Freed, P. Gardner,
F.J.M. Geurts , W. Li , J. Lin , O. Miguel Colin , B.P. Padley , R. Redjimi, J. Rotter 

E. Yigitbasi , Y. Zhang 
















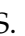


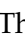


University of Rochester, Rochester, New York, USA

A. Bodek , P. de Barbaro , R. Demina , J.L. Dulemba , A. Garcia-Bellido , O. Hindrichs , A. Khukhunaishvili , N. Parmar , P. Parygin⁸⁹ , E. Popova⁸⁹ , R. Taus 






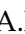




The Rockefeller University, New York, New York, USA

K. Goulianos 















Rutgers, The State University of New Jersey, Piscataway, New Jersey, USA

B. Chiarito, J.P. Chou , S.V. Clark , D. Gadkari , Y. Gershtein , E. Halkiadakis , M. Heindl , C. Houghton , D. Jaroslawski , O. Karacheban²⁷ , S. Konstantinou , I. Laflotte , A. Lath , R. Montalvo, K. Nash, J. Reichert , H. Routray , P. Saha , S. Salur , S. Schnetzer, S. Somalwar , R. Stone , S.A. Thayil , S. Thomas, J. Vora , H. Wang 

University of Tennessee, Knoxville, Tennessee, USA

H. Acharya, D. Ally , A.G. Delannoy , S. Fiorendi , S. Higginbotham , T. Holmes , A.R. Kanuganti , N. Karunarathna , L. Lee , E. Nibigira , S. Spanier 












Texas A&M University, College Station, Texas, USA

D. Aebi , M. Ahmad , T. Akhter , O. Bouhali⁹⁰ , R. Eusebi , J. Gilmore , T. Huang , T. Kamon⁹¹ , H. Kim , S. Luo , R. Mueller , D. Overton , D. Rathjens , A. Safonov 







Texas Tech University, Lubbock, Texas, USA

N. Akchurin , J. Damgov , N. Gogate , V. Hegde , A. Hussain , Y. Kazhykarim, K. Lamichhane , S.W. Lee , A. Mankel , T. Peltola , I. Volobouev 

Vanderbilt University, Nashville, Tennessee, USA

E. Appelt , Y. Chen , S. Greene, A. Gurrola , W. Johns , R. Kunnawalkam Elayavalli , A. Melo , F. Romeo , P. Sheldon , S. Tuo , J. Velkovska , J. Viinikainen 





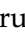
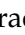

















University of Virginia, Charlottesville, Virginia, USA

B. Cardwell , B. Cox , J. Hakala , R. Hirosky , A. Ledovskoy , C. Neu 

Wayne State University, Detroit, Michigan, USA

S. Bhattacharya , P.E. Karchin 


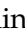




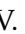








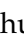

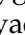


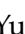

University of Wisconsin - Madison, Madison, Wisconsin, USA

A. Aravind , S. Banerjee , K. Black , T. Bose , S. Dasu , I. De Bruyn , P. Everaerts , C. Galloni, H. He , M. Herndon , A. Herve , C.K. Koraka , A. Lanaro, R. Loveless , J. Madhusudanan Sreekala , A. Mallampalli , A. Mohammadi , S. Mondal, G. Parida , L. Pétré , D. Pinna, A. Savin, V. Shang , V. Sharma , W.H. Smith , D. Teague, H.F. Tsoi , W. Vetens , A. Warden 

Authors affiliated with an international laboratory covered by a cooperation agreement with CERN

G. Gavrilov , V. Golovtcov , Y. Ivanov , V. Kim⁹² , P. Levchenko⁹³ , V. Murzin , V. Oreshkin , D. Sosnov , V. Sulimov , L. Uvarov , A. Vorobyev[†], T. Aushev 

Authors affiliated with an institute formerly covered by a cooperation agreement with CERN

S. Afanasiev , V. Alexakhin , D. Budkouski , I. Golutvin , I. Gorbunov , V. Karjavine , V. Korenkov , A. Lanev , A. Malakhov , V. Matveev⁹² , V. Palichik , V. Perelygin , M. Savina , V. Shalaev , S. Shmatov , S. Shulha , V. Smirnov , O. Teryaev , N. Voytishin , B.S. Yuldashev⁹⁴, A. Zarubin , I. Zhizhin , Yu. Andreev , A. Dermenev 

S. Gninenko , N. Golubev , A. Karneyeu , D. Kirpichnikov , M. Kirsanov , N. Krasnikov , I. Tlisova , A. Toropin , V. Gavrilo , N. Lychkovskaya , A. Nikitenko^{95,96} , V. Popov , A. Zhokin , R. Chistov⁹² , M. Danilov⁹² , S. Polikarpov⁹² , V. Andreev , M. Azarkin , M. Kirakosyan, A. Terkulov , E. Boos , V. Bunichev , M. Dubinin⁸¹ , L. Dudko , A. Ershov , A. Gribushin , V. Klyukhin , O. Kodolova⁹⁶ , S. Obraztsov , S. Petrushanko , V. Savrin , A. Snigirev , V. Blinov⁹², T. Dimova⁹² , A. Kozyrev⁹² , O. Radchenko⁹² , Y. Skovpen⁹² , V. Kachanov , D. Konstantinov , S. Slabospitskii , A. Uzunian , A. Babaev , V. Borshch , D. Druzhkin⁹⁷ , E. Tcherniaev , V. Chekhovsky, V. Makarenko 

†: Deceased

¹Also at Yerevan State University, Yerevan, Armenia

²Also at TU Wien, Vienna, Austria

³Also at Institute of Basic and Applied Sciences, Faculty of Engineering, Arab Academy for Science, Technology and Maritime Transport, Alexandria, Egypt

⁴Also at Ghent University, Ghent, Belgium

⁵Also at Universidade do Estado do Rio de Janeiro, Rio de Janeiro, Brazil

⁶Also at Universidade Estadual de Campinas, Campinas, Brazil

⁷Also at Federal University of Rio Grande do Sul, Porto Alegre, Brazil

⁸Also at UFMS, Nova Andradina, Brazil

⁹Also at Nanjing Normal University, Nanjing, China

¹⁰Now at The University of Iowa, Iowa City, Iowa, USA

¹¹Also at University of Chinese Academy of Sciences, Beijing, China

¹²Also at China Center of Advanced Science and Technology, Beijing, China

¹³Also at University of Chinese Academy of Sciences, Beijing, China

¹⁴Also at China Spallation Neutron Source, Guangdong, China

¹⁵Now at Henan Normal University, Xinxiang, China

¹⁶Also at Université Libre de Bruxelles, Bruxelles, Belgium

¹⁷Also at an institute formerly covered by a cooperation agreement with CERN

¹⁸Also at Suez University, Suez, Egypt

¹⁹Now at British University in Egypt, Cairo, Egypt

²⁰Also at Purdue University, West Lafayette, Indiana, USA

²¹Also at Université de Haute Alsace, Mulhouse, France

²²Also at Department of Physics, Tsinghua University, Beijing, China

²³Also at The University of the State of Amazonas, Manaus, Brazil

²⁴Also at University of Hamburg, Hamburg, Germany

²⁵Also at RWTH Aachen University, III. Physikalisches Institut A, Aachen, Germany

²⁶Also at Bergische University Wuppertal (BUW), Wuppertal, Germany

²⁷Also at Brandenburg University of Technology, Cottbus, Germany

²⁸Also at Forschungszentrum Jülich, Jülich, Germany

²⁹Also at CERN, European Organization for Nuclear Research, Geneva, Switzerland

³⁰Also at HUN-REN ATOMKI - Institute of Nuclear Research, Debrecen, Hungary

³¹Now at Universitatea Babes-Bolyai - Facultatea de Fizica, Cluj-Napoca, Romania

³²Also at MTA-ELTE Lendület CMS Particle and Nuclear Physics Group, Eötvös Loránd University, Budapest, Hungary

³³Also at HUN-REN Wigner Research Centre for Physics, Budapest, Hungary

³⁴Also at Physics Department, Faculty of Science, Assiut University, Assiut, Egypt

³⁵Also at Punjab Agricultural University, Ludhiana, India

³⁶Also at University of Visva-Bharati, Santiniketan, India

³⁷Also at Indian Institute of Science (IISc), Bangalore, India

- ³⁸Also at IIT Bhubaneswar, Bhubaneswar, India
- ³⁹Also at Institute of Physics, Bhubaneswar, India
- ⁴⁰Also at University of Hyderabad, Hyderabad, India
- ⁴¹Also at Deutsches Elektronen-Synchrotron, Hamburg, Germany
- ⁴²Also at Isfahan University of Technology, Isfahan, Iran
- ⁴³Also at Sharif University of Technology, Tehran, Iran
- ⁴⁴Also at Department of Physics, University of Science and Technology of Mazandaran, Behshahr, Iran
- ⁴⁵Also at Department of Physics, Isfahan University of Technology, Isfahan, Iran
- ⁴⁶Also at Italian National Agency for New Technologies, Energy and Sustainable Economic Development, Bologna, Italy
- ⁴⁷Also at Centro Siciliano di Fisica Nucleare e di Struttura Della Materia, Catania, Italy
- ⁴⁸Also at Università degli Studi Guglielmo Marconi, Roma, Italy
- ⁴⁹Also at Scuola Superiore Meridionale, Università di Napoli 'Federico II', Napoli, Italy
- ⁵⁰Also at Fermi National Accelerator Laboratory, Batavia, Illinois, USA
- ⁵¹Also at Consiglio Nazionale delle Ricerche - Istituto Officina dei Materiali, Perugia, Italy
- ⁵²Also at Department of Applied Physics, Faculty of Science and Technology, Universiti Kebangsaan Malaysia, Bangi, Malaysia
- ⁵³Also at Consejo Nacional de Ciencia y Tecnología, Mexico City, Mexico
- ⁵⁴Also at Trincomalee Campus, Eastern University, Sri Lanka, Nilaveli, Sri Lanka
- ⁵⁵Also at Saegis Campus, Nugegoda, Sri Lanka
- ⁵⁶Also at National and Kapodistrian University of Athens, Athens, Greece
- ⁵⁷Also at Ecole Polytechnique Fédérale Lausanne, Lausanne, Switzerland
- ⁵⁸Also at Universität Zürich, Zurich, Switzerland
- ⁵⁹Also at Stefan Meyer Institute for Subatomic Physics, Vienna, Austria
- ⁶⁰Also at Laboratoire d'Annecy-le-Vieux de Physique des Particules, IN2P3-CNRS, Annecy-le-Vieux, France
- ⁶¹Also at Near East University, Research Center of Experimental Health Science, Mersin, Turkey
- ⁶²Also at Konya Technical University, Konya, Turkey
- ⁶³Also at Izmir Bakircay University, Izmir, Turkey
- ⁶⁴Also at Adiyaman University, Adiyaman, Turkey
- ⁶⁵Also at Bozok Universitetesi Rektörlüğü, Yozgat, Turkey
- ⁶⁶Also at Marmara University, Istanbul, Turkey
- ⁶⁷Also at Milli Savunma University, Istanbul, Turkey
- ⁶⁸Also at Kafkas University, Kars, Turkey
- ⁶⁹Now at Istanbul Okan University, Istanbul, Turkey
- ⁷⁰Also at Hacettepe University, Ankara, Turkey
- ⁷¹Also at Erzincan Binali Yildirim University, Erzincan, Turkey
- ⁷²Also at Istanbul University - Cerrahpasa, Faculty of Engineering, Istanbul, Turkey
- ⁷³Also at Yildiz Technical University, Istanbul, Turkey
- ⁷⁴Also at Vrije Universiteit Brussel, Brussel, Belgium
- ⁷⁵Also at School of Physics and Astronomy, University of Southampton, Southampton, United Kingdom
- ⁷⁶Also at IPPP Durham University, Durham, United Kingdom
- ⁷⁷Also at Monash University, Faculty of Science, Clayton, Australia
- ⁷⁸Also at Università di Torino, Torino, Italy
- ⁷⁹Also at Bethel University, St. Paul, Minnesota, USA
- ⁸⁰Also at Karamanoğlu Mehmetbey University, Karaman, Turkey

⁸¹Also at California Institute of Technology, Pasadena, California, USA

⁸²Also at United States Naval Academy, Annapolis, Maryland, USA

⁸³Also at Ain Shams University, Cairo, Egypt

⁸⁴Also at Bingol University, Bingol, Turkey

⁸⁵Also at Georgian Technical University, Tbilisi, Georgia

⁸⁶Also at Sinop University, Sinop, Turkey

⁸⁷Also at Erciyes University, Kayseri, Turkey

⁸⁸Also at Horia Hulubei National Institute of Physics and Nuclear Engineering (IFIN-HH), Bucharest, Romania

⁸⁹Now at another institute formerly covered by a cooperation agreement with CERN

⁹⁰Also at Texas A&M University at Qatar, Doha, Qatar

⁹¹Also at Kyungpook National University, Daegu, Korea

⁹²Also at another institute formerly covered by a cooperation agreement with CERN

⁹³Also at Northeastern University, Boston, Massachusetts, USA

⁹⁴Also at Institute of Nuclear Physics of the Uzbekistan Academy of Sciences, Tashkent, Uzbekistan

⁹⁵Also at Imperial College, London, United Kingdom

⁹⁶Now at Yerevan Physics Institute, Yerevan, Armenia

⁹⁷Also at Universiteit Antwerpen, Antwerpen, Belgium